ΠΑΝΕΠΙΣΤΗΜΙΟ ΚΡΗΤΗΣ, ΤΜΗΜΑ ΙΑΤΡΙΚΗΣ

Ο ρόλος της φυσικής ανοσοαπάντησης στην παθογένεση παρεγχυματικών και αγγειακών παθήσεων του πνεύμονα

Ελένη Βεργαδή

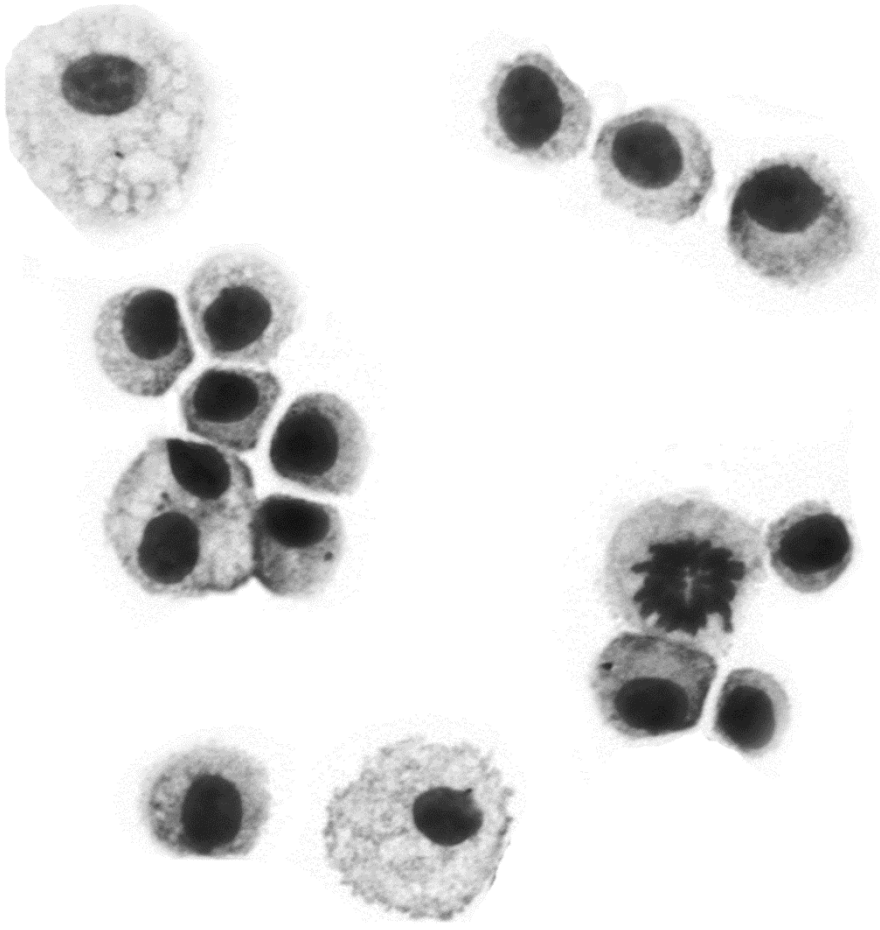

Διδακτορική Διατριβή

Ηράκλειο, 2015

*Title picture: Alveolar macrophages isolated from bronchoalveolar lavage from mice exposed to hypoxia.

UNIVERSITY OF CRETE, SCHOOL OF MEDICINE

The role of innate immune response in the pathogenesis of parenchymal and vascular lung diseases

Eleni Vergadi

PhD Thesis

Heraklion, 2015

Τριμελής Συμβουλευτική Επιτροπή

Χρήστος Τσατσάνης: Αναπληρωτής Καθηγητής Κλινικής Χημείας, Τμήμα Ιατρικής, Πανεπιστήμιο Κρήτης

Δημήτριος Γεωργόπουλος: Καθηγητής Εντατικής Ιατρικής, Τμήμα Ιατρικής, Πανεπιστήμιο Κρήτης

Stella Kourembanas: Καθηγήτρια Παιδιατρικής- Νεογνολογίας, Τμήμα Ιατρικής, Πανεπιστήμιο Harvard

Επταμελής Συμβουλευτική Επιτροπή

Χρήστος Τσατσάνης: Αναπληρωτής Καθηγητής Κλινικής Χημείας, Τμήμα Ιατρικής, Πανεπιστήμιο Κρήτης

Δημήτριος Γεωργόπουλος: Καθηγητής Εντατικής Ιατρικής, Τμήμα Ιατρικής, Πανεπιστήμιο Κρήτης

Stella Kourembanas: Καθηγήτρια Παιδιατρικής- Νεογνολογίας, Τμήμα Ιατρικής, Πανεπιστήμιο Harvard

Δημήτρης Καρδάσης: Καθηγητής Βιοχημείας, Τμήμα Ιατρικής, Πανεπιστήμιο Κρήτης

Κατερίνα Βαπορίδη: Επίκουρος Καθηγήτρια Εντατικής Ιατρικής, Τμήμα Ιατρικής, Πανεπιστήμιο Κρήτης

Ευμορφία Κονδύλη: Επίκουρος Καθηγήτρια Εντατικής Ιατρικής, Τμήμα Ιατρικής,

Πανεπιστήμιο Κρήτης

Πρόδρομος Σιδηρόπουλος: Επίκουρος Καθηγήτης Ρευματολογίας, Τμήμα Ιατρικής, Πανεπιστήμιο Κρήτης

This research has been conducted in three collaborating research laboratories under the Graduate Program "The Molecular Basis of Human Disease" of the Medical School, University of Crete. The first part of this research on the pathogenesis of Acute Lung injury was conducted in the Laboratory of Clinical Chemistry and the laboratory of Intensive Care Unit of the University of Crete under the supervision of Dr Christos Tsatsanis, Dr Dimitrios Georgopoulos and Dr Katerina Vaporidi. Some of the experiments were also conducted by the author in Cenix Biosciences, located in Dresden, Germany.

The second part of the thesis on the pathogenesis of pulmonary hypertension has been conducted in the Laboratory of Neonatology, Department of Newborn Medicine in Children's Hospital Boston and Harvard Medical School under the supervision of Dr Stella Kourembanas and Dr Alex S. Mitsialis.

The first part of this work was supported by the European Union within the 7th framework program (FP7-PIAP-GA-2008-230725-TACIT and FP7-2011-REGPOT-1-TransPOT), the Association for International Cancer Research (AICR11-0505) and from National and EU funds under the 'ARISTEIA' grant to Christos Tsatsanis. The second part was supported by the National Institutes of Health grants (RO1 HL 055454 and RO1 HL085446) to Drs Kourembanas and Mitsialis.

Eleni Vergadi acknowledges personal funding from State Scholarships Foundation-IKY, Propondis Foundation and Manassaki's Scholarship Awards program.

Ευχαριστίες

Η παρούσα διατριβή είναι το αποτέλεσμα της πενταετούς ενασχόλησης μου με την βασική εργαστηριακή έρευνα, μια πορεία ευχάριστη και συναρπαστική, γεμάτη εκπλήξεις αλλά και απογοητεύσεις. Στην πορεία μου αυτή, με βοήθησαν καθοριστικά καθηγητές - δάσκαλοι, φίλοι, συνεργάτες και συγγενείς που επιθυμώ να ευχαριστήσω βαθύτατα.

Ιδιαίτερη σημασία είχε για μένα η καθημερινή συνεργασία με τους επιβλέποντες της διατριβής μου, καθηγητές Χρήστο Τσατσάνη, Κατερίνα Βαπορίδη και Δημήτρη Γεωργόπουλο στο Πανεπιστήμιο Κρήτης και καθηγητές Στέλλα Κουρεμπάνα και Αλέξανδρο Μιτσιάλη στο Πανεπιστήμιο Harvard στην Βοστώνη. Οι άνθρωποι αυτοί διέθεσαν πολύ χρόνο, γνώση και επιστημονική εμπειρία ώστε να με συμβουλεύουν και να με καθοδηγούν καθημερινά προς την σωστή κατεύθυνση και να με στηρίζουν επιστημονικά, ηθικά και οικονομικά. Την περίοδο συνεργασίας μου μαζί τους αποκόμισα ανεκτίμητη γνώση και εμπειρία καθώς και αυτογνωσία και προσωρική ωρίμανση.

Πολλές ευχαριστίες οφείλω επίσης στον καθηγητή Βασίλειο Ζαννή, τον άνθρωπο που αποτέλεσε δάσκαλο και μέντορα μου στην σταδιοδρομία μου μέχρι σήμερα καθώς μου μετέδωσε την αγάπη για την έρευνα και με βοήθησε ουσιαστικά να συνεχίσω τις μεταπτυχιακές μου σπουδές στην Βοστώνη.

Ευχαριστώ επίσης όλους τους συνεργάτες μου και μέλη του εργαστηρίου Κλινικής Χημείας, την Ελευθερία Ιερωνυμάκη, Χριστίνα Δοξάκη, Alicia Arranz, Κωνσταντίνα Λυρώνη, Έφη Καραγιάννη, Όλγα Ρασούλη, Μαρία Βενυχάκη, Ρένα Δερμιτζάκη, Ιωάννα Πλατή, Ισμήνη Αλεξάκη και τον Μανώλη Θεοδωράκη, Βαγγέλη Κανιάρη και Ανδρέα Πάτσαλο για τις χαρές και δυσκολίες που περάσαμε μαζί και την βοήθεια τους “on the bench”. Θα ήθελα να ευχαριστήσω και την Ελένη Λαγουδάκη από το παθολογοανατομικό εργαστήριο για την χρήσιμη βοήθειά της στην επεξεργασία και ερμηνεία των ιστολογικών πειραμάτων.

Θερμά ευχαριστώ και στους συνεργάτες μου στο εργαστηρίο Νεογνολογίας, Helen Christou, Angeles Fernandez Gonzalez, Xianlan Li, Sally Vitali, Changjiin Lee, Annette Scheid και Muhammad Aslam για τις καθημερινές συμβουλές τους στο ερευνητικό μου ξεκίνημα και τις χρήσιμες ερευνητικές και μη συζητήσεις.

Τους καθηγητές της επταμελούς επιτροπής Δημήτριο Καρδάση, Ευμορφία Κονδύλη και Πρόδρομο Σιδηρόπουλο για τον χρόνο τους και τις συμβουλές τους καθώς και τον καθηγητή Δημητριο Μπούμπα για τις συμβουλές και την υποστήριξή του.

Τέλος, θέλω να ευχαριστήσω τους γονείς μου Γιάννη και Κωνσταντίνα και τον σύζυγό μου Ζαχαρία για την συνεχή υποστήριξή τους, την ανοχή και την υπομονή τους όλα αυτά τα χρόνια.

Στους γονείς μου Γιάννη και Κωνσταντίνα,

και στον σύζυγό μου Ζαχαρία

Curriculum Vitae Eleni Vergadi

Medical/Scientific Education and Qualifications

2001-2007	M.D Degree (University of Crete / Faculty of Medicine) Grade "Excellent" (8.88/10)
2007-2009	Master of Science: «Molecular Basis of Human Disease» (University of Crete/Faculty of Medicine) Grade "Excellent" (10/10)"
2010-2015	PhD Thesis: "The role of innate immune response in the pathogenesis of parenchymal and vascular lung disease" University of Crete, Faculty of Medicine.

Previous and Current posts and positions

11/2008-12/2010	Research Fellow in Pediatrics, Division of Newborn Medicine Children's Hospital Boston, Harvard Medical School
12/2010-12/2014	PhD student - researcher in the laboratory of Clinical Chemistry in collaboration with the laboratory of Intensive Care Medicine, University of Crete, Faculty of Medicine.
9/2011-12/2011	Marie Curie Fellowship under TACIT program (Targeted Carriers in Immunotherapy) IAPP project (Industry-Academia Partnerships and pathways). Bioinnovation Center, Dresden, Germany. The goal was to develop siRNA molecules for endotracheal delivery
4/2012 – 5/2013	Resident in Pediatrics, St. Nicolas General Hospital, Crete
5/2013- today	Resident in Pediatrics, University General Hospital of Heraklion, Crete

Publications:

1. Vergadi E, Vaporidi K, Theodorakis EE, Doxaki C, Lagoudaki E, Ieronymaki E, Alexaki VI, Helms M, Kondili E, Soennichsen B, Stathopoulos EN, Margioris E, Georgopoulos D, Tsatsanis C. Akt2 Deficiency Protects from Acute Lung Injury via Alternative Macrophage Activation and miR-146a Induction in Mice. J immunology. 2014; an 1;192(1):394-406.

2. Kaniaris E, Vaporidi K, Vergadi E, Theodorakis EE, Kondili K, Lagoudaki E, Tsatsanis C, Georgopoulos D. Genetic and pharmacologic inhibition of Tpl2 kinase is protective in a mouse model of ventilator-induced lung injury. Intensive Care Medicine Experimental 2014; 2:15

3. Karakasilioti I, Kamileri I, Chatzinikolaou G, Kosteas T, Vergadi E, Robinson AR, Tsamardinos I, Rozgaja TA, Siakouli S, Tsatsanis C, Niedernhofer LJ, Garinis G. DNA Damage Triggers a Chronic Autoinflammatory Response Leading to Fat Depletion in NER Progeria. Cell Metabolism 2013; 18, 403–415.

4. Vaporidi K, Vergadi E, Kaniaris E, Hatziapostolou M, Lagoudaki E, Georgopoulos D, Zapol WM, Bloch KD, Iliopoulos D. Pulmonary microRNA profiling in a mouse model of ventilator-induced lung injury. Am J Physiol Lung Cell Mol Physiol. 2012;109(3):L199-207.

5. Arranz A, Doxaki C, Vergadi E, Martinez de la Torre Y, Vaporidi K, Lagoudaki ED, Ieronymaki E, Androulidaki A, Venihaki M, Margioris AN, Stathopoulos EN, Tsichlis PN, Tsatsanis C. Akt1 and Akt2 kinases differentially regulate macrophage polarization. Proc Natl Acad Sci U S A. 2012;303(24):9517-22.

6. Lee C, Mitsialis SA, Aslam M, Vitali SH, Vergadi E, Konstantinou G, Sdrimas K, Fernandez-Gonzalez A, Kourembanas S. Exosomes mediate the cytoprotective action of mesenchymal stromal cells on hypoxia-induced pulmonary hypertension. Circulation. 2012;126(22):2601-11.

7. Paraskakis E, Vergadi E, Chatzimichael A, Bouros D. Current evidence for the management of the paediatric parapneumonic effusions. Curr Med Res Opin. 2012 J;28(7):1179-92.

8. Vergadi E, Chang MS, Lee C, Liang OD, Liu X, Fernandez-Gonzalez A, Mitsialis SA, Kourembanas S. Early macrophage recruitment and alternative activation is crucial for the development of the hypoxia-induced pulmonary hypertension. Circulation. 2011;123(18):1986-95.

9. Liang OD, Mitsialis SA, Chang MS, Vergadi E, Lee C, Aslam M, Fernandez-Gonzalez A , Liu X, Baveja R, Kourembanas S. Mesenchymal Stromal Cells Expressing Heme Oxygenase-1 Reverse Pulmonary Hypertension. Stem Cells. 2011;29(1):99-107.

Selected Presentations

1. Bitsori M, Vergadi E, Perdikogianni C, Raissaki M, Galanakis E. Renal abscesses in children: A ten year experience. 7th training course. European and Mediterranean ESPID. Romania. 2014
2. Vergadi E, Vaporidi K, Doxaki C, Kondili E, Georgopoulos D, Tsatsanis C. Akt2 deficiency and alternative activation of macrophages protects from acid aspiration induced ARDS via induction of miR-146a. Intensive Care Medicine European Society, 26th Annual Congress. Paris, France. 2013
3. Vergadi E, Vaporidi K, Kondili E, Georgopoulos D, Tsatsanis C. Akt2 ablation promotes alternative activation of macrophages via induction of miR146 and protects from

acute lung injury. 2nd Inflammation & Cancer Summer School. Infla-Care (Inflammation and Cancer Research in Europe). Malia, Crete, Greece. 2012

4. Vergadi E, Helms M, Boehm S, Doxaki C, Alexaki I, Soennichsen B, Tsatsanis C. In vivo pulmonary delivery of small RNAs: Efficiency and Limitations. 2nd Inflammation & Cancer Summer School. Infla-Care (Inflammation and Cancer Research in Europe). Malia, Crete, Greece. 2012
5. Vergadi E, Arranz A, Doxaki C, Kaniaris E, Vaporidi A, Georgopoulos D, Tsatsanis C. Akt2 deficiency promotes alternative activation of macrophages via regulation of miR155 and C/EBPβ and abrogates the development of acute lung injury. 62o Hellenic Congress of Biochemistry and Molecular Biology. Athens, Greece. 2011.
6. Vergadi E. The role of alternatively activated macrophages in the pathogenesis of pulmonary hypertension. 17th Scientific Conference of Greek Medical Students. Heraklion, Greece. 2011
7. Yeny Martínez de la Torre; Eleni Vergadi; Alicia Arranz; Christina Doxaki; Andrew N Margioris; Philip N. Tsichlis; Christos Tsatsanis. Akt2 kinase is a key determinant of M2 macrophage polarization and Tumor Associated Macrophage formation. European Macrophage and Dendritic Cell Society, 25th Annual meeting. Brussels, Luxemburg. 2011
8. Vergadi E. "Macrophage accumulation and activation in hypoxic lungs is critical for the later development of hypoxia-induced pulmonary hypertension. Graduate Program in "the Molecular Basis of Human Disease". 2nd Scientific Annual Retreat. Heraklion, 2010.
9. Kourembanas S, Liang OD, Chang MS, Aslam M, Vergadi E, Mitsialis SA. Hypoxia, Lung Inflammation and Stem Cell Therapy. New York Academy of Science. Hypoxia and Consequences: From Molecule to Malady. New York, USA. 2009
10. Paraskakis E, Galanakis E, Vergadi H, Maraki S, Georgiladakis A, Kalmanti M. Risk factors for MRSA staphylococcal carriage in children with chronic allergic diseases. Eur Respir J 2006; 28: Suppl. 50, 265s.
11. Vergadi E, Giahnakis E, Vasilaki E, Spanaki AM, Michailoudi E, Fitrolaki N, Briasoulis G. Patients that required hospital treatment in regional Pediatric Intensive Care Unit in a 16-month time. 44th Pan-Hellenic Pediatric Conference, Rhodes, Greece, 2006.
12. Vergadi E, Giahnakis E. Clinical characteristics of the patients of regional Pediatric Intensive Care Unit. 12th Scientific Conference of Greek Medical Students. Larissa, Greece, 2006.
13. Vergadi E, Giahnakis E. Correlations of morbidity and outcome scores in patients of Pediatric Intensive Care Unit. 12th Scientific Conference of Greek Medical Students. Larissa, Greece, 2006.
14. Vergadi E. Inhibitors of Tyrosine Kinases. 1st Pan-Hellenic student meeting: modern proceedings in Clinical Oncology. Heraklion, Greece, 2006.
15. Vergadi E. Influenza. Clinical presentation, diagnosis and treatment. 12th Scientific Conference of Greek Medical Students. Larissa, Greece, 2006.

Awards and Honors:

2012	Award "Gardiki-Kouidou" from the Hellenic Society of Biochemistry and Molecular Biology as the most qualified PhD candidate of the year, member of the society
2011	Manassaki scholarship award to contact PhD studies (University of Crete)
2011	“Large size research projects” University of Crete Research Funding «The impact of macrophage activation state in the pathogenesis of acute lung injury» 10/2011 (14000€) To Dr Vaporidi K and phD student Eleni Vergadi
2008	Scholarship for graduate studies from the State Scholarship Foundation
2007	Scholarship for graduate studies from the graduate program “Molecular Basis of Human Disease” (University of Crete, Faculty of Medicine)
2007	First student in grading order at the graduation of the University of Crete, Faculty of Medicine (valedictorian of the graduating class, class of 102 students). Dean's List and First Rank University Graduation Honors award.
2007	Scholarship for conducting graduate studies abroad from GlaxoSmithKline pharmaceutics.
2007	“Dretaki” Award from University of Crete for ranking first in the graduation ceremony.
2007	Award from “Cretan Hestia” Foundation, for having the 2nd greater grade among Cretan graduates.
2006	First Award for best abstract: Vergadi E, Giahnakis E. Clinical characteristics of the patients of regional Pediatric Intensive Care Unit. 12th Scientific Conference of Greek Medical Students. Larissa. Greece. 2006

Member of professional societies

1. European Society of Pediatric Neonatal Intensive Care (ESPNIC)
2. European Society of Pediatric Infectious diseases (ESPID)
3. European Society of Intensive Care Medicine (ESCIM)
4. European Respiratory Society (ERS)
5. Hellenic Society of Neonatology
6. Hellenic Society of Perinatal Medicine
7. Hellenic Society of Biochemistry and Molecular Biology

"We live on an island surrounded by a sea of ignorance.
As our island of knowledge grows, so does the shore of our ignorance"

- John Archibald Wheeler

TABLE OF CONTENTS

TABLE OF CONTENTS

TABLE OF CONTENTS cont.

ABSTRACT

Περίληψη

Το σύνδρομο αναπνευστικής δυσχέρειας (ARDS) ως αποτέλεσμα μηχανικού αερισμού, πνευμονικής λοίμωξης, εισρόφησης ή προωρότητας, αποτελεί την συχνότερη αιτία νοσηρότητας και θνητότητας στις μονάδες εντατικής θεραπείας ενηλίκων, παίδων και νεογνών. Αντίστοιχα, η πνευμονική υπέρταση πρωτοπαθής ή δευτεροπαθής σε προϋπάρχουσα διαταραχή, προκαλεί εξίσου σοβαρή νοσηρότητα, υποξαιμία, αναπνευστική και καρδιακή ανεπάρκεια. Καθώς οι μοριακοί και κυτταρικοί μηχανισμοί της βλάβης του πνεύμονα και της δημιουργίας πνευμονικής υπερτάσεως δεν είναι επαρκώς χαρακτηρισμένοι, η σε βάθος κατανόηση τους είναι απαραίτητη για το σχεδιασμό θεραπευτικών προσεγγίσεων. Η ενεργοποίηση της φυσικής ανοσίας και στις δύο καταστάσεις συγκαταλέγεται ανάμεσα στους πιθανούς παθογενετικούς μηχανισμούς.

Με την χρήση μοντέλων μυών γενετικά τροποποιημένων σε γονίδια-κλειδιά για την φλεγμονή και την αγγειακή λειτουργία (Akt2 kinase deficient, lung specific inducible heme oxygenase HO-1 transgenic), στην παρούσα μελέτη διερευνούμε την φύση της φλεγμονώδους ανοσοαπάντησης και του φαινότυπου ενεργοποίησης των κυψελιδικών μακροφάγων που αναπτύσσεται πρώιμα σε ζωικά πρότυπα οξείας βλάβης πνεύμονα και πνευμονικής υπέρτασης και επιδιώκουμε να διασαφηνίσουμε τον πιθανά αιτιολογικό τους ρόλο στην ανάπτυξή τους.

Για να διασαφηνίσουμε τον ρόλο της φυσικής ανοσίας και της ενεργοποίησης των μακροφάγων στην οξεία βλάβη πνεύμονα, προκαλέσαμε άσηπτη πνευμονική βλάβη κυρίως με εισρόφηση υδροχλωρικού οξέους σε ποντικούς φυσικού τύπου (WT) και σε Akt2-/- ποντικούς. Η οξεία βλάβη πνεύμονα σε ποντικούς φυσικού τύπου οδήγησε σε μειωμένη πνευμονική ενδοτικότητα, εξοίδηση πρωτείνης και έκκριση κυτταροκινών στο βρογχοκυψελιδικό υγρό. Τα κυψελιδικά μακροφάγα απέκτησαν κλασσικό φαινότυπο ενεργοποίησης (M1). Η οξεία βλάβη πνεύμονα από υδροχλωρικό οξύ ήταν λιγότερο σοβαρή στα Akt2-/- ποντίκια συγκριτικά με τα WT ποντίκια. Τα κυψελιδικά μακροφάγα των Akt2-/- ποντικών ενέδειξαν εναλλακτικό φαινότυπο ενεργοποίησης (M2). Παρόλο όμως που η παρουσία M2 μακροφάγων σχετίστηκε με προστασία από την άσηπτη βλάβη πνεύμονα, οδήγησε σε αυξημένο μικροβιακό φορτίο στα Akt2-/- ποντίκια που μολύνθηκαν με ενδοτραχειική έγχυση Pseudomonas aeruginosa συγκριτικά με τα WT ποντίκια.

Για να κατανοήσουμε την M1 ενεργοποίηση των μακροφάγων, μελετήσαμε το σηματοδοτικό μονοπάτι του υποδοχέα TLR στα μακροφάγα. Βρήκαμε ότι τα mRNA επίπεδα των σηματοδοτικών πρωτεινών TRAF6, IRF5 και STAT1 αυξήθηκαν στα κυψελιδικά μακροφάγα WT ποντικών μετά απο έκθεση σε υδροχλωρικό οξύ. Αντίθετα, τα Akt2-/- μακροφάγα είχαν χαμηλότερα επίπεδα TRAF6, IRF5, STAT1 και IRAK1 σε σύγκριση με τα

μακροφάγα φυσικού τύπου. Τα επίπεδα mRNAs των IRAK1, TRAF6, STAT1 και IRF5 είναι γνωστό ότι ρυθμίζονται από το αντι-φλεγμονώδες miRNA miR-146a.

Πράγματι, το μικρο-RNA miR-146a, αυξήθηκε στην όψιμη φάση της πνευμονικής βλάβης στα ποντίκια φυσικού τύπου ενώ η επαγωγή του στα Akt2-/- ποντίκια παρατηρήθηκε νωρίτερα, στην οξεία φάση. Μάλιστα, η υπερέκφραση του miR-146a στα μακροφάγα φυσικού τύπου κατέστειλε την επαγωγή της επαγώμενης συνθάσης του νιτρικού οξειδίου (iNOS) από τον LPS και οδήγησε σε M2 ενεργοποίηση των μακροφάγων. Η καταστολή του miR-146a στα Akt2-/- μακροφάγα αποκατέστησε την έκφραση της iNOS. Επιπλέον, η χορήγηση εξωγενούς miR-146a ή η σίγαση του γονιδίου Akt2 σε ποντίκια φυσικού τύπου που είχαν εκτεθεί σε υδροχλωρικό οξύ οδήγησε σε καταστολή της iNOS στα κυψελιδικά μακροφάγα.

Συμπεραίνοντας, η καταστολή του Akt2 και η επαγωγή του miR-146a προάγει την εναλλακτική ενεργοποίηση των μακροφάγων και προστατεύει από την οξεία πνευμονική βλάβη. Τροποποίηση του φαινότυπου των κυψελιδικών μακροφάγων μέσω των Akt2 και miR- 146a θα μπορούσε να εφαρμοστεί θεραπευτικά σε περιπτώσεις μη – λοιμώδους ARDS. Όμως, μια τέτοια θεραπεία δεν θα ήταν ωφέλιμη σε περιπτωσεις λοιμώδους ARDS καθώς επηρεάζει την μικροβιοκτόνο δράση των μακροφάγων.

Η πνευμονική αρτηριακή υπέρταση είναι μια σπάνια νόσος που χαρακτηρίζεται από αγγειοσυστολή και πάχυνση του αγγειακού τοιχώματος με τελικό αποτέλεσμα υπερτροφία και ανεπάρκεια της δεξιάς κοιλίας. Παρά την σημαντική πρόοδο σε αυτό το ερευνητικό πεδίο, οι μηχανισμοί που οδηγούν στην ανάπτυξη της νόσου παραμένουν ασαφείς. Η φλεγμονή του πνευμονικού παρεγχύματος όλο και περισσότερο και εμπλέκεται στην ανάπτυξη πνευμονικής υπερτάσεως.

Η ιστική υποξία, ένα ευρέως γνωστό ερέθισμα που προκαλεί πνευμονική υπέρταση, προάγει μια φλεγμονώδη ανοσοαπάντηση στον πνεύμονα που προηγείται χρονικά της ανάπτυξης της υπερτάσεως. Η ιστοειδική, στους πνεύμονες, συστασιακή έκφραση της οξυγενάσης της αίμης (heme oxygenase-1, HO-1) μπορεί να καταστείλει τόσο την φλεγμονώδη απάντηση αλλά και μετέπειτα ανάπτυξη της νόσου. Στην παρούσα μελέτη, χρησιμοποιήσαμε ένα διαγονιδιακό μοντέλο ποντικού που υπερεκφράζει HO-1 στα επιθηλιακά κύτταρα του πνεύμονα υπό τον έλεγχο της δοξυκυκλίνης με επαγόμενο τρόπο (tetON σύστημα). Ελέγχοντας έτσι την δράση της HO-1 και κατ' επέκταση της πνευμονικής φλεγμονής, στόχος μας ήταν να διασαφηνίσουμε την φύση της φλεγμονώδους ανοσοαπάντησης στην υποξία και τον ρόλο της στην ανάπτυξη της πνευμονικής υπέρτασης.

Η έκθεση των ποντικών στην υποξία σύντομα οδήγησε στην συγκέντρωση μονοκυττάρων/μακροφάγων και στην παραγωγή κυτοκινών/ κυτταροκινών στο βρογχοκυψελιδικό έκπλυμα. Η υπερέκφραση της HO-1 κατέστειλε αυτην την φλεγμονώδη απάντηση. Τα κυψελιδικά μακροφάγα των υποξικών ποντικών εκδήλωσαν *in vivo*

φαινότυπο ενεργοποίησης τυπικό της εναλλακτικής οδού, με έκφραση των δεικτών Fizz1, Ym1 και arginase-1 ενώ απέτυχαν να εκφράσουν δείκτες κλασσικής ενεργοποίησης όπως την επαγόμενη συνθάση του νιτρικού οξειδίου (iNOS), παράγοντα νέκρωσης των όγκων (TNF-a) και ιντερλευκίνη-12 (IL-12p40).

Για να επισημάνουμε το ρόλο της παραπάνω φλεγμονώδους απάντησης στην παθογένεση της νόσου, διακόψαμε την συνεχή χορήγηση δοξυκυκλίνης στα ζώα ώστε να επανέλθουν τα επίπεδα της HO στα φυσιολογικά. Η βραχεία – για 2 ημέρες – χορήγηση δοξυκυκλίνης (και επομένως βραχεία επαγωγή της HO-1) καθυστέρησε αλλά δεν κατέστελε την μέγιστη αύξηση των μονοκυττάρων/μακροφάγων και την ενεργοποίηση της εναλλακτικής οδού, 7 ημέρες μετά τα οποία επακολούθησε πνευμονική υπέρταση. Όμως, παρατεταμένη χορήγηση – για 7 ημέρες - δοξυκυκλίνης (και επομένως συνεχή επαγωγή της HO-1) κατέστη επαρκής να αναστείλει τόσο την συγκέντρωση μονοκυττάρων/μακροφάγων και την εναλλακτική ενεργοποίηση των μακρόφάγων, να προκαλέσει υπερέκκριση IL-10 από τα μακροφάγα και να αναχαιτήσει την μετέπειτα εμφάνιση πνευμονικής υπέρτασης. Επιπλέον, το υπερκείμενο από τα υποξικά M2 μακροφάγα προήγαγε τον πολλαπλασιασμό και των λείων μυικών κυττάρων της πνευμονικής αρτηρίας ενώ η θεραπεία με μονοξείδιο του άνθρακα, κύριο ενζυματικό προϊόν της HO-1, κατέστειλε αυτό το φαινόμενο. Η πνευμονική διήθηση μακροφάγων και η εναλλακτική ενεργοποίησή τους στην υποξία είναι κρίσιμο φαινόμενο για την μετέπειτα ανάπτυξη πνευμονικής υπέρτασης. Η οξυγενάση της αίμης δρα προστατευτικά εν μέρει μέσω της τροποποίησης του φαινοτύπου ενεργοποίησης των μακροφάγων.

Τα ευρήματα της παρούσας μελέτης δύναται να βοηθήσουν στον σχεδιασμό στοχευμένων θεραπειών που πιθανά να βελτιώσουν την πρόγνωση που παραμένει πενιχρή.

Abstract

The acute respiratory distress syndrome (ARDS), due to mechanical ventilation, lung infection, aspiration, sepsis or prematurity, is the major cause of morbidity and mortality in Intensive Care Units of adults, children and neonates. Pulmonary hypertension, primary or secondary to existing condition, promotes similarly severe morbidity that may also lead to respiratory and cardiac failure. Limited therapies are effective nowadays in the management of both conditions. Since the molecular and cellular mechanisms of acute lung injury (the pathologic picture of ARDS) and pulmonary hypertension have not been clearly elucidated, their understanding is crucial to develop targeted and effective therapies. Lung inflammation and specifically innate immunity and macrophage accumulation appears to be a common denominator that contributes to pathology in both diseases.

By utilizing wild-type (WT) mice and mice genetically modified in key – genes for inflammation and vascular function (Akt2 knock-out, lung specific inducible HO-1 transgenic), in the current study we investigate the nature of inflammatory response and the phenotype of macrophage activation in animal models of acute lung injury and pulmonary hypertension and we aim to elucidate its potential causative role in the pathogenesis of disease.

To investigate the role of macrophage activation in aseptic lung injury and identify molecular mediators with therapeutic potential, lung injury was induced in WT and Akt2-/- mice by hydrochloric acid aspiration. Acid-induced lung injury in WT mice was characterized by decreased lung compliance and increased protein and cytokine concentration in bronchoalveolar lavage fluid. Alveolar macrophages acquired a classical activation (M1) phenotype. Acid-induced lung injury was less severe in Akt2-/- mice compared with WT mice. Alveolar macrophages from acid-injured Akt2-/- mice demonstrated the alternative activation phenotype (M2). Although M2 polarization suppressed aseptic lung injury, it resulted in increased lung bacterial load when Akt2-/- mice were infected with Pseudomonas aeruginosa.

To understand macrophage activation in our model and the role of Akt2, we studied the TLR pathway. We found that mRNA levels of TRAF6, IRF5, STAT1 but not IRAK1 were increased in alveolar macrophages in WT mice exposed to acid. On the other hand, macrophages from Akt2-/- mice exposed to acid had lower levels of TRAF6, IRF5, STAT1 and IRAK1 compared to WT mice. The mRNA levels of IRAK1, TRAF6, STAT1 and IRF5 are known to be targeted by the anti-inflammatory microRNA miR-146a.

Indeed, miR-146a was found to be induced during the late phase of lung injury in WT mice, whereas it was increased early in Akt2-/- mice. MiR-146a overexpression in WT macrophages suppressed LPS induced inducible NO synthase (iNOS) and promoted M2 polarization, whereas miR-146a inhibition in Akt2-/- macrophages restored iNOS expression.

Furthermore, miR-146a delivery or Akt2 silencing in WT mice exposed to acid resulted in suppression of iNOS in alveolar macrophages. In conclusion, Akt2 suppression and miR-146a induction promote the M2 macrophage phenotype, resulting in amelioration of acid-induced lung injury. *In vivo* modulation of macrophage phenotype through Akt2 or miR-146a could provide a potential therapeutic approach for aseptic ARDS; however, it may be deleterious in septic ARDS because of impaired bacterial clearance.

Pulmonary hypertension is a rare disease that is characterized by vasoconstriction, thickening and remodeling of vascular wall and finally leads to right heart hypertrophy and failure. Despite the significant progress in the field the molecular mechanisms that lead to disease remain unclear. Lung inflammation has been found to precede the development of hypoxia induced pulmonary hypertension (HPH); however, its role in the pathogenesis of HPH is poorly understood. We sought to characterize the hypoxic inflammatory response and to elucidate its role in the development of HPH. We also aimed to investigate the mechanisms by which heme oxygenase-1 (HO-1), an anti-inflammatory enzyme, is protective in HPH.

We generated bitransgenic mice that overexpress human heme oxygenase-1 under doxycycline control in an inducible, lung-specific manner. Hypoxic exposure of mice in the absence of doxycycline resulted in early transient accumulation of monocytes/macrophages in the bronchoalveolar lavage. Alveolar macrophages acquired an alternatively activated phenotype (M2) in response to hypoxia, characterized by the expression of found in inflammatory zone-1 (Fizz1), arginase-1, and chitinase-3-like-3 (CHI3L3 or Ym1). A brief 2-day pulse of doxycycline (and therefore transient HO-1 induction) delayed, but did not prevent, the peak of hypoxic inflammation, and could not protect against HPH. In contrast, a 7-day doxycycline treatment sustained high heme oxygenase-1 levels during the entire period of hypoxic inflammation, inhibited macrophage accumulation and activation, induced macrophage interleukin-10 expression and prevented the development of HPH. Supernatants from hypoxic M2 macrophages promoted the proliferation of pulmonary artery smooth muscle cells, whereas treatment with carbon monoxide, a heme oxygenase-1 enzymatic product, abrogated this effect. Early recruitment and alternative activation of macrophages in hypoxic lungs are critical for the later development of HPH. Heme oxygenase-1 may confer protection from HPH by effectively modifying the macrophage activation state in hypoxia.

The findings of the current study can potentially lead to the development of targeted therapies that may improve prognosis and morbidity that remain too dismal.

INTRODUCTION

Normal Lung Structure and Physiology

Structural Elements of the Lung

In air-breathing animals, the respiratory system is the vital system of the body that carries out a critical function, the exchange of gases, oxygen and carbon dioxide, between inspired air and blood. In order to perform this vital function the lungs have a large surface area where the internal environment is exposed to external air.

The respiratory system can be subdivided in an upper and a lower respiratory tract, the first being considered the conductive part, while the latter can be referred to as the respiratory part where the actual gas exchange takes place (1-5). The lung airways arise from the trachea and the main bronchi and they systematically branch over an average of 23 generations of dichotomous branching to progressively to smaller airways, the bronchioles (1). Further branching of bronchioles leads to the terminal bronchioles, which are less than 2 cm in diameter. The part of the lung parenchyma that is distal to terminal bronchioles is composed by respiratory bronchioles and alveoli and forms a terminal respiratory unit, the site where oxygen diffuses from inspired air to the blood, and through the same way, the metabolic byproducts, carbon dioxide (CO_2) and CO, pass for elimination in the exhaled air (Figure 1) (1, 3-5). The adult lung contains anatomic channels that permit ventilation distal to an area of obstruction (Figure 2); the inter-alveolar pores of Kohn and the bronchoalveolar Lambert's channels (2). Next to the branching airways the pulmonary and bronchial arteries offer a double arterial supply that leads to the capillary endothelium in the terminal respiratory units (1). Lymphatic vessels clear the parenchyma from extra fluid.

A thin basement membrane with or without surrounding interstitial tissue separates the endothelial cells from the alveolar lining epithelial cells (Figure 2) (1, 4). At the thick parts of the air-blood barrier where epithelial and endothelial basement membranes are separated, there are elastic fibers and bundles of collagen as well as interstitial cells, mainly fibroblasts eosinophils and rarely lymphocytes and monocytes (1, 3, 4). The connective tissue fibrils (collagen, elastin) around the alveolar walls and the peribronchiolar space form a three-dimensional basket-like structure that allows the lung to expand in all directions without developing excessive tissue recoil (6).

Looking at the tissue organization of the lung, the airways and the blood vessels extend all the way out to the gas-exchange region, but they show different properties and different structural components in conducting as compared with respiratory structures (Figure 3) (3). The principal cell types of the lung include epithelial cells of the airway, bronchi, and alveoli; bronchiolar Clara cells, mucus-producing goblet cells, interstitial cells of the airway and fibroblasts, endothelial cells of the pulmonary vasculature; smooth muscle cells of pulmonary vasculature; and alveolar macrophages.

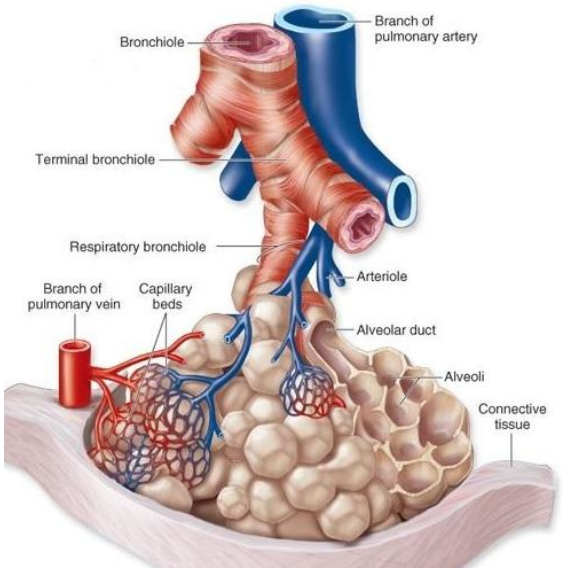

Figure 1. Terminal bronchioles, respiratory bronchioles, and alveoli. Terminal bronchioles branch into respiratory bronchioles, which then branch further into alveolar ducts and individual alveoli. The figure shows the branching relationship, as well as the pulmonary blood vessels that travel with the bronchioles and the dense layer of branching capillaries that surrounds each alveolus for gas exchange between blood and air. *Source: Mercher AL. Junqueira's Basic Histology. Text and Atlas. 12th Edition. Copyright: the McGraw-Hill companies*

The alveolar epithelium consists of two types of cells, the flattened type I pneumocytes that cover the 95% of the alveolar surface and offer mainly mechanical support and the cuboeidal rounded type II pneumocytes the main source of pulmonary surfactant (4, 5, 7). Type II pneumocytes retain proliferation capacity and together with Clara cells in the bronchioles are important in the regeneration of alveolar epithelium after type I cell injury (Figure 3) (4, 5, 7)**.** Alveolar macrophages are the scavenger cells loosely attached to the epithelial cells or lie free in the alveolar space where they travel around the alveolar wall phagocytosing foreign particles and bacteria (Figure 3). Smooth muscle cells form circular bands around the airway epithelium and respiratory bronchioles (Figure 1) (3, 6).

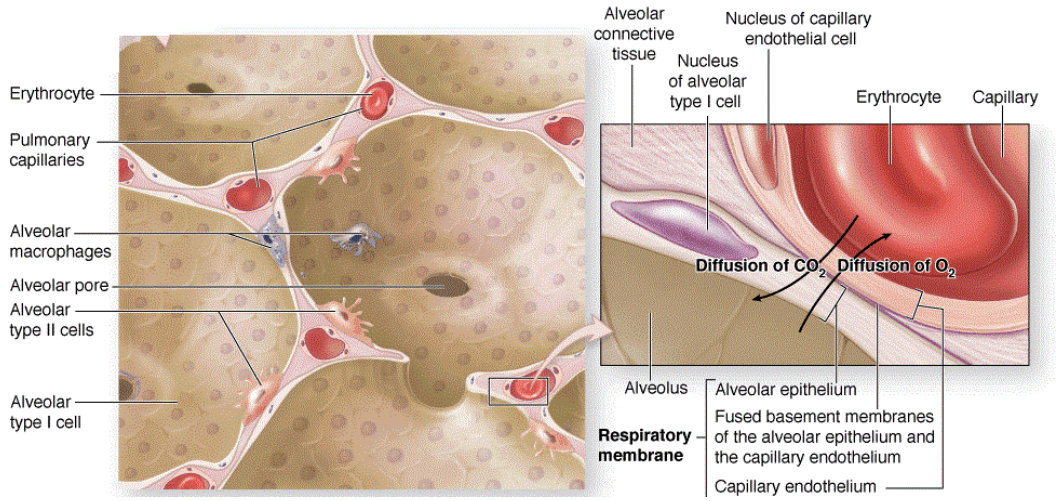

Figure 2. Detailed anatomy of the alveolar spaces and the respiratory membrane. Structural components of an alveolus such as type I and type II alveolar cells and the relationship between capillaries and sac like alveoli and are depicted. In the left, closer view of the air-blood barrier that consists of an alveolar type I cell, a capillary endothelial cell, and their fused basement membranes. Source: Mercher AL. Junqueira's Basic Histology. Text and Atlas. 12th Edition. Copyright: the McGraw-Hill companies.

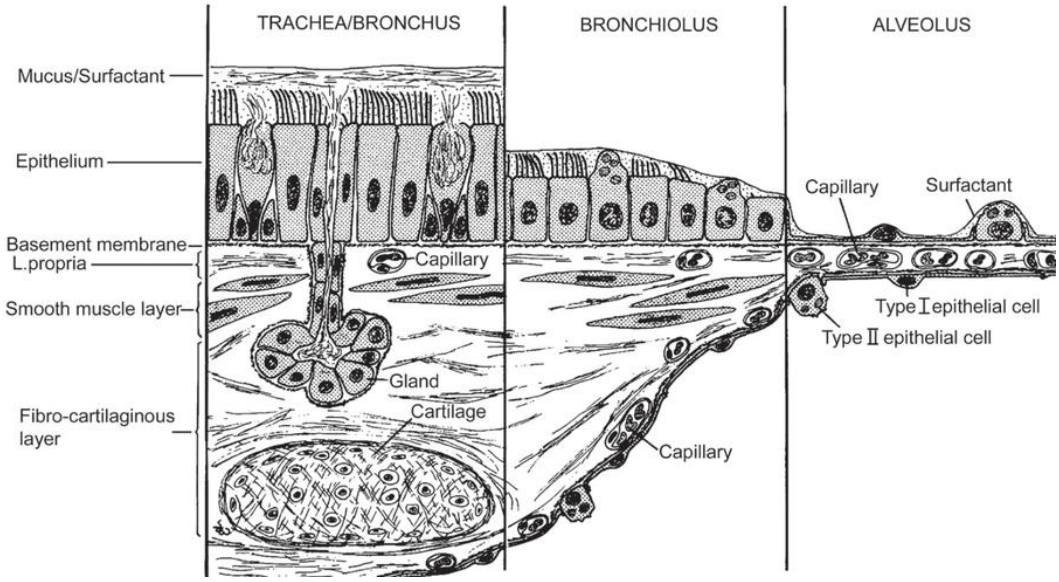

Figure 3. Airway wall structure at the three principal levels. The epithelial layer gradually becomes reduced from pseudostratified to cuboidal and then to squamous. The smooth muscle layer disappears in the alveoli. The fibrous layer contains cartilage only in bronchi and gradually becomes thinner as the alveolus is approached. Source: Weibel ER: The Pathway for Oxygen. Cambridge: Harvard University Press, 1984.

Physical properties of the Lung

Physiology of respiration and alveolar ventilation

The flow of air in the lungs is a complex procedure. The respiration center is located in medulla oblongata and is controlled by the peripheral and central chemoreceptors for pH and pO_2. The respiratory center stimulates the neurons that are located in the anterior horns of spinal cord (A3-A5) via the phrenic nerve and regulates the functions of the respiratory muscles (1, 4). During inspiration, the respiratory center signals the contraction of diaphragm and inspiratory intercostal muscles that lead to increase in lung volume and consequent fall in transthoracic pressure. The contraction of respiratory muscle produces pressure (P_{muscle}) that drives the flow of air in the lungs. The flow of air ceases when there is no pressure difference among alveolar spaces and atmospheric air (1, 4).

Alveolar ventilation is defined as

$$VA = f \times (VT - VD)$$

VT is tidal volume, VD is dead space volume, and f is the respiratory frequency

The partial pressure of oxygen in the alveolus (PAO_2) is determined by the classic alveolar gas equation:

$$PAO_2 = FiO_2 \times (P_{atm} - P_{H2O}) - PaCO_2/RQ$$

The latter equation yields a PAO_2 of 100 to 120 mm Hg in room air at sea level. The difference between the partial pressure of oxygen in the alveolus (PAO_2) and that in the pulmonary capillary (PaO2), approximately 10 mm Hg under normal conditions, is caused by the diffusion barrier of alveolar–capillary membrane and the overall ventilation–perfusion (V/Q) ratio of the lung (2, 3). While the former is easily overcome by increasing inspired oxygen concentration and rarely is a cause for clinically significant hypoxemia, the same cannot be said for the latter (2). The principal etiology for clinically significant hypoxemia is pulmonary pathology associated with decreased lung volumes, reduced lung compliance, and an increased proportion of low V/Q compartments of the lung (2, 3).

Alterations in VT and/or f, which are the components of minute alveolar ventilation (VE), will result in changes in $PaCO_2$ (hypocapnia, hypercapnia).

Lung volumes and capacities

Volumes and capacities of the lungs are affected by several factors, specifically muscle strength, the static–elastic characteristics of the chest wall and lungs, and patient age. They are estimated based on the traditional spirometric technique (2). Understanding of static lung volumes is critical to evaluating and subsequently treating patients with respiratory disease.

Tidal volume is defined as the amount of gas moved during normal breathing, and residual volume is defined as the amount of gas that remains in the lung after a maximal expiration (2, 5). Total lung capacity is defined as the volume of gas in the lungs after a maximal inspiration (5). Functional residual capacity (FRC) is the volume or air that remains in the lung at the end of a tidal breath. This gas serves as a reservoir of oxygen during expiration. Functional residual capacity is determined by the static balance between the outward recoil of the chest wall and the inward recoil of the lung (2, 5).

Elastance and Compliance

Respiratory system as a whole consists of the lung and the thoracic wall, two structures that have the ability to expand and they are connected to each other via the pleura (5). The lung is an elastic structure and tends to passively recoil and return in their previous volume after inspiration (2). However, the presence of the chest wall, which, in contrast to the lung, pulls outward at low volumes and inward at high volumes, retards this tendency (2, 3).

If we consider the lung and the chest wall to operate in series, the elastic recoil pressure of the total respiratory system (Prs) can be calculated as the sum of the pressures exerted by the elastic recoil of the lung (transpulmonary pressure) and the elastic recoil of the chest wall (2, 3). Since the elastic recoil of the lung is determined (under static conditions of zero airflow) as the difference between alveolar pressure (Palv) and pleural pressure (Ppl) (Pa – Ppl) and the elastic recoil of the chest wall is determined (while the respiratory muscles are completely at rest) as the difference between pleural pressure and the pressure at the external surface of the chest (Pbs, atmospheric pressure) (Ppl – Pbs), the elastic recoil of the entire respiratory system can be expressed as the sum of the two:

$$Prs = (Pa - Ppl) + (Ppl - Pbs) = Pa - Pbs$$

The change in transpulmonary pressure required to cause a given change in the volume of air in the lungs is a measure of the distensibility, or compliance, of the lungs (2). Pulmonary compliance is calculated as shown:

$$C_{(L/cmH2O)} = \Delta V / \Delta P$$

C = lung compliance, ΔP = transpulmonary pressure, ΔV = change in lung volume

Lung elasticity, conversely, is the resistance to lung expansion (elastance) that describes the stiffness or the tendency to resist to distortion and to return to the original configuration when the distorting force is removed (3, 6). Elastance is calculated as follows:

$$E_{(cmH2O/L)} = \Delta P/\Delta V \text{ and } \Delta P = \Delta V.E \text{ or } E = 1/C$$

Lung compliance is not a constant value but it is dependent to lung volume. As lung volume increases, the elastic elements approach their limits of distensibility, and a given change in transpulmonary pressure produces smaller and smaller increases in lung volume (4, 5, 8). Thus, the compliance of the lung is least at high lung volumes and greatest as the residual volume is approached.

In practice, pulmonary compliance is determined by the slopes of a curve relating the changes in transpulmonary pressures to the changes in lung volume in the course of an expiration after a maximal inspiration, the pressure - volume curve of the respiratory system (Figure 4) (8). The pressure-volume characteristics of the lung are nonlinear but sigmoidal with upward concavity at low inflation pressure and downward concavity at higher inflation pressure (Figure 4) (8).

The acquisition of pressure volume culve requires static conditions and the measurement of transthoracic wall pressure (Palv-Pbs) in different lung volumes. Factors

affecting compliance are sex and age of the patient, posture, consolidation, atelectasis, lung edema, fibrosis (2).

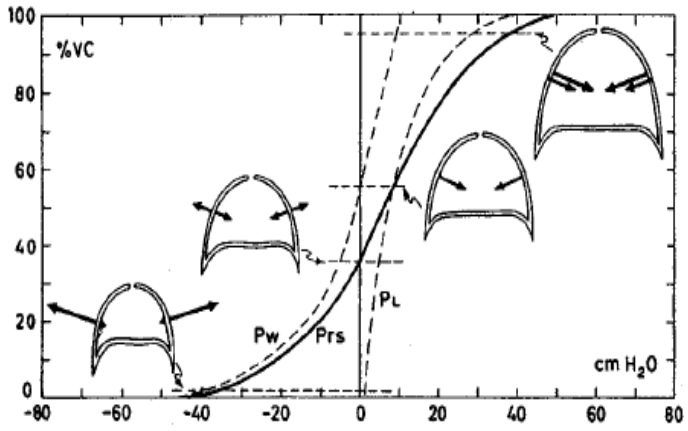

Figure 4. The normal pressure-volume curve (P-V curve). The P-V curve of the respiratory system is the sum of the pressures generated by the chest wall (PW) and lungs (PL) (dotted lines). Functional residual capacity (FRC) occurs where the sum of the 2 pressures are equal and opposite. %VC: percent of vital capacity. Adapted from Agostoni E, Hyatt RE. Static behavior of the respiratory system. In: Geiger SR Handbook of physiology, 2nd edition.

Alveolar Surface Tension

Surface tension is the force that acts across the surface of a liquid, as the attractive forces between liquid molecules are stronger than the forces between liquid and gas molecules (2). The interior surfaces of the alveoli are lined by a thin liquid layer of osmotic fluid. The surface tension at the air-liquid interface of the alveoli, in addition to the elastic properties of the parenchyma, contributes importantly to the elastic recoil of the lungs and acts to decrease lung compliance (2).

By considering the alveolus to be a sphere, we can apply Laplace's law. Laplace's law states that the pressure inside a spherical structure—e.g., the alveolus—is directly proportional to the tension in the wall and inversely proportional to the radius of curvature:

$$\text{Alveolar pressure} = 4T / r$$

T = tension (dyn/cm) r = radius

When the water comes in contact with air, among the water molecules more tension is produced. This results in decrease of water surface and a tendency to collapse the alveolar surface and to expel the air from the alveoli (2). The surface tension of each alveolus is inversely related to the radius of the alveoli. That's why the neonatal alveoli have higher surface tension that the adults lungs and are prone to collapse (2). The surface tension

remains constant as lung volume changes, and the recoil pressure of small airspaces exceeds that of larger ones. As a result, small alveoli tend to empty into larger ones (Figure 5).

To minimize this phenomenon, type II pneumocytes produce surfactant, a mixture of phospholipids proteins and anions that reduce the surface tension of the alveolar fluid (2, 4, 5). The presence of surfactant in the lungs is crucial for the avoidance of this phenomenon since it can reduce surface tension of the alveolar fluid at 5-30dynes/cm. Without the presence of surfactant, the alveolar fluid has a tension of 72dynes/cm that leads to alveolar collapse (4, 5).

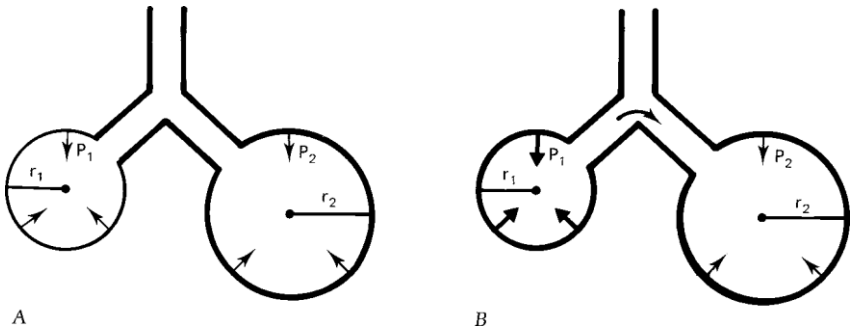

Figure 5. The effects of surfactant in maintaining alveolar stability. Model of the distal lung in which individual alveoli are controlled by Laplace's law. A. Surfactant lowers the tension (T) of the alveolar walls at low lung volumes. Consequently, the transpulmonary pressure (P) of large and small communicating airspaces is the same. r1 < r2, T1 < T2, P1← P2. B . Without surfactant, the surface tension remains constant as lung volume changes, and the recoil pressure of small airspaces exceeds that of larger ones. As a result, small alveoli tend to empty into larger ones. r1 < r2, T1 = T2, P1 > P2. Adapted from Fishman, et al. Fishman's pulmonary diseases and disorders. 2008.

Airway Resistance

In order for air to move in and out of the lungs, gas must flow from an area of higher pressure to one of lower pressure. According to Ohm's law, the pressure gradient that faces a substance (gas or liquid) is equal to the product of the flow rate times the resistance to flow (pressure gradient [P] = flow rate [V] x resistance [R]) (2). Lung Resistance is the ability of the lung airways to resist to the movement of air along its airway tree due to friction power. The movement of air can be expressed by flow of air (V', L/sec) and is driven by the pressure gradient among alveolar space and atmosphere. The pressure gradient is necessary to overcome the airway resistance (4, 5).

$$R = \Delta P/V' \text{ και } \Delta P = R \cdot V'$$

Resistance to air flow is related to the length of the airway and inversely related to the 4^{th} power of the radius of the airway according to Poiseuille's law (4, 5).

$$R = \mu L 8/\pi r^4$$

A large fraction of the resistance to airflow is in the upper respiratory tract, including the nose, mouth, pharynx, larynx, and trachea. Most of the remainder of airway resistance is in medium-sized lobar, segmental, and subsegmental bronchi up to about the seventh generation of airways (3). The small peripheral airways, particularly those less than 2 mm in diameter, constitute only about 10 to 20 percent of the total airway resistance (3).

The pressure surrounding intrathoracic airways approximates pleural pressure. As the lung volume increases, the elastic recoil forces of the lung increase; the traction applied to the walls of the intrathoracic airways also increases, widening the airways and decreasing their resistance to airflow. Conversely, at low lung volumes, the transmural airway pressure is lower and airway resistance increases (3).

Pulmonary circulation

Anatomically, the pulmonary blood vessels can be divided into two groups; vessels lying in the loose connective tissue and "alveolar" blood vessels within the alveolar walls (2). The latter are subject to whatever forces operate at the alveolar level (2). Depending on the gravity, pulmonary blood flow is different in the upper areas of the lung compared to the lower lung zones, and the radius of these arteries may differ in different lung zones.

Following the initial fall after birth, pulmonary arterial pressures remain fairly constant in the disease-free state throughout life, with systolic, diastolic, and mean pressures of 25, 8, and 15 mm Hg, respectively (2, 4, 5). Pulmonary venous pressure is routinely just higher than the left atrial pressure, near 5 mm Hg. The wall of the vessels of the pulmonary circulation is approximately five times thinner and larger in diameter than the systemic circulation. The smooth-muscle fibers encircle the vessel lumen; they can modify the vessel's diameter and can thus regulate blood flow (2). The arterioles that have a diameter of 100 μm contribute significant to arterial resistance since they contain a single muscle layer in their medial wall (2, 4, 5). The arterial bed continues out to the precapillaries, which consist of vessels 20 to 40 μm in diameter that are enwrapped by an incomplete smooth muscle sheath and to capillaries are lined by continuous large, flat cells endothelial cells (3).

The pressure of pulmonary arteries is affected by factors such as the volume of air or fluid in the alveoli, the lung volumes, the recruitment of capillaries with low or no blood flow, increases in pulmonary venous pressure and hypoxic stimuli (that causes local vasoconstriction) (2). Also, neurogenic stimuli, vasoactive compounds, and chemical mediators have been demonstrated to alter pulmonary vascular resistance (2). Vascular endothelial cells are capable of producing a variety of vasoactive substances that participate in the regulation of normal vascular tone (9). These substances, such as NO, endothelin-1, Fizz1, and prostacyclin are capable of producing vascular relaxation and/or constriction inducing and/or inhibiting smooth muscle cell migration and replication (10).

The immune system of the Lung

Together with oxygen, antigenic material present in atmospheric air, containing microorganisms, dust and other particles, also enters the lungs in inspiration. These incoming antigens make contact with the respiratory epithelium from the nasal cavity to the most distal part, the alveolus. Considering the large surface area and the volume of air inspired on a daily base, the low prevalence of inflammation under normal conditions is remarkable (2, 11, 12). Thus, to maintain normal lung function, the respiratory system is equipped with an efficient immune system. This system comprises immunocompetent cells of innate and adaptive immunity in the respiratory epithelium and alveolar space.

Innate immunity is an evolutionarily ancient and universal system that is directed by cells with capacity to recognize pathogen patterns and eliminate infection, thus provides the first line of host defense (13). Such cells are macrophages, neutrophils, eosinophils, basophils and NK cells, or non – professionally immune cells such as epithelial cells. The innate immunity has no memory compared to adaptive or acquired immunity which is characterized by antigenic specificity, diversity, memory, and self/non-self recognition and is mediated mainly via B and T lymphocytes (13).

The pulmonary host defenses start in the level of conducting airways and consist primarily by anatomic barriers (such as larynx, mucosal layer, cilia, cough reflex) and physiologic barriers such chemical mediators (i.e. lysozyme), local immunoglobulin production and iron-containing proteins (transferrin, lactoferrin) (13). The lung epithelium contributes to host defense in a number of ways, including ciliary beat activity and mucus production, but also production of chemokines, cytokines, antimicrobial peptides, proteinase inhibitors and surfactant proteins (11). The cells of the immune system that reside in the airways are mainly B plasma cells located in the seromucous glands of bronchi where they produce antibodies into the mucous blanket. Also, antigen presenting dendritic cells (DCs) are located in the bronchi and upon activation they migrate to lymph nodes to further activate antigen-specific T cells; thus, providing a link between innate and adaptive immunity (14, 15). DCs are most numerous in large airway epithelium and decrease in quantity as the airways become smaller (3). Also, localized subepithelial collection of lymphocytes forming the Bronchus Associated Lymphoid Tissue (BALT) form a secondary lymphoid tissue analogous to other types of mucosa-associated lymphoid tissue (15). This structure is uncommon or absent in adult humans; are only transiently expressed during childhood in humans and may appear and proliferate in response to infection or chronic inflammation. BALT is also present in normal rodent airway (3).

The above defenses in the airways eliminate the majority of inhaled particles and microbes into the lungs and thus alveoli are usually sterile in normal subjects (3). However, some small-size particles and some pathogenic microorganisms can reach the air-exchange

surface of the alveoli. When this occurs another set of host defense mechanisms in the alveolar level must take over. The first defense line resides at the alveolar space and consists mostly of alveolar macrophages (90% of cells retrieved by bronchoalveolar lavage studies), lymphocytes (7-10%), mainly T cells and to a lesser extent B cells (IgG- and IgA-secreting) as well as lung dendritic cells (3, 14). Also, humoral factors such as the lipoproteins, antimicrobial peptides (e.g., lysozyme, lactoferrin, defensins), opsonins, immunoglobulins, surfactant proteins and complement factors are secreted in the alveolar space. Granulocytes (neutrophils, eosinophils, and basophils) are present in the human lung, but they are also very rare (3).

Just beneath the alveolar epithelium, the second defense line, in the interstitial space is represented by the interstitial macrophages. These macrophages are in close proximity with lung lymphatic system and they are constantly being replenished by blood monocytes migrating into the interstitial space (3, 15, 16). In this second defense levels, other cells than interstitial macrophages play a role in lung defense such as interstitial lymphocytes mostly T cells and to a less extend B cells and NK cells. Most if not all NK activity in the lung has been localized to the interstitial compartment. Memory T cells can also found here.

The third defense line is constituted by the lymph nodes that protects the blood and hence the entire organism from dissemination of indigestible foreign matter and also, in most instances, of infective agents (3). Moreover, activation of adaptive immunity by migrating macrophages DCs takes place in the lymph nodes. Depending on the type and dose of antigen, the DC subset, and the regional cytokine microenvironment, different effector T cells can be generated; T helper 1 (Th1), Th2 or Th17 responses or regulatory T cells (Treg) responses that prevent inflammation (15).

Lung innate immunity

As mentioned above, the normal lung contains multiple populations of innate immune cells with the great majority of them to be macrophages and dendritic cells while mast cells, basophils, neutrophils and monocytes are also present but their numbers are relatively low (15). Lung macrophages consist of two distinct populations, alveolar macrophages that represent long lived tissue-resident macrophages, and short-lived monocyte derived interstitial macrophages (15). Alveolar macrophages play an important role in maintaining lung homeostasis by removing pathogens and noxious particles. The role of alveolar macrophage in lung normal state and in disease is discussed in detail in the following section.

Dendritic cells (DCs) are leukocytes specialized in the uptake, processing, and presentation of antigen in cells of adaptive immunity and thus are fundamental in regulating both innate and adaptive immune functions. They are mainly localized at the interface

between body surfaces and the environment. In the absence of inflammation, lung conventional DCs (cDCs) can be subdivided into three distinct subsets based on the expression of a combination of specific cell surface markers and on their distinct ontogeny: the myeloid DC (mDC) or monocyte-derived CD11b$^+$ DCs, plasmacytoid DCs, and CD103$^+$ DCs, which originate from distinct precursors and play a crucial role in the induction and suppression of innate immune responses (15-17). The CD103$^+$ DCs form a highly developed network in the epithelial layer of the conducting airways and this particular subset of DCs displays long cellular protrusions in between the basolateral space made up by basal epithelial cells (18, 19). Monocyte-derived DCs (moDCs) and plasmacytoid dendritic cells (pDCs) have been described to populate the lungs upon inflammation (18, 19). The different subsets of dendritic cells in the lung are illustrated in Figure 6.

Mast cells reside in human airways and they also play an important role in the lung in both health and disease (20). Their primary role is to initiate inflammation and repair in response to tissue damage initiated by a variety of diverse stimuli (20).

Neutrophils are short-lived cells (average life span is about 24 to 48 hours) equipped with numerous antimicrobial effector mechanisms. Unlike resident macrophages, mast cells and dendritic cells, neutrophils do not reside in the lungs prior to infection but they are recruited from the circulation upon inflammation (21). Recruited neutrophils accumulate at the site of infection and phagocytose and kill pathogens using several microbicidal mechanisms (21). They also produce reactive oxygen and nitrogen intermediates and they release a number of antimicrobial proteins and peptides that are stored in neutrophil granules (21).

Antibody-based recognition of cell-surface markers has been widely used for the identification of myeloid immune cells in the lung (22). In figures 6 and 7 the types of myeloid cells in mouse lung and their main expression markers are depicted (22). Alveolar

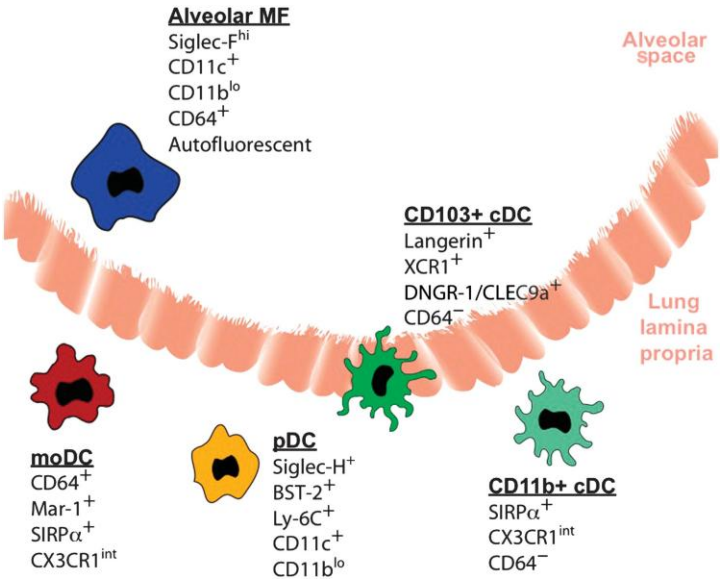

Figure 6. Lung dendritic cell and macrophage phenotype. cDC, conventional dendritic cell; DC, dendritic cell; MF, macrophage; moDC, monocyte-derived DC; pDC, plasmacytoid DC. Adapted from Guilliam et al, Mucos Immunol, 2013.

macrophages differ from other macrophages since they do not express CD11b, a classic macrophage marker, and they express high levels of CD11c, a dendritic cell marker and Siglec F, which is typically considered an eosinophil marker (18, 22).

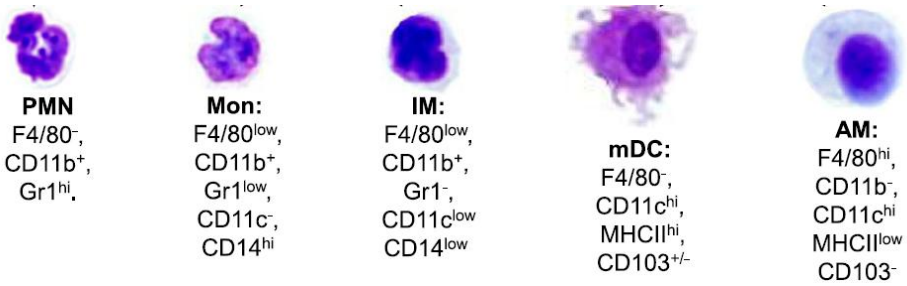

Figure 7. Myeloid cell subsets in murine lungs. AM, alveolar macrophages; IM, interstitial macrophages; mDC, myeloid dendritic cells; Mon,monocytes; PMNs, polymorphonuclear cells. Adapted from Zaynagerdinovet al, Cell Mol Biol, 2013

Mouse models are widely used for lung immune system studies however, we must have in mind that there are significant differences between mice and humans in immune system development, activation, and response to challenge, in both the innate and adaptive arm. One difference worth noting is that whereas mice have significant bronchus associated lymphoid tissue, this is largely absent in healthy humans, possibly reflecting a higher breathable antigen load for animals living so much closer to the ground (23). Also, several antimicrobial peptides such as defensins are not produced in mice (23). Furthermore, there are significant differences between human and murine lung dendritic cells and macrophages in their function, expression markers and secreted factors (24). The main differences between human and murine alveolar macrophages are analyzed in the following sections.

Molecular control of innate immunity

The network of cells discussed above, especially dendritic cells (DCs) and macrophages, are well equipped with various pathogen-associated molecular pattern recognition receptors (PRRs) or damage associated molecular pattern receptors to recognize these wide variety of microbes, dusts, and pollutants. PRRs recognize relatively invariant highly conserved molecular patterns expressed by microorganisms, the pathogen-associated molecular patterns (PAMPs) and endogenous danger signals, damage-associated molecular patterns (DAMPs) (25). The best-known examples of PAMPs include lipopolysaccharide (LPS) of gram-negative bacteria; lipoteichoic acids of gram-positive bacteria; peptidoglycan; lipoarabinomannan of mycobacteria; double-stranded RNA, which is produced by most viruses during the infection cycle; and ß-glucans and mannans found in fungal cell walls (21).

Several families of PRRs have been characterized so far, including Toll-like receptors, RIG-I-like receptors, NOD-like receptors, and C-type lectin receptors (26). These PRRs are expressed not only in macrophages and DCs but also in various nonprofessional immune cells such as epithelial cells (16, 26).

The mammalian Toll-like receptors (TLRs) are important signaling receptors in innate host defense (21). There are at least twelve TLRs in mammalian species that differ from one another in their expression pattern, their ligand specificities, the signaling pathways they utilize, and the cellular responses they induce. Some of the TLRs can recognize more than one ligand, and again, these ligands can be structurally unrelated to each other (21). Available evidence suggests that TLRs respond also to endogenous molecules, most of which are released from dead cells (DAMPs), suggesting that TLRs can survey danger signals and are associated with sterile inflammation and have important roles in the pathogenesis of inflammatory diseases (16, 21, 26).

Engagement of TLRs activates multiple signaling cascades leading to the induction of genes involved in innate immune responses. Binding of ligands followed by dimerization of TLRs recruits adapter proteins such as myeloid differentiation factor 88 (MyD88), TIR-domain-containing adaptor protein-inducing IFN-β (TRIF), TIR-associated protein (TIRAP), and TRIF-related adaptor molecule (TRAM). MyD88 associates with IL-1R-associated kinases (IRAKs), TNFR-associated factor 6 (TRAF6), while TRIF activates interferon related factors (IRFs). Both pathways result in activation of nuclear factor NF-kB (27).

Inhibition of inflammatory response

The innate immune response is activated rapidly (within hours) compared with adaptive immunity. Activation of the innate immune system, however, can be a double-edged sword for the host. Pro-inflammatory cytokines mediate a positive feedback loop on the innate immune system, and overproduction of cytokines, if unchecked, is hazardous to the host and may cause severe outcomes. If inflammation is not resolved promptly, it progresses into a chronic state in which the persistence of immune cells infiltrating the tissue is associated with its destruction and fibrotic alteration. Also, overproduction of cytokines by immune cells to overwhelm pathogens can lead to sepsis and can be fatal (28).

To avoid harmful and inappropriate inflammatory responses, the initial inflammatory response is followed by a stage of resolution where the same cells that participated in the initiation of inflammation have to be inactivated and the process of healing and debris scavenging has to be initiated (28). This mechanism is there to prevent excessive innate immune activation and negatively regulate the initial triggering signals. Inhibition of Toll-like receptor signaling is a major mechanism in suppression of immune response. Mediators that negatively regulate TLR signaling are interleukin-1 receptor-associated kinase- M (IRAK-M),

mitogen and stress activated protein kinase (MSK) 1 and 2, TGF-β-activated kinase 1 (TAK1), A20 and the Src homology 2 domain-containing protein tyrosine phosphatase-1 and -2 (SHP-1, -2) (25, 28).

MicroRNAs (miRNAs), newly discovered oligonucleotides important to gene regulation which bind to the 3' untranslated region of target mRNA and direct their post-transcriptional repression, have been shown to directly target components of the TLR signaling system. Among them miR-155, miR-21, miR-146a and let-7 appear to have a central role (Figure 8) (28-30). MiR-155 positively regulates TLR signaling by suppressing Tab2, the activator of TAK1, an inhibitor of NF-kB. MiR-146a blocks TLR signaling by targeting IRAK1 and TRAF6, proteins that are important components of the myeloid differentiation primary-response protein 88 (MyD88)-dependent pathway for NF-κB activation downstream of TLR2, TLR4, TLR5, TLR7–TLR8 and TLR9. In mouse peritoneal macrophages, the induction of let-7e expression decreases cell surface expression of TLR4, the mRNA of which contains a let-7 target site (31). Finally, transfection of cells with a miR-21 precursor blocked NF-kB activity and promoted IL-10 production in response to LPS via targeting PDC4, a proinflammatory protein that promotes activation of the transcription factor NF-kB and suppresses interleukin 10 (IL-10) (32).

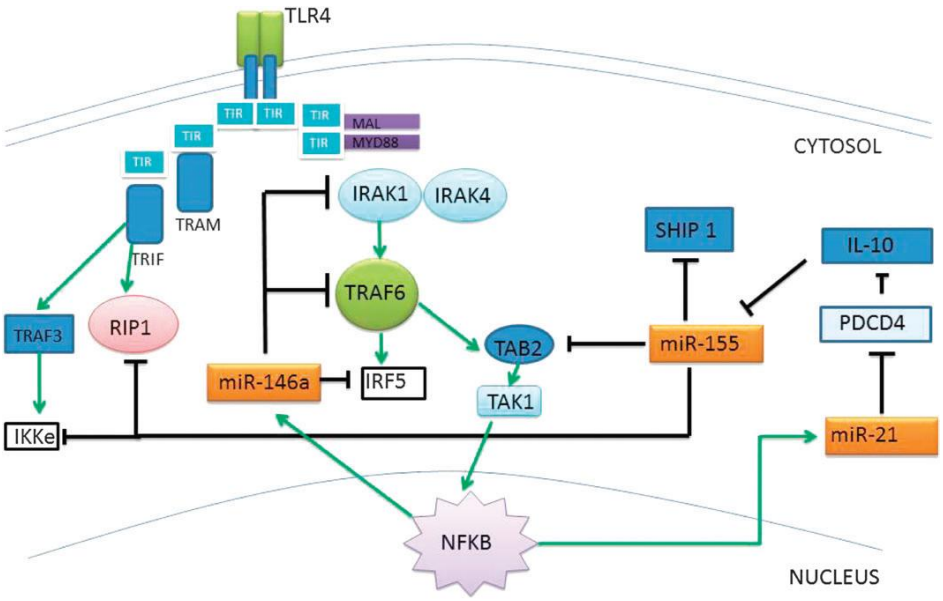

Figure 8. Regulation of TLR signaling by microRNAs. Adapted from Quinn et al, Int Immunol, 2011

The Alveolar Macrophages

Macrophages are cells of innate immunity that are widely distributed throughout the body, within and outside lympho-hemopoietic organs. They are derived from mononuclear leukocytes (monocytes) that reside in bone marrow or circulate in the blood (21, 33).

Resident macrophages are conditioned by the requirements of the tissue during both normal and pathological processes. In normal conditions, they have a scavenger and housekeeping role by recognizing and engulfing dead, senescent or abnormal cells or cell debris (21). Unlike other myeloid granulocytic phagocytes, macrophages can be long-lived and retain the ability to synthesize RNA and protein to a marked extent, at least for several months even after phagocytosis has occurred. They are also capable of handling repeated bacterial and other microbial challenges (reusable phagocytes) (3).

In pathological conditions, macrophages sense the endogenous danger signals that are present in the debris of necrotic cells through Toll-like receptors (TLRs), intracellular pattern recognition receptors and the interleukin-1 receptor (IL-1R)′(34). This function makes macrophages one of the primary sensors of danger in the host. Élie Metchnikoff, who won the Nobel Prize in Physiology or Medicine in 1908 for his description of phagocytosis, suggested that the key to immunity was to “stimulate the phagocytes”(35). Since his discovery, immunologists have been occupied with the concept of macrophages as immune effector cells and with understanding how these cells participate in host defense.

Lung macrophages can be differentiated into several populations in the lung according to the compartment they are found in intravascular, interstitial, airway, and alveolar macrophages. Of these, the alveolar macrophages, the cell population of the surface lining layer, are of particular importance.

The alveolar macrophages are freely moved cells, which are transiently attached to the surface of the alveolar epithelium by pseudopodia and can crawl over this surface by amoeboid movement (Figure 9) (21). They can also move from alveoli to alveoli via passage through a pore of Kohn. They populate the lung tissue during early embryogenesis and remain viable for prolonged periods (17). They derive from monocytes but in the alveoli they constitute a partly self-reproducing cell population (17, 36). It is estimated that macrophages make up 90 percent of cells found in the alveolar spaces (3).

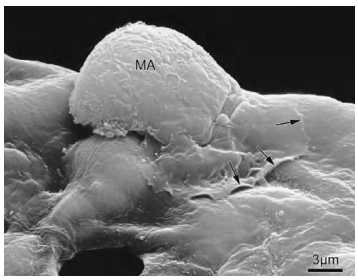

Figure 9. Alveolar macrophage (MA) seen sitting on epithelial surface of human lung. Note cytoplasmic lamella *(arrows)* which represents the advancing edge of the cell. Adapted from Fishman and Elias. Fishman’s pulmonary diseases and disorders, 2008.

Alveolar macrophages are the most abundant antigen-presenting cells in lung tissue and they play a major role in lung immunity and homeostasis. The unique tissue location and function of alveolar macrophages distinguish them from other macrophage populations since the majority of them are in close contact with the respiratory epithelium (37). In steady state conditions, alveolar macrophage is tightly controlled through several cell–cell and soluble mediator interactions; and receives anti-inflammatory signals from microenvironment such as IL-10 and TGF-β (Figure 10) resulting in poor ability to present antigen to T cells, decreased phagocytic activity and reduced respiratory burst (37). This creates a regulatory environment with inhibitory signals that is highly controlled in order to limit unwanted inflammatory responses (37, 38).

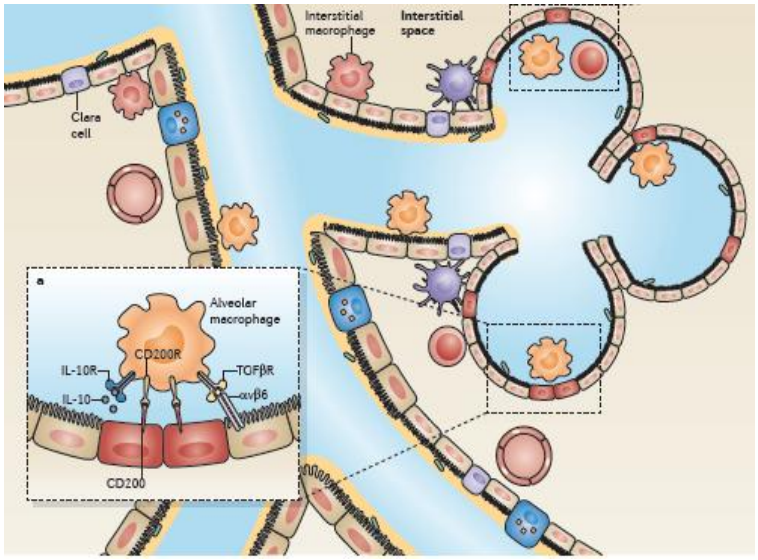

Figure 10. Leukocyte interactions in the healthy lungs. Alveolar macrophages reside in the airspaces attached to type I or type II alveolar epithelial cells. Alveolar macrophages are regulated by the airway epithelium through their interactions with CD200, which is expressed by type II alveolar cells, with transforming growth factor-β (TGFβ), which is tethered to the epithelial cell surface by αvβ6 integrin, and with secreted interleukin-10 (IL-10). Adapted from Hussel et al, Nat Rev Immunol, 2014.

However, alveolar macrophages have contradictory functions. They are essential for steady-state clearance of daily cellular debris but are also ideally placed to initiate a strong inflammatory response to pathogenic invading material. The interaction with airway epithelium and whether the cells that are cleared by alveolar macrophages are apoptotic or necrotic determine whether alveolar macrophages will respond in an anti-inflammatory or in a pro-inflammatory manner (37). Therefore, the initiation of inflammation requires a combination of events that override the inhibitory mechanisms that regulate alveolar macrophages. Once initiated, the outcome of their activation is determined by pathogen-specific properties and by the host immune response to them (37).

Activation of macrophages is a key event in the inflammatory cascade in the lung and defines a functional state characterized by extrusion of pseudopodia and an increase in cell size and membrane ruffling. The smaller the macrophage may represent younger, recently emigrated phagocytes and the larger may represent previously activated cells (2). Upon activation, lung macrophages release a variety of cytokines (MCP-1, MIP-2, IL-8, TNF-α, IL-6,

INF-γ), arachidonate metabolites, leukotrienes, reactive oxygen metabolites (nitric oxide, superoxide anion) and constitutive enzymes such as metalloproteases and elastase (3). These mediators impact extracellular matrix, fibrin deposition as well as the function of nearby cells, including T cells, B cells, endothelial cells, and fibroblasts (7). By the secretion of pro-inflammatory chemotactic factors, alveolar macrophages then also recruit neutrophils and lymphocytes, monocytes, eosinophils, dendritic cells and other cells into the alveoli to promote acute lung inflammation (7).

A wide array of receptors is expressed by alveolar macrophages, of which most mediate activation, migration, or phagocytosis. Most important are the toll-like receptors. Other receptors expressed by alveolar macrophages include chemokine receptors, cytokine receptors, Fc receptors that recognize opsonizing antibodies IgG (Fcγ), receptors for IgA, receptors for phagocytosis, lectin receptors, bacterial endotoxin (CD14) receptors, insulin receptors, receptors for Class II MHC (HLA-DR, DP, DQ), mannose receptors and scavenger receptors (such as MARCO, Dectin -1) (3). Also in macrophage surface, several proteins and glycoproteins are expressed such as β2 Integrins (CD18; CD11α, b, c), cell surface proteins that are essential for antigen presentation and lymphocyte activation, including MHC, cell-cell adhesion molecules (e.g., ICAM/CD54, LFA 3/CD58), CD4 and the CD28 (3).

Macrophage activation phenotypes

However, alveolar macrophage activation is not simple phenomenon. Macrophages have remarkable plasticity that allows them to efficiently respond to environmental signals and change their phenotype respectively. These changes can give rise to different populations of cells with distinct functions. It has been recognized that these changes can be roughly categorized in classical activation (M1) and alternative macrophage activation (M2) (39).

In general, classically activated macrophages are “effector” macrophages, activated through Toll-like receptors, interferon-γ (INF-γ), LPS and tumor necrosis factor (TNF-α) (39). These cytokines prime the cells towards high production of iNOS and reactive oxygen species (ROS), IL-12β secretion and high capacity to present antigen, leading to a type I response (39). These cells exhibit enhanced microbicidal or tumoricidal capacity, increased secretion of cytokines and mediators, and higher expression of co-stimulatory molecules (40, 41). Thus, M1 macrophages contribute to the development of inflammation and tissue injury.

On the other hand, alternatively activated macrophages are activated mostly by interleukin-4 (IL-4) or IL-13 although various M2 like subtypes have been described (40, 41). PAMPs that are expressed by helminthes and parasites as well as metabolic pathways of obesity and insulin resistance may also drive the alternative activation of macrophages (42-44). M2 is characterized by high levels of arginase-1 (Arg-1), found-in-inflammatory-zone-1

(Fizz1), chitinase-3-like-3 (Ym1), and macrophage galactose C-type lectin 1 and 2 (MGL1, 2) expression (7, 45, 46). M2 macrophages participate in the resolution of inflammation, and are known to be beneficial in the outcome of several inflammatory diseases (39, 47-49). In M2 macrophages, arginase-1 antagonizes iNOS for the same substrate, L-arginine, but produces urea instead of nitric oxide, compromising by this way the generation oxidative stress (Figure 11) (39, 48).

However, since their initial description, the functional and phenotypical characteristics of macrophages within the M1 phenotype have remained mostly unaltered, but the M2 macrophage category has been expanded to accommodate a broad range of macrophage functions. The study of macrophage activation in different models, disease states and activating agents revealed that different versions of M2 macrophages with distinct spectrum of markers and function may exist depending on the environmental conditions. As a result, widespread use of many definitions of macrophage activation has been noted. The most common definition that was emerged was the "M2-like macrophages" that share many markers with M2 macrophages but they produce high levels of IL-10 (50). M2 like macrophages were also considered to be all the M2 macrophages that were produced in an Th2 independent way such as the tumor-associated macrophages (TAM) that were noted in hypoxic sites of tumors (50).

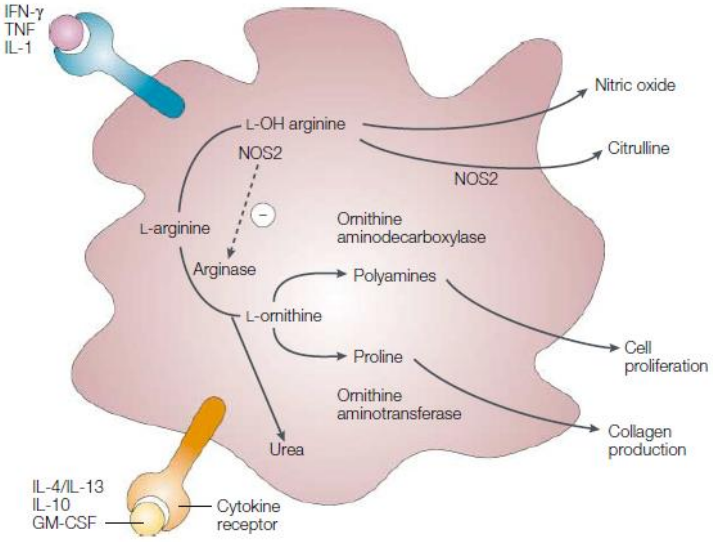

Figure 11. Differential utilization of L-arginine by activated macrophages. Adapted from Gordon et al. Nat Rev Immunol, 2003.

The M2 nomenclature became also more confusing by the fact that the term "M2 macrophages" has also been applied in a loose way to macrophages exposed to immune complexes (Ic), IL-10, glucocorticoids (GC) with transforming growth factor β (TGF-β) or glucocorticoids alone (40, 50-52). For these reason several groups have proposed that M2 designation should expand into three different subtypes of macrophages M2a, induced by IL-4 or IL-13; M2b induced by exposure to immune complexes (IC) and agonists of Toll-like receptors (TLRs) or IL-1R; and M2c (immunosuppressive or deactivated), induced by IL-10 and glucocorticoid hormones (51, 53-55). The term ''regulatory'' macrophages has been also emerge to describe macrophages that mainly secrete IL-10 and TGF-β (52, 56). Also, confusion was emerged with the types of activation caused by GM-CSF-

1 as M1 and macrophages grown in CSF-1 as M2 since significant differences have been documented in the transcriptomes of macrophage populations primarily generated with the use of CSF-1 or GM-CSF (52).

Another population of macrophages is the 'tolerant macrophages". Tolerance is defined as the reduced capacity of a cell to respond to a stimulus after an initial exposure to this stimulus ensuring that cells will not over-react to sustained TLR stimuli (57). Endotoxin tolerance is characterized by a decreased production of cytokines in response to the pro-inflammatory stimulus of LPS. These cells combine potent phagocytic activity with impaired capability for Ag presentation (58). Recent findings have shown that tolerant macrophages share many similar characteristics with M2 macrophages and represent a distinct state of M2 polarization (58, 59).

In the literature, M2 designation persists despite a growing body of evidence indicating that the macrophages called after M2 encompass cells with dramatic differences in their biochemistry and physiology (51-55). To avoid complexity, it was recently proposed that in each experimental setting, activation methods, i.e. IL-4, Ig, IL-10, GC, IFN-γ, LPS, should be clearly stated and where ambiguity exists— for example, in a macrophage population isolated from an *in vivo* system—researchers should emphasize the marker combinations used and state the closest relative(s) along the spectrum of macrophage activation shown in Figure 12 (52).

Although murine M1 and M2 polarized macrophage subsets are relatively easy to distinguish based on combinatorial gene expression profiles, the identification of equivalent subsets in humans has been more challenging. There are scarce data for definition and categorization of human activated macrophages. It should be noted that classical M2 macrophage markers in mice (such as resistin-like-α, chitinase 3-like 3 and arginase 1) are not induced in human macrophages even in the presence of IL-4, so direct comparisons with mouse studies are difficult (52). Studies in human involve mainly blood monocyte-derived macrophages and not tissue resident macrophages as in animal models (52). For example, interferon regulatory factor 5 (IRF5) seems to be crucial for human M1 macrophage gene expression. However, neither Arg1 nor iNOS is expressed by *in vitro* polarized human macrophages stimulated with IL-4 or IFN-γ, respectively (60).

Human "alternatively activated" macrophages that were polarized using IL-4 and IL-13 included those encoding the mannose receptor (also known as CD206), matrix metalloproteinase 2 (MMP2), MMP7, MMP9, the tyrosine protein kinase MER, growth arrest-specific protein 7 (GAS7), CD163, stabilin 1 (STAB1) and the adenosine A3 receptor (37, 61). Some of the markers that characterize human macrophage activation are noted with asterisk in Figure 12 and in comparison with murine M2 macrophages in Figure 13.

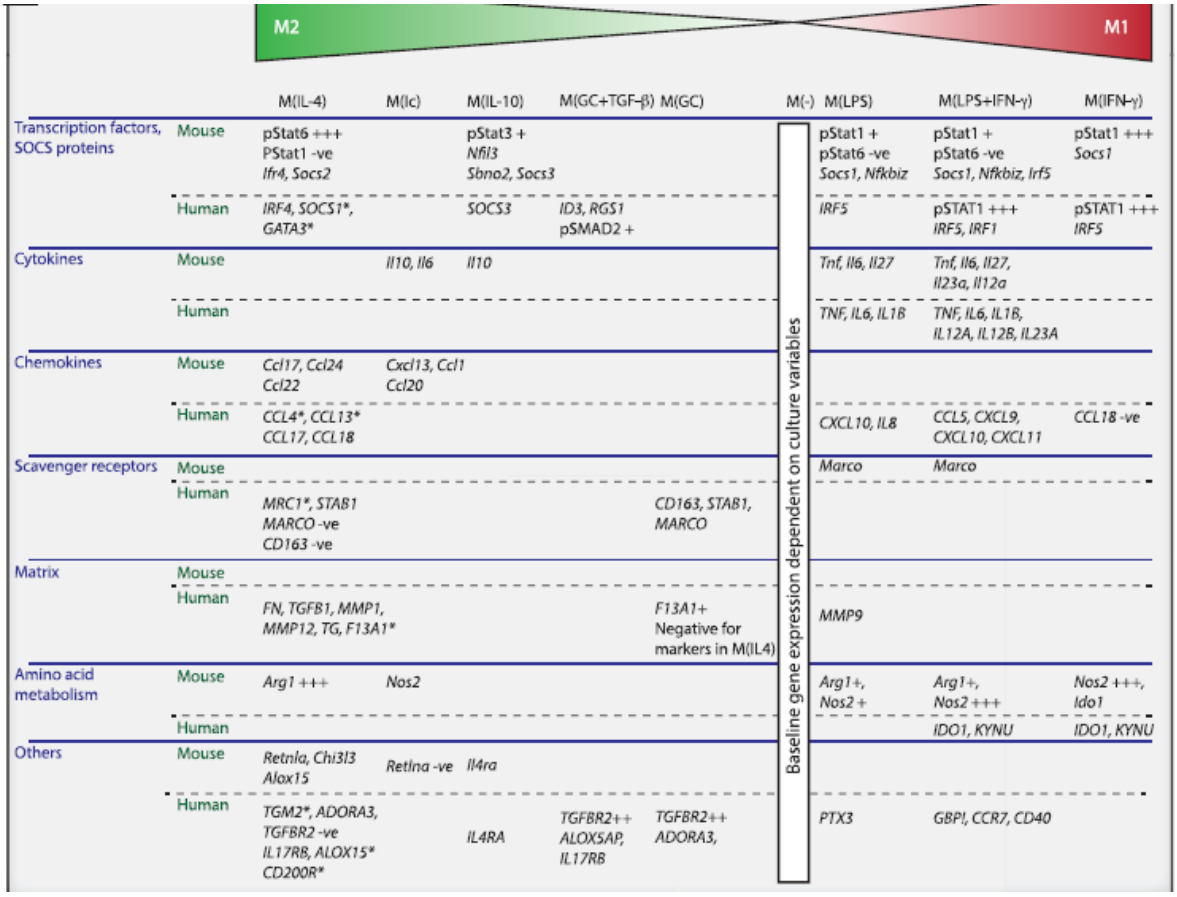

Figure 12. Framework for Describing Activated Macrophages. Marker systems for activated macrophages. Shown are functional subdivisions according to stimulation of CSF-1 macrophages with the existing M1-M2 spectrum concept. Stimulation conditions are IL-4, immune complexes (Ic), IL-10, glucocorticoids (GC) with transforming growth factor β (TGF-β), glucocorticoids alone, LPS, LPS and IFN-g, and IFN-g alone. Marker data were drawn from a wide range of published and unpublished data from the authors' laboratories and represent a starting consensus. An asterisk indicates corroboration of human IL-4 genes by deep sequencing. Adapted from Murray et al, Immunity, 2014.

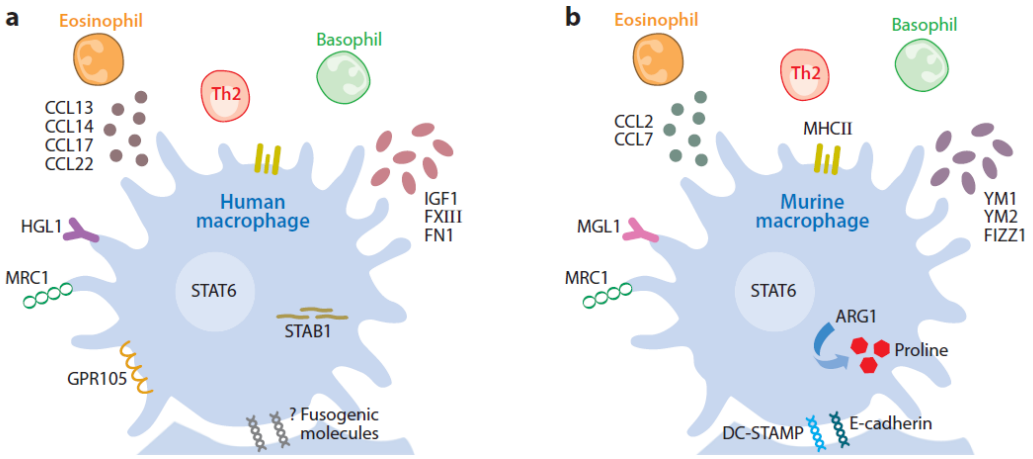

Figure 13. Human and murine macrophage alternative activation markers. There are differences between human (a) and murine (b) alternative activation markers. IL-4 and IL-13 induce genes conserved in both species such as MHC class II (MHCII) and MRC1, as well as divergent ones such as ARG1, YM1 in mouse, and GPR105 in humans. Adapted from Martinez et al, Ann Rev Immunol, 2009.

Regulation of macrophage activation

Apart from the signaling cascades elicited by receptor stimulation, there is a group of regulatory genes and pathways which partially or totally tune the polarization program (63). Several signaling pathways such as NFkB p65 subunit, STAT-1 phosphorylation and IRF-5 upregulation as well as suppression of suppressor of cytokine signaling SOCS1 have been shown to promote M1 activation (7, 48, 64-68). For example, forced expression of IRF5 in M2 macrophages drove M1-specific cytokines, chemokines, and costimulatory molecules and led to a potent Th1 response whereas induction of M1-markers was impaired in irf5−/− macrophages (65).

Several other genes have been found to specifically alter the ability of macrophages to undergo alternative activation. The elements identified so far belong to the same families that control classical activation, such as the NF-kB member p50, the IRF family member IRF4 controlled by Jmjd3, the C/EBP family member C/EBP - β controlled by Creb, the STAT member STAT6 and NF-kB competitor PPAR- γ (69-72). In figure 14 the major transcription factor pathways that control M1 and M2 activation are depicted.

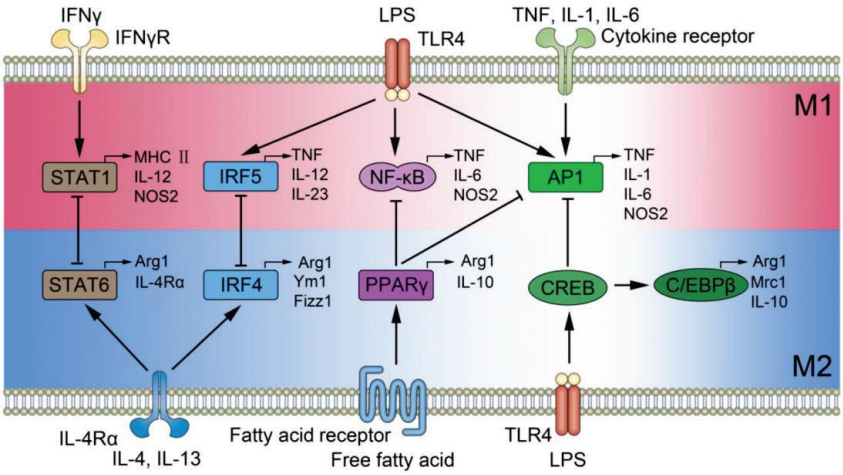

Figure 14. Signal pathways of macrophage polarization. The figure illustrates several mechanisms underlying macrophage polarization and shows the feedback regulation between M1 and M2 signal pathways. The feedback regulation between M1 and M2 are implemented by STAT1-STAT6, IRF5-IRF4, NF-κB-PPARγ, AP1-CREB, and AP1-PPARγ, and they play essential roles in the initiation, development, and cessation of inflammatory diseases. Adapted from Liu et al, Int J Biol Sci, 2014.

Evidence shows that not only pathway-specific transcription factors and receptors, but also cytosolic enzymes, and functionally distant genes can be regulators and contribute to tuning and determining the macrophage activation profile. For example, galectin-3 a carbohydrate-binding lectin present on macrophages is required for alternative activation (74). IKK-β inhibits the M1 macrophage phenotype during infection through negative

crosstalk with the Stat1 pathway (75). SHIP-deficiency and SOCS3 suppression have been also shown to regulate M2 activation (48, 64, 66, 67, 76, 77).

Within the different signaling complexes, the PI3K pathway and its downstream mediators are emerging as central for the elicitation and control of M1 and M2 macrophages. The PI3K/Akt pathway do regulate macrophage activation pathways by regulating cytokine and TLR4 receptor signaling (78) and by modulation of IKK phosphorylation and NF-kB suppression (13). However, the potential district function Akt isoforms in macrophage differentiation remains elusive. Recently, our work has shown that Akt1 and Akt2 kinase isoforms have a major role in macrophage polarization.

The role of Akt Kinases in macrophage activation

Akt, also known as protein kinase B (PKB), is a family of three serine/threonine protein kinases, Akt1, Akt2 and Akt3, important to control cell survival, proliferation and differentiation (79, 80). The first two are being expressed in most tissues including myeloid cells while the third is expressed primarily in neuronal tissues. Akt isoforms perform similar as well as unique functions within cells as were revealed by knock-out mouse models. Knock out mice of Akt-1 exhibit global growth defects (growth retardation) and reduced life duration, knockout of Akt-2 results to insulin resistance and development of diabetes and Akt-3 knock out seems to be implicated in the development of brain and neuronal survival (81-83).

Despite their high homology, Akt isoforms regulate distinct physiological functions via mechanisms including distinct tissue distribution of the Akt isoforms, differential activation of the Akt isoforms by different PI3K kinases, and isoform specific subcellular compartmentalization (84). In the present study we focus on the role of Akt2 in macrophage activation.

The Akt2 gene (Akt2) was first isolated in 1987 from non-viral sequences of the acute transforming retrovirus AKT8 genome (v-akt, viral proto-oncogene) (85). The protein Akt-2, also known as Protein kinase B β was later found to belong to AGC (cAMP-dependent, cGMP-dependent and protein kinase C) serine/threonine protein kinase family, containing SH2-like (Src homology 2-like) domains (86). Akt2 is a 56-kDa cytosolic protein, with three conserved domains among all the isoforms: an N-terminal pleckstrin homology (PH) domain, a central catalytic kinase domain and an AGC-kinase C-terminal domain (figure 15) (86, 87). The PH domain of just over 100 amino acids forms a small pocket that binds phosphatidylinositol 3, 4, 5-trisphosphate (PIP3) with high affinity. The kinase domain of approximately 250 amino acids in length is very similar to cAMP dependent kinases (PKA), protein kinase G (AGC kinases), serum and glucocorticoid-regulated protein kinases (SGK)

PKC and aPKC (87, 88). The C-terminal domain, approximately 40 amino acids in length, contains a phosphorylation site into a hydrophobic pocket with a characteristic motif of AGC kinases (F-X-X-F/Y-S/T-Y/F where X is any amino acid) (87, 88).

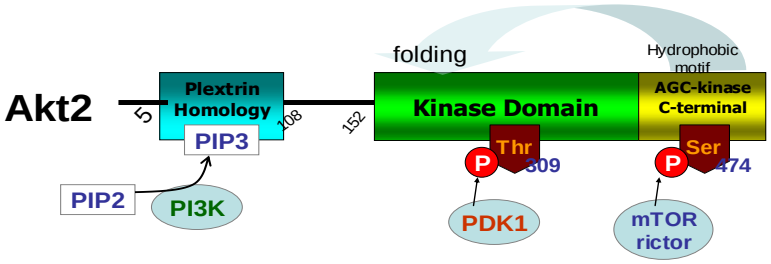

Figure 15. Schematic presentation of human Akt2 structure and activation sites. The district domains of the protein and the phosphorylation sites are illustrated. Designed by the author

PI3 kinase is the major upstream regulator and activator of Akt2 (Figure 15) (89). PI3K catalyzes the formation of a lipid second messenger, PIP3 from PIP2. Then proteins that contain PH domains such as Akt kinases can bind to PIP3 and can be activated. Activation of Akt is a complex process that can be divided in three steps. First, Akt must translocate to the cell membrane through the interaction of its PH domain with PIP3 (90). Binding to PIP3 induces a conformational change in Akt (unfolding) which facilitates its further activation through two additional independent phosphorylation events, in two specific sites (Thr309 and Ser474) by upstream serine/threonine kinases, the PDK-1 and mammalian target of rapamycin (mTOR) complex 2 (mTORC2/Rictor) (90). Both phosphorylation events are essential for the full activation of Akt (86, 87).

Once upon activation, Akt dissociates from the plasma membrane and phosphorylates many substrates in the cytoplasm and the nucleus. Most of the substrates contain conserved AKT phosphorylation sites (RXRXXS/T) (87).

There are also several proteins that are direct or indirect inhibitors of Akt. Protein phosphatase-2A (PP2A) and the PHLPP-1 (PH-domain Leucine-rich repeat protein phosphatase-1) directly dephosphorylate the hydrophobic motif phosphorylated serine and Drosophila Tribbles) and especially TRB3 binds to unphosphorylated Akt and inhibit its phosphorylation and activation *in vivo* (91). Apart from the above there are also several inhibitors of the upstream molecules that indirectly inhibit the activation of Akt and the insulin signaling in general. SHIP2 (SH2-containing inositol polyphosphate 5-phosphatase-2) is a PIP3 phosphatase that inhibits phosphorylation and subcellular redistribution of Akt2 (92). Additionally, the levels of cellular PIP3 are regulated primarily by a phosphatase called PTEN that mainly act in the inhibition of phosphorylation of Thr309 of Akt2 (93). Moreover, several natural and synthetic inhibitors of PI3K, wortmannin and LY294002 respectively, reduce the level of PIP3 and prevent the phosphorylation and activation of Akt (94).

Akt kinases play central roles in innate immunity as they are activated by TLRs and cytokine receptors and contribute to the inflammatory response. Akt1 and Akt2 kinases were recently found that hold a key role in the regulation of macrophage activation phenotype (68, 95, 96). Deletion of Akt1 results in M1 polarization and reduced arginase-1 activity and expression. Surprisingly, Akt2 deficiency had the opposite effect from Akt1-/- macrophages, rendering them hypo-responsive to LPS and M2 –prone (49, 68). Another study reported that Akt1 inhibition resulted in enhanced clearance and reduced intracellular growth of Salmonella typhimurium and Mycobacterium tuberculosis (97). Furthermore it was found that, SHIP1 repression, by miR-155, increases AKT1 signaling and by this way promoted alternative macrophage activation (98).

The precise mechanism by which Akt isoforms regulate macrophage activation is not known; work from our group has shown that Akt1 mediates LPS-driven negative regulatory signals by promoting the expression of miRNAs, including miR-155, miR-125b and let-7e (68). MiR-155 controls the expression of SOCS1 (68), SHIP1 (99) and of the transcription factor C/EBPβ (100). SOCS1 suppresses IFN-γ signaling (101), thus blocking M1 polarization, SHIP1 deficiency leads to M2 polarization (102) while C/EBPβ regulates Arg1 expression (103) and M2 differentiation (Figure 16). Depletion of Akt2 isoform in peritoneal macrophages triggered with LPS abrogates M1 activation and promotes M2 phenotype by inducing C/EBPβ (49, 68), a transcriptional regulator of Arg-1 expression (104) via suppression of the LPS- mediated miR-155 induction (Figure 16).

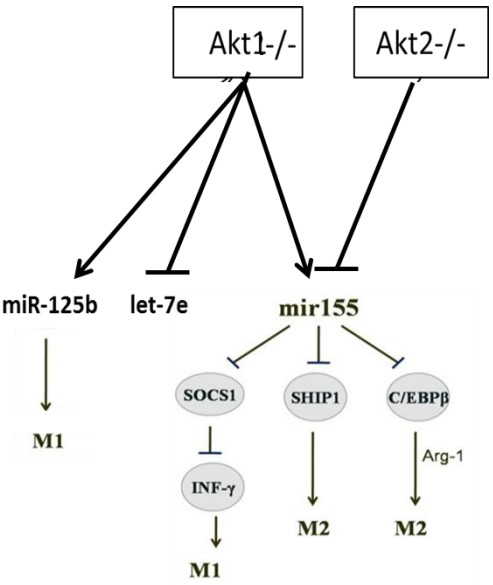

Figure 16. Schematic presentation of a potential mechanism of Akt1 and Akt2 regulation of macrophage differentiation via miRNAs.

MiRNA regulation of macrophage activation

Several recent studies implicate microRNAs in the regulation of innate immune responses and macrophage activation. MicroRNAs (miRNAs) are small non-coding RNA molecules that bind to the 3' untranslated region (3'-UTR) of a specific complementary mRNA sequence, resulting in cleavage, translational repression and gene silencing (105). MicroRNAs are transcribed by RNA polymerase II as part of capped and polyadenylated primary transcripts that are then cleaved by the Drosha ribonuclease III enzyme to produce an approximately

70-nt stem-loop precursor microRNA, which is further cleaved by the cytoplasmic Dicer ribonuclease to generate the mature microRNA and antisense microRNA products (105). The mature microRNA is incorporated into a RNA-induced silencing complex, which recognizes target mRNAs through base pairing with the microRNA and most commonly results in translational inhibition or destabilization of the target mRNA (105). The miRNAs that are consistently found to be expressed in macrophages are depicted in Table 1.

Macrophage MicroRNAs					
let-7a	miR-19b	miR-29a	miR-107	miR-181a	miR-324-5p
let-7b	miR-20a	miR-30a	miR-125a-5p	miR-181b	miR-328
let-7c	miR-21	miR-30b	miR-128	miR-185	miR-331-3p
let-7d	miR-22	miR-30c	miR-130b	miR-186	miR-342-3p
let-7d*	miR-23a	miR-30d	miR-132	miR-191	miR-345
let-7e	miR-23b	miR-34a	miR-133a	miR-197	miR-361-5p
let-7f	miR-24	miR-92a	miR-133b	miR-210	miR-362-5p
let-7g	miR-25	miR-93	miR-140-3p	miR-212	miR-378*
let-7i	miR-26a	miR-99b	miR-146a	miR-221	miR-425*
miR-15a	miR-26b	miR-103	miR-146b-5p	miR-222	miR-484
miR-15b	miR-27a	miR-106a	miR-151-3p	miR-223	miR-498
miR-16	miR-27b	miR-106b	miR-155	miR-320a	miR-500*
miR-17	miR-28-5p				

Table 1. Macrophages microRNAs consistently detected using two microarray techniques. Adapted from Luers et al, Cell Immunol, 2010.

Several of the above miRNAs have been recently associated with macrophage activation phenotypes. Among them miR-155, miR-146a, miR125b appear to exert the most important role.

MiR-155, rapidly upregulated by NF-kB, is best characterized as a pro-inflammatory miRNA because it enhances the production of inflammatory cytokines in macrophages and other immune cell types. MiR-155 has been reported to increase TNF-α production by stabilizing the TNF-α transcript thus promoting M1 response and to targets the IL-13 receptor and CEBPβ transcription factor which promotes alternative macrophage activation (107, 108). Interestingly, a recent study has shown that miR-155 delivery in alternatively activated macrophages is sufficient to reprogram these cells toward a more pro-inflammatory M1 phenotype (109). MiR-155 has been also shown to target key molecules involved in TLR signal transduction TGF-beta-activated kinase 1 (TAK1)-binding protein (TAB)2 and SHIP1 (110). SHIP1 negatively regulates the PI3K/AKT1 pathway, therefore, SHIP1 repression by miR-155 may increase AKT1 signaling and promote alternative macrophage activation (98, 111). Also, Akt2 promotes M2 macrophages via inhibition of miR-155 (49). The aforementioned data suggest that miR-155 induction by inflammatory signaling sustains or even amplifies classical pro-inflammatory macrophage activation (98, 112, 113).

MiR-125b expression is upregulated in macrophages in response to pro-inflammatory stimuli and finely tunes TNF-α production, NF-kB activation, and IFN-γ signaling in

macrophages (98, 114). Enforced expression of miR-125b drives macrophages to M1 activation, whereas anti–miR-125b treatment decreases CD80 surface expression (115). MiR-125b can also sustain pro-inflammatory cell activation by targeting the transcription factor IFN regulatory factor (IRF)4 (116), which promotes alternative macrophage activation.

MiR-146a is another miRNA that in contrast to miR-155 and miR125b can function as a potent inhibitor of inflammation. Mice with a targeted deletion of the miR-146a locus were found to be hypersensitive to bacterial challenge to produce excessive amounts of pro-inflammatory cytokines in response to endotoxin and succumb to septic shock faster than the wild type littermates (117). MiR-146 deficient mice also display severe tissue inflammation increased basal cytokine production, as well as elevated titers of autoantibodies, all classical signs of autoimmunity. Furthermore, aged knockout mice develop tumors in their secondary lymphoid organs and undergo myeloproliferation, suggesting that miR-146a regulates proliferation in immune cells (117, 118). Furthermore, miR-146a is necessary for the *in vivo* suppressor function of Tregs (119).

MiR-146, also activated by NF-kB, has been identified as a major negative regulation of TLR signaling and classical NF-kB activation by targeting IL1R-associated kinase (IRAK1) and TNF receptor-associated factor (TRAF)6, two key adaptor molecules in the TLR/NF-kB pathway (98). MiR-146a has been found elevated in tolerant "M2-like" macrophages (120). MiR-146a has target sites in additional, though less well-validated targets, which include IRAK2, STAT1, IRF5, SMAD4 and CXCR4 (119).

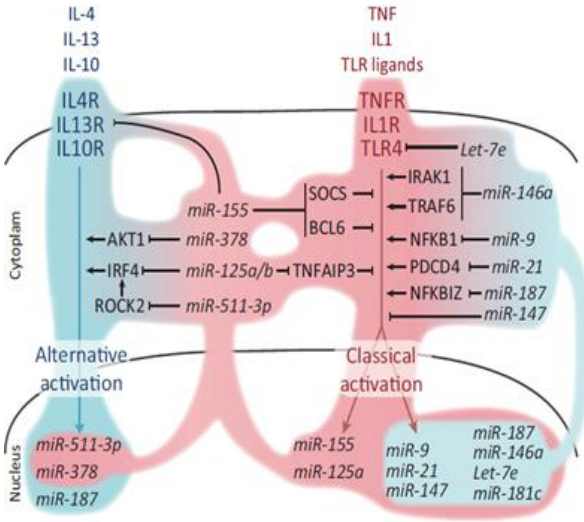

Figure 17. Regulation of classical and alternative macrophage activation by microRNAs. Several miRNAs are induced upon either type of macrophage activation. These include miRNAs that primarily sustain classical activation (pink-shaded) either by enhancing pro-inflammatory signaling (e.g., miR-155 and miR-125b) or by attenuating alternative activation (e.g., miR-511-3p, miR-378, and miR-155). Other miRNAs conversely attenuate classical activation (blue-shaded) by repressing several positive regulators of proinflammatory signaling (e.g., miR-146a and Let-7e). Adapted from Squadrito et al, Trends Immunol, 2013.

Other miRNAs that are important in controlling innate immune responses and macrophage activation include let-7e, miR-223, miR-9, miR-21, miR-187 and miR-147 (98, 114, 121, 122). They can be induced by several TLR agonists in a MyD88 and NF-kB-dependent manner and, like miR-146, are thought to inhibit pro-inflammatory responses in monocytes/macrophages by suppressing NF-kB activation through a negative feedback loop

mechanism (98, 114). MiR-378-3p and miR-511-3p expression is upregulated in macrophages by alternative activation (98, 114). In figure 17 a schematic diagram of miRNA implicated in macrophage activation is depicted.

The role of activated macrophages in the pathogenesis of lung diseases

Activated macrophages are prominent in many lung diseases but it is unclear whether macrophage activation is a cause or result of lung disease, it is probably both. In certain noninfectious lung diseases there is similarity of inflammatory responses to those in response to infections in which the consequences are deleterious rather than beneficial (3). Thus, understanding ways to control lung innate and acquired immune responses will be essential in developing appropriate therapies for inflammatory lung diseases.

There is conflicting evidence about the beneficial or harmful role of alternatively activated macrophages in the course of lung disease. There are many reports that point out the pathogenic, harmful role of M2 in and airway and inflammatory diseases (54, 123). M2 are typically but not exclusively associated with Th2 responses where they are thought to increase fibrosis by expressing profibrotic factors such as fibronectin, matrix metalloproteinases and IL-1β (53). The presence of M2 has been associated with the pathogenesis of several inflammatory diseases such as of parasitic diseases, atherosclerosis, asthma, allergic disease, obesity and insulin resistance, cancer and sepsis (73, 124). M2s are also actually more susceptible to some infections like in tuberculosis as they do not have the microbicidal properties of M1s (40). In case of tumor associated macrophages (TAMs), they are considered to be harmful as they promote tumor growth via their angiogenic and mitogenic properties and their inability to destroy tumor cells (125, 126).

However, M2 macrophages that have an M2-like phenotype have been shown to play a significant role in the resolution of aseptic inflammatory conditions such in models of DSS induced colitis (127, 128). In Th1 mediated autoimmune responses switch to Th2 is considered beneficial. Similarly, in M1 mediated diseases, switch to M2 is considered “less harmful” and beneficial or anti-inflammatory (53, 129). However, the timing of M1 to M2 switch *in vivo* is of great importance.

The role of M2 macrophages in lung inflammatory disease such as acute lung injury and pulmonary hypertension have not been investigated yet.

Acute Lung Injury

Acute lung injury (ALI) is a general term that describes the pathogenetic changes in the lung triggered by any injurious event affecting directly or indirectly the lung tissue and is arbitrarily used to describe the pathologic presentation of a clinical syndrome, ARDS. It was previously used by the American-European Consensus Conference in 1994 as a term that described a less severe form of ARDS. ALI as a "clinical term" was recently abandoned in the 2012 Berlin classification and it was replaced by the term "mild ARDS" (130).

However ALI is still currently used in experimental setting; the Official Workshop of American Thoracic Society Task force has determined specific criteria for the definition of experimental ALI (Table 2). The main features of experimental ALI are rapid onset (within 24hours) and histological evidence of tissue injury, alteration of the alveolar capillary barrier, presence of an inflammatory response, and evidence of physiological dysfunction (Table 2). They recommended that, to determine if ALI has occurred, at least three of these four main features of ALI should be present (131). Specifically, the presence of the main features of experimental lung injury can be established with the measurements listed in table 2.

The clinical picture of ALI, Acute Respiratory Distress Syndrome (ARDS) is a severe, life-threatening medical condition characterized by widespread inflammation and injury in the lungs that result in pulmonary edema, hypoxemia and finally

Table 2. Experimental ALI. Features and measurements

Histological Evidence of Tissue Injury
- Accumulation of neutrophils in the alveolar or the interstitial space
- Formation of hyaline membranes
- Presence of proteinaceous debris in the alveolar space (such as fibrin strands)
- Thickening of the alveolar wall
- Enhanced injury as measured by a standardized histology score

Alteration of the Alveolar Capillary Barrier
- An increase in extravascular lung water content
- Accumulation of an exogenous protein or tracer in the airspaces or the extra vascular compartment
- Increase in total bronchoalveolar (BAL) protein concentration
- Increase in concentration of high molecular weight proteins in BAL fluid (e.g., albumin, IgM)
- Increase in the microvascular filtration coefficient

Inflammatory Response
- Increase in the absolute number of neutrophils in BAL fluid
- Increase in lung myeloperoxidase (MPO) activity or protein concentration
- Increase in the concentrations of proinflammatory cytokines in lung tissue or BAL fluid

Physiological Dysfunction
- Hypoxemia
- Increased alveolar–arterial oxygen difference

respiratory failure. The incidence of ARDS is estimated 15 to 30 cases per 100,000 population per year (2, 132) and is a frequent cause of morbidity and mortality in critically ill patients (133, 134). There is no effective treatment reported so far for ARDS.

ARDS is characterized by the following criteria: 1, lung injury of acute onset, within one week of an apparent clinical insult and with progression of respiratory symptoms, 2, bilateral opacities on chest imaging not explained by other pulmonary pathology (e.g. pleural effusion, pneumothorax or nodules), 3, respiratory failure not explained by heart failure or volume overload and 4, decreased arterial PaO_2/FiO2 ratio (130). Specifically, in mild ARDS, ratio is 201 - 300 mmHg (≤ 39.9 kPa), moderate ARDS, 101 - 200 mmHg (≤ 26.6 kPa) and severe ARDS ≤ 100 mmHg (≤ 13.3 kPa) (a minimum PEEP of 5cmH_2O is required; it may be delivered noninvasively with CPAP to diagnose mild ARDS). The above characteristics are the "Berlin criteria" of 2012 by the European Society of Intensive Care Medicine, endorsed by the American Thoracic Society and the Society of Critical Care Medicine (130).

Table 3. Common causes of ARDS

Pulmonary (direct causes)
- Pneumonia
- Aspiration
- Mechanical ventilation
- Near drowning
- Inhalation injury
- Pulmonary contusion

Extrapulmonary (indirect causes)
- Sepsis
- Pancreatitis
- Trauma
- Transfusion RELATED
- DIC

The clinical syndrome of ARDS may be triggered from either a direct insult to the lungs as in pneumonia or aspiration (pulmonary ARDS) or it may be the end result of remote or systemic injuries such as sepsis or trauma (extrapulmonary) (2). The common causes are listed in table 3.

Clinical Course and Histopathology

ARDS is the clinical presentation of the pathological changes in the lung upon injurious stimuli that can be divided in two phases. The acute, or exudative, phase is manifested by disruption of the capillary-endothelial interface that involves damage to both the alveolar epithelium and pulmonary vascular endothelium (Figure 18) (133). Cell injury and alveolar barrier disruption leads to endothelial permeability and thus results in exudation of protein rich fluid in the alveolar space (135). This exudate may form sheets lining alveoli hyaline membrane (Figure 18). There is also impaired surfactant production due to either alveolar epithelial injury or secondarily from the effects of therapy (5, 133). Moreover, neutrophils and macrophages are attracted in the lung by chemokines (Figure 18) (2, 3). Vascular endothelial injury is a key feature of acute lung injury, as well as intravascular thrombosis

and capillary permeability that increases alveolar fluid (2, 3). In fact, pulmonary vascular injury, in the setting of acute lung injury, can lead to pulmonary arterial hypertension, resulting in increased intrapulmonary shunting, hypoxia, right ventricular dysfunction and worse outcome (2).

Fluid filled airspaces, loss of surfactant, microvascular thrombosis and disorganized repair reduces resting lung volumes (decreased compliance), increasing ventilation-perfusion mismatch, right to left intrapulmonary shunting and the work of breathing (2, 5, 6). Arterial hypoxemia that is refractory to treatment with supplemental oxygen is characteristic of acute phase. Radiographically, the findings are bilateral infiltrates, patchy or asymmetric, due to interstitial and alveolar edema (2).

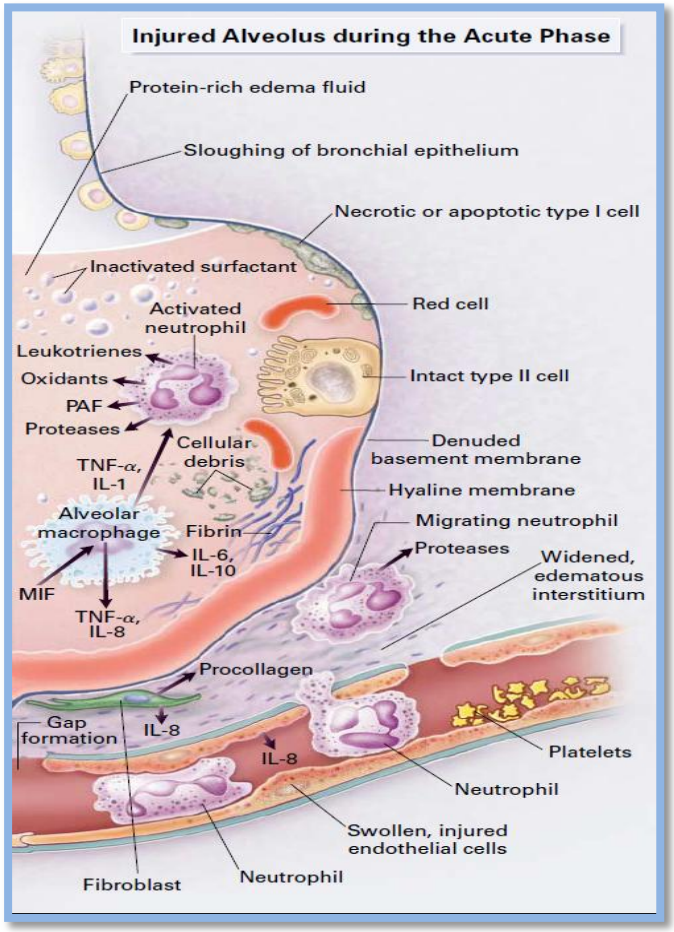

Figure 18. Injured Alveolus in the Acute Phase of ARDS
There is injury of both the bronchial and alveolar epithelial cells, with the formation of protein-rich hyaline membranes. Neutrophils are shown adhering to the injured capillary endothelium and marginating through the interstitium into the air space, which is filled with protein-rich edema fluid. In the air space, an alveolar macrophage is secreting cytokines, interleukin-1, 6, 8, and 10, (IL-1, 6, 8, and 10) and tumor necrosis factor *a* (TNF-*a*), which act locally to stimulate chemotaxis and activate neutrophils. Neutrophils can release oxidants, proteases, leukotrienes, and other proinflammatory molecules. The influx of protein rich edema fluid into the alveolus has led to the inactivation of surfactant. Adapted from Ware et al, N Eng J Med, 2000.

Some patients rapidly recover from acute ARDS. However, prolonged inflammation and destruction of pneumocytes leads to fibroblastic proliferation and lung fibrosis (2). This fibrosing alveolitis may become apparent 3 to 7 days after initial onset of ARDS with persistent hypoxemia, and a further decrease in pulmonary compliance (3, 136). As a result, there is thickening of the endothelium, epithelium and interstitial space, there is less edema,

but the spaces are still filled with inflammatory cells, to a lesser extent compared to the acute phase (2, 6).

Subsequent recovery phase is characterized by the gradual resolution of hypoxemia and improved lung compliance (136). In this phase granulocyte and monocyte recruitment from the circulation ceases, phagocytosis of apoptotic neutrophils or parenchymal cells and debris by macrophages is taking place (136). The clearance of alveolar edema fluid is taken over by active sodium transport via apical membrane epithelial Na^+ channels (ENaC) is pumped into the lung interstitium by basolaterally located Na/K-ATPase, thus creating a local osmotic gradient to reabsorb the water fraction of the edema fluid from the airspaces of the lungs via aquaporins (137). Also, there is differentiation of type II cells to type I (7).

Typically, the radiographic abnormalities resolve completely and in many patients pulmonary function returns to normal. If the underlying disease or injurious factor is not removed, the quantity of inflammatory mediators released by the lungs in ARDS may result in a systemic inflammatory response syndrome and multiple organ failure (136).

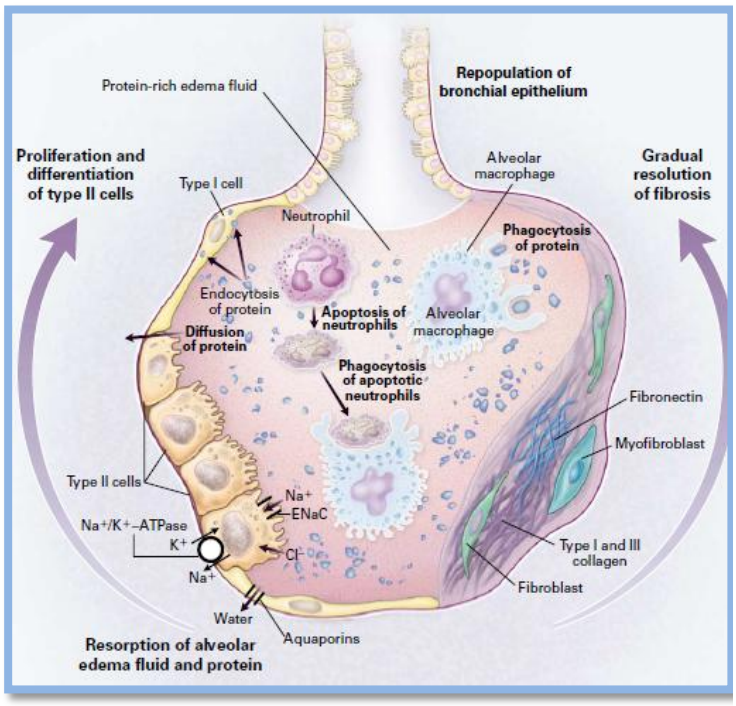

Figure 19. Resolution of ARDS. The alveolar epithelium is being repopulated by the proliferation and differentiation of alveolar type II cells. Resorption of alveolar edema fluid is shown at the base of the alveolus. Sodium is taken up by the epithelial sodium channel (ENaC) and through the basolateral membrane of type II cells by the sodium pump (Na+/K+–ATPase). Water is moving through aquaporins. Macrophages remove insoluble protein and apoptotic neutrophils by phagocytosis. The gradual remodeling and resolution of intraalveolar and interstitial granulation tissue and fibrosis are shown. Adapted from Ware et al. N Eng J Med. 2000

To summarize the pathophysiology of acute respiratory distress syndrome is divided into eight categories: innate immunity, alveolar fluid transport, surfactant, apoptosis, coagulation and direct alveolar epithelial injury (138). Although the triggering mechanisms are not completely understood, recent research has examined the role of inflammation in ALI and is reviewed in detail in the following pages.

Current Management of ARDS – The clinical paradox of Mechanical Ventilation

Maintaining adequate tissue oxygenation (PaO_2>60 mmHg) and gas exchange without increasing excessively inspired oxygen concentration is an important therapeutic goal in the management of ARDS. For the patient with ARDS, this goal is achieved with respiratory support, most typically in the form of mechanical ventilation. Surfactant-replacement therapy is also of outmost importance in infants with the neonatal respiratory distress syndrome followed by mechanical ventilation, either invasive or non-invasive. The usual strategies of fluid management, achievement of adequate hematocrit and the use of appropriate inotropes and vasopressors to maintain adequate cardiac output are adjunct therapies in critically ill patients with ARDS (2, 136).

Mechanical ventilation works by increasing mean alveolar pressure (mPalv) and augmenting by this way the pressure that comes from respiratory muscles. Increased mPalv allows for recruitment of partially flooded or atelectatic alveoli, thereby restoring normal V/Q matching and decreasing intrapulmonary shunt. The restoration of lung volumes frequently is followed by a reduction in the inspired oxygen concentration as well as improvement of respiratory mechanics and work of breathing. These improvements may allow for the partial or complete restoration of spontaneous ventilation (2, 136).

However, during the 1980s and 1990s, several studies showed that mechanical ventilation can produce lung inflammation and injury in animals, termed ventilator-induced lung injury (VILI) (133). These studies provided the basis for a large multicenter study comparing different ventilator strategies in patients with ALI/ARDS, which changed the clinical management of patients in intensive care units (133, 139, 140). It is necessary herein to distinguish between ventilator- induced lung injury, in which mechanical ventilation is the sole method used to generate injury, and ventilator-associated lung injury, in which mechanical ventilation modifies lung injury due to a clinically relevant cause, such as pneumonia, acid aspiration or sepsis (133).

It has soon recognized that high peak inspiratory pressure was fatally injurious. Alveolar epithelial cells and vascular endothelial cells undergo stretching during high pressure mechanical ventilation and excessive alveolar distension produces rupture at the junction of the alveolar wall and vascular sheath, allowing air to track along the bronchovascular sheath into the mediastinum and subcutaneous tissues or to rupture into the pleural spaces (air leak syndromes) (2, 133). Given that the development of air leaks appeared to be related to the use of high airway pressures, the term “barotrauma” was applied (2, 141).

Elevated tidal volume, as opposed to airway pressure per se, was also paramount in inducing ventilator-associated lung injury, thus establishing the concept of volutrauma. Overstretching of alveolar walls results in endothelial and epithelial breaks and interstitial edema that can cause failure of the alveolar epithelial–endothelial barrier or the plasma membrane and alterations in cytoskeletal structure (142, 143). But, the concept “the lower the tidal volume, the better the outcome” that was emerged is also a complex issue since

atelectasis may develop through the use of low tidal volume ventilation and cause *atelectotrauma,* and is attributed to the repeated collapse and re-expansion of alveoli. The latter can be overcome by the application of PEEP (2, 133).

Next, several studies showed that physical forces can change gene expression patterns in the lung, leading to increased inflammatory mediator release and alterations of ion channels; described as biotrauma and *mechanotransduction* (Figure 20) (2, 142). Mechanical cell deformation can be converted to biochemical changes, including production of proinflammatory cytokines and changes in lipid trafficking (142). Cyclic stretch stimulates alveolar epithelial cells through mechanosensitive membrane-associated proteins and stretch-activated ion channels but also through recruitment of additional phospholipids in the plasma membrane (144). Hyperinflation and deformation per se can trigger activation of monocytes, alveolar epithelial type II cells and endothelial cells and promote chemokine and cytokine release in the lung (143, 145-148). The clinical relevance of biotrauma is not only that it can aggravate ongoing lung injury but also that it may have important systemic consequences via spillover of lung inflammatory mediators into the systemic circulation leading to multiple organ failure (143, 149, 150).

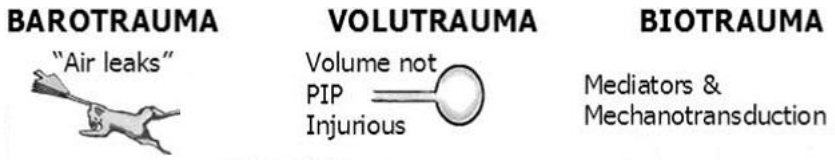

Figure 20. Time line illustrating a the major basic science observations that have influenced our understanding of ventilator-induced lung injury. Adapted from Tremblay et al, Int Care Med, 2006.

As a result of the recognition of the influence of VILI on the course of ARDS, physicians have mandated the clinical use of lung protective strategies that attempt to use minimal forces (whether pressure or volume triggered) in a manner that limits VILI (2). Current ventilation strategies involve using "gentle lung treatment approach" in the conventional tidal volume control ventilator; tidal volumes 4-6ml/kg in adults and children and 3-5ml/kg in neonates are considered a safe normal physiological range (141, 152). PEEP is also equally important to VT since in the presence of atelectasis, even a normal physiologic VT will result in overexpansion of the aerated alveoli that are more compliant to expansion based on Laplace law. Typically, PEEP levels are increased incrementally until the FiO_2 can be reduced below toxic levels (<0.6 in adults <0.40 in neonates) while maintaining a systemic oxygen saturation above 90% (2, 141, 152). The mode of ventilation is also important. Assisted synchronized mechanical ventilation whenever feasible is a more favorable alternative since it is associated with reduced incidence of ventilator-associated lung injury (VALI) (153).

Other strategies that are usually utilized to avoid lung injury are prone positioning, recruitment maneuvers and reduction in respiratory rate (154). Permissive hypercapnia and

mild hypoxemia (SO_2 as low as 88%) and respiratory acidosis are considered tolerable (2, 152, 155-157) but their benefit is controversial (155, 158, 159). Adjunctive treatments such as nitric oxide and extracorporeal membrane oxygenation in neonates and steroids and β2-agonists in adults may be also used (152, 160). B2 agonists and high frequency oscillatory ventilation (HFOV) have been found to increase epithelial ion channels and aquaporin but their benefit in ARDS has not been proven (161). Also, a number of clinical trials and animal studies have addressed the use of glucocorticoids in early and late phase ARDS with contradictory results (162-164). Steroids in some studies did increase the number of ventilator-free days during the first 28 days, accompanied by improved compliance and oxygenation, however given the failure of multicenter, randomized, controlled trials to demonstrate a benefit of high-dose corticosteroids in patients with ARDS, the administration of corticosteroids cannot be recommended (163, 165, 166).

However, even after the application of protective lung ventilation strategies and the improvement in survival in patients with ARDS that was noticed, it was recognized that the proportion of patients receiving protective ventilation remains modest (167). In many patients, the severity of lung disease renders inevitable the use of high concentrations of oxygen and high tidal volume to achieve adequate gas exchange. However, even ventilation with low tidal volume can harm the lungs since, although ventilation with 5–7 ml/kg is considered to be in “physiological” range, there is also diversity in breathing patterns from patient to patient and breath to breath fluctuation of the same patient. This breathing pattern in ARDS may be further influenced by the metabolic demand, dead space and the acid–base status or each patient (2, 138). Furthermore, it was been found that protective mechanical ventilation in preterm lambs exposed to acute chorioamnionitis does not reduce ventilation-induced lung or brain injury (168). Other complications of mechanical ventilation irrespectively of strategy used involve upper airway trauma, subglottic edema/stenosis, alveolar overdistention, reduced cardiac output secondary to increased intrathoracic pressure and impaired venous return and preload. Thus, the use of mechanical ventilation presents a clinical paradox. On the one hand, it provides life-sustaining support to allow sufficient time for recovery. On the other hand, it can be directly injurious to the lung.

To conclude, mechanical ventilation, the currently indicated life-saving intervention in patients with ALI, may further provoke and/or exacerbate lung injury (133). Also, the use of pharmacologic agents such as b2 agonists or corticosteroids are controversial and proven not efficacious in ARDS. In order to minimize the iatrogenic consequences of mechanical ventilation and to improve survival in ARDS, there must be a greater understanding of the signal transduction mechanisms that lead to ARDS.

To this direction, the molecular biology has expanded to the field of critical care. Basic research in ARDS has improved our understanding of biologic responses and has promising results on potential novel therapeutic applications; biological treatments. In the following

section we describe the basic scientific evidence reported for ARDS in animal models so far. Based on these facts we made the hypothesis of this study aiming to expand the existing knowledge in field of acute lung injury and to identify novel therapeutic targets.

Experimental Acute Lung Injury: animal models

In order to study ARDS in animals, several animal models have been described that are based on clinical disorders that are associated with ARDS in humans (table 4) (133). The term "Acute lung injury" (ALI) describes the pathologic presentation of ARDS and the specific features and measurements that define ALI in animals were recently determined and discussed above (131).

Table 4. Animal models of ALI

- Mechanical ventilation
- LPS
- Live bacteria
- Acid aspiration
- Hyperoxia
- Bleomycin
- Oleic acid
- Cecal ligation and puncture

In this study we focused on three models of acute lung injury; hydrochloric acid induced ALI (169), high tidal volume induced ALI (VILI) (133), and a septic pneumonia- associated lung injury (170). All of them recapitulate the main characteristics of human ALI, which are lung inflammation and high permeability pulmonary oedema.

In acid aspiration induced lung injury, investigators have used hydrochloric acid (HCl) to simulate lung injury due to gastric acid aspiration in humans caused mainly by altered level of consciousness (133, 171). Critically ill patients have an increased risk of aspiration due to gastroparesis, high gastric residual volume, nasogastric intubation and gastroesophageal reflux. But apart from the aspiration pneumonitis, acid induced ALI is a model that targets primary the alveolar epithelium and endothelium and recapitulates the pathology of human ARDS (133). Exposure of lung epithelial cells to HCl resulted in neutrophilic inflammation in the lung, alveolar hemorrhage, intra-alveolar and interstitial edema and impairment in the alveolar fluid clearance (133, 172).

The ventilation induced lung injury model (VILI) is the only model of lung injury that has affected clinical practice and improved survival in humans. Injurious ventilation per se, without preceding lung injury, can initiate cytokine-mediated pulmonary inflammation and is used to elucidate the mechanism of ARDS as well as potential treatments (133). The mechanisms of VILI (volutrauma, biotrauma) were described above in the consequences of mechanical ventilation. High tidal volume is usually applied that results in alveolar hemorrhage, hyaline membrane formation, neutrophilic infiltration, decreased compliance and gas-exchange abnormalities (133, 173).

While the above two methods study the aseptic acute lung injury, the administration of live bacteria in the lungs is a widely used method to study septic lung injury. Pulmonary infections are the main risk factor of ARDS. In animals, local administration of bacteria into the lungs can be achieved by using an intra-tracheal catheter, by transtracheal instillation or by aerosolization. Depending on the size of the bacterial inoculum, systemic manifestations of sepsis may be also evident. Bacteria that have been mostly used for this purpose are Pseudomonas aeruginosa, E. coli and S. aureus. Intra-tracheal injection of P.aeruginosa leads to lung inflammation, alveolar epithelial barrier leakiness and alveolar cell death (174). The injury was resolved 7 days from the initiation of P. aeruginosa injection (170).

Pathogenesis of experimental Acute lung injury

The majority of studies in animal models of ALI have focused on two mechanisms that contribute to pathology: the inflammatory response and the removal of pulmonary edema fluid from the alveolar space. In the present study we will focus on the inflammatory response that takes place in ALI, and specifically in the role of innate immune response and alveolar macrophages.

The role of inflammation in the development of Acute Lung Injury

Lately, in an increasing number of human and animal studies, it is becoming apparent that lung inflammation, either septic or aseptic, plays a central role in the promotion of ALI (175-181). One of the pathologic hallmarks observed in lungs from patients succumbing to ARDS is pronounced neutrophil and monocyte infiltration (182). Once in the interstitial and/or alveolar space, leukocytes release a series of oxygen- and nitrogen-based radical species, proteases, and arachidonic acid metabolites all of which can contribute to impaired endothelial barrier function and high permeability pulmonary edema that results in respiratory failure (2, 183).

Also pro-inflammatory mediators such as TNF-α, IL-1β, IL-6, IL-8 and chemokines such as macrophage inflammatory protein (MIP)-1, monocyte chemoattractant protein (MCP)-1 and CXCL-1, released by inflamed epithelial cells or activated innate immune cells, have been detected in the lungs of mouse and rat models of ALI (184-187). This inflammatory response is not limited to the lung but it has been shown to lead to a systemic inflammatory response that promotes distal organ injury and multi-systemic organ failure (188).

Thus innate immunity plays a major role in the pathogenesis of ALI. In agreement with the above, many studies have shown that anti-inflammatory treatment with exogenous IL-10, TNF-α neutralizing antibodies or IL-1ra can ameliorate ALI in animal models (2, 189-191).

Also, regulatory T cell expansion or recruitment in lung may facilitate recovery from ALI (111, 192-195). Administration of Keratinocyte growth factor-2 (KGF-2), a potent epithelial cell mitogen that also down-regulates pro-inflammatory responses (reducing IL-1β and TNF-α) and up-regulate anti-inflammatory responses (increasing cytokine IL-10 and IL-1Ra) has been found to be protective in many models of ALI (191, 196-198).

However, the timing of anti-inflammatory treatment in the course of ALI is crucial since for example an increased T-regulatory cell ratio in BAL in the very early phase of ARDS in humans was found to be an important risk factor for increased mortality (199).

The role of alveolar macrophages in ALI

Among the inflammatory cells implicated in ALI, alveolar macrophages appear to exert the most important role (169, 178, 179, 200, 201). Studies support the importance of macrophages to initiate and maintain the inflammatory response, as well as a determinant of resolution of lung inflammation and repair (202).

Alveolar macrophages, the primary sensors of injurious insult in the lung, accumulate upon stimuli in the acute phase of ALI, sense the endogenous danger signals that are present in the debris of necrotic cells and can initiate the lung inflammatory response and promote neutrophilic infiltration, tissue damage and oxidative stress (7, 45, 46, 169, 178, 179, 182, 200, 203). The importance of alveolar macrophage in the pathogenesis of lung inflammation and injury is demonstrated in macrophage depletion experiments. It has been showed that macrophage depletion by aerosolized clondronate resulted in decreased inflammation, diminished neutrophil recruitment in the lung and less severe lung injury in three animal models of ALI; hydrochloric acid aspiration, ventilation-induced ALI and ALI due to gram negative bacterial endotoxin (178, 179, 182, 201). Also LPS activated macrophages were found to decrease ENaC expression and activity and interfere with fluid removal of the alveoli (7).

In the resolving phase of ALI, alveolar macrophages also play a major role. Macrophages can actively terminate and resolve neutrophilic influx and induce neutrophil apoptosis (7). They are also capable of producing growth factors such as vascular endothelial growth factor (VEGF) (204), platelet derived growth factor A and B (PDGF-A and B), insulin-like growth factor-1 and tumor growth factor (TGF)-β, being crucial for tissue repair after injury, regulation of scaring resolution and matrix degradation (7).

According to the above, obviously, the macrophages of the acute phase and the macrophages of the resolving phase have a different function. It is well established in the literature that alveolar macrophages acquire classical M1 activation state in models of acute lung injury in rats and mice; they overexpress iNOS and pro-inflammatory cytokines, contributing by this way to inflammation and to the severe outcome of the disease (169,

178, 179, 200, 201). iNOS knock-out mice or rats treated with a specific iNOS inhibitor developed ameliorated ALI upon high tidal volume or acid-aspiration (205-207). In another study, induction of iNOS in alveolar macrophages exacerbated the outcome of ALI (31). Furthermore, in a septic model of ALI, alveolar macrophage depletion in iNOS-/- mice and subsequent reconstitution with WT macrophages resulted in significant sepsis-induced pulmonary protein leak and injury (208). Thus, M1 macrophages seem to represent a common denominator that contributes to pathology in ALI.

Though, the molecular mechanisms that regulate macrophage phenotype in ALI have not been fully described yet. It has been found that the activation of TLR4 signaling in alveolar macrophages and specifically the TLR4-TRIF-TRAF6-NF-kB signaling is important in acid-aspiration induced ALI, as TLR4-/-, TRIF-/- or TRAF6-/- mice are incapable to develop ALI (200, 209). TLR4 signaling plays also a critical role in other models of ALI (210).

Apart from M1 macrophages, the presence of M2 alveolar macrophages has been also noticed in the resolving phases in several models of ALI (7, 45). They appear after the acute phase and play a central role in tissue healing and recovery (7, 45, 46). In fact, both populations of M1 and M2 alveolar macrophages exist in the same time in the lung and their equilibrium will determine the type or response. But also M1 macrophages upon the proper environment can be transformed to M2 (7). In contrast to alveolar macrophages that can have either M1 or M2 phenotype, interstitial macrophages are considered to have an M2 phenotype (45, 46). The role of M2 macrophages has been studied, among others, in lung fibrosis and asthma, but the role of M2 macrophages in the outcome of ALI has not been clarified yet.

Biological treatments targeting inflammation in ALI

Up to now, many experimental treatments have been shown to alleviate inflammatory response in ALI. The great majority of studies have been focused in two fields of research; miRNAs and stem cells and their products (211). Accumulating evidence suggested that targeting disease-associated miRNAs might be a potential therapeutic strategy for inflammatory diseases (212, 213). MicroRNAs expression is affected in ARDS in humans and in animal models (214-217). Recently, miR-155, a distinct miRNA molecule, important in inflammatory and immune response, was found upregulated in lung tissue in an ALI animal model (7, 33). Targeting miR-155 in ALI could ameliorate from the disease via regulation of macrophage and Treg activation (111). Similarly, recent research work reported that silencing of miR-21 using antagonist of miR-21 could reduce the BAL protein level and affect the development of VILI in mice (215). Also, miR-146a upregulation in LPS induced lung injury resulted in suppression of lung inflammatory response (217). These studies could

highlight an important fact that miRNAs including miR-155 might be potential targets for the development of novel therapeutic strategy for ALI.

A number of cell types, particularly mesenchymal stem/stromal cells (MSCs), bone marrow-derived mononuclear cells, endothelial progenitor cells, and embryonic stem cells have been demonstrated to reduce mortality and modulate the inflammatory and remodeling processes in relevant preclinical ARDS models (218). Mesenchymal stem cells appear closest to clinical translation, given the evidence that they may favorably modulate the immune response to reduce lung injury, while maintaining host immune-competence and also facilitating lung regeneration and repair (193, 219, 220). The MSCs may exert their effect via diverse paracrine mechanisms, including the release of cytokines and growth factors and/or by transfer of cellular contents such as peptides, nucleic acids, and mitochondria via either microvesicular or direct cell-cell contact-mediated transfer (218). MSC secretome and, specifically, MSC-derived microvesicles have emerged as potential key mediators of therapeutic action that can be the focus of future therapies (221, 222).

Other experimental treatments that have been effectively used are inhibition of NF-kB signaling (223), promotion of autophagy in alveolar macrophages (224, 225), blocking oxidative stress via HO-1 upregulation, anti-inflammatory treatment with IL-10 (189, 190), antibody neutralization (e.g., anti-TNF-antibody) or receptor blockade (e.g., IL-1Ra) (2, 191), and inhibition of leucocytes infiltration by adhesion molecule blocking (182). Despite these encouraging results, to date no human trials have been successful. None of the studies reported so far have investigated the role of the alternatively activated macrophage in the development of ALI.

Despite considerable basic science and clinical research, therapeutic options for established ALI are limited. The cellular and molecular mechanisms that lead to ALI remain incomplete. It is necessary to further understand ALI pathology and identify novel treatments targeting the pathways that may prevent or ameliorate lung injury.

Pulmonary Arterial Hypertension

Pulmonary hypertension is defined as a mean pulmonary arterial pressure (mPAP) ≥25 mmHg at rest as assessed by right heart catheterization (226). In fact, pulmonary hypertension is a hemodynamic and pathophysiological state and not a disease *per se* (227). It can be found in multiple clinical conditions that usually but not always share similar histological and pathophysiological abnormalities (Table 5) (227).

Since the first international conference by the World Health Organization (WHO) in Geneva in 1973, the classification of clinical conditions that lead to pulmonary hypertension was subjected to many changes. The current classification is based on the WHO Conference in Nice (2013) and separates the term pulmonary arterial hypertension (PAH) (group 1) from pulmonary hypertension (PH) due to left heart disease (group 2), pulmonary disease (group 3), chronic thromboembolic pulmonary hypertension (CTEPH) (group 4) and PH of miscellaneous etiologies (group 5) (Table 5) (228, 229).

In the present thesis we will mainly focus in the subgroup of pulmonary hypertension known as pulmonary arterial hypertension (PAH). PAH is further defined by a mean pulmonary arterial pressure (mPAP) ≥25 mmHg and the addition of the criterion that the pulmonary capillary wedge pressure must be normal, less than 15 mm Hg and elevated pulmonary vascular resistance (PVR >3 WU) (226, 230). PAH is characterized by increased

Table 5. Updated clinical classification of pulmonary hypertension (Nice, 2013)

1. Pulmonary arterial hypertension (PAH)
1.1. Idiopathic PAH
1.2. Heritable PAH
1.2.1. BMPR2
1.2.2.ALK1,ENG,SMAD9,CAV1, KCNK3
1.2.3. Unknown
1.3. Drug- and toxin-induced
1.4. Associated with
1.4.1. Connective tissue diseases
1.4.2. HIV infection
1.4.3. Portal hypertension
1.4.4. Congenital heart diseases
1.4.5. Schistosomiasis
1’ Pulmonary veno-occlusive disease and / or pulmonary capillary hemangiomatosis
1” Persistent pulmonary hypertension of the newborn (PPHN)

2. Pulmonary hypertension due to left heart disease
2.1. Left ventricular systolic dysfunction
2.2. Left ventricular diastolic dysfunction
2.3. Valvular disease
2.4 Congenital/acquired left heart inflow/outflow tract obstruction and congenital cardiomyopathies

3. Pulmonary hypertension owing to lung diseases and/ or hypoxia
3.1. Chronic obstructive pulmonary disease
3.2. Interstitial lung disease
3.3. Other pulmonary diseases with mixed restrictive and obstructive pattern
3.4. Sleep-disordered breathing
3.6. Chronic exposure to high altitude
3.7. Developmental abnormalities

4. Chronic thromboembolic pulmonary hypertension (CTEPH)

5. Pulmonary hypertension with unclear multifactorial mechanisms
5.1. Hematologic disorders: chronic hemolytic anemia, myeloproliferative disorders, splenectomy
5.2. Systemic disorders: sarcoidosis, pulmonary histiocytosis, lymphangioleiomyomatosis
5.3. Metabolic disorders: glycogen storage disease, Gaucher disease, thyroid disorders
5.4. Others: tumoral obstruction, fibrosing mediastinitis, chronic renal failure, segmental

PVR leading to right ventricular overload, hypertrophy, and eventually to right ventricular failure and death (231). This progressive and sometimes fatal disease occurs as an idiopathic disease, familial/hereditary or as a component of other disease states (232) such as connective tissue disease, congenital heart disease, portal hypertension and human immunodeficiency virus (HIV) infection. Persistent pulmonary hypertension of the newborns and some other conditions and environmental factors, such as drugs, viruses, or toxins are also included in PAH definition (233).

PAH has an estimated incidence of 2 cases per million individuals per year and a prevalence of approximately 10 to 15 cases per million individuals (227, 231). International registries show that approximately 57% of adult and children with PAH had idiopathic PAH (IPAH) or familial PAH. PAH associated with congenital heart disease (CHD) is relatively more frequent in children (36%) than adults (10–11%), while PAH associated with connective tissue disease and other associated forms are very rare in children compared with the adult population (9, 226, 234, 235).

Persistent Pulmonary Hypertension of the Newborn (PPHN) results from the failure of relaxation of the pulmonary vasculature at birth, leading to shunting of non-oxygenated blood from the pulmonary to the systemic circulation via open ductus arteriosus and/or foramen ovale (236). PPHN has an incidence of 2 per 1,000 live births (141, 229). The most common etiology results from a failure to undergo the normal fall in pulmonary vascular resistance due to various conditions of perinatal stress such as hemorrhage, aspiration, hypoxia, hypoglycemia, polycythemia, acidosis and hypothermia or drug use during pregnancy (such as serotonic uptake inhibitors) (141, 236).

Prior to the advent of modern therapies, life expectancy for adults with idiopathic pulmonary arterial hypertension was less than 3 years from diagnosis; for children, it was less than 10 months and for newborns less than 5 days (237). Untreated patients with PAH have a 1-, 3-, and 5-year survival rate of 68%, 48%, and 34%, respectively(232). Treated, the survival rates improve to 91% to 97% after 1 year and 84% to 91% after 2 years (232).

Clinical Course and Histopathology

The clinical presentation of PH is non-specific; it begins with shortness of breath and chest pain with exercise and progress to dyspnea with normal activities and, finally, dyspnea at rest (238). Given this lack of specificity of PAH symptoms, the mean delay before diagnostic characterization is 2.8 years, during which time PAH worsens and the majority of cases have moderate to severe PAH at time of diagnosis (238). By then, patients have severe pulmonary vascular remodeling and RV dysfunction (238).

Pathologic findings show intimal hyperplasia and fibrosis, medial hypertrophy, and in situ thrombi of the small pulmonary arteries and arterioles. Peripheral arteries are muscularized while medial hypertrophy and neointima formation is noticed in proximal arteries with formation of plexiform lesions (figure 21) (232).

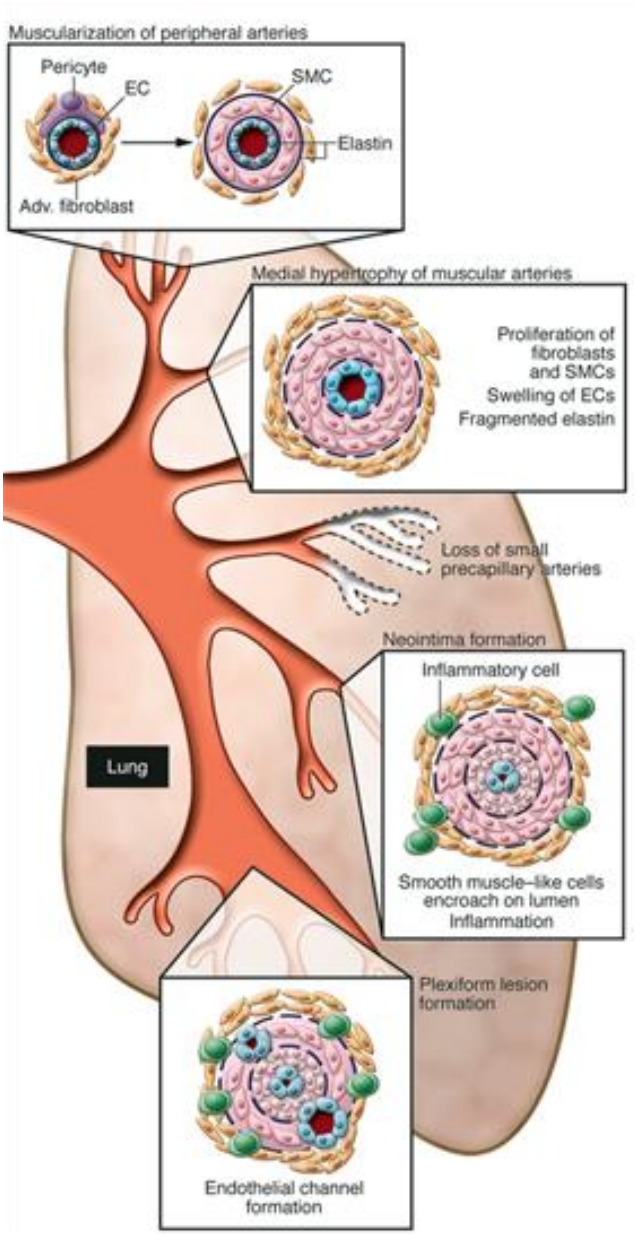

Figure 21. Vascular abnormalities associated with PAH. This schema depicts the abnormalities throughout the pulmonary circulation: abnormal muscularization of distal and medial precapillary arteries, loss of precapillary arteries, thickening of large PAs, and neointimal formation that is particularly occlusive in vessels less than 500–100 uM and in plexiform lesions therein. Adapted from Rabinovitch et all. J Clin Invest, 2013

Current Management of PAH

In the past 20 years, there have been progress in terms of PAH treatment and three classes of pulmonary vasodilators (defined as PAH-targeted therapy) have been approved for treatment of PAH in adults and children that target the prostacyclin pathway, the endothelin pathway or the nitric oxide pathway. Currently, there are 12 FDA-approved drugs for PAH available in the United States, each one targeting 1 of these 3 pathways. These include intravenous or subcutaneous prostanoids (epoprostenol or treprostinil), endothelin receptor antagonists (bosentan and ambrisentan) and phosphodiesterase type 5 inhibitors (PDE-5, Sildenafil and Tadalafil). PDE-5 inhibitors exert their pharmacological effect by increasing the intracellular concentration of cGMP. The soluble guanylate cyclase (sGC) stimulator, acting on NO pathway as PDE-5 inhibitors, riociguat was recently added (9, 239). Treatment with a single agent is usually started and in non-responders with severe disease combined therapy is recommended (240, 241).

General measurements for the management of PH also include exercise limitations, avoidance of physical activity after meals or in extreme temperatures, psychological

assistance and use non-specific pharmacological treatment with oral anticoagulant treatment, diuretics, digitalis and calcium-channel blockers as needed and only in "vasoreactive" patients that have a positive response to acute vasoreactivity testing (10-15% of IPAH) (231).

In case of PPHN, the current mainstay of therapy is first the treatment of the underlying condition along with several promising therapeutic modalities such as oxygen supplementation, mechanical ventilation, nitric oxide inhalation, phosphodiesterase inhibitors (pde-5; sildenafil, pde-3; milrinone), prostaglandins analogs, endothelin receptor antagonists and finally extracorporeal membrane oxygenation (141, 236, 242, 243).

The introduction of targeted PAH therapy have increased therapeutic options and potentially reduced morbidity and mortality; yet, none of the current therapies have been curative (244). Intravenous vasodilators dilate both the systemic and pulmonary vasculature and cause significant problems, including systemic hypotension, increased intrapulmonary shunting (i.e., increased V/Q mismatch), and increased hypoxemia (244). Consequently, selective pulmonary vasodilation with inhaled NO has only transient effects (244). Despite treatment advancements, there was no improvement in mortality, which still remains high.

Experimental Pulmonary Hypertension: animal models

Numerous animal models of PAH are currently available but the most commonly used ("classic" models) for the study of PAH are rodents exposed to either hypoxia or monocrotaline (245-247). These animal models have been extensively used and have undoubtedly contributed to a better understanding of the pulmonary hypertensive process.

The monocrotaline and hypoxic models resemble the basic features of human PAH but they do not recapitulate the pathologic picture of neointimal and plexogenic arteriopathy in patients with PAH (248). PH development in mice is of necessity faster and weaker compared to human disease. Despite the disadvantages, transgenic mouse models are a perfect tool for studying the processes involved in pulmonary vascular function and disease as it can effectively be used to test interventions designed against particular molecular pathways and processes (249).

In the monocrotaline model of PAH, the toxic pyrrolizidine alkaloid monocrotaline is injected in animals and is metabolized by hepatic oxidases to monocrotaline pyrrole and this active compound causes vascular injury through endothelial damage and adventitial inflammation, particularly macrophage accumulation, resulting in pulmonary hypertension and subsequent right heart failure (249, 250).

In the hypoxic model, chronic hypoxic exposure is utilized to induce PH reproducibly in a wide variety of animal species, but most frequently in mice and rats. Hypoxia induces changes in lung vasculature that most closely recapitulates human disease in comparison

with the monocrotaline model. The main advantage to hypoxia is its simplicity and reliability. This is probably why it is by far the most common model of PH found in the literature (249). In the current study we utilized the hypoxic model of pulmonary hypertension.

Upon exposure to low oxygen concentration (8% or 10%), vasoconstriction rapidly occurs and it is responsible for the rapid elevation of pulmonary arterial pressure (245, 247). Apart from acute vasoconstriction, oxygen deprivation results in dysfunction of oxidative phosphorylation/mitochondrial respiration and reduction in ATP production (251). Cells then rely on specific transcription factors; hypoxia inducible factors 1 and 2 (HIFs) for survival and adaptation to hypoxia. HIFs induce a transcriptional program of genes that regulate glucose and energy metabolism, cell survival and apoptosis, erythropoiesis, vascular tone and angiogenesis (252, 253).

Long term, chronic exposure of mice in hypoxia, via HIF or HIF cross talk with other transcription factors (such as NF-kB), induces smooth muscle cell proliferation and vessel wall remodelling in the vasculature by transcriptional activation of genes encoding vascular smooth muscle cell (VSMC) mitogens and inflammatory mediators such as vasoconstrictors (PDGF-B, VEGF, FGF, endothelin), growth factors, adhesion molecules (P selectin, ICAM, VCAM), cytokines and matrix proteins (fibronectin, laminin, proteoglycans) (247, 252, 254, 255). Sustained hypoxia leads also to the development of a complex, pro-inflammatory microenvironment, capable of promoting recruitment, retention and differentiation of circulating monocytic cell populations that contribute to vascular remodeling (256).

After 2 weeks of hypoxic exposure, muscularization and remodeling of small pulmonary arteries takes place as well as thickening and fibrosis and peripheral extension of smooth muscle in the media of small non- muscular arteries and arterioles. These pathogenetic changes recapitulate the elevation of right ventricular systolic pressure and right ventricular hypertrophy of human disease (247, 250, 257). In contrast with human disease, hypoxic animal models can be partially reversible upon return to normoxia. Thus, the chronic hypoxic models of PH in rodents could be regarded as models for less severe PH (247).

Pathogenesis of experimental PAH

Pulmonary arterial hypertension (PAH) is a devastating disease without effective treatment. Despite decades of research and development of novel treatments, PAH remains a fatal disease. The pathophysiological mechanisms of pulmonary hypertension are not fully understood, suggesting an urgent need for better understanding of the pathogenesis of PAH.

Despite the clinical heterogeneity of the entities listed in ‘Updated clinical classification of pulmonary hypertension (Nice, 2013) a common pathway resulting from a combination of genetic susceptibility and environmental factors seems to play a pivotal role in the

pathogenesis of pulmonary hypertension. This pathway is characterized by vasoconstriction due to constrictive agents, an imbalance of vasodilators as well as vascular remodeling.

Pulmonary vascular tone is regulated through a balance of vasoconstrictive and vasodilatory stimuli. The imbalance of vasoconstrictors and vasodilators leads to endothelial dysfunction early in the course of disease (258-260). Numerous vasoactive substances such as endothelin, carbon dioxide, thromboxanes, angiotensin II, platelet-derived growth factor-B (PDGF-B) and vascular endothelial growth factor (VEGF) and the recently recognized Fizz1 or HIMF are released from endothelial, smooth muscle cells and inflammatory cells in response to hypoxia or other stimuli and regulate vascular tone (2, 257, 261-263). When growth factors and mitogens bind to their receptors, various signaling pathways are activated which increase cytosolic calcium levels and activate the MAPK signaling pathway–stimulating transcription factors (c-fos, c-jun, c-myc, and so on) and increase cell proliferation (257). Prostacyclin's antagonistic effects act by increasing cAMP concentration, which simultaneously inhibits MAPK signaling. Also nitric oxide diffuses into the cell and stimulates cGMP production via guanylyl cyclase that results in relaxation of the SMC, leading to vasodilation (257). An increase in vasoconstricting factors such as angiotensin-II, endothelin-1 (ET-I), thromboxane A2 (TXA2), serotonin, Fizz1 and decrease in vasodilating factors such as nitric oxide (NO), prostacyclin, apelin, adrenomedulin, vasoactive intestinal peptide and atrial natriuretic peptide lead to endothelial dysfunction.

Following an initial endothelial injury, smooth muscle proliferation and progressive structural remodeling occurs characterized by a proliferative and anti-apoptotic state of cells within the vascular wall (smooth-muscle cells, fibroblasts, and endothelial cells) (235, 264). Clones of endothelial cells proliferate and give rise to plexiform lesions, the pathologic hallmark of this condition, while smooth-muscle cells and myofibroblasts proliferate and lead to medial hypertrophy and adventitial hyperplasia (235, 264, 265). Disruption of the extracellular matrix, infiltration of inflammatory cells, and thrombosis in situ combine to reduce the cross-sectional area of the small pulmonary arteries and stiffen the large pulmonary arteries, increasing the right ventricular afterload and leading to right heart failure (235, 264, 266).

All vessels layers, intima, media and adventitia are involved in the remodeling process. The thickening of the medial wall of previously muscularized pre-capillary pulmonary arteries is usually due to proliferation of local smooth muscle cells. Muscularization of non-muscular pulmonary arteries has also been noted in hypoxic animal models (267, 268). The appearance of SM-like cells (as defined by the expression of a-SM-actin) so called "distal extension of smooth muscle," has been noted in these vessels (267). Differentiation of pericytes, recruitment and differentiation of local fibroblasts to myofibroblasts and transdifferentiation of endothelial cells and recruited leukocytes into mesenchymal-like cells where it ultimately adapt a SMC-like phenotype have been proposed as the cause of

muscularization of previous non-muscular arterioles (267-270). In addition, there is medial and adventitial thickening of the muscular and elastic vessels. The medial thickening is believed to be attributable to hypertrophy and increased accumulation of smooth muscle cells as well as increased deposition of extracellular matrix proteins, predominantly collagen and elastin (267). The adventitial thickening is assumed to be caused by accumulation of fibroblasts and myofibroblasts and an often marked increase in extracellular matrix accumulation (collagens, elastin, fibronectin, tenascin) (267).

In the past few years our knowledge regarding the molecular mechanisms responsible for the pathobiology of PAH was remarkably increased. Key components has been revealed like as the Rho GTPases: Rac1 and RhoA (271), Wnt signaling (272), nitric oxide and prostacyclin (PGI2), serotonin (5-HT), serotonin transporter and receptors (273) angiopoietin (274, 275), Kv channels (233, 276, 277) and dysregulation of the insulin signaling machinery (e.g., decreased peroxisome proliferation activating receptor gamma signaling, increased insulin‑like growth factor signaling) (249, 278, 279).

Epigenetic mechanisms such as methylation of CpG islands, modification of histone proteins, and microRNAs have been also implicated in PAH pathogenesis (280). Over the past few years, an exponential increase in the number of publications on the role of miRNAs in PAH pathogenesis has emerged. Indeed, many features of PAH, such as inflammation and hypoxia, are known to modulate miRNA expression and could explain miRNA deregulation in PAH (238). MicroRNAs (miRNAs) are dysregulated in patients with PAH and in experimental pulmonary hypertension (281). Furthermore, normalization of a few miRNAs is reported to inhibit experimental pulmonary hypertension (282). MicroRNA-21, miR-124, miR-138, miR-424, miR-503, miR-204 and miR-206 play a significant role in regulating in pulmonary artery smooth muscle cell (PASMC) proliferation (278, 280, 283-287). MicroRNA-190 regulates hypoxic pulmonary vasoconstriction by targeting a voltage-gated K^+ channel in arterial smooth muscle cells (288). MiR-199a2 expression can ameliorate PH by reduction of ET-1 levels (289). Other microRNAs, such as miR-145, miR-21 and the miR17/92 cluster, have been associated with the disrupted BMPR2 pathway (283).

Furthermore, a genetic disposition appears to be important in some subtypes of pulmonary vascular disease (familiar PAH). In 2000, bone morphogenetic protein receptor type 2 (BMPR2) mutations was identified by linkage analysis as a genetic cause of PAH (290-292). In up to 70% of familial PAH and in up to 30% of idiopathic PAH patients are carriers of BMPR2 mutations (228, 290, 293-296). Since the landmark discovery that bone morphogenetic protein receptor type II (BMPR2) mutations cause the majority of cases of familial PAH, investigators have discovered mutations in genes that cause PAH in families without BMPR2 mutations, including the activin–like kinase type 1 (ALK1) and the endoglin (ENG) (both associated with hereditary hemorrhagic telangiectasia), caveolin-1 (CAV1), and a gene (KCNK3) encoding a two-pore potassium channel. Also endothelin receptor

polymorphism, nitric oxide synthase 3 polymorphisms, genetic variations in the Kv1.5 channel gene (KCNA5), potassium channel KCNK3, TGF-β, SMAD-9, Notch mutations mutations in eukaryotic initiation factor 2 alpha kinase 4 (EIF2AK4), carbamyl-phosphate synthetase gene and other genes have been associated with hereditary PAH (297-303).

In figure 22, a schematic diagram that summarizes the major components of PAH pathogenesis is illustrated.

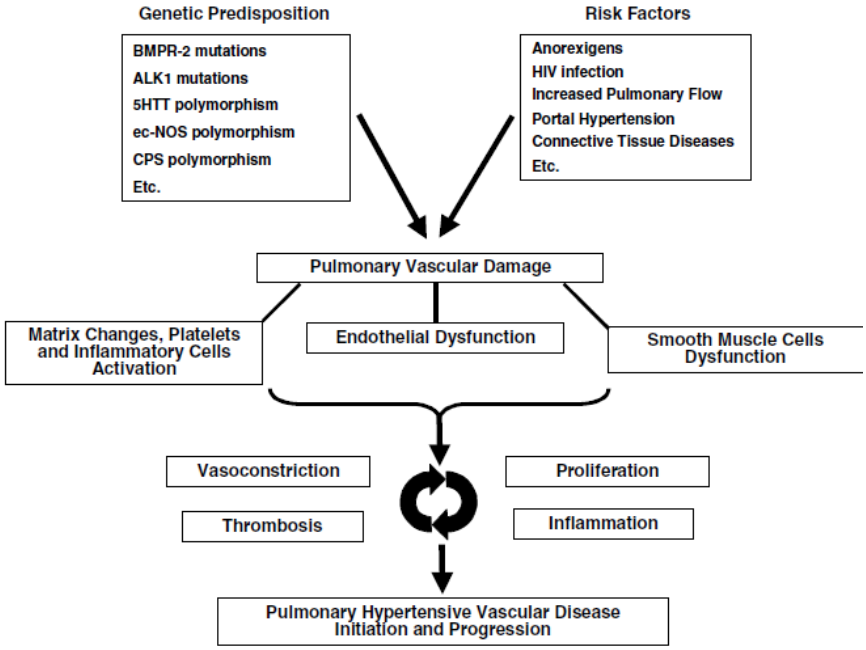

Figure 22. Pulmonary arterial hypertension: potential mechanisms. BMPR-2: bone morphogenetic receptor protein 2 gene; ALK 1: activin-receptor-like kinase 1 gene; 5-HTT: serotonin transporter gene; ec-NOS: nitric oxide synthase gene; CPS: carbamyl-phosphate synthetase gene. Adapted from Galie et al, Eur Heart J, 2004.

The role of inflammation in the pathogenesis of PAH

Inflammation has been recently demonstrated to play a significant role in various types of pulmonary hypertension in human and animal studies. An increasing number of studies support the idea of inflammation-mediated remodeling as a potential cause for the development of pulmonary hypertension (Figure 23). The development of hypoxia-induced pulmonary hypertension has been also recently associated with an inflammatory response in the lung (304).

Within a few years, upregulation of inflammatory markers has been extensively correlated with PAH. Fractalkine (CX3CL1), a chemokine that facilitates leukocyte recruitment, has been found upregulated in the T lymphocytes of PAH patients (305). The chemoattractant Regulated upon Activation, Normal T cell Expressed and Secreted (RANTES or CCL5) has been also reported to play a role in PAH via the induction of the vasoconstrictor endothelin-1 (306). Mediators of the lipoxygenase pathway were found to be highly expressed in animal models of PAH (307, 308). Other growth factors have been involved in

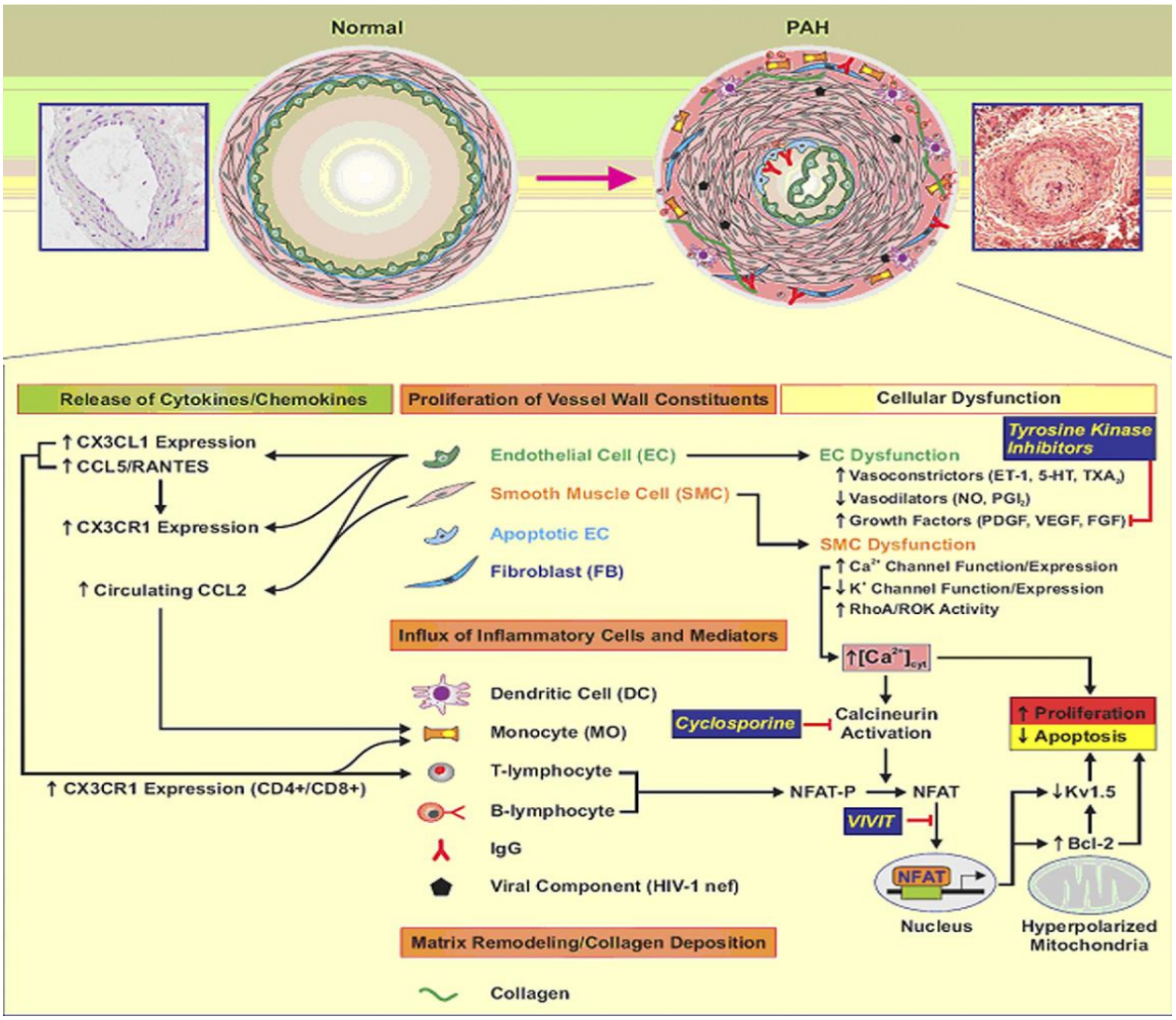

Figure 23. Mechanisms of Inflammation-Mediated Remodeling. Schematic diagram of inflammatory mediators, cells, and mechanisms involved in pulmonary vascular remodeling. Release of cytokines and chemokines in remodelled vessels (e.g., plexiform lesions) or in the circulation, from activated endothelial cells (ECs) and smooth muscle cells (SMCs), mediate the influx of inflammatory cells (e.g., monocytes, T and B lymphocytes). Cellular dysfunction (particularly involving EC and SMC) contributes to release of vasomotor and growth mediators, activation of transcriptional factors (e.g., nuclear factor of activated T lymphocytes [NFAT]), influx of calcium, and mitochondrial dysfunction. The net effect is a shift of balance in favour of cell proliferation and decreased apoptosis, leading to remodeling and narrowing of the pulmonary vascular lumen. Potential therapeutic target sites include inhibition with tyrosine kinase inhibitors, calcineurin with cyclosporine, and prevention of NFAT activation with VIVIT polypeptide. bcl2 = B-cell lymphoma 2; CCL2= chemokine (C-C motif) ligand 2; CCL5= chemokine (C-C motif) ligand 5 or RANTES (Regulated upon Activation, Normal T cell expressed and secreted); CX3CL1 _ chemokine (C-X3-C motif) ligand 1 (fractalkine); CX3CR1 = chemokine (C-X3-C motif) receptor 1; DC =dendritic cells; ET1= endothelin 1; FB = fibroblasts; FGF= fibroblast growth factor; 5-HT = serotonin; HIV-1 = human immunodeficiency virus 1; IgG = immunoglobulin G; MO = monocyte; NO = nitric oxide; PAH = pulmonary arterial hypertension; PDGF= platelet-derived growth factor; PGI2 = prostacyclin; ROK = Rho kinase; VEGF = vascular endothelial growth factor. Adapted from Hassoun et al, Eur Resp J, 2009.

vascular remodeling in animals such as VEGF, platelet derived Growth Factor (PDGF), epithelial Growth Factor (EGF), and Fibroblast Growth Factor (FGF-2) (228, 308).

The association between inflammation and vascular remodeling was further strengthened by the observation of elevated cytokine levels, such as IL-1b and IL-6, IL-8, TNF-α, IL-18, MCP-1, MIP-1α and adiponectin were found in the serum of patients with severe idiopathic PAH, in connect tissue disease associated PAH and in animal models of PAH (309-314). These cytokines are known to have pro-angiogenic and anti-apoptotic activities and acts as a growth factor for endothelial cells. Cytokines have been also demonstrated to promote proliferation and migration of VSMC *in vitro* (228, 315). Studies utilizing transgenic mice overexpressing IL-6 or IL-6 knock out mice showed a correlation between IL‑6 expression and the development of vasculopathy, reproducing conditions characteristic of severe PH in humans (249). Importantly, levels of certain cytokines, such as IL1β , IL-6, and tumor necrosis factor α, are predictive of outcome in patients with PAH (228).

Furthermore, upregulation of anti-inflammatory IL-10 have been found in patients with PAH, which could serve as counter-regulating mechanisms against the inflammation in lung tissue. Treatment with IL-10 in experimental PAH resulted in reduced mean pulmonary arterial pressure and significant improvement in survival from disease (228, 316).

Apart from the chemokine/cytokines involved in PAH, cellular immunity has been found to be of crucial importance. Increased infiltration of macrophages, dendritic cells, mast cells, T lymphocytes and to a lesser extent B cells have been found in the walls of pulmonary arteries and perivascular areas of the plexiform lesions from patients with PAH (317-320) and the degree of perivascular inflammation correlates with both vascular wall thickness as well as mPAP (308).

Adaptive immunity is active in patients with PAH. T cells are abundant in pulmonary vasculature in lungs from PAH patients. Cytotoxic CD8+ T cells even constitute the major part of the inflammatory component in plexiform vascular lesions. But T cells mostly adapt Th17 polarization implicating autoimmune inflammatory responses in PAH patients (321, 322). Also of regulatory T cells have been found in the lesions of PAH and their presence has been correlated with ameliorated disease (322, 323). B cells are also present in PAH lesions, and upon stimulation they produce autoantibodies which may explain the increased levels of antinuclear antibodies generally found in PAH patients (322).

The role of macrophages in PAH

Among the inflammatory cells implicated in PAH, cells of the monocyte/macrophage lineage appear to exert the most important role. Bone marrow-derived cells of the monocyte/macrophage lineage have been reported to mobilize to the hypertensive pulmonary arteries and contribute to the pulmonary vascular remodeling in rat, calf and mice models of hypoxia-induced pulmonary hypertension and in human idiopathic PAH (228, 324, 325). Accumulation of mesenchymal stem cell precursors of a monocyte/macrophage

lineage and upregulation of various inflammatory mediators in the pulmonary artery adventitia of neonatal rat and calf models of disease have been recently reported to play a critical role in hypoxic vascular remodeling (325-327).

Macrophages accumulate in large numbers in such hypoxic/ischemic tissues and respond to hypoxia by upregulating a number of transcription factors such as hypoxia-inducible factors (HIFs) 1 and 2 and NF-κB (328, 329) leading to activation of the pro-inflammatory cytokines IL-1β, MIP-2 and MCP-1 (330, 331). Activation of macrophages induces the release of IL-1β, IL-6, tumor necrosis factor-α, and IL-10, which all play an important role in the pathogenesis of PAH (figure 24) (228). Furthermore activated macrophages may present antigens to T cells resulting in T-cell activation and T-cell derived cytokine production, which further facilitates the inflammatory process associated with PAH (228). Also the macrophages that are recruited in the vessel wall, together with fibrocytes can be differentiated into mesenchymal cells/myofibroblasts and contribute to muscularization of arteries (figure 24) (267, 332). The contribution of circulating mononuclear cells in vascular remodeling process was confirmed by depletion studies in hypoxic animal models of PAH. A striking reduction in adventitial thickening as well as a near complete inhibition of the accumulation of collagen, fibronectin, and tenascin-C were documented in which the number of these cells was reduced in the circulation of hypoxic rats (256, 267). Macrophage elimination results in attenuated inflammatory response in the lung and systemic inflammation (333, 334).

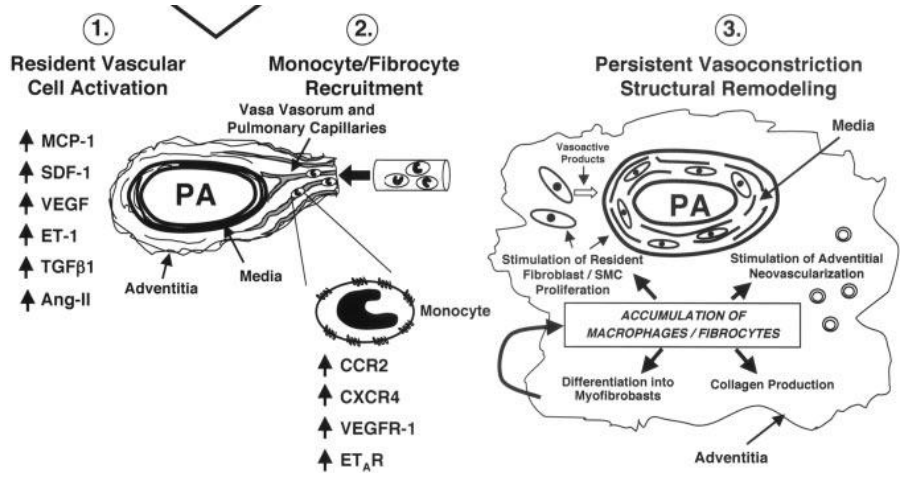

Figure 24 . Schematic representation of the potential roles of resident and circulating monocytes and fibrocytes in the hypoxia-induced structural vascular remodeling process. (1) Hypoxia activates resident endothelial cells, adventitial fibroblasts or medial SMCs to secrete chemokines/cytokines that (2) induce recruitment of circulating monocytes/ fibrocytes to the pulmonary perivascular space, where (3) these recruited cells promote differentiation into mesenchymal cells/myofibroblasts, production of collagens, and stimulation of resident vessel wall cell contraction and proliferation. Adapted from Stenmark et al, Circ Res, 2006.

The Heme Oxygenase in PAH

Heme Oxygenase -1 (HO-1), also known as heat shock protein 32, is a 32-kDa protein induced by heat, heme, hypoxia, hyperoxia, oxidative stress, acidosis, shear stress, stretch and several cytokines (335). Under normal physiological conditions, HO-1 is expressed at low levels in vascular smooth muscle cells (VSMCs) and cardiomyocytes (335, 336). However, under pathophysiological conditions, only HO-1 is induced in the heart and blood vessels (335, 336).

HO-1 is a major antioxidant and cytoprotective enzyme that catalyses the rate-determining step in the breakdown of heme to three enzymatic end-products: CO, free Fe^{2+} and biliverdin which is reduced subsequently to bilirubin (337, 338). The role of HO-1 is vital in the cells since its activity helps the cells to cope with the problem of free heme accumulation, a potential pro-oxidant molecule when accumulated in high levels. By degradation of the pro-oxidant heme and generation of the anti-oxidant bilirubin, HO protects cells against oxidative injury (339, 340). These three metabolites of heme by HO reactions have also additional important functions and are involved in various critical cellular events (338).

HO-1 has been reported by our group and others to be induced by hypoxia and to be protective in hypoxia-induced pulmonary hypertension (246, 304, 341-343). This protection, up to now, has been mainly attributed to the relaxation of vascular tone and inhibition of VSMC proliferation by CO (342, 344). However, studies have shown that HO-1 has anti-inflammatory properties (345-350). These findings were supported by the fact that HO-1-deficient mice develop a chronic inflammatory state that progresses with age (341, 351). Moreover, the only human reported to lack HO-1 died of a chronic systematic inflammatory syndrome and inability to handle oxidative stress (348). Mice deficient in HO-1 have a maladaptive response to hypoxia and develop right ventricular dilation with fibrosis, formation of thrombus and inflammation (341).

Although the anti-inflammatory mechanisms of HO-1 are largely unknown, HO-1 and its enzymatic products, carbon monoxide and bilirubin, downregulate the inflammatory response by either attenuating the expression of adhesion molecules in endothelial cells and thus inhibiting leukocyte recruitment, by repressing the induction of cytokines and chemokines, and by suppressing excessive macrophage and antigen presenting cell activation while enhancing anti-inflammatory effects like upregulating IL-10 cytokine in macrophages and inducing regulatory T cells (352-358).

Among the end products of HO-1, CO has been demonstrated to be critical for the anti-inflammatory properties of HO-1 in models of acute lung injury, endotoxin, shock, and from our studies in pulmonary hypertension (345-350). Like nitric oxide, CO is a gas that freely diffuses in the adjacent cells and can reach its target molecules independently of receptors

and transporters (245). It can stimulate soluble guanylyl cyclase and thus increases intracellular levels of cGMP, an important regulator of vascular tone and smooth muscle growth (342, 344).

The transient effects of hypoxia are mediated by the smooth muscle cells via the increased expression of HO-1 resulting in increased CO production. Increased CO levels inhibit smooth muscle cell growth in an autocrine manner and inhibit the endothelial expression of ET-1 and PDGF-B, thereby inhibiting smooth muscle cell contractility and proliferation in a paracrine manner (245). Exogenous CO administration is protective in PAH and can reverse the disease in animal models of PAH (359). However, under prolonged periods of hypoxia, HO-1 and CO production is not sustained and thus the endothelial cell pathway predominates, leading to active and sustained vasoconstriction with structural remodeling of the pulmonary vasculature (245). Based on this model, a sustained expression of HO-1 leading to increased CO levels could prevent or reduce the development of hypoxic pulmonary hypertension *in vivo* (245).

Physiological roles for CO, both exogenously applied or hypoxia induced CO, involve modulation of cGMP levels, vasodilation, the inhibition of platelet aggregation, and anti-proliferative effects on smooth muscle (343, 360). There is growing interest in the role of CO in the anti-inflammatory and cytoprotective function of HO-1, but the pathways involved in the anti-inflammatory effect of CO are poorly understood. CO application has been found protective in several models of acute lung injury caused by LPS, hyperoxia, acid aspiration of ischemia/reperfusion (361-365). CO can modulate mitogen-activated protein kinase and guanylate cyclase/guanylate cyclic monophosphate (cGMP) pathway to inhibit secretion of pro-inflammatory cytokines (361-365). CO also modulates several transcription factors, including NF-kB and activating protein-1 (AP-1), which are involved in inflammation (361-365). Both *in vivo* and *in vitro*, carbon monoxide at low concentrations differentially and selectively inhibited the expression inhibited Toll-like receptor (TLR) 2, 4, 5, and 9 signaling in macrophages and the lipopolysaccharide-induced pro-inflammatory cytokines tumor necrosis factor-a, interleukin-1b, and macrophage inflammatory protein-1 and increased the lipopolysaccharide-induced expression of the anti-inflammatory cytokine interleukin-10 (343, 363, 364, 366).

Apart from CO, biliverdin and bilirubin also protect from vascular remodelling in chronic hypoxia (367). Bilirubin, in low concentrations, is a scavenger of ROS *in vitro*, reduces oxidant-induced cellular injury and attenuates oxidant stress *in vivo* (340). Biliverdin exert their protective effects largely though its anti-oxidant properties (339, 368). Similar to CO, biliverdin administration has been found to protect against LPS induced acute lung injury in rats, via reduction of serum levels of the LPS-induced proinflammatory cytokine IL-6 and augmented expression of the anti-inflammatory cytokine IL-10 (369).

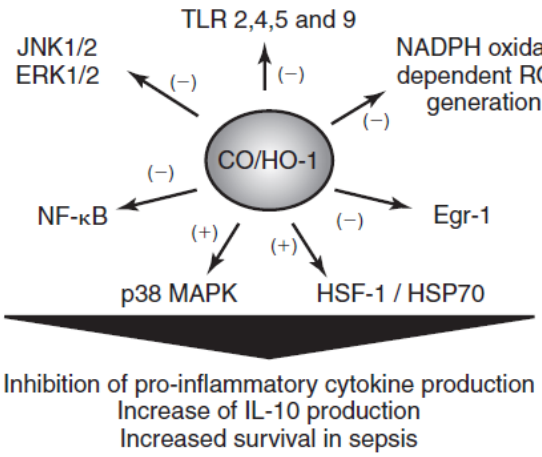

Figure 25. Role of HO-1/CO in inflammation. HO-1/CO can downregulate inflammation by several mechanisms. CO inhibits LPS-inducible proinflammatory cytokine production in macrophages by modulation of p38 MAPK, and through inhibition of ERK1/2 and JNK-dependent pathways. CO can downregulate ROS production, Toll-like–receptor trafficking and inhibit nuclear transcription factor activities during inflammatory signaling such as NF-kB or EGR-1. Upregulation of the heat-shock protein-70 (hsp70) through heat-shock factor-1 (HSF-1) has also been implicated in CO-mediated anti-inflammatory tissue protection. Adapted from Ryter et al, Antiox Redox Signal, 2007.

Biological treatments targeting inflammation in PAH

The aforementioned inflammatory pathways involved in PAH may serve as novel potential specific therapeutic targets. Although current PAH treatments possess immunomodulatory properties there is no approved therapeutic specifically targeting the inflammatory processes. Up to now many experimental treatments specifically targeting inflammation are of interest and appear to work in experimental PH.

A great majority of studies have been focused in the immunomodulatory effect of stem cells and their products (370). There is a wide range of cell types that could be used to repair and regenerate the lung microvasculature in PAH via modulation of inflammatory response and are currently tested in clinical trials. Although autologous adult stem and progenitor cells present the least risk, they likely offer the least potential for direct tissue repair and regeneration. In contrast, pluripotent stem cells have the greatest capacity for transdifferentiation and regeneration. Mesenchymal stem cells (MSCs), endothelial progenitor cells and adipose-derived stem cells (ADSCs) have been found to colonize the pulmonary arteries, attenuate pulmonary arterial hypertension and ameliorate pulmonary arterial remodeling (371-374). MSCs, whose mechanism of action is predominantly paracrine, are being widely tested for the treatment of a variety of human diseases. No one factor has been proven sufficient to mediate the therapeutic effects of MSCs. However, exosomes-membrane vesicles secreted by MSCs, can transport and deliver a large variety of proteins, lipids, and nucleic acids and can modify cell and organ function are also are appealing candidates as vectors of their efficacy (221, 375, 376). Because of the efficacy of cell-based gene transfer with non-regenerative “carrier” cells, the genetic enhancement of these cells could result in synergistic benefits from the reparative cell activity and the therapeutic transgene. And lately a number of different therapeutic transgenes have been assessed in combination with MSCs (377).

Glucocorticoids have been shown to prevent experimentally‐induced PH when used early in the course of disease via anti-inflammatory mechanisms and been shown efficacy in several case series in PAH associated with SLE or with mixed connective tissue disease (378). But in the latter case, there was a dramatic clinical deterioration of PAH symptoms after completion of GC treatment (378).

Inflammatory processes appear to play an important role in the vascular remodeling characteristic of PAH and might be important targets for PAH therapy. Deciphering their exact mechanisms of action in the process of pulmonary vascular remodeling will provide a wide spectrum of potentially novel targets that are desired considering the currently limited array of modern PAH therapies.

OBJECTIVES

Biological significance-Objectives

Aim of this study is to examine the role of innate immunity and specifically macrophages in the pathogenesis of two models of acute and chronic lung disease; in acute lung injury and pulmonary arterial hypertension. In this study we will characterize the temporal pattern of innate immune response and macrophage activation phenotype during the course of the above lung diseases and we will investigate the role of this response in the outcome of the disease. We will also utilize methods to modify the inflammatory response and the macrophage activation state *in vivo* in an effort to prevent disease development.

Part 1: Acute lung injury

In the first part of this study on acute lung injury, we will use three mouse models of ALI, two aseptic; acid aspiration-induced ALI and ventilation –induced lung injury and one septic; P. aeruginosa associated lung injury. Our first goal is to determine the nature of macrophage activation among different types of experimental acute lung injury and inflammation and to determine whether an M1 to M2 response takes place in the course of disease. Since M1 activation is known in ALI, we aim to define the critical time window in which M1 macrophages are the predominant population in ALI and whether this response if followed by M2 activation.

Subsequently, to evaluate the contribution of macrophage polarization in the development of ALI we aim to enhance M2 macrophage activation, using Akt2 knock-out mice. We have previously shown that macrophage polarization is controlled by the Akt kinases; deletion of Akt2 renders macrophages M2–prone (49). By inducing in Akt2-deficient mice, we will investigate the role of alternative macrophage polarization in the development of ALI.

Since the signaling pathways that lead to M2 have not been characterized yet we aim to shed light on the role of macrophage polarization towards the alternative pathway and improve our understanding of the function of these cells, focusing on the role of Akt kinases and their downstream signaling molecules. Finally, to expand this result to a potential therapeutic application and to facilitate M1 to M2 switch *in vivo* during the course of ALI, we will test the effectiveness of targeting critical molecules of M2 polarization such as Akt2 and downstream targets of Akt2 kinases, aiming at modulating the course of disease.

Part 2: Pulmonary hypertension

In the second part of the study, the primary goal is to delineate the nature of the inflammatory response that leads potentially, in a causative way, to pulmonary vascular

remodeling and hypertension. We will use the hypoxic model of pulmonary hypertension, aiming to highlight the specific components of inflammatory response caused by hypoxia and to pose a putative link between hypoxia-induced lung inflammation and pulmonary hypertension.

It has been previously reported by our laboratory that constitutive overexpression of heme oxygenease-1 can block both hypoxic inflammatory response and pulmonary hypertension in mice (304). Therefore, in order to shed light on the role of inflammation in the development of pulmonary hypertension we generated a bitransgenic mouse model with dox - inducible, lung-specific expression of HO-1. This model allow us to turn on and off HO-1 expression, by this way, turn off and on the inflammatory response in the lung respectively, and investigate its role in the development of pulmonary hypertension. By the use of a bitransgenic mouse model with inducible HO-1 overexpression we will be also able to assess the anti-inflammatory properties of HO-1 in this context and elucidate the critic al temporal therapeutic "window" that is adequate for HO-1 to exert its protective effects.

Recognition of inflammatory cells and mediators as major players in the smooth muscle cell hyperplasia and growth may introduce new therapeutic options for the treatment of pulmonary hypertension.

Summary – Significance of the study

ARDS and pulmonary hypertension are devastating disorders characterized with high morbidity and mortality. Still the present pharmacological interventions for ARDS and PH are primarily supportive in nature. Despite the growing evidence in the field, the cellular and molecular mechanisms that lead to the development of ARDS and PH remain incomplete. Their understanding is the basis to tailor targeted therapies and reduce mortality.

In summary this study will provide information on inflammatory response and macrophage polarization during the course of experimental ALI and PH. Additionally it will investigate molecular mechanisms that regulate lung inflammatory response and macrophage phenotype switch, and examine methods to promote macrophage switch *in vivo* as a therapeutic strategy in these diseases.

METHODS AND MATERIALS

Materials and Methods

Acute lung injury

- **Aseptic Acute Lung Injury: Hydrochloric Acid - induced Acute Lung Injury in mice**

To induce acute lung injury with hydrochloric acid (HCL), 8-10 weeks old C57BL/6 mice, either WT mice or mice lacking the *Akt2* gene, were anesthetized with intraperitoneal (i.p) injection of a mixture of ketamine (100mg/kg) and xylazine (6mg/kg). Then, mice were endotracheally intubated, external trans-illumination of the neck was used to facilitate visualization of the trachea through the oropharynx and various concentrations of HCL, 0.01N, 0.025N, 0.05N, and 0.1N diluted in normal saline (0.9% NaCl) that correspond to gradually reduced solution pH (Table 6), were instilled in the trachea (Figure 26).

Figure 26: Expression of glottis for intratracheally intubation in mice

Among the above HCL concentrations, 0.05N was chosen as optimal as it could provoke reproducibly significant lung injury of moderate severity with relatively mild neutrophilic response compared to 0.1N concentration. It is more clinically relevant since it correlates with gastric acid pH.

Mice were endotracheally intubated and 0.05N HCL solution (pH≈1.5) in a volume of 2ml/kg diluted in normal saline (0.9% NaCl) was instilled in the trachea; while age and gender matched mice received 2ml/kg of normal saline and served as controls. A bolus of 0.5ml of air was given to ensure that HCL solution reaches the distal lung. Mice were then extubated and left to recover from anesthesia. Administration of 100% O_2 for 5-10 minutes allowed restoration of a normal breathing pattern after HCL administration.

HCL concentration	Solution pH
0.01N	1.8
0.025N	1.5
0.05N	1.25
0.1N	1.1

Table 6: Approximate pH values of HCL solutions diluted in Normal Saline.

Then, at specific time points following HCL administration, mice were sacrificed and pressure-volume curve of the respiratory system was measured, bronchoalveolar lavage (BAL) and blood serum was collected and lung tissue was harvested for RNA analysis and histology.

In total, 486 mice (WT; n=278, Akt2-/-; n= 208) for acid-induced lung injury were used. Due to sample insufficiency, not all mice were used for all assays. The specific number of samples used is mentioned in the figure legends. A large number of animals were used as alveolar macrophage donors for *ex vivo* experiments.

The indices of lung injury examined were lung compliance, obtained from the pressure volume curve of the respiratory system, protein concentration, inflammatory cells, cytokines in bronchoalveolar lavage (BAL) and lung histology (Table 7).

Table 7. Indices of Acute Lung Injury

-Lung Compliance
-Protein extravasation
-Cellular and humoral lung inflammatory response
-Histological injury

All mice were kept in the pathogen free environment of the animal house of Institute of Molecular Biology and Biotechnology in Heraklion, Crete. All procedures described above were approved by the Veterinary Department of the Heraklion Prefecture (Heraklion, Crete, Greece).

- **Aseptic Acute Lung Injury: Ventilation Induced acute lung injury (VILI) in mice**

To induce ventilator-induced lung injury (VILI), we used an established model of VILI in our lab as previously described (154, 183), in which C57BL/6 mice are ventilated with high tidal volume for 3.5 hours. Specifically, 8-10 weeks old C57BL/6 mice, mice, either WT mice or mice lacking the *Akt2* gene, were anesthetized, with intraperitoneal (i.p.) injection of ketamine 100 mcg/g and fentanyl 0.12 mcg/g [33], subjected to tracheostomy and connected to a rodent ventilator (SAR-830, IITC Life Science, Woodland Hills, CA, USA) (Figure 27).

Figure 27
Mouse ventilator SRA -830

Initially mice were ventilated with normal rate and volume (VT 10 ml/kg resulting in peak inspiratory pressure (PIP) = 9 ± 0.5 cmH_2O, PEEP 1.5cmH_2O, FiO2 30%, f 135bpmin, with recruitment manoeuvres performed every 30 min.), while receiving intravascular volume resuscitation to prevent hypotension. Fluids and anaesthetics (fentanyl, ketamine) were continuously infused from a catheter placed in the carotid artery. Subsequently, after 30 min of haemodynamic stabilization, ventilator settings were changed to high tidal volume (approximately 45 ml/kg, targeted to a PIP = 35 ± 0.5 cmH_2O, FiO2 30%, f 60 breaths/min, PEEP = 1.5 cmH_2O, without recruitment maneuvers) and mice were ventilated for another four hours to induce VILI, while another group of mice were left in low volume ventilation and served as controls. Inhaled carbon dioxide (CO_2) was added in high VT groups to prevent hypocapnia. Arterial blood pressure, PIP, PEEP, and VT were monitored throughout the study. Airway pressure, flow and volume were measured using a pneumotachograph (8431B Hans Rudolf Inc, USA) and a transducer (Micro-Switch 140PC, Honeywell, Ontario, Canada). All signals will be sampled at 150 Hz using Windaq software (Windaq Instruments Inc, OH, USA). Throughout

the experiment, rectal temperature will be monitored and maintained within the normal range using a heating lamp.

At the end of the experiment, blood was collected from the arterial line for blood gas analysis, followed by inspiratory pressure volume curve and bronchoalveolar lavage fluid (BALF) and tissue collection.

Septic Acute Lung Injury: Pseudomonas aeruginosa lung infection

To induce a septic model of lung injury (pneumonia), a clinical strain of *Pseudomonas aeruginosa* (kindly provided by Dr E. Skoulika, Department of Microbiology, Medical School, University of Crete) was maintained frozen in glycerol stocks. One day before lung infection, bacteria were thawed, inoculated into Luria-Bertani (LB) broth and incubated overnight at 37°C. From this culture, an aliquot was taken to start a fresh culture that lasted 6-7 hours. Bacterial concentrations were estimated from a standard curve based on optical density (OD600). *P. aeruginosa* was then harvested by centrifugation (3,500rpm 10min), followed by washes and an appropriate final dilution with sterile NS. The inoculum number was retrospectively confirmed through plating of serial dilutions and counting of colony forming units (CFU) on LB plates.

C57BL/6 WT and Akt2-/- mice were anaesthetized as described above and a volume of 40 μL of bacterial solution (2×10^7 bacteria approximately) or the corresponding vehicle solution (NS) was applied intratracheally. Animals were sacrificed 12 hours after inoculation, and pressure volume curve of the respiratory system, bronchoalveolar lavage and lung tissue for histology was obtained. Protein levels, cytokine concentration and WBCs numbers were determined in BALF. To determine bacterial load (colony forming units, CFUs), serial 10-fold dilutions of the BAL fluid were plated on agar plates. The results are expressed as mean CFU per mL of BAL fluid.

In total, 28 mice (WT; n=14, Akt2-/-; n= 14) were used. The specific number of samples used is mentioned in the figure legends. All mice were kept in the pathogen free environment of the animal house of Institute of Molecular Biology and Biotechnology in Heraklion, Crete. All procedures described above were approved by the Veterinary Department of the Heraklion Prefecture (Heraklion, Crete, Greece).

Vascular Lung injury

Hypoxia – induced lung inflammation and pulmonary hypertension

Hypoxic exposure is well known to promote the development of lung oxidative stress and pulmonary hypertension. To induce chronic lung inflammation and pulmonary

hypertension, animals were introduced to normobaric hypoxia (8.5% O2) for at least 2-3 weeks inside a chamber where oxygen was tightly regulated by an Oxycycler controller (Biospherix, Ltd., Lacona, NY). Nitrogen was automatically introduced as required to maintain the proper FiO_2 and ventilation was adjusted to keep CO_2 levels less than 8,000 ppm (0.8%). Ammonia was removed by charcoal filtration using an electric air purifier. Age and sex-matched littermates were exposed to identical conditions in normoxia and served as controls.

From each animal, hemodynamic measurements took place prior to sacrifice, followed by bronchoalveolar lavage, harvesting of heart and inflation of lungs for histology. One lobe was sutured prior to inflation, frozen in liquid nitrogen and stored at -80°C for mRNA and protein analysis.

In total, 1832 mice (WT FVBs; n=160, CC77; n=1580, CCTA; n=135) for hypoxia induced PAH were used. Due to sample insufficiency, not all mice were used for all assays. The specific number of samples used is mentioned in the figure legends. A large number of animals were used as alveolar macrophage donors for *ex vivo* experiments.

Animals were maintained in a pathogen-free environment in the Children's Hospital Animal Care facility and all animal experiments were approved by the Children's Hospital Boston Animal Care and Use Committee.

Use of HO-1 bitransgenic mice to study hypoxia induced lung injury

To evaluate the role of macrophages in hypoxic induced lung injury, we utilized a bitransgenic mouse line (CC77 is our working designation) that overexpresses human HO -1 in an inducible lung-specific way. HO-1 overexpression was chosen since the HO-1 is well recognized anti-inflammatory enzyme known to protect from hypoxia induced PAH. In order to regulate HO-1 expression and thus inflammatory response, bitransgenic mice have been generated in our lab by crossing of Balb/c transgenic mice that harbor the reverse tetracycline transcriptional activator (rtTA, tetON system) under the control of the Clara Cell secreted protein (CCSP) promoter (CCTA line: a kind gift from Dr. J.A Whitsett) (379) with FVB transgenic mice that carry the human HO-1 transgene under the control of the tetracycline response element (TH77 line: CCSP-rTTA x TRE-hHO1xSV40 polyA). The latter was generated by microinjection of a $(TetO)_7$-CMV-human HO-1 transgene that consists of seven copies of the tet operator linked to a minimal CMV promoter, the human HO-1 cDNA, and SV40 polyadenylation signals (figure 28).

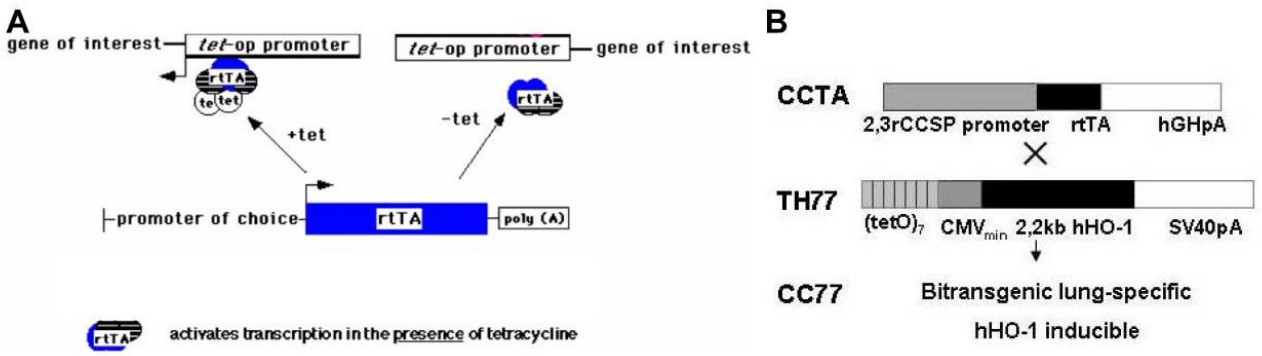

Figure 28. Inducible HO-1 expression by a bitransgenic mouse line A, The tetON System for inducible tissue specific expression of the gene of interest. Only upon the presence of dox, the tetracycline transactivator initiates transcription. B. Outline of the constructs designed. Bitransgenic mice (CC77) were produced by crossing of mice bearing the reverse tetracycline transactivator (rtTA) under the control of the 2.3-kb rat CCSP (Clara cells secreted protein) promoter (CC10) (CCTA mouse line) with transgenic mouse line (TH77) generated by microinjection of a (TetO)7-cmv-hHO-1-polyA transgene.

Expression of human HO-1 in the lung was achieved by the addition of 1 mg/ml doxycycline (dox) (Sigma-Aldrich, Inc., St. Louis, MO) in the drinking water. The CCTA (CCTA is our working designation) mouse line that lacks the human HO-1 transgene, treated with dox, served as control to eliminate any potential effects imparted by dox itself, independent of human HO-1 expression.

After two days pretreatment with dox, animals were introduced to normobaric hypoxia (8.5% O_2). Dox administration was either continued for the entire duration of the hypoxic exposure or terminated at two days or after seven days of hypoxia (overview of experimental design is illustrated in figure 29. Age and sex-matched littermates were exposed to identical conditions in hypoxia or normoxia and served as controls.

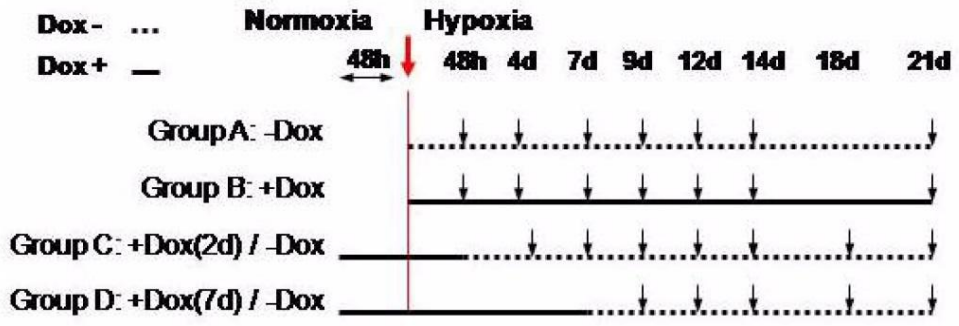

Figure 29. Overview of the duration of hypoxic exposure, dox administration and withdrawal in different animal groups. Arrows indicate time points were animals were sacrificed, BAL was collected, lungs and hearts were harvested.

***In vivo* treatments**

Depletion of alveolar macrophages with liposomal clodronate and macrophage reconstitution

Suspensions of multilamellar liposomes encapsulating clodronate were prepared according to Van Rooijen method (380). Clodronate and lyophilized liposomal preparations were obtained from Sigma (St. Louis, MO). Specifically, the liposomes were resuspended with 1ml clodronate and mixed thoroughly. Liposomes were maintained in suspension for 2h at room temperature (for liposome swelling). Empty liposomes were made by the addition of sterile PBS alone. This solution was ultra-centrifuged at 10,000*g* for 30min at 4C. The liposomal pellets were then removed and resuspended in PBS, followed by ultra-centrifugation at 10,000g for 30min at 4C. Subsequently, liposomes were resuspended in 1 ml of sterile PBS, stored at 4C, and used within 48 h. The final concentration of the liposomal clodronate suspension was approximately 20 mg/ml and was diluted 1: 3 prior to intratracheal administration (6,5mg/ml).

Based on preliminary experiments and on published observations (208, 381), maximum macrophage depletion is achieved 1 day after i.t clodronate administration and may last for up to 3days. Fifty microliters of the diluted liposomal suspension were intratracheally instillated in a single dose 3days before the induction of ALI in WT and Akt2-/- mice. Subsequently, approximately 250.000 naïve alveolar macrophages harvested from BALF from WT and Akt2-/- mice were transferred to WT and Akt2-/- mice 1hour prior to HCL administration. Macrophages collected from different mice of the same genotype were pooled together prior to transfer, washed twice with PBS, and filter via a cell strainer to eliminate transfer or epithelial cell debris. The groups of mice and the treatment they received are depicted in table 8. Mice were sacrificed 12hour after HCL intratracheal instillation.

Table 8. Macrophage adoptive transfer- experimental groups.

	Mouse genotype	***Mφ transferred***	***Lung Injury***
Control Group	WT	WT Mϕ	w/o
Group 1	WT	WT Mϕ	12h HCL
Group 2	WT	Akt2-/- Mϕ	12h HCL
Group 3	Akt2-/-	WT Mϕ	12h HCL
Group 4	Akt2-/-	Akt2-/- Mϕ	12h HCL

Application of siRNA and miRNAs *in vivo*

Before the application of the siRNA targeting *Akt2*, several experiments utilizing siRNA targeting GAPDH took place in order find out the optimal effective dose needed. SiRNA targeting *GAPDH* or siRNA targeting *Luciferase* was initially instilled intratracheally in the lung in three different concentrations (0.5nmoles, 2.5nmoles or 5nmoles per mouse) and 5nmoles per mouse was chosen as the minimal concentration that promoted reproducibly significant GAPDH mRNA and protein suppression, 48h and 72h post administration respectively, with minimal lung toxicity. Toxicity was assessed by the grade of neutrophilic infiltration in the lung, the amount of protein extravasation and the induction of TNF-α and IL-6 in BALF caused by the siRNA itself, in mice subjected to siRNA instillation compared to normal saline.

The percentage of alveolar macrophages that received the siRNA was assessed by flow cytometry analysis (described below) 12h, 48h and 72hours after administration of Cy3 labeled siRNA targeting *Luciferase*. The effectiveness of GAPDH mRNA suppression in alveolar macrophages was also assessed by mRNA analysis via qPCR, 12h and 48h after siGADPH administration.

To evaluate distribution of siRNA in the lung, Cy3 conjugated siRNA targeting *Luciferase* was used. 5nmoles per mouse were intra-tracheally administrated and lungs were harvested 24 hours later. Lungs were inflated in 4% PFA, fast frozen, then immersed in 20% sucrose and prepared for microtome sections. DAPI staining (Thermo Fisher Scientific, Inc., Waltham, MA) was carried out and tissues were observed under fluorescent microscopy. Lungs from mice that received normal saline exhibited mild fluorescence signal attributed to high autofluorescence of lung tissue.

The sequence of siRNA targeting *Akt2* is depicted in table 9. However, the siRNA used *in vivo* targeting *Akt2* contain 2'-O-Methyl modifications increasing their *in vivo* stability and reducing immune response activation (382, 383). Its effectiveness in suppressing *Akt2* was verified *in vitro* before *in vivo* application. Based on the aforementioned dose response experiments and on previously reports that applied naked siRNA and miRNA in the lung (215, 384-386); 5nmoles of siRNA targeting *Akt2,* 1nmole of miR-146a mimic or 0,6nmoles of miR-146a inhibitor (Anti-miR-146a) (Life technologies Corp, Carlsbad, CA) were instilled intra-tracheally in each mouse in volume of 50μl normal saline prepared from nuclease free water. In case of siRNA experiments, two doses of siRNA were administered, the first 48hours before the instillation of HCL acid and the second, one hour after acid-aspiration. MiR-146a mimic and inhibitor were instilled one hour after the instillation of HCl acid. In both cases, mice were sacrificed 24 hours post acid-aspiration. SiRNA targeting *Luciferase* and non-targeting miRNA control (scramble) were used as experimental controls respectively.

Table 9. SiRNA targeting Akt2	
Sense siRNA sequence	ACC/OmeU/UAUGUUGGACAAA/OmeG/A/OmeU/OmeU/
Antisense siRNA sequence	/5Phos/UCUUUGUCCAACA/OmeU/AAG/OmeG/Utt

Administration of HO-1 products, CO and biliverdin

To find out which of the H0-1 products is responsible for HO-1 effect and to recapitulate HO-1 response in WT mice without genetic intervention, HO-1 products CO and biliverdin were administrated in WT mice exposed to hypoxia.

Specifically, CO treated mice inhaled CO gas intermittently: 250 ppm for 1 hour prior to hypoxic exposure and then received 250 ppm for 1 hour twice daily, inside the hypoxic chamber for a total of 48 hours. A group of mice underwent i.p injections of 50 μmol/kg biliverdin IX hydrochloride (Frontier Scientific, Inc., Logan, UT) as previously reported (387), prior to the onset of hypoxia and twice daily thereafter. Finally, a third group received both CO and biliverdin as above. Control mice were injected i.p with the same volume of PBS and inhaled room air or hypoxic air (8.5% O2) without CO.

Assessment of Lung Injury

Pressure volume curve of the respiratory system

A pressure-volume curve of the respiratory system was obtained by slow lung inflation to peak airway pressure of 25cmH_2O, as previously described (supersyringe method) (183, 388). Briefly, myochalasis was induced by i.p injection of pancuronium (4mg/kg) and mice were mechanically ventilated for 5 minutes (tidal volume 8 ml/kg, respiratory rate 125 breaths/min, PEEP 1cm H_2O, and FiO_2 0.5). Once myochalasis was achieved, the mice were disconnected from mechanical ventilator and were left to exhale. Then the lungs were gradually inflated via the tracheal tube from FRC (Pressure 0cmH_20) with a steady flow of air of 100ml/sec, from a syringe in which the flow was mechanically controlled, until the peak inspiratory pressure reached 25cmH_20.From the correlation of volume and the pressure measure in that volume in the specific time point the P=V curve is developed.

The pressure volume curve is reported here using the percentage of predicted TLC (total lung capacity) on the vertical axis rather than using the actual lung volume in liters. This procedure helps to normalize for differences in body size and sex among mice. As an indicator of lung compliance we used the inspiratory capacity (IC), defined as the volume inflated at airway pressure of 25 cmH_2O, normalized to body weight, and expressed as % of control.

Hemodynamic and ventricular weight measurements

After hypoxic exposure for the indicated time periods, mice were anesthetized and hemodynamic and ventricular weight measurements were performed. Right ventricular systolic pressure (RVSP) was measured trough a trans-thoracic route: a pressure transducer (ADI Instruments, Inc., Colorado Springs, CO) attached to a 23g needle was used and data were collected and analyzed using the PowerLab hardware and software (ADI Instruments, Inc., Colorado Springs, CO). Right ventricular hypertrophy was assessed by harvesting hearts, removing atria, dissecting the RV and deriving Fulton's Index, i.e. the weight ratio of (Right ventricle)/ (left ventricle and septum) [(RV)/(LV+S)].

Morphometric analysis

Alveolar/distal pulmonary arterioles of 50-100 μm in diameter, not associated with bronchi, from lung sections immunostained with α-SMA (as described above), were captured with light microscopy. At least 10 representative pulmonary arterioles were chosen from three different sections from each animal. Morphometric analysis of medial vessel wall thickness was performed using the software package Metamorph v.6.2r (Universal Imaging, Downingtown, PA). The entire vessel area including the lumen was identified as "Total Area" and the area of brown-color (α- SMA stained) that represents the medial smooth muscular layer was labeled "Threshold Area". Medial Wall Thickness Index was determined by using the quotient of Threshold Area x 100 over Total Area [(%Threshold Area x 100)/ total Area].

Lung Histology and Immunohistochemistry

For histology purposes, lungs were first perfused with PBS through the right ventricle. The perfusion flow was kept at approximately 1ml/min by the use of a peristaltic pump with Platinum L/S Masterflex silicone tubing. An incision at the left atrium allowed the outflow of the blood. Lungs were then intra-tracheally inflated with 10% formalin at 25 cmH_2O pressure, fixed overnight at 4°C, then stored in 70% ethanol before embedding in paraffin. Lung tissue sections of 5μM were prepared and further deparaffinized and rehydrated. Sections were stained with hematoxylin and eosin (H&E) and evaluated by a pathologist blinded to the interventions.

To determine lung injury score, in acid induced lung injury model, due to the patchy nature of the lesions random High power fields (400x) were scored. The selection was effectuated by successive haphazard displacements, each of which was at least one High power field in length. To perform the histological assessment of lung injury, five

independent variables were evaluated: **A**. Neutrophils in alveolar spaces, **B**. Neutrophils in the interstitial spaces, **C**. Hyaline membranes, **D**. Proteinaceous debris filling the airspaces, **E**. Alveolar septal thickening, and weighted according to the relevance ascribed to by the Official American Thoracic Society Workshop Report on Features and Measurements of Experimental Acute Lung Injury in Animals (131). The resulting injury score is a continuous value between 0 and 1.

Immunohistochemical assessment of vascular remodeling was performed by staining for alpha-smooth muscle actin (anti-α-SMA antibody, Sigma-Aldrich, Inc., St. Louis, MO), a marker of smooth muscle cells (389). Endogenous peroxidase activity was inhibited with 3% H_2O_2 (Sigma- Aldrich, Inc., St. Louis, MO) in methanol. Next, the sections were incubated with a biotinylated horse antimouse IgG (Vector Laboratories, Inc., Burlingame, CA), treated with the avidin–biotin complex (Vectastain Elite ABC kit, Vector Laboratories, Inc., Burlingame, CA), and stained with 3,3'-diaminobenzidine substrate (KPL, Inc., Gaithersburg, MD). Slides were counterstained with 1% Methyl Green (Sigma-Aldrich, Inc., St. Louis, MO).

Bronchoalveolar Lavage – Inflammatory Cell Counts

Bronchoalveolar lavage fluid (BALF) was obtained through intratracheal instillation of ice-cold PBS (Ca^{2+} and Mg^{2+} free, supplemented with 0.1mM EDTA) and filtered via a 35μm cell strainer to exclude contamination from epithelial cells that mostly appeared in clusters. First, 0.3ml/kg PBS was instilled, and the supernatant was used to evaluate cytokine concentrations in the BALF. Then, to collect alveolar macrophages, BAL was further applied for 5 times with 1ml PBS.

Total white blood cell (WBC) counts of BAL isolated cells were estimated by hemocytometer counting using Kimura stain,(390) while differential counts were determined by flow cytometry (see below). For cytospin preparations, the cell suspension was cytocentrifuged at 300g for 5 min using the Shandon Cytospin 4 (Thermo Scientific, Rockford, IL). Slides were air-dried overnight, stained with May-Grünwald Giemsa (Merck, Frankfurt, Germany) and evaluated under light microscope.

BAL fluid protein and cytokine profile

Protein Concentration of the BALF was assessed by the BCA method (BCA Protein Assay, Thermo Scientific, Rockford, IL). IL-6, TNF-α, CXCL-1 and IL-1β protein levels in the lavage fluid were determined using a commercially available sandwich enzyme linked immunosorbent assay kit (Quantikine, R&D Systems, Abingdon, UK) according to the manufacturer's instructions.

The BALF supernatant was analyzed using a multiplex mouse cytokine kit (FGFβ, MIP-1α, IL-1β, IL-17, IL-2, IL-13, IL-4, TNF-α, IL-12, INF-γ) (Invitrogen Corporation, Carlsbad, CA) in the Luminex 200™ System (Luminex Corporation, Austin, TX). BALF supernatant samples from animals treated with either dox or regular water in normoxia versus two and four days in hypoxia were analyzed in duplicate. Standard Luminex protocol was followed as suggested by the manufacturer.

Assessment of alveolar macrophage phenotype

Alveolar Macrophage isolation

BAL was collected at the indicated time periods after acid administration, pseudomonas infection or hypoxic exposure as described above. The red blood cells were removed from the cell suspension using ammonium chloride lysis buffer (Sigma-Aldrich, Inc., St. Louis, MO). To discriminate alveolar macrophages, cells were stained with FITC-anti mouse CD45 antibody (BD Biosciences, Franklin Lakes, NJ), APC– anti-mouse CD11c (BD Biosciences, Franklin Lakes, NJ) , PE-anti-mouse Ly-6G (BioLegent, San Diego,CA), antibodies specific for WBCs, alveolar macrophages and neutrophils, respectively. Cells were evaluated in a MoFlo Cell Sorter (Beckman-Coulter) and macrophage and neutrophil percentage were analyzed with Summit Software (Summit Software, Inc., Fort Wayne, IN). The $CD45^{+}CD11c^{+}Ly\text{-}6G^{-}$ cells (alveolar macrophages) were further sorted and isolated with purity >90%.

In the hypoxic models of PAH, more than ninety percent of the cells isolated this way appeared to be of the monocyte/macrophage lineage and this was confirmed by cell-specific markers in flow cytometry (below). Isolated cells were used for RNA extraction, flow cytometry, or immunocytochemistry.

Cytospin preparation and Immunocytochemistry

BAL isolated cells were cytocentrifuged as mentioned above and placed on microscope slides. Immunocytochemistry for Fizz1, galectin -3, iNOS, Arg-1 and IRF5 was performed by immersion of the slides in 2% paraformaldehyde, incubation with blocking serum, followed by incubation at 4°C overnight with rabbit polyclonal anti-mouse-Fizz1 antibody (Abcam, Cambridge, MA), rabbit polyclonal anti mouse galectin-3 (Abcam, Cambridge, MA), rabbit polyclonal anti-mouse iNOS antibody (Santa Cruz Biotechnology, Inc., Santa Cruz, CA), rabbit polyclonal anti-mouse IRF5 antibody (Cell Signaling Technology, Inc., Beverly, MA) or mouse monoclonal anti-mouse Arg-1 (BD Biosciences, Franklin Lakes, NJ). Goat biotinylated anti-rabbit IgG or horse biotinylated anti-mouse IgG (both from Cell Signaling Technology, Inc., Beverly, MA) were used as secondary antibodies. FITC- avidin or Texas Red- Avidin conjugate

(Vector Laboratories, Inc., Burlingame, CA) were further used. Nuclei were counterstained with DAPI (Thermo Fisher Scientific, Inc., Waltham, MA).

RNA isolation and quantitative PCR

RNA from alveolar or thioglycolate-elicited peritoneal macrophages or total lung was isolated using Trizol reagent (Life technologies Corporation, Carlsbad, CA). In the case of *in vivo* isolated and sorted alveolar macrophages, RNA precipitation was facilitated with addition of 250 μg/μl RNAase free glycogen (Fermentas Gmbh, St.Leon-Rot, Germany). One μg of total DNA digested RNA was used for cDNA synthesis (Thermoscript RT, Invitrogen Corporation, Carlsbad, CA). The SYBR Green method was followed in the PCR reaction. Primer sequences are shown in Table 10. Ribosomal Protein S9 (RPS9) served as housekeeping gene. Annealing was carried out at 60˚C for 30 sec, extension at 72˚C for 30 sec, and denaturation at 95˚C for 15 sec for 40 cycles.

To isolate micro-RNAs from alveolar macrophages, total RNA was isolated as above. For cDNA synthesis and qPCR of specific miRNAs, TaqMan MicroRNA Assays (Life technologies Corp, Carlsbad, CA) were used. The miRNA sequence is described in the table 10. SnoRNA135 served as housekeeping miRNA. Annealing and extension was carried out at 60˚C for 30 sec and denaturation at 95˚C for 15 sec for 40 cycles in a 7500 Fast Real-Time PCR System (Life technologies Corp, Carlsbad, CA). Analysis of the fold change was performed based on the Pfaffl method (391).

Table 10. Primer Sequence

Ym1	Fwd	: 5’-GCAGAAGCTCTCCAGAAGCAATCCTG-3’
	Rev	5’-ATTGGCCTGTCCTTAGCCCAACTG-3’
Fizz1	Fwd	5’-GCTGATGGTCCCAGTGAATAC-3’
	Rev	5’-CCAGTAGCAGTCATCCCAGC-3’
Arginase-1	Fwd	5’-CAGAAGAATGGAAGAGTCAG-3’
	Rev	5’- CAGATATGCAGGGAGTCACC-3’
iNOS	Fwd	5’-TCCTGGAGGAAGTGGGCCGAAG-3’
	Rev	5’ -CCTCCACGGGCCCGGTACTC-3’
IL-12β	Fwd	5’- GGAGGGGTGTAACCAGAAAGGTGC-3’
	Rev	: 5’-CCTGCAGGGAACACATGCCCAC-3’
C/EBPβ	Fwd	5’- GGGGTTGTTGATGTTTTTGGTT-3’
	Rev	: 5’- TCACTTTAATGCTCGAAACGGA-3’
IRF5	Fwd	5’- ACATGCCACCTCAGCCGTACAAG-3’
	Rev	5’- CCCTACAGGTGGCTGGAGAGCAG-3’

IRF4	Fwd	5’- CAGGTGACTCTGTGCTTTGGTGAGG-3’
	Rev	5- CGGAGGGAGCGGTGGTAATCTGG-3’
TRAF6	Fwd	5’- GGTGTAAGGCCTAGCAGCAGAT-3’
	Rev	5’- AAATAGCCCATGGAAGCACAGT-3’
IRAK1	Fwd	5’- GTGCCGCTTCTACAAAGTGATG-3’
	Rev	5’- GTGAGGATGTGAACGAGGTCAG-3’
Akt2	Fwd	5’- GCCTGAGGTGCTAGAGGACAAT-3’
	Rev	5’- GAAGCCGATCTCCTCCATAAGA-3’
RPS9	Fwd	5’-GCTAGACGAGAAGGATCCCC-3’
	Rev	5’-. CAGGCCCAGCTTAAAGACCT -3’
Human HO-1	Fwd	5’- GCAGTCAGGCAGAGGGTGATA-3’
	Rev	5’-AGCCTGGGAGCGGGTGTTGAG-3’
Arginase-2	Fwd	5’-CACGGGCAAATTCCTTGCGTCC-3’,
	Rev	5’-GGTTGGCAAGGCCCACTGAACG-3’
Mannose Receptor, C type 1 (MR)	Fwd	5’-TTTCCATCGAGACTGCTGC-3’
	Rev	5’-ACCAAAGCCACTTCCCTTC-3’
TNFa	Fwd	5’-GCCCACGTCGTAGCAAACCACC-3’
	Rev	5’-CGGGGCAGCCTTGTCCCTTG-3’
CCL2(MCP-1)	Fwd	5’-GGCTGGAGCATCCACGTGTTGG-3’
	Rev	5’-TTGGGGTCAGCACAGACCTCTCTC-3’
IL-6	Fwd	5’-CAAAGCCAGAGTCCTTCAGAG-3’
	Rev	5’-CACTCCTTCTGTGACTCCAGC-3’
IL-10	Fwd	5’- GCGCTGTCATCGATTTCTCCCCTG-3’
	Rev	5’-GGCCTTGTAGACACCTTGGTCTTGG-3’
PDGF-BB	Fwd	5’-GGGAGCAGCGAGCCAAGACG-3’
	Rev	5’-TGCCCACACTCTTGCCGACG-3’
GADPH	Fwd	5’-CGTCCCGTAGACAAAATGGT-3’
	Rev	5’- GAATTTGCCGTGAGGGAGT-3’

MicroRNA Sequence

mmu-miR-155	UUAAUGCUAAUUGUGAUAGGGGU
hsa-miR-146a	UGAGAACUGAAUUCCAUGGGUU
hsa-miR-125b	UCCCUGAGACCCUAACUUGUGA
SnoRNA135	CUAAAAUAGCUGGAAUUACCGGCAGAUUGGUAGUGGUGAGCCUAUG GUUUUCUGAAG

Flow cytometry

Total white blood cell (WBC) counts of BAL isolated cells (see above) were accessed by hemocytometer counting using Kimura stain (392), and reconfirmed by flow cytometry analysis by the use of FITC-anti mouse CD45 antibody (BD Biosciences, Franklin Lakes, NJ) and flow cytometry absolute count standard beads (Bangs Laboratories, Fishers, IN). Differential WBC analysis was performed using APC–anti-mouse F4/80 (eBioscience, Inc., San Diego, CA), PE-anti-mouse Ly-6G/L (BD Biosciences, Franklin Lakes, NJ), and Pacific Blue-anti-mouse CD3 (eBioscience, Inc., San Diego, CA) antibodies specific for macrophages, neutrophils and T cells, respectively. Expression profile of BAL isolated alveolar macrophages was assessed by APC-anti mouse F4/80 (eBioscience, Inc., San Diego, CA),(393) FITC-anti-mouse CD11c, and PE-anti-mouse CD45 (BD Biosciences, Franklin Lakes, NJ) in separate analysis.

Expression of protein levels of iNOS, IL-12β, Arg-1, Fizz1, MGL-1/2 and IL-10 were determined by flow cytometry cell surface and intracellular staining, as previously described (394, 395) Fizz1, iNOS, Arg-1, expression was assessed by performing fixation with paraformaldehyde, intracellular permeabilization and staining with primary rabbit anti-mouse- Fizz1 antibody (Abcam, Cambridge, MA) followed by secondary rabbit FITC-conjugated anti-rabbit antibody (BD Biosciences, Franklin Lakes, NJ). In order to evaluate the IL-12b and IL-10- expressing alveolar macrophages, BALF-isolated cells were incubated with Golgi inhibitor (monensin, BD Biosciences, Franklin Lakes, NJ) fixed and permeabilized, and stained with APC-conjugated monoclonal antibody against murine IL-10 (BD Biosciences, Franklin Lakes, NJ)

Cell surface staining was carried out by incubation with PerCP-Cy5.5 anti-mouse CD11c (Biolegent, San Diego, CA), then fixed and permeabilized (BD Fixation and Permeabilization Solution Kit, BD Biosciences, Franklin Lakes, NJ) and stained with APC-conjugated monoclonal antibody against murine IL-10 (BD Biosciences, Franklin Lakes, NJ), FITC conjugated monoclonal antibody against murine iNOS (BD Biosciences, Franklin Lakes, NJ) and PE conjugated monoclonal antibody against murine IL-12β (BD Biosciences, Franklin Lakes, NJ). Mouse monoclonal anti-mouse Arginase-1 (BD Biosciences, Franklin Lakes, NJ) and rabbit polyclonal anti-mouse Fizz1 (Abcam, Cambridge, UK) were used in separate analyses. FITC Goat Anti-Rabbit IgG (BD Biosciences, Franklin Lakes, NJ) and APC Rat anti mouse IgG1 (Biolegent, San Diego, CA) were used as secondary antibodies for Fizz1 and Arginase-1 staining respectively. PE anti-mouse MGL1/2 (RnD systems, Minneapolis, MN), FITC anti mouse CD80 and/or PE anti mouse CD86 and anti-mouse STAT1 were used for cell

surface staining in a separate analyses. The proper isotype controls were used in each case. The flow cytometry events were acquired in a MoFlo Legacy Cell Sorter (Beckman Coulter, Inc., Brea, CA) and analyzed with the use of Summit Software (Summit Software, Inc., Fort Wayne, IN). Flow cytometry events were first gated based on forward and side scatter and then the CD11c positive cells (alveolar macrophages) were further selected in order to evaluate the expression of activation markers.

Last, the evaluation of siRNA uptake from alveolar macrophages took place by staining of alveolar macrophages with CD11c-PECy3 (eBioscience, Inc., San Diego, CA) and identification of siRNA – positive macrophages by detection of the emission of Cy3 labeled Luciferase. Although cyanine dye Cy3 does not give fluorescence intensity comparable to that of PE or APC and is most used in fluorescent microscopy, Cy3 is excited at 488 nm by an argon laser and can be used directly in flow cytometry (ref. Fluorochrome Conjugates For Flow Cytometry - Applications Guide- Caltag Technologies).

Western blot analysis

Protein concentration from macrophage lysates was determined by the BCA assay. Macrophage protein lysates were resuspended in SDS-containing loading dye. Twenty μg of protein was electrophoresed on 13.3% denaturing polyacrylamide gel prior to wet transfer to 0.45 μm PVDF membrane (Biorad, Hercules, CA). Briefly, after blocking with 5% skim milk in phosphate buffered saline (pH 7.4) containing 0.1% Tween 20 (PBST) for an hour at room temperature, the membranes were incubated with rabbit polyclonal anti-mouse IRF5 antibody (Cell Signaling Tech, Beverly, MA), rabbit polyclonal anti-mouse IRF4 antibody (Cell Signaling Tech, Beverly, MA), mouse polyclonal anti-mouse TRAF6 antibody (Santa Cruz Biotechnology, Inc., Santa Cruz, CA), rabbit polyclonal anti-mouse Fizz1 antibody (Abcam, Cambridge, MA), rabbit polyclonal anti-human and anti-mouse HO-1 antibody (Enzo Life Sciences International, Inc., Plymouth Meeting, PA), rabbit polyclonal anti-mouse polyclonal anti-mouse IgA Ab (Millipore, Billerica, MA), rat anti-mouse IL-10 antibody (Abcam, Cambridge, MA) or mouse monoclonal anti-mouse b actin (Cell Signaling Tech, Beverly, MA) at 4°C overnight.at 4°C overnight.

The membranes were then incubated with 40 ng/ml of peroxidase-conjugated anti-rabbit or anti-mouse secondary antibody (Santa Cruz Biotechnology, Inc., Santa Cruz, CA), respectively, for 30 min at room temperature followed by reaction with Lumi-Light ECL substrate (Thermo Fisher Scientific, Waltham, MA). Densitometric analysis was performed with the NIH ImageJ program.

BALF samples were concentrated with 20% trichloroacetic acid (TCA, Sigma-Aldrich, Inc., St. Louis, MO) overnight, washed with ice-cold acetone and resuspended in SDS-containing loading dye.

Nitrite concentration and arginase activity assay

Determination of nitric oxide metabolite, nitrite concentration in BALF (based on Griess reaction). BAL supernatants from control mice and mice with acid-induced lung injury for twelve hours were utilized. 50 μL sulfanilamide solution (1% w/v sulfanilamide, 5% w/v phosphoric acid) were added to equal volume of sample. Samples were incubated for 10 minutes in the dark and 50μL of 0.1% w/v N-(naphthyl) ethyl-enediamidedihydrochloride was added, followed by a second incubation for 10 minutes at RT in the dark). Absorbance at 550 nm was measured, and the amount of nitrite was determined using a $NaNO_2$ standard curve.

In the Griess reaction, nitrite and nitrate concentration in BALF supernatant were measured by the Total NO/Nitrite/Nitrate Assay (R&D Systems, Minneapolis, MN). Proteins were removed before analysis with ultrafiltration using 10,000 molecular weight (MW) cut-off filters (Amicon Ultra; Millipore, Billerica, MA). Supernatants from RAW 264.7 macrophages stimulated with 100 μg/ml LPS or 100 U/ml INF-γ for 48 hours served as positive controls.

Arginase activity was assessed indirectly by measuring the concentration of urea generated by the arginase-dependent hydrolysis of L-arginine as previously described (396). Alveolar macrophages from animals with acid-induced lung injury (twelve-hour time point) and control mice were harvested, washed, and lysed with 10 mM Tris.HCl (pH 7.4) containing 0.4% (w/v) Triton X-100 and protease inhibitor cocktail (Complete, Roche, Basel, Switzerland). After 30 min on a shaker, 100 μL of 25 mM Tris.HCl was added. Into 100 μL of this lysate, 10 μL of 10 mM $MnCl_2$ was added, and the enzyme was activated by heating for 10 min at 55 °C. Arginine hydrolysis was conducted by incubating the lysates with 100 μL of 0.5ML-arginine (pH 9.7) at 37 °C for 60 min. The reaction was stopped with 800 μL of H_2SO_4 (96%)/H_3PO_4 (85%)/H_2O (1/3/7, v/v/v). The urea concentration was measured at 550 nm after addition of 40 μL of α-isonitrosopropiophenone (Sigma-Aldrich Corp, St. Louis, MI) (dissolved in 100% ethanol), followed by heating at 100°C for 30 min. One unit of enzyme activity is defined as the amount of enzyme that catalyzes the formation of 1 μmol•urea/min.

In vitro cell treatments

Cell Cultures-Cell transfections

For cell transfection experiments, peritoneal or bronchoalveolar lavage from control animals was obtained through instillation of 5 x 1 ml Hank's Balanced Salt Solution (without calcium and magnesium) supplemented with 10 mM EDTA and 1 mM HEPES and filtered twice via a 35 μm cell strainer to exclude contamination of epithelial cells. $1x10^5$ macrophages per well (4 wells per group) were seeded in 48-well tissue-culture plates in a volume of 0.2 ml macrophage complete medium (DMEM, GIBCO, Life technologies Corp, Carlsbad, CA) supplemented with 10% (v/v) FBS, 10 mM L-glutamine, 100 IU/ml penicillin and 100 μg/ml streptomycin. Cells were incubated at 37°C for 4 hours and then their medium was replaced with serum-free, antibiotic-free DMEM prior to transfection. Lipofectamine served as transfection reagent (RNAimax, Life technologies Corp, Carlsbad, CA) and cells were transfected with either 30nM of siRNA (small interfering RNA) for *Akt2* (sense seq: ACC/OmeU/UAUGUUGGACAAA/OmeG/A/OmeU/OmeU/, antisense seq: 5Phos/UCUUUGUCCAACA/OmeU/AAG/OmeG/Utt, designed at Cenix Bioscience, Dresden, Germany) or negative control dsRNA. For miR-146a experiment, transfection was carried out with 30nM miR-146a mimic, anti-miR-146a inhibitor and not-targeting controls (NTC) that were purchased from Ambion (Life technologies Corp, Carlsbad, CA). Transfection efficiency and biological effect was assessed 72 hours post transfection.

To induce M1 phenotype in alveolar macrophages and to recapitulate the *in vivo* stimuli, BAL fluid (0,3ml/kg) samples from WT mice 6 hours after acid-aspiration were obtained. After 24 hour serum starvation, BAL fluid was applied in cultured WT and Akt2-/- BAL isolated alveolar macrophages in 1:1 dilution with fresh serum–free DMEM. Control cells received same ratio of normal saline. Cells were harvested 12 hours post stimulation.

LPS stimulation in peritoneal macrophages, that were transfected with miR146a mimic, miR146a inhibitor or scramble miRNA (all from Life technologies Corporation, Carlsbad, CA), was carried out by introduction of a final concentration of 100ng/ml LPS *E.coli* in the cell medium. Stimulation was applied 4 hours or 24 hours prior to cell harvesting.

Macrophages were cultured for 48 hours at 0.5-1% O2 (pO2 in the media was 14-18 torr) in a hypoxic work station (in Vivo2, Ruskinn Technology, Ltd., Bridgend, UK) and/or Billups chambers that were flushed with a mix of 0.5% O_2 and 5% CO_2 (N2 balance). Alternatively, macrophages were stimulated with 20 ng/ml murine recombinant interleukin-4 (IL-4) (R&D Systems, Minneapolis, MN) in order to be polarized towards M2. CO treatment was

performed in Billups chambers that were flushed with a mix of 0.5% O_2, 5% CO_2, 500 ppm CO (N2 balance). Cells were pretreated with CO for 1 hour in normoxia prior to hypoxic exposure. Cell viability was greater than 80% in all groups as assessed by trypan blue exclusion.

Primary alveolar macrophages stimulated with 100 μg/ml LPS *E.coli* and 100 U/ml INF-γ for 48 hours served as positive controls. Nuclei were counterstained with DAPI (Thermo Fisher Scientific, Inc., Waltham, MA) and samples were observed with fluorescent microscopy.

Primary alveolar macrophage culture

For cell culture experiments, BALF was obtained through intratracheal instillation of 5 x 1 ml Hank's Balanced Salt Solution (without calcium and magnesium) supplemented with 10 mM EDTA and 1 mM HEPES and filtered twice via a 35 μm cell strainer to exclude contamination of epithelial cells. 3.5x105 macrophages per well were seeded in 48-well tissue-culture plates in a volume of 0.25 ml macrophage complete medium (DMEM/10: Dulbecco's Modified Eagle Medium) (GIBCO, Invitrogen Corporation, Carlsbad, CA) supplemented with 10% (v/v) FBS, 10 mM L-glutamine, 100 IU/ml penicillin and 100 ug/ml streptomycin). Cells were incubated at 37°C for 4 hours and then their medium was replaced with serum-free DMEM prior to hypoxic exposure or IL-4 stimulation.

Macrophage activation and CO treatment

Macrophages were cultured for 48 hours in a hypoxic work station (inVivo2, Ruskinn Inc.) and/or Billups chambers that were flushed with a mix of 0.5% oxygen and 5% CO_2 (N2 balance). Alternatively, macrophages were stimulated with 20 ng/ml murine recombinant interleukin -4 (IL-4) (R&Dsystems) in order to be polarized towards M2. CO treatment was performed in Billups chambers that were flushed with a mix of 0.5% oxygen, 5% CO2, 500 ppm carbon monoxide (N2 balance). Cells were pretreated with CO for 1 hour in normoxia prior to hypoxic exposure. Cell viability was greater than 80% in all groups as assessed by trypan blue exclusion.

PASMC proliferation assay

Mouse primary pulmonary artery smooth muscle cells (PASMCs) were cultured ($2x10^3$ cells per well) in a volume of 100 μl of DMEM (GIBCO, Invitrogen Corporation, Carlsbad, CA) supplemented with 10% FBS, 10 mM L-glutamine, 100 IU/ml penicillin and 100 μg/ml streptomycin, using 96-well tissue culture plates. Two days prior to proliferation assay, the

medium was replaced with DMEM supplemented with 0.1% FBS, 10 mM L-glutamine, 100IU/ml penicillin and 100 μg/ml streptomycin. Macrophage-conditioned media, diluted two-fold with fresh low-serum media, were then applied to PASMCs and the cultures were incubated for an additional three days. Cell proliferation was assessed by cell proliferation reagent WST-1 (Roche Diagnostics, Mannheim, Germany) by applying 10 μl of WST-1 reagent to each well and measuring OD440-OD690 after two hours of incubation at 37^0C. Treatment of PASMCs with 25ng/ml PDGF-BB served as a positive control. Fresh cell culture medium (DMEM) or medium equilibrated in 0.5% Oxygen for 48 hours were used as negative controls. Mouse recombinant IL-10 (R&D Systems, Minneapolis, MN) was used in the range of 1-100 ng/ml.

Statistical analysis

All data were evaluated for normality using Kolmogorov – Smirnov test (with Dallal – Wilkinson – Lilliefor P value). The data that passed the normality test were analyzed with one way analysis of variance with Bonferroni's multiple comparison post test. Comparison of non-parametric results between different groups was performed by Mann Whitney U test or Kruskal-Wallis test with Dunn's multiple comparison post test, using GraphPad InStat (GraphPad Software, San Diego, CA). P value <0.05 was considered significant. Results are expressed as mean ± SD or median (5-95 percentiles) as indicated and are representative of at least three independent.

RESULTS

PART ONE

M2 MACROPHAGES PROTECT FROM THE DEVELOPMENT OF ACUTE LUNG INJURY

Main Findings

Upon HCL aspiration, WT mice developed impaired lung compliance, increased vascular permeability, and lung inflammatory response with prominent M1 activation characterized by induction of iNOS and IL-12β. Akt2-/- mice exhibited ameliorated ALI; improved compliance and reduced alveolar protein levels and lung inflammatory response. Upon high tidal volume ventilation also, Akt2-/- mice exhibited ameliorated ALI; improved lung compliance, reduced protein extravasation and improved alveolar-arterial O_2 gradient. We utilized the acid-induced acute lung injury model in order to further study the inflammatory response and the role of macrophages in ALI and the mechanism by which Akt2-/- ablation confers protection.

Alveolar macrophages of Akt2-/- mice with HCL induced ALI, not only had suppressed iNOS and IL-12β production, but were activated towards the alternative M2 pathway (Arg-1, Fizz1 and Ym1 up-regulation). To investigate the mechanism of protection in the absence of Akt2 in macrophages we investigated molecular pathways already known to affect macrophage activation; several miRNAs such as miR-155 and miR-125b, already known to promote M1 activation, via suppression of c/EBPβ and IRF4 transcription factors respectively and the TLR4 pathway.

Although miR-155 levels were suppressed in alveolar macrophages of Akt2-/- mice resulting in enhanced c/EBPβ production, miR-155 levels were not up-regulated in WT macrophages upon acid administration thus miR155 did not play a significant role in the pathogenesis of acid induced ALI. In terms of miR-125b, there was a mild non-significant increase of miR125b in alveolar macrophage upon ALI and there was no change in miR-125b levels among WT and Akt2-/- macrophages.

Next, we investigated signaling molecules downstream the TLR4 signaling in alveolar macrophages that may be affected by Akt2 deficiency. We found that the mRNA and protein levels of downstream proteins such as TRAF6, STAT1 and IRF5 were elevated in WT macrophages upon HCL stimulation while Akt2-/- macrophages did not respond accordingly. Based on this finding we sought to investigate the role of miR-146a, a miRNA well known to

mute TLR4 signaling via targeting or TRAF6, STAT1, IRF5 and IRAK1, in Akt2-/- mice. We found that miR-146a was significantly up-regulated in Akt2-/- macrophages compared to WT. Moreover, transfection of LPS-treated WT macrophages with a precursor of miR146a abrogated M1 activation. Application of an inhibitor of miR146a in Akt2-/- macrophages abolished iNOS suppression and the development of M2.

To further clarify the importance of macrophage activation in the pathogenesis of ALI, we sought to deplete alveolar macrophages from WT mice in ALI and reconstitute them with Akt2-/- macrophages. WT mice that received Akt2-/- macrophages exhibited reduced iNOS expression and improved inspiratory capacity compared to WT mice that received WT cells. We then attempted to modulate WT alveolar macrophage phenotype *in vivo* without depleting host macrophages. MiRNA targeting miR-146a and siRNA targeting Akt2 was delivered endotracheally in WT animals exposed to acid. MiR-146 delivery or Akt2 silencing in WT mice exposed to acid resulted in suppression of iNOS in alveolar macrophages.

To expand the role of alveolar macrophages in models of septic lung inflammation and lung injury, we utilized a model of Pseudomonas aeruginosa induced lung injury. Although M2 polarization was beneficial in aseptic lung injury, it resulted in increased lung bacterial load when Akt2-/- mice were infected with Pseudomonas aeruginosa.

Development of acid induced lung injury in mice

To pursue our hypothesis, we opted for a mouse model of acute lung injury with reproducibility, moderate severity and minimal neutrophilic accumulation compared to macrophage infiltration that will allow us to study the macrophage response. Thus, ALI was first induced with various concentrations of hydrochloric acid, 0.01N, 0.025N, 0.05N and 0.1N HCL diluted in normal saline (0.9% NaCl). The protein levels in BALF, the total number of WBCs in BALF and the relative expression of iNOS in alveolar macrophages were increased by the increasing concentration of HCL (Figure 30).

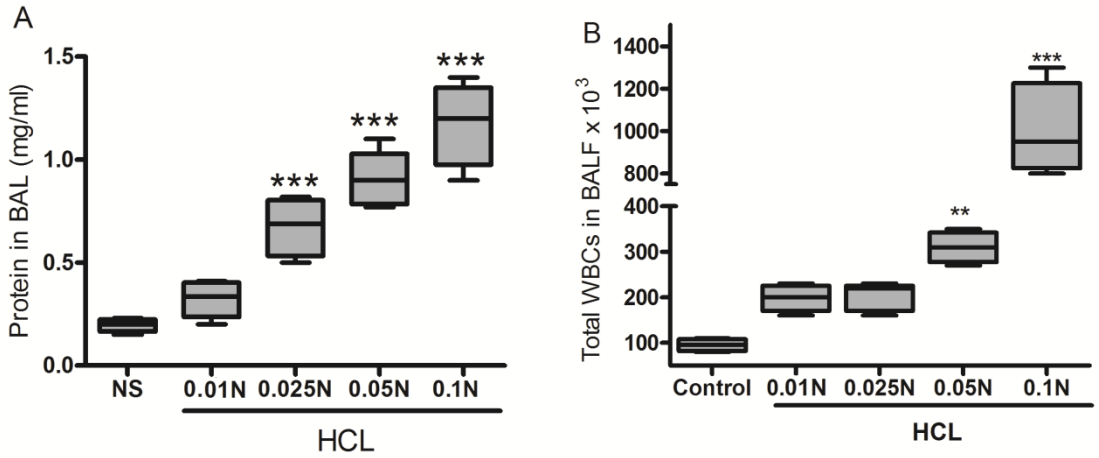

Figure 30. Protein concentration in BALF in WT mice and (B) total WBCs in BALF at several concentrations of HCL solution 24h after HCL intratracheal administration. n = 4–5 mice/group. Box plots: box shows 5–95 percentiles, horizontal line represents median, and whiskers represent minimum and maximum. **p, 0.01, ***p, 0.001, acid treatment versus NS (control) treatment.

However, 0.01N and 0.025N HCL concentrations could not promote a significant iNOS overexpression compared to control. Also, 0.1N administration promoted robust accumulation of neutrophils in the alveolar space (approximately 80-90% of the BAL cells) (Figure 31 and 32). Among the above HCL concentrations, 0.05N was chosen as optimal and capable to produce significant injury, M1 macrophage activation without excessive neutrophilic inflammation.

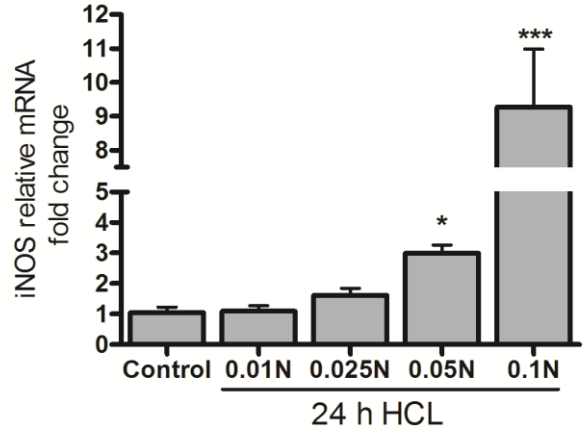

Figure 31. Relative mRNA levels of iNOS in alveolar macrophages from WT mice exposed to various concentrations of HCL solution. n = 4 mice/group.
Graphs represent mean +/- SD.*p, 0.05, ***p, 0.001, acid treatment versus NS treatment.

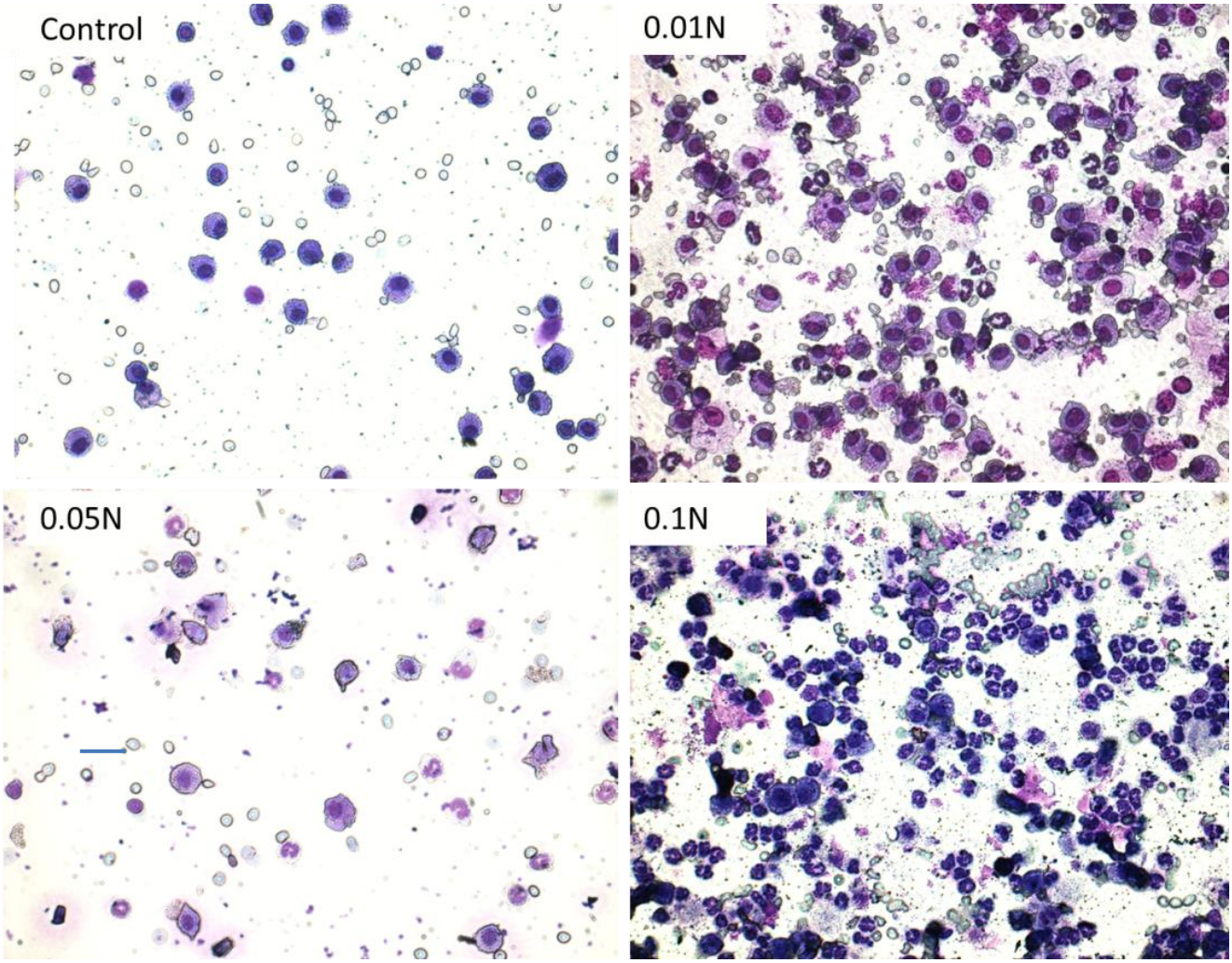

Figure 32. Representative cytospin images of cells isolated from BAL from WT mice exposed to 0.01N, 0.05N and 0.1N of HCL solution respectively. Note the presence of numerous neutrophils in 0.1N HCL concentration. Scale bar, 25 mm.

Akt2 deficiency protects from the development of acid-induced lung injury and ventilator induced lung injury

To describe the nature of inflammatory response in ALI and to determine the role of Akt2 and M2 macrophages in aseptic lung injury we exposed Akt2-/- mice, which possess M2-type macrophages, and WT mice to acid-induced lung injury and to ventilator induced lung injury. These models induce tissue injury, either chemical or mechanical (volutrauma, barotrauma) which initiate an aseptic inflammatory cascade. The development of acute lung injury in our model was assessed at several time points following acid instillation or after 4hour of high tidal volume ventilation based on the measurement of the pressure volume curve of the respiratory system (PV curve), estimation of total lung capacity (lung compliance), measurement of protein levels in BALF (an indirect index of vascular permeability), assessment of arterial oxygenation as well as with lung histology (Figure 33).

Akt2 deficiency in Hydrochloric acid induced ALI

Within 12hours of acid-aspiration in WT mice, the pressure volume curve of the respiratory system and lung compliance (Figure 33A, B) were severely compromised. Also, protein concentration in BALF was significantly elevated compared to mice treated with normal saline (Figure 33C). The severity of lung injury peaked at 12 hours post acid-aspiration and declined thereafter (Figure 33B, C). Lung compliance and protein concentration levels returned to baseline at 72 hours after acid-aspiration (Figures 33B, 33C, 34A, 34B). Acid-induced lung injury was less severe in Akt2-/- mice compared to WT mice (Figure 33A-C) although still significantly compromised compared to mice in normal saline group. There was a decrease in lung compliance and an increase in BAL fluid protein concentration in acid-treated Akt2-/- mice compared to saline-treated mice, but less than in WT mice (Figure 33A-C).

Histology on lung sections from WT mice 12 hours post acid-aspiration demonstrated destruction of normal tissue architecture characterized by thickening of the alveolar walls due to increased cellularity and edema (Figure 33D-b). Proteinaceous debris in the alveoli and extravasated red blood cells were also observed (Figure 33D-c). Lung sections from acid-treated Akt2-/- mice 12 hours post injury demonstrated less severe lung injury compared to WT mice (Figure 33D-d). Only mild thickening of the alveolar walls with inconspicuous presence of inflammatory cells and focal congestion of capillaries, with mild red cell extravasation were observed in Akt2-/- mice (Figure 33D-e, f).

Apart from the impaired lung compliance and the development of edema, accumulation of macrophages and neutrophils took place within 6 hours post HCL exposure (Figure 34A, B). Macrophage and neutrophil infiltration increased within 6 hours after acid-aspiration in

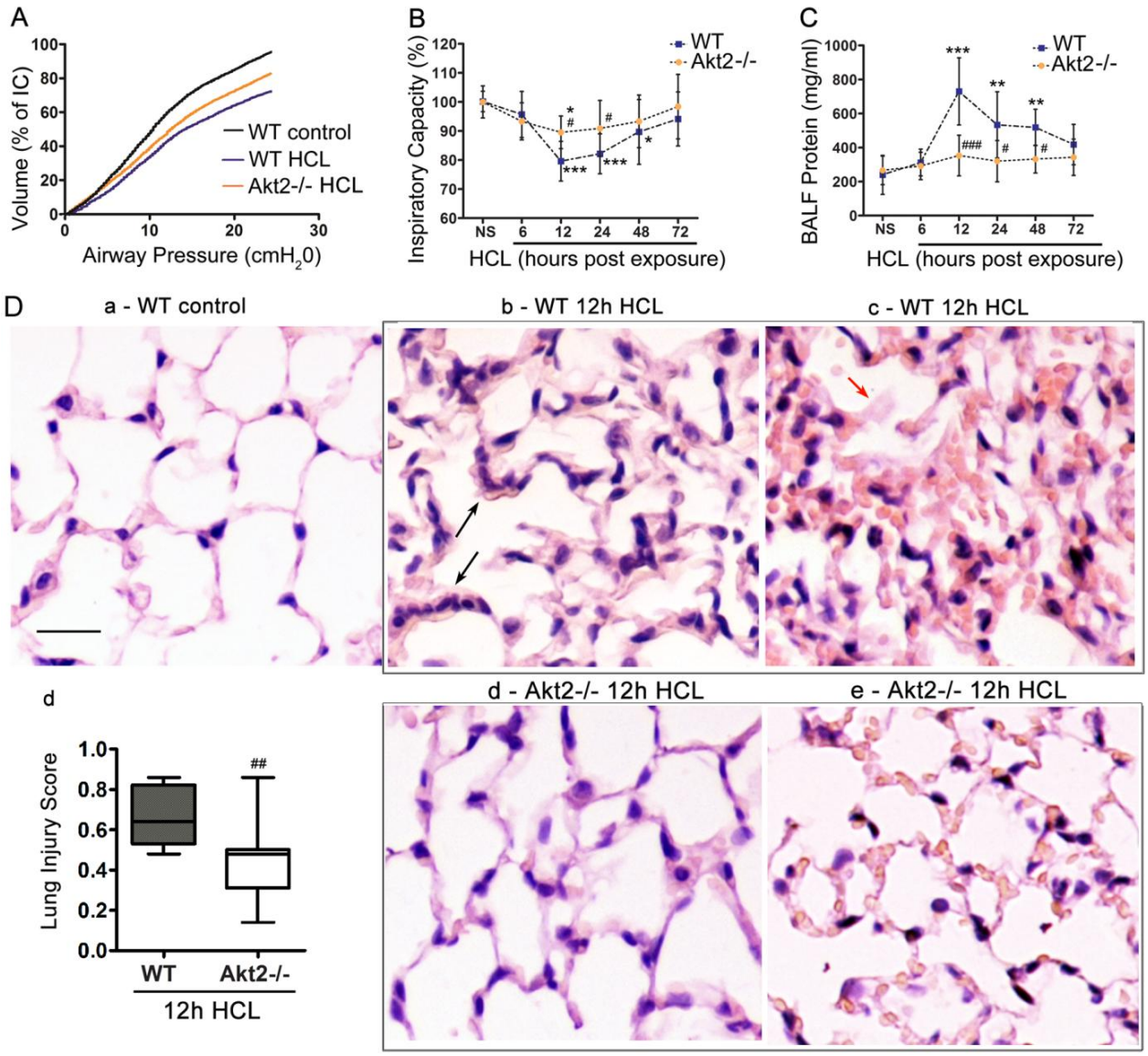

FIGURE 33. Acid aspiration–induced lung injury is reduced in Akt2-/- mice. (A) Pressure Volume Curve of the respiratory system, (B) Inspiratory Capacity (IC), and (C) protein concentration in bronchoalveolar lavage fluid (BALF) in WT and Akt2-/- mice at several time points after acid (HCL) aspiration compared to normal saline (NS) group. (D) Histological analysis of lung tissue of untreated control WT mice (D-a), WT (D-b,c) and Akt2-/- mice (D-e,f) twelve hours after HCL administration (H&E stain, magnification x400), as well as analysis of acute lung injury score (D-d). Black arrows in (D-b) demonstrate thickening of the alveolar walls due to increased cellularity. Red arrow in (D-c) indicates proteinaceous debris in the alveoli. Extravasated red blood cells are also depicted. Scale bar is representative of 25μm. N=5-8 mice per group. Line graphs represent median ±SD. Box Plot: box shows 5-95 percentiles, line at median and whiskers at min-max. *: acid- vs. NS-treated; *p<0.05, **p<0.01, ***p<0.001. #: Akt2-/- vs. WT; #p<0.05, ##p<0.01, ###p<0.001.

WT mice and reached its highest level at 12 hours (Figure 34A-C). Furthermore, chemokines and cytokines such as TNF-α, IL-6, CXCL-1 and IL-1β also accumulated in BAL fluid and reached their highest level at 6 hours post acid-aspiration (Figure 34D). The severity of lung

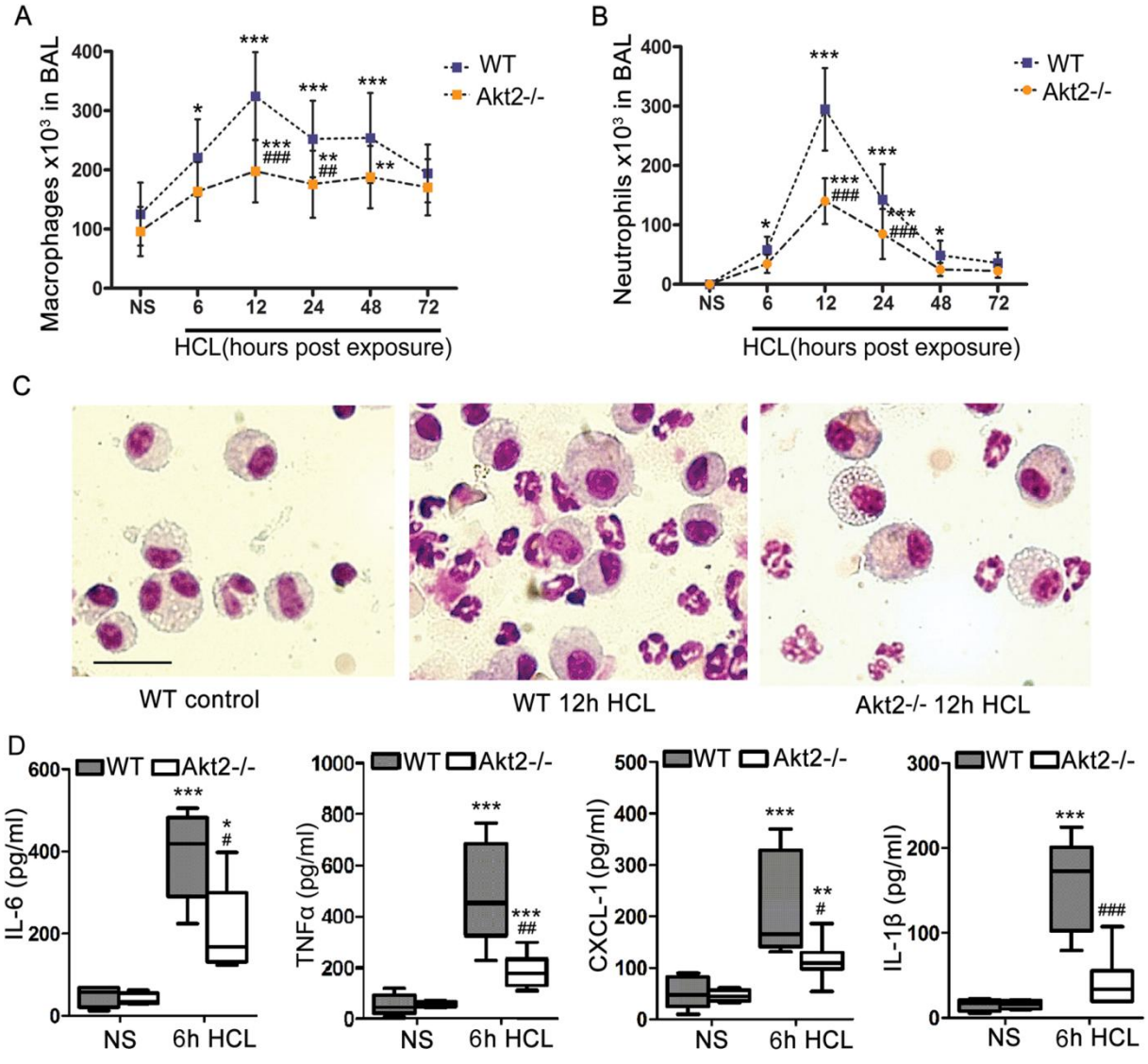

Figure 34. Lung inflammation upon acid aspiration was reduced in Akt2-/- mice. (A) Macrophages and (B) neutrophils are accumulated in bronchoalveolar lavage (BAL) soon after acid instillation. (C) Representative cytospin images of BAL isolated cells from WT and Akt2-/- mice twelve hours after acid exposure. Scale bar is representative of 25μm. (D) Levels of TNF-α, IL-6, CXCL-1 and IL-1β in BAL fluid of WT and Akt2-/- mice six hours after acid-aspiration compared to normal saline (NS) aspiration group. N=5-8 mice per group. Line graphs represent median ±SD. Box Plot: box shows 5-95 percentiles, line at median and whiskers at min-max. *: acid- vs. NS-treated; *p<0.05, **p<0.01, ***p<0.001. #: Akt2-/- vs. WT; #p<0.05, ##p<0.01, ###p<0.001.

inflammation peaked at 12 hours after acid-aspiration and declined thereafter; BAL cell counts and cytokines returned to baseline at 72 hours after acid-aspiration (Figure 34A, 34B). The severity of inflammatory cell infiltration (Figure 34A-C) and the cytokine levels in the BAL fluid (Figure 34D) were lower in Akt2-/- compared to WT mice.

Akt2 deficiency in Ventilation induced ALI

To assess the inflammatory response in VILI and the role of Akt2 deficiency we utilized an established model of high tidal volume ventilation model in our lab (154, 183). After 3.5hours of high VT ventilation, lung compliance decreased in WT mice to 65% of control, but not in Akt2−/−mice (83% of control; Figure 35). The development of lung injury was associated with impaired oxygenation (Figure 35). Akt2−/−mice subjected to high VT ventilation had higher PaO_2 than WT mice (Figure 35). There were no differences in $PaCO_2$, pH, and lactate between the two genotypes after high VT ventilation (data not shown).

Mechanical ventilation with high VT induced an inflammatory response in the lungs of mice of both genotypes, characterized by neutrophilic infiltration that was less severe in Akt2-/- mice (Figure 36).

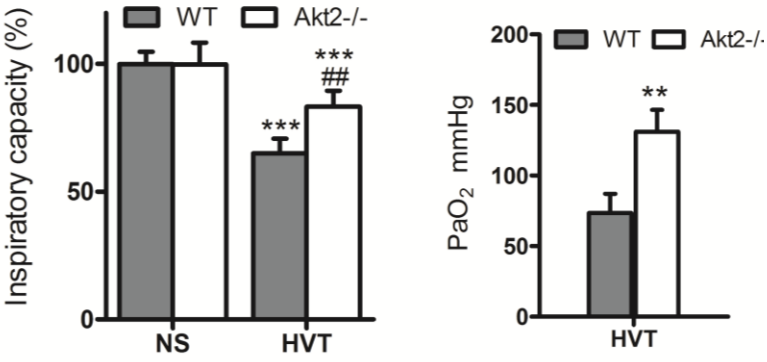

Figure 35. Inspiratory capacity and arterial oxygenation in WT and Akt2-/- mice exposed to high tidal volume ventilation for 3,5 hours. Compared to NS. Box Plot: box shows 5-95 percentiles, line at median and whiskers at min-max. *: HVT - vs. NS-treated; *p<0.05, **p<0.01, ***p<0.001. #: Akt2-/- vs. WT; #p<0.05, ##p<0.01, ###p<0.001.

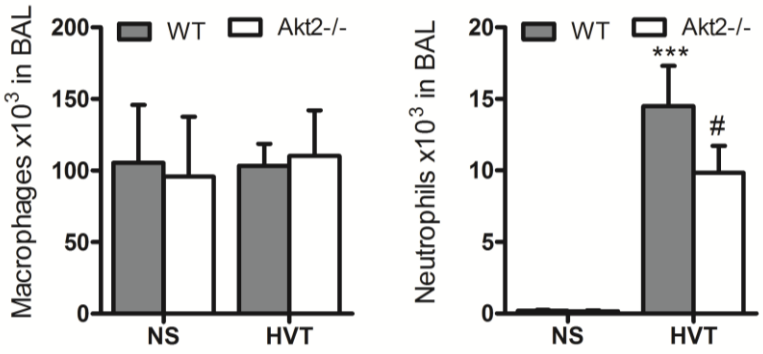

Figure 36. Macrophage and neutrophil cell numbers in BAL from WT and Akt2-/- mice exposed to high tidal volume ventilation for 3,5 hours. Box Plot: box shows 5-95 percentiles, line at median and whiskers at min-max. *: HVT- vs. NS-treated; *p<0.05, **p<0.01, ***p<0.001. #: Akt2-/- vs. WT; #p<0.05, ##p<0.01, ###p<0.001.

These results suggested that ablation of Akt2 resulted in reduced lung inflammation and ameliorated acid – induced lung injury and ventilation induced lung injury compared to WT mice.

Akt2 deficiency regulates alveolar macrophage phenotype

Akt2 ablation suppresses M1 polarization and promotes M2 phenotype in Alveolar Mϕ in acid-induced lung injury

To determine the inflammatory phenotype of infiltrated macrophages in the model of acid-induced lung injury, we measured the concentration of inflammatory mediators in the BALF and the presence of M1 and M2-type of macrophages in the lungs of WT and Akt2-/- mice during the acute phase (12 hours following acid aspiration) and at the resolution stage (24 hours following acid aspiration). In the acute phase of injury, twelve hours after acid-aspiration, M1 activation of macrophages was observed in WT mice; alveolar macrophages overexpressed iNOS (Figure 37A, C, D, F) and IL-12β (Figure 37B, E). The expression of M1 markers returned to basal levels at 48 hours of injury (Figure 37A, B). However, antigen presentation was not induced by HCL-aspiration as was assessed by CD80 and CD86 protein expression (data not shown).The concentration of NO metabolite Nitrite in the BAL fluid was increased in WT mice 12 hours post-injury (Figure 37G). Expression of M1 markers and the levels of NO after acid aspiration-induced lung injury were lower in Akt2-/- mice compared to WT (Figure 37A-G).

The expression of M2 activation markers, Arg-1, Fizz1 and Ym1, 12 hours post acid-aspiration was evident in both WT and in Akt2-/- macrophages. The mRNA and protein levels of Arg-1, Fizz1 and Ym1, as well as arginase activity and MGL1 and MGL2 protein expression, were higher in Akt2-/- macrophages compare to WT ones (Figures 38A-G and 391A). The above M2 markers were elevated in Akt2-/- macrophages compared to WT Mϕ both at basal levels in normal saline treatment and upon 12 and 24 hours of acid-aspiration, however there were no significant difference between these groups at 48hours, were significant up-regulation of M2 response took place in WT macrophages as well (Figure 38E,G,I). Arg1 mRNA was upregulated both in WT and Akt2-/- macrophages 12h following acid aspiration however upregulation of its protein and its activity was not statistically significant at 12h in WT MΦ, but was further induced at later time points (24hours following HCL instillation - data not shown).

MGL1 and 2 protein expression was also higher in Akt2-/- alveolar macrophages compared to macrophages from WT mice (Figure 39A), while IL-10 expression was not significantly different among the WT and Akt2-/- macrophages (Figure 39B).

In vitro application of siRNA targeting Akt2 in isolated alveolar macrophages from WT mice, resulted in downregulation of Akt2 and concomitant up-regulation of C/EBPβ, an M2 polarization-associated transcription factor (49), as well as Arg-1 and Fizz1 (Figure 38H, I), further supporting the impact of Akt2 suppression in promoting M2 polarization in alveolar macrophages.

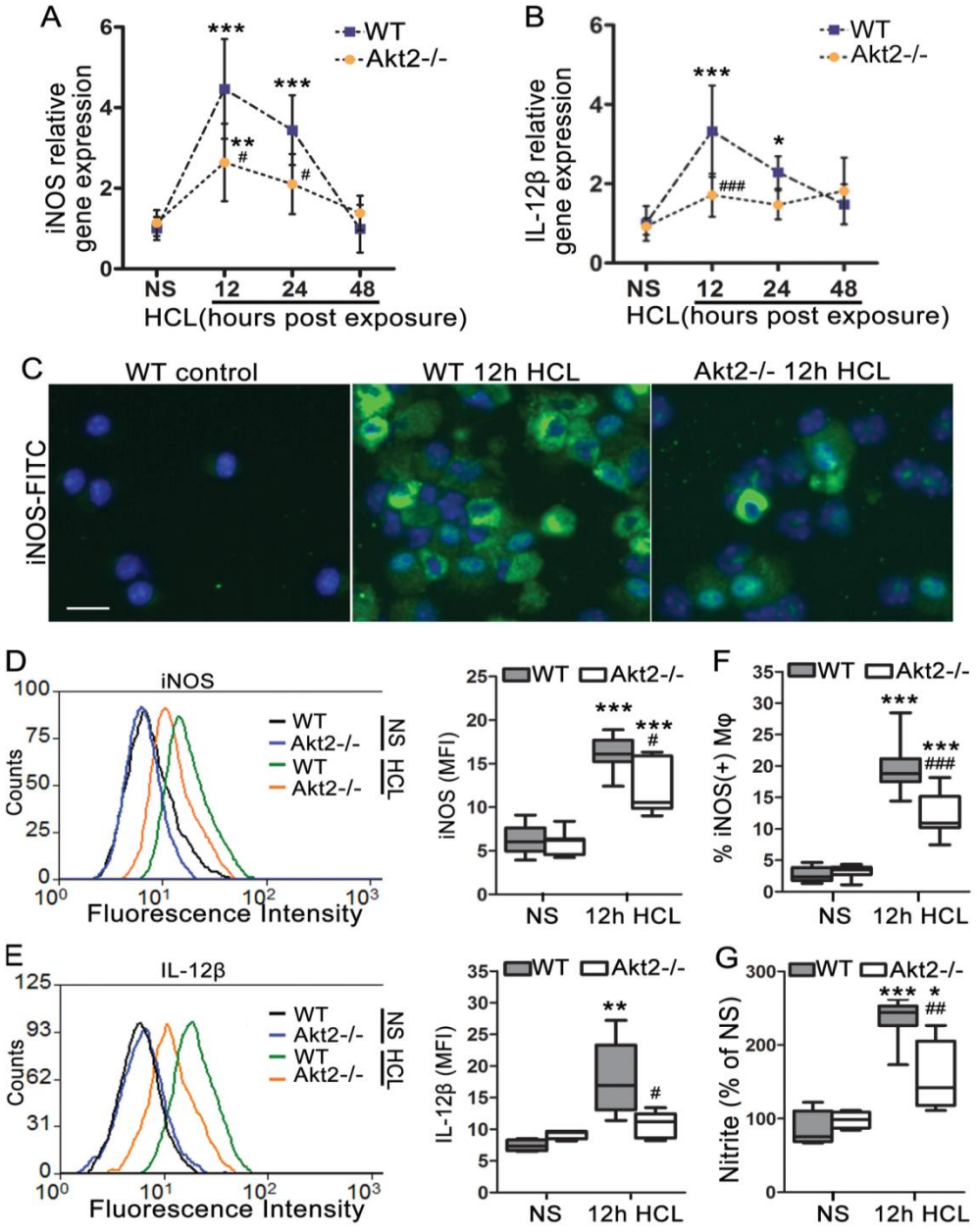

Figure 37. Classical (M1) macrophage activation in acid-induced lung injury was reduced in Akt2-/- mice. iNOS and IL-12β, markers of M1 activation were evaluated in alveolar macrophages from WT and Akt2-/- mice at basal levels and upon acid aspiration. (A) iNOS and (B) IL-12β mRNA induction was assessed at different time points after acid aspiration compared to the normal saline (NS) aspiration group. iNOS protein levels in WT and Akt2-/- alveolar macrophages were assessed by (C) immunofluorescence and (D) fluorescence intensity (measured by flow cytometry, MFI) twelve hours after acid exposure. Similarly IL-12β protein levels were evaluated by (E) fluorescence intensity (MFI) twelve hours after acid exposure and compared to mice receiving normal saline. (F) iNOS positive WT and Akt2-/- macrophages based on flow cytometry cell counts and (K) nitrite levels in BAL fluid from WT and Akt2-/- mice after acid exposure. Scale bar in (C) is representative of 25μm. MFI: mean fluorescence intensity of cells gated for CD11c. N=5-8 mice per group. Bar graphs represent mean ± SD. Box Plot: box shows 5-95 percentiles, line at median and whiskers at min-max. *: acid- vs. NS-treated; *p<0.05, **p<0.01, ***p<0.001. #: Akt2-/- vs. WT; #p<0.05, ##p<0.01, ###p<0.001.

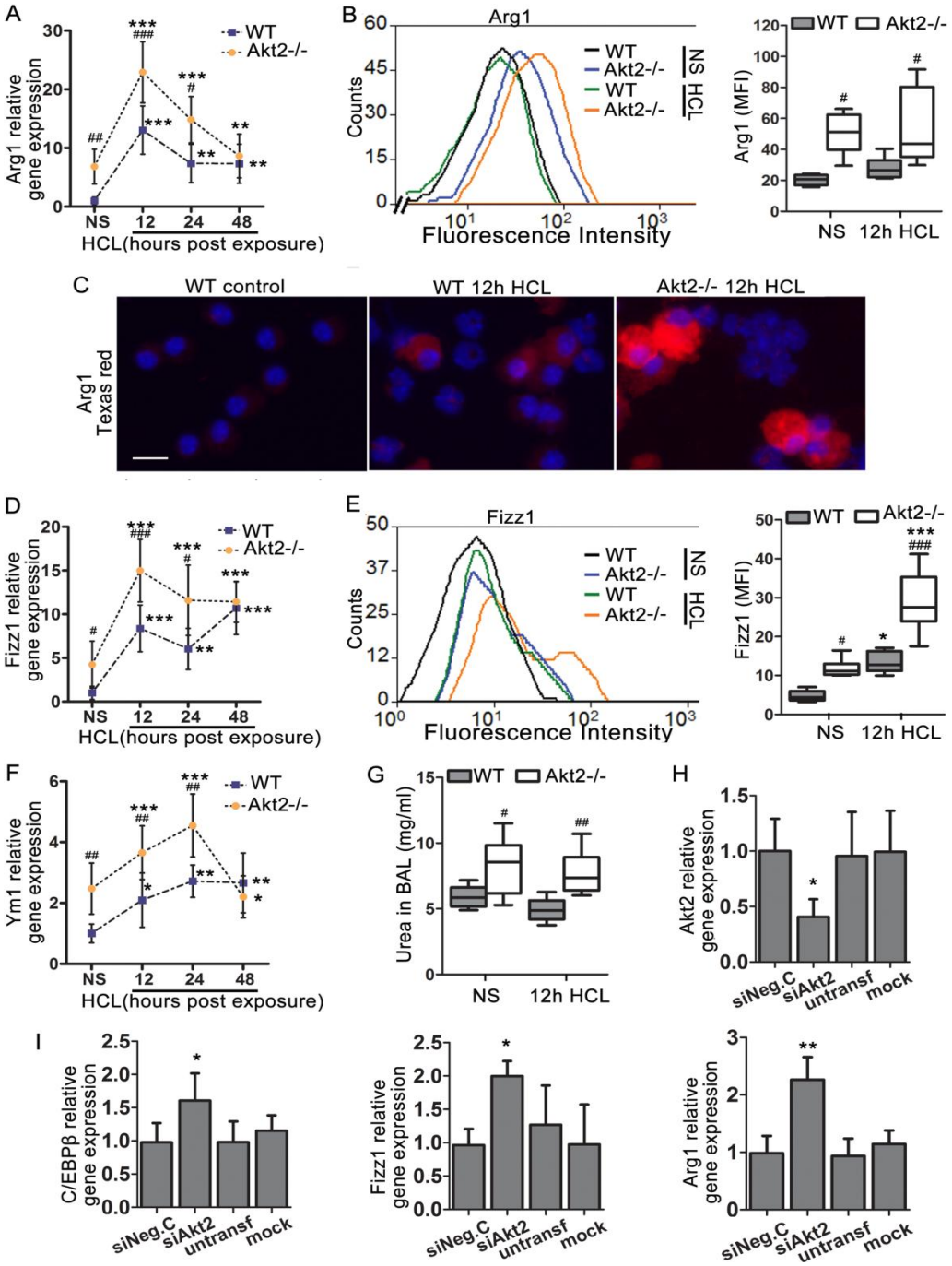

Figure 38. Akt2-/-alveolar Mϕ exhibit M2 phenotype following acid-induced ALI. Arg1, Fizz1 and Ym1, markers of M2- macrophage activation were evaluated in WT and Akt2-/- mice at basal levels and upon acid aspiration . Arg1 expression was assessed at (A) mRNA levels and (B) protein levels by flow cytometry (MFI) and (C) immunofluorescence, 12h after acid aspiration. Similarly, Fizz1 (D) mRNA levels and (E) protein levels (MFI) were evaluated in the same conditions.F) Ym1 mRNA levels in WT and Akt2-/- Mf in acid treated mice compared to NS - treated mice (G) Urea production, an index of arginase activity, was evaluated in WT and Akt2-/- alveolar macrophages after acid exposure. mRNA levels of (H) Akt2 and (I) C/EBPβ, Arg1 and Fizz1 in isolated alveolar macrophages transfected with siRNA for Akt2 (siAkt2) or non-targeting siRNA (siNegC). Cells that received only transfection reagent (mock) or left without treatment (untransfected) were used as controls. Scale bar in (C) corresponds to 25μm. MFI: mean fluorescence intensity of cells gated for CD11c. N=5-8 mice per group. Bar graphs represent mean ± SD. Box Plot: box shows 5-95 percentiles, line at median and whiskers at min-max. *: acid- vs. NS-treated; *p<0.05, **p<0.01, ***p<0.001. #: Akt2-/- vs. WT; #p<0.05, ##p<0.01, ###p<0.001

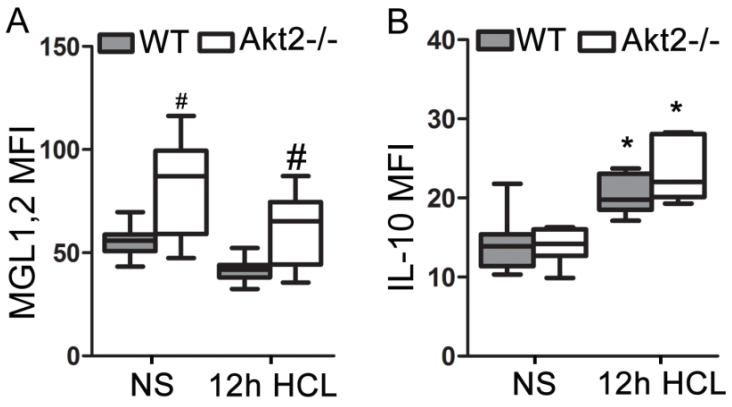

Figure 39. MGL-1,2 and IL-10 protein levels in alveolar macrophages. (A) MGL-1,2 and (B) IL-10 protein levels in alveolar macrophages of WT and Akt2-/- mice exposed to acid-aspiration for twelve hours. NS: normal saline. MFI: mean fluorescence intensity. Box Plot: box shows 25-75 percentiles, line at median, and whiskers at 5-95 percentiles. N=5-8 per group. *: acid- vs. NS-treated; *p<0.05. #: Akt2-/- vs. WT; #p<0.05

Mechanisms of protection from ALI in Akt2 deficient mice

Involvement of miR-155 and miR-125b in macrophage activation phenotype in acid-induced lung injury and the role of Akt2

Next, we sought to elucidate the mechanisms via which Akt2 deficiency regulates macrophage polarization and protects from acid-induced lung injury. Earlier studies from our group have shown that miR-155 plays a central role in promoting M1 activation in macrophages following LPS stimulation and is under the control of Akt kinases (49, 68). Furthermore, in the recent literature, miR155 and miR-125b have been found to promote M1 phenotype in macrophages via regulation of C/EBPb and IRF4 respectively (49, 116). Whether or not miR-155 and/or miR- 125b play a role in regulation of M1 macrophage activation in HCL lung injury remains elusive.

To investigate the involvement of miR-155 in the regulation of M1 phenotype in our model of aseptic lung injury, we measured miR-155 levels in alveolar macrophages from WT and Akt2-/- mice exposed to acid. We found that the expression of miR-155 did not increase in WT alveolar macrophages at twelve hours after acid–aspiration, but was suppressed at 24 hours post injury (Figure 40A). In order to exclude miR-155 involvement in M1 activation in our model, we stimulated alveolar macrophages *in vitro* with BAL fluid collected from WT mice, six hours after acid-aspiration. We found that exposure to BAL fluid did not cause an increase in miR-155 levels although it promoted iNOS expression (Figure 40C, D), suggesting that miR-155 does not contribute to M1 activation of macrophages in this model of aseptic lung injury.

The development of M2 phenotype in WT alveolar macrophages 24 hours after acid-aspiration was associated with a decrease in miR-155 expression (Figure 40A). The expression of miR-155 in Akt2-/- alveolar macrophages was lower compared to WT both at basal levels and 12 hours post acid-aspiration (Figure 540A), in agreement with their inherent M2 phenotype. C/EBPβ levels, a target of miR155, were inversely correlated with miR-155 levels (Figure 40B). C/EBPβ expression increased in WT macrophages at 12 hours after acid-aspiration, and it was higher in Akt2-/- macrophages compared to WT (Figure 40B). These results suggest that even though miR-155 does not participate in the initial M1 activation of alveolar macrophages in aseptic lung injury, its suppression coincides with the emergence of M2 status.

MiR-125 is a miRNA recently reported by other groups to play major role in M1 macrophage activation, mainly via the suppression of IRF4 (116). To investigate the involvement of miR-125b in the regulation of M1 phenotype in our model of aseptic lung injury, we measured miR-125b levels in alveolar macrophages from WT and Akt2-/- mice exposed to acid. We found that there was a mild non- significant increase in expression of

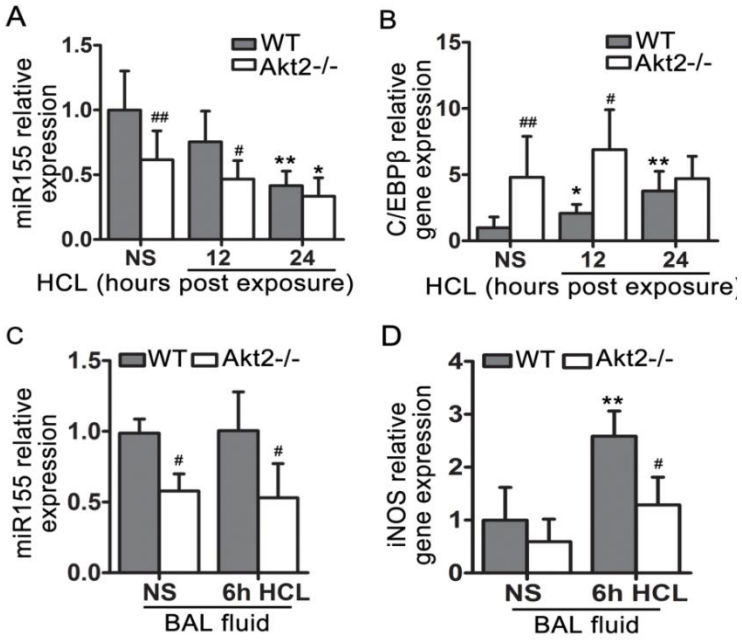

Figure 40. MiR-155 expression in acid-induced lung injury. Expression of (A) miR-155 and (B) its target mRNA C/EBPβ in WT and Akt2-/- alveolar macrophages from mice exposed to acid for 12 and 24 hours. (C) MiR-155 and (D) iNOS mRNA levels in WT and Akt2-/- alveolar macrophages treated *in vitro* with bronchoalveolar lavage (BAL) fluid from WT mice that received either normal saline (NS) or HCL for 6 hours in vivo. Mean ± SD is depicted of n=4-8 mice or samples per group. *: acid- vs. NS-treated; *p<0.05, **p<0.01. #: Akt2-/- vs. WT; #p<0.05, ##p<0.01.

miR-125 in WT alveolar macrophages at twelve hours after acid–aspiration compared to control mice (Figure 41). Also, there was no difference in miR-125b levels in WT and Akt2-/- macrophages (Figure 41).

We also examined the levels of IRF4 in alveolar macrophages from WT and Akt2-/- animals exposed to acid, since IRF4 is target of mir-125b and a positive regulator of M2 activation (116). The expression of IRF4 in naïve Akt2-/- alveolar macrophages was higher compared to WT both at basal levels and 12 hours post acid-aspiration (Figure 41). However, we failed to detect IRF4 protein expression in alveolar macrophages.

These results suggest that miR-125b does not participate in the initial M1 activation of alveolar macrophages in aseptic lung injury. Akt2-/- alveolar macrophages have higher levels of IRF4 mRNA but compared to WT but this upregulation was not correlated with miR-125b levels and was not confirmed in protein level.

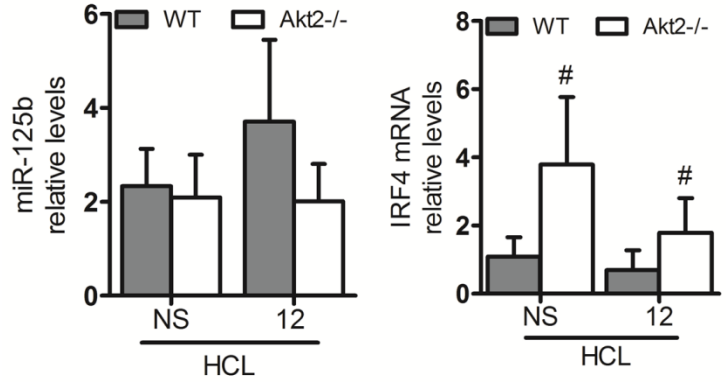

Figure 41. Mir-125b and IRF4 expression in acid induced lung injury.
Expression of (A) miR-125b and (B) its target mRNA IRF4 in WT and Akt2-/- alveolar macrophages from mice exposed to acid for 12 and 24 hours. Mean ± SD is depicted of n=4-7 mice or samples per group. #: Akt2-/- vs. WT; #p<0.05.

Akt2 deficient macrophages exhibit suppressed TLR4 signaling, via the upregulation of miR-146a

Since macrophage activation and lung inflammation depend on TLR4 signals, we examined the impact of Akt2 ablation on TLR4 signaling components. We found that mRNA levels of TRAF6 and IRF5 but not of IRAK1, three downstream mediators of TLR4 signaling, were increased in WT alveolar macrophages 12 hours after acid-aspiration (Figure 42A, B). On the contrary, Akt2-/- macrophages expressed less TRAF6, IRF5 and IRAK1 compared to WT macrophages both at basal levels and 12 hours after acid-aspiration (Figure 42A, B). Furthermore, application of siRNA targeting Akt2 in isolated alveolar macrophages resulted in downregulation of TRAF6 and IRF5 compared to cells that received non-targeting siRNA (Figure 42C).

STAT1 signaling activation is also crucial for M1 activation and it was recently found that apart from interferon receptors it can also be activated downstream TLR4 via interaction with TRAF6 (397, 398). STAT1 mean fluorescence intensity was upregulated in WT macrophages exposed to acid. STAT1 levels were significantly reduced at basal levels and after 12hours of exposure to hydrochloric acid in macrophages from Akt2-/- mice compared to WT ones (Figure 43).

IRAK1, TRAF6, STAT1 and IRF5 mRNAs are regulated by the anti-inflammatory miRNA miR-146a (399, 400). We, therefore, evaluated the expression of miR-146a in alveolar macrophages after acid-aspiration. MiR-146a expression did not change significantly at 12 hours after acid-aspiration, but increased at 24 hours (Figure 42E). Interestingly, in Akt2-/- macrophages the expression of miR-146a was higher compared to WT prior to acid aspiration, as well as after 12 and 24 hours (Figure 42E). To further support that suppression of Akt2 results in miR-146a induction, we transfected macrophages with siRNA for Akt2 and found that miR-146a was upregulated (Figure 42D). Additionally, miR-146a expression was higher, while TRAF6 and IRF5 mRNA and protein expression were lower in Akt2-/- peritoneal macrophages compared to WT macrophages (Figure 42F, G). These findings suggested that miR-146a and its targets TRAF6 and IRF5 were affected by Akt2 deletion or suppression.

To verify if the above mechanism is equivocal in macrophages, we assessed miR-146a, TRAF6 and IRF5 levels in peritoneal macrophages as well. MiR-146a levels were higher and TRAF6 and IRF5 mRNA levels were lower in Akt2-/- peritoneal macrophages compared to WT (Figure 42C). Moreover, protein levels of TRAF6 and IRF5 were also lower in Akt2-/- peritoneal macrophages compared to WT (Figure 42F,G).

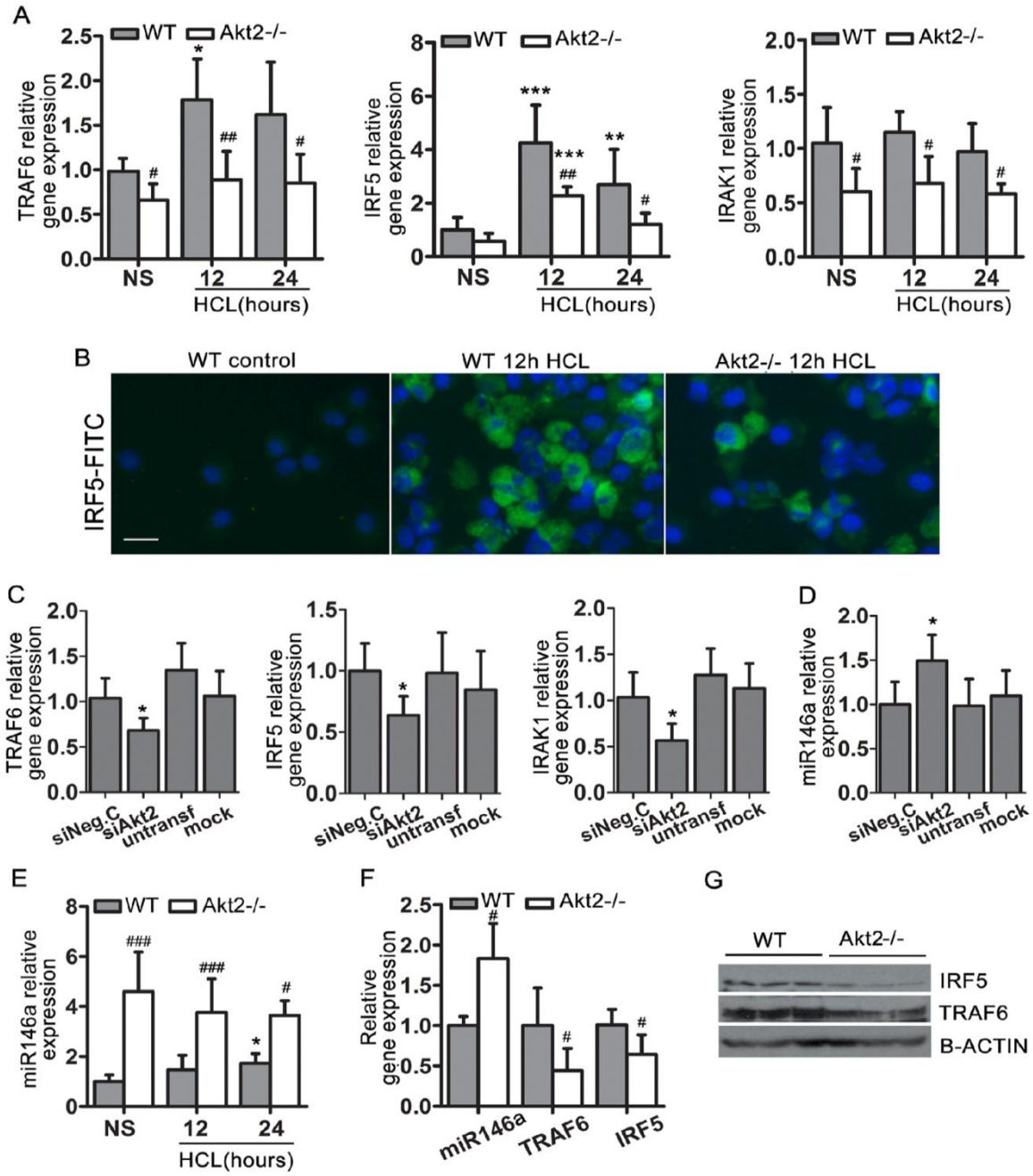

Figure 42. TLR4 signaling and miR-146a expression in acid-induced lung injury. (A) mRNA levels of TRAF6, IRF5 and IRAK1 and (B) protein expression of IRF5 in WT and Akt2-/- alveolar macrophages from mice exposed to acid aspiration for 12hours. Scale bar corresponds to 25μm. (C) mRNA levels of TRAF6, IRF5 and IRAK1 and (D) miR-146a in alveolar macrophages treated with either siRNA for Akt2 (siAkt2) or non-targeting siRNA (siNegC). Cells that received only transfection reagent (mock) or left without treatment (untransfected) were used as controls. (E) Levels of miR-146a in WT and Akt2-/- alveolar macrophages from mice that received acid for 12 or 24 hours. (F) Comparison of miR-146a, TRAF6 and IRF5 mRNA levels in unstimulated WT and Akt2-/- peritoneal macrophages. (G) Protein levels of IRF5 and TRAF6 in WT and Akt2-/- unstimulated peritoneal macrophages. B-actin was used as control. NS: normal saline. Mean ± SD is depicted of n=4-8 mice or wells per group. *: acid- vs. NS-treated; *p<0.05, **p<0.01, ***p<0.001. #: Akt2-/- vs. WT; #p<0.05, ##p<0.01, ###p<0.001.

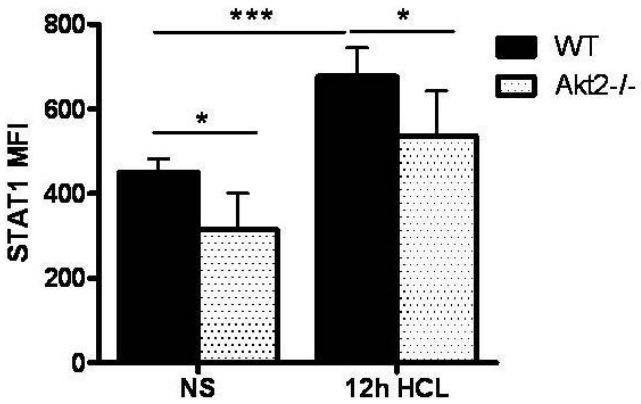

Figure 43. STAT1 Mean fluorescence intensity (MFI) levels in BAL alveolar macrophages from WT and Akt2-/- mice, 12h post HCL administration, n=8. *p<0.05, ***p<0.001.

MiR-146a prevents M1 activation *in vitro* and is critical for the protection observed in the absence of Akt2

To investigate whether miR-146a upregulation is essential for amelioration of the M1 response in Akt2-/- mice, we isolated peritoneal macrophages from WT and Akt2-/- mice, induced M1 polarization by treating them with LPS, a stimulus that promotes macrophage activation and transfected them with either a miR-146a mimic or a miR-146a inhibitor. As controls, we used cells treated with negative control miRNA (scramble), cells treated solely with transfection reagent (mock) and cells that remained untreated (i.e. non transfected). Akt2-/- macrophages are hypo-responsive to LPS and maintain an M2 phenotype both *in vitro* and *in vivo* when mice were subjected to LPS-induced endotoxin shock (49).

Transfection of WT macrophages with miR-146a resulted in suppression of TRAF6 and IRF5. The effect of miR-146a in suppressing TRAF6 and IRF5 in Akt2-/- macrophages was less prominent compared to WT (Figure 44A, B). Inhibition of miR-146a by a miR-146a inhibitor did not affect the expression of TRAF6 and IRF5 in WT macrophages but upregulated their expression in the absence of Akt2 (Figure 44A, B).

Furthermore, miR-146a transfection inhibited LPS-induced iNOS expression in WT macrophages (Figure 46A) and led to up-regulation of C/EBPβ, Arg1 and Fizz1 in control and LPS treated WT macrophages (Figures 46B-D and 45). Moreover, IL-6 and TNFα expression was reduced in LPS stimulated WT macrophages transfected with miR-146a (Figure 46E, F). In contrast, transfection of miR-146a in Akt2-/- macrophages did not affect LPS-induced iNOS, IL-6 and TNFα, when compared to LPS treated Akt2-/- macrophages that received negative control miRNA (Figure 46A, E, F). However, inhibition of miR-146a in Akt2-/- macrophages increased LPS-induced iNOS, IL-6 and TNFα, but did not appear to cause reduction in C/EBPβ, Arg-1 and Fizz1 suggesting that these molecules are regulated by a different Akt2-dependent mechanism (Figure 46B-F).

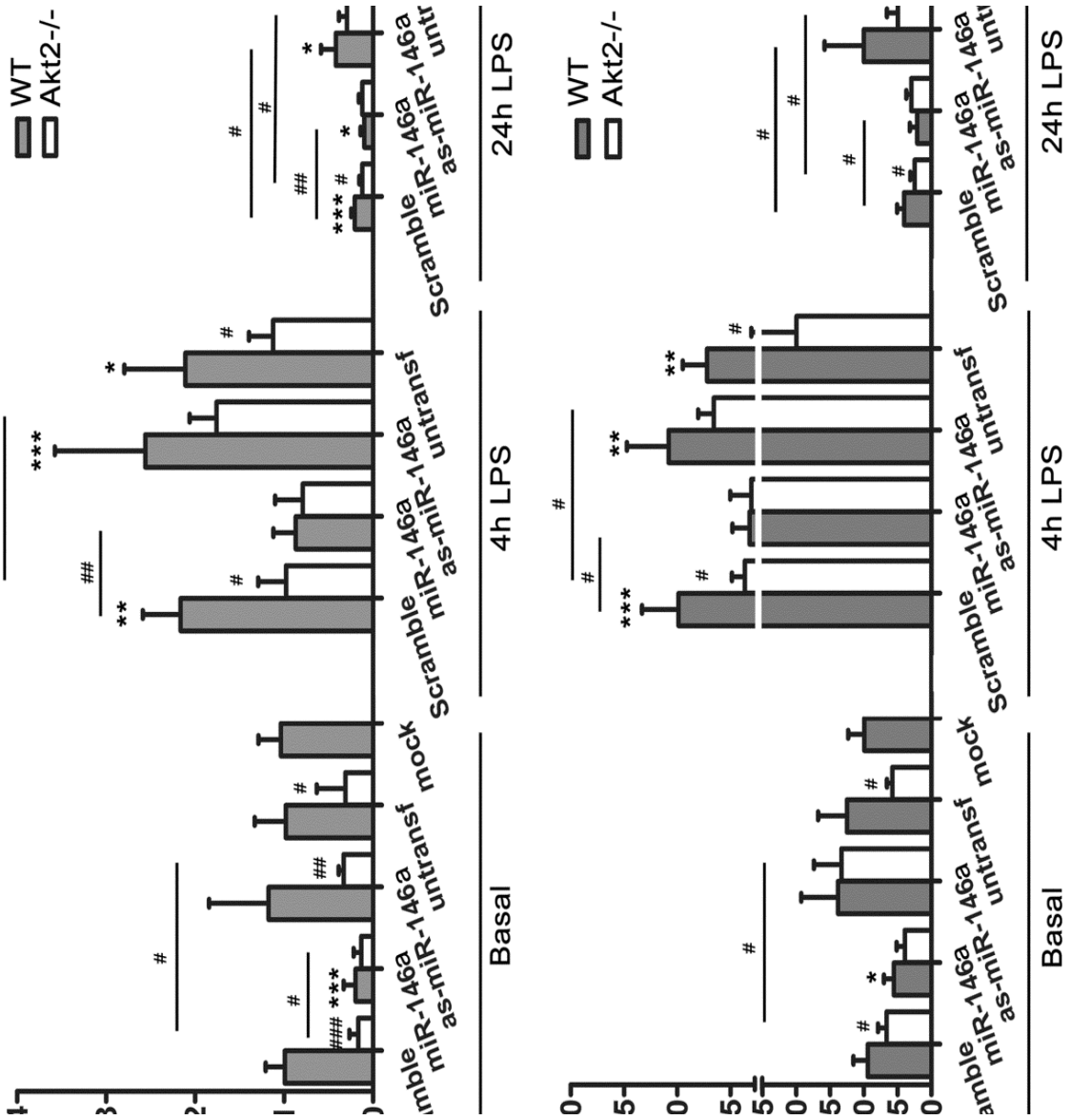

Figure 44. Modulation of miR-146a expression in WT and Akt2-/- macrophages in culture. mRNA levels of (A) TRAF6 and (B) IRF5 in WT and Akt2-/- peritoneal macrophages that were transfected with a miR-146a mimic, an inhibitor of miR-146 or a non-targeting control RNA (scramble). Untransfected cells as well as cells that received only transfection reagent (mock) were used as experimental controls. Mean ± SD is depicted of n=4-5 wells per group. In X- axis, miR-146a represents the miR-146a mimic while as-miR146a the miR146a inhibitor (antisense). *: LPS- vs. NS-treated; *p<0.05, **p<0.01, ***p<0.001. $^{\#}$: Akt2-/- vs. WT; $^{\#}$p<0.05, $^{\#\#}$p<0.01, $^{\#\#\#}$p<0.001.

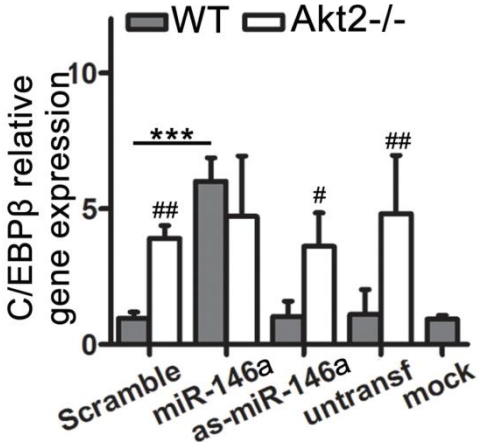

Figure 45. MiR-146a upregulates C/EBPβ. C/EBPβ mRNA levels in unstimulated WT and Akt2-/- macrophages that were treated with either miR-146a mimic, miR-146a inhibitor of non-targeting control (scramble). Untransfected cells as well as cells that received only transfection reagent (mock) were used as experimental controls. Mean ± SD is depicted of n=4-6 wells per group. *: acid- vs. NS-treated; ***p<0.001. $^{\#}$: Akt2-/- vs. WT; $^{\#}$p<0.05, $^{\#\#\#}$p<0.001.

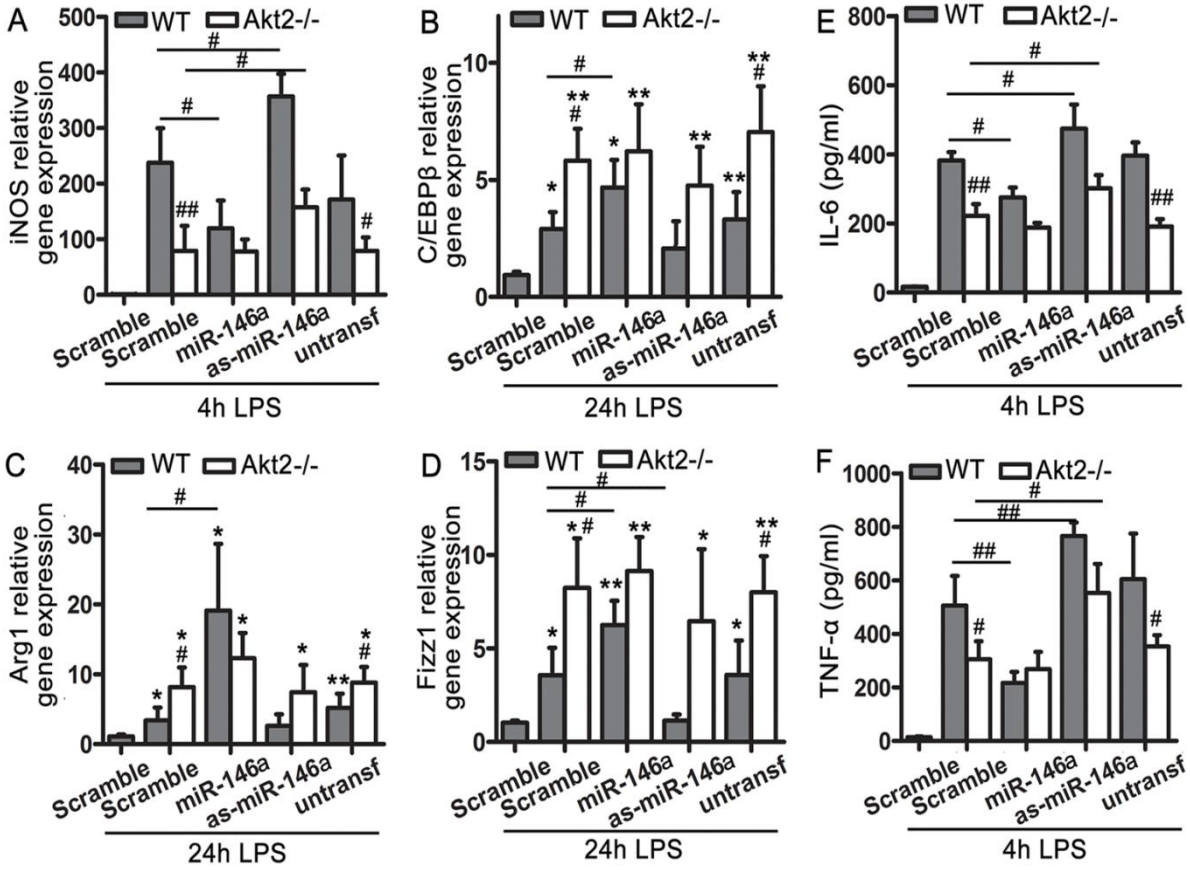

Figure 46. MiR-146a modulates macrophage activation in WT and Akt2-/- macrophages. mRNA levels of (A) iNOS, (B) C/EBPb, (C) Arg-1 and (D) Fizz1 in WT and Akt2-/- peritoneal macrophages that were treated with either a miR-146a mimic, an inhibitor of miR-146 or an non-targeting control RNA (scramble) are demonstrated. iNOS levels were assessed 4 hours post LPS stimulation, while C/EBPb, Arg-1 and Fizz1 24 hours post LPS. Protein levels of (E) IL-6 and (F) TNFα in supernatants of LPS-stimulated WT and Akt2-/- macrophages that were transfected with either miR-146a mimic, an inhibitor of miR-146a or a non-targeting control RNA. Non-transfected cells as well as cells that received only transfection reagent (mock) were used as experimental controls. NS: normal saline. N=5-8 mice per group. Bar graphs represent mean ± SD. *: acid- vs. NS-treated; *p<0.05, **p<0.01, ***p<0.001. $^{\#}$: Akt2-/- vs. WT; $^{\#}$p<0.05, $^{\#\#}$p<0.01.

The role of M2 macrophages in the pathogenesis of ALI

Adoptive transfer of Akt2-/- macrophages partially protects WT mice from the development of ALI

With the results presented so far, we show that Akt2-/- mice exhibit M2 alveolar macrophage phenotype and are protected from the development of ALI. However, to understand the importance of M2 macrophages in our model we opted to deplete alveolar macrophages from WT mice and to transfer akt2-/- macrophages intratracheally prior to HCL administration. First, we utilized the liposomal – mediated macrophage "suicide" phenomenon described by van Rooijen, according to which, liposomal encapsulated - dichloromethylene bisphosphonate (clodronate) is phagocytosed by monocytes and macrophages and results in their selective apoptosis (380, 381). Minimal uptake is demonstrated in neutrophils and endothelial cells, but this does not result in apoptosis and liposomal clodronate does not accumulate in T lymphocytes or epithelial cells (381).

First, various concentrations of clodronate were given either intratracheally or i.v and the extend of macrophage depletion as well as the neutrophilic infiltration in the lung were assessed 24h later. Based on the literature and on preliminary experiments, substantial depletion of alveolar macrophages occurs within 24h of intratracheal (IT) administration of liposomal clodronate and persists for at least 72h (381).

The administration of liposomes containing PBS did not affect macrophage viability but it cause a minor neutrophilic response (approximately 5.000-10.000 cells /ml of BALF). The extend of macrophage depletion was directly dependent on the concentration of liposomal clodronate, but high concentrations of clodronate also caused a robust neutrophilic response, probably due to extensive macrophage apoptosis (Figure 47). The working concentration was chosen with the criterion of adequate macrophage depletion with the minimal neutrophilic response (Figure 47, 1:3 dilution). Intravenous (IV) administration of clodronate failed to eliminate pulmonary macrophages (Figure 47), thus only i.t route was applied in the following experiments.

Next, we measured the effect of macrophage depletion on lung inspiratory capacity (compliance) upon ALI. The animals that received liposomes filled with either PBS or clodronate exhibited reduced inspiratory capacity, 20% and 10% less respectively, compared to normal saline controls (Figure 48).

The WT animals that received liposomal clodronate 24h before ALI had no difference with animals that received PBS liposomes (they showed a mild trend towards increased inspiratory capacity compared to WT animals that received PBS containing clodronate, but this effect did not reach statistical significance) (Figure 48). Similarly, there was no difference in the inspiratory capacity in Akt2-/- mice that received PBS or clodronate containing

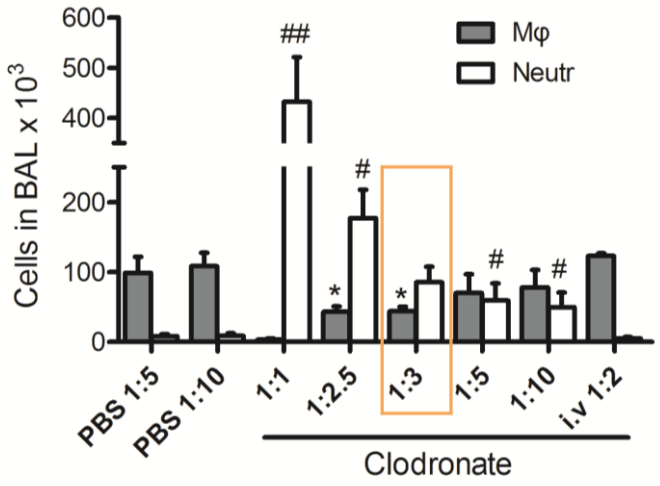

Figure 47. Effect of clodronate containing liposomes on lung inflammatory cell population. Macrophages and neutrophils accumulated in bronchoalveolar lavage (BAL) 24h after i.t administration and 48h after i.v administration of either PBS or clodronate containing liposomes. N=3-4 mice per group. *: Clodronate vs. PBS-; *p<0.05. #: Clodronate vs. PBS; #p<0.05, ##p<0.01.

liposomes and were exposed to HCL injury (Figure 48). Interestingly, we found no difference between WT and Akt2-/- animals with acid induced ALI that received PBS containing liposomes, and we hypothesized that WT and Akt2-/- mice may respond differently in this experimental setting.

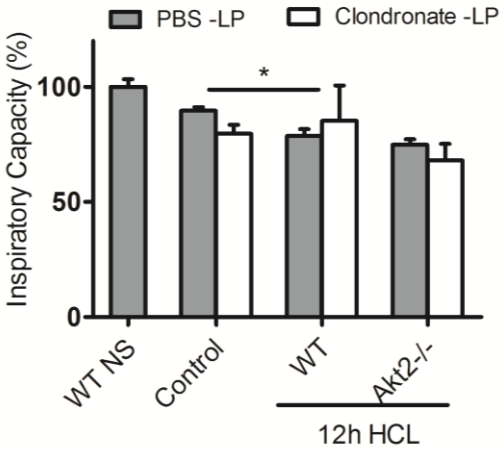

Figure 48. Inspiratory Capacity in WT and Akt2-/- mice treated with PBS or clodronate containing liposomes, 12h after HCL administration compared to normal saline (NS) group. N=4-5 mice per group. Graphs represent mean ±SD. *: acid- vs. NS-treated; *p<0.05.

To elucidate whether or not M2 macrophages can confer protection from ALI, in mice where alveolar macrophages have been depleted, we transferred WT or Akt2-/- alveolar macrophages, 1hour prior to HCL administration. As depicted in figure 49, WT animals with ALI that received akt2-/- macrophages had less iNOS positive macrophages and improved inspiratory capacity (Figure 50), compared to WT animals that received WT macrophages. On the contrary, they had no difference in neutrophilic infiltration (figure 50). Akt2-/- animals with ALI that received WT macrophages had more iNOS positive macrophages (although non-significantly) and reduced inspiratory capacity (Figure 50), compared to Akt2-/- animals that received Akt2-/- macrophages. Again, they had no difference in neutrophilic infiltration (Figure 50). Overall, Akt2-/- mice had a reduced neutrophilic response compared to WT mice mice regardless the macrophage population transferred (Figure 50), meaning that

neutrophilic chemotaxis is inherently defective in Akt2-/- mice and it is not dependent on macrophage activation state at this setting. Also, there was no change in the inspiratory capacity in WT and Akt2-/- animals that received WT and Akt2-/- cells respectively (Figure 50), as it has been shown among WT and Akt2-/- mice (Figure 48). This finding may indicate that the invasive nature of the experiment interferes with animals' physiology and normal lung responses.

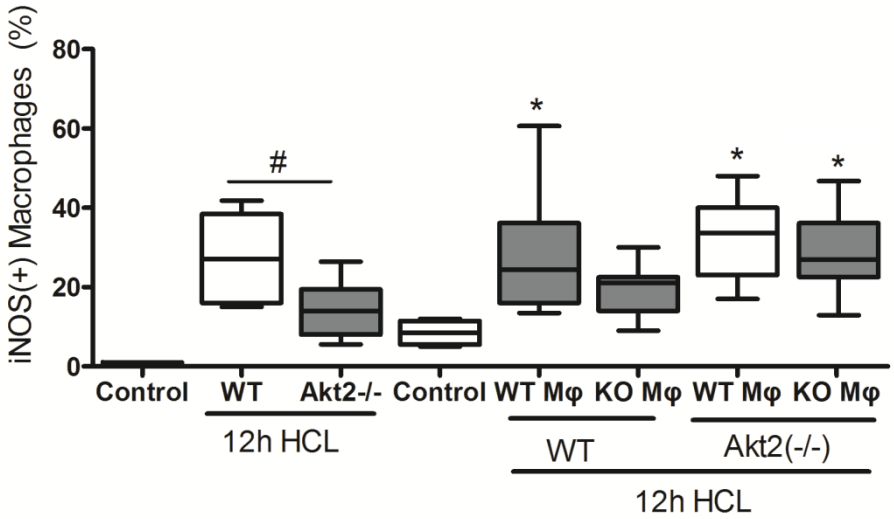

Figure 49. iNOS expression in ALI after macrophage adoptive transfer. iNOS positive alveolar macrophages, based on flow cytometry cell counts on CD11c+ cells in BALF , from WT and Akt2-/- mice after acid exposure and in WT and Akt2-/- mice treated with liposomal clodronate and subsequently received either WT or Akt2-/- alveolar macrophages i.t 1h before HCl administration. N=4-5 mice per group. Box Plot: box shows 5-95 percentiles, line at median and whiskers at min-max. *: acid- vs. NS-treated; *p<0.05.. #: Akt2-/- vs. WT; #p<0.05.

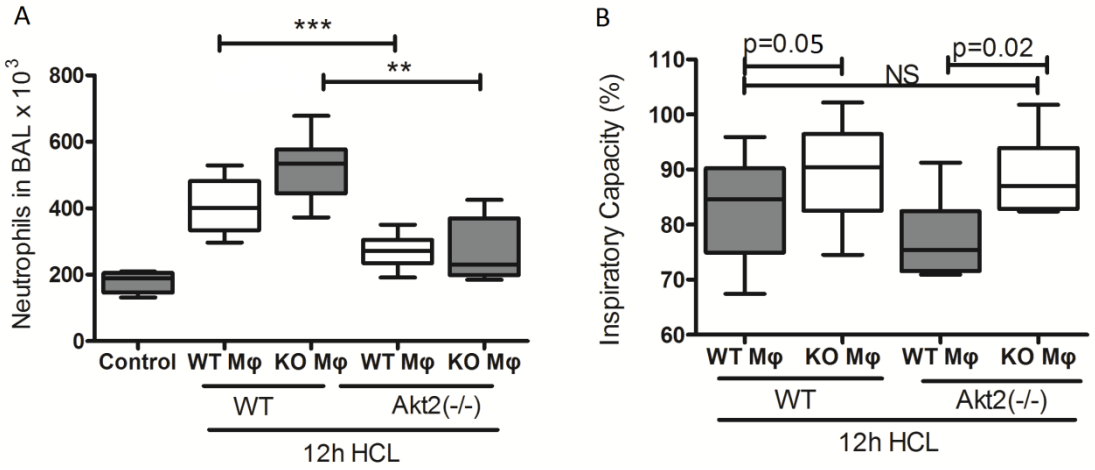

Figure 50. Effect of macrophage adoptive transfer in ALI. (A) the numbers of neutrophils accumulated in bronchoalveolar lavage (BAL) and the (B) lung inspiratory capacity 12h after HCL in WT and Akt2-/- animals macrophage depleted and reconstituted with WT or Akt2-/- alveolar macrophages. N=4-5 mice per group. Box Plot: box shows 5-95 percentiles, line at median and whiskers at min-max. *p<0.05.***p<0.001. #: NS : no- significant.

Therapeutic inhibition of Akt2 or induction of miR-146a by *in vivo* administration of siAkt2 or miR146a

To further confirm that inhibition of Akt2 and induction of miR-146a inhibit M1 activation of alveolar macrophages *in vivo*, and to show that induction of M2 polarization *in vivo* can ameliorate ALI, we attempted to administrate to acid-treated WT mice intratracheally siAkt2, miR-146a mimic or miR-146a inhibitor to modulate Akt2 or miR-146a expression respectively.

Before the application of the siRNA and miRNAs, several experiments utilizing siRNA targeting GAPDH took place in order find out the optimal effective dose needed. SiRNA targeting GAPDH was validated *in vitro* before *in vivo* application (data not shown). SiRNA targeting *GAPDH* or siRNA targeting *Luciferase* was initially instilled intratracheally in the lung in three different concentrations (0.5nmoles, 2.5nmoles or 5nmoles per mouse) and mRNA levels (Figure 51) and protein levels of GAPDH were assessed 48h and 72h later respectively (Figure 51). 5nmoles per mouse was chosen as the minimal concentration that promoted significant GAPDH mRNA suppression, with minimal lung toxicity (e.g. neutrophilic response). The application of modified siRNA targeting Luciferase in control animals without lung injury provoked a mild neutrophilic response, but there was no increase in numbers of macrophages (Figure 52), inflammatory mediators in the lung such as TNF-α (Figure 52) or protein concentration in BALF (Figure 52). Distribution of siRNA into the lung parenchyma following its intratracheal administration was assessed by Cy3-conjugated control siRNA (Figure 53 and 54).

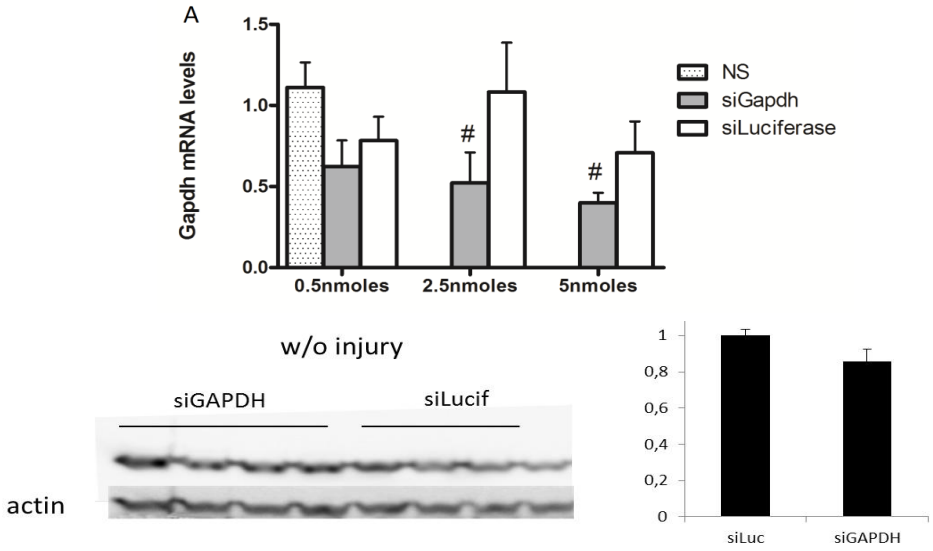

Figure 51. Effect of target suppression after local delivery of siRNA targeting GAPDH. (A) mRNA and (B) protein levels of GAPDH in total lung lysates from mice treated with 0.5, 2.5 or 5nmoles of siRNA targeting GAPDH i.t The mRNA levels were assessed 48h after siRNA administration while protein levels 72 hours later. B-actin was used as control. NS: normal saline. Mean ± SD is depicted of n=4-5 mice or wells per group. #: siGAPDH- vs.siLuciferase; #p<0.05.

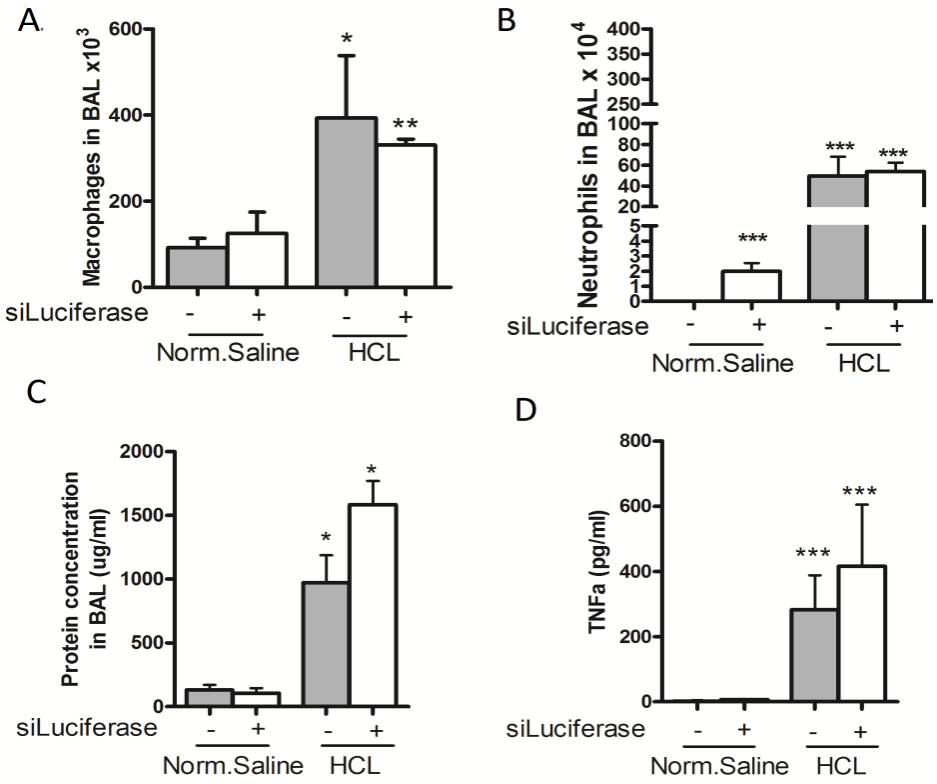

Figure 52. Effect of siRNA delivery in lung injury and inflammation. (A) Macrophages, (B) neutrophils, (C) protein concentration in BAL and (D) TNF-α levels in BALF in NS or HCL instilled WT mice treated or not with siRNA targeting Luciferase. Mean ± SD is depicted of n=4-5 mice or wells per group. #: siGAPDH- vs.siLuciferase; #p<0.05.

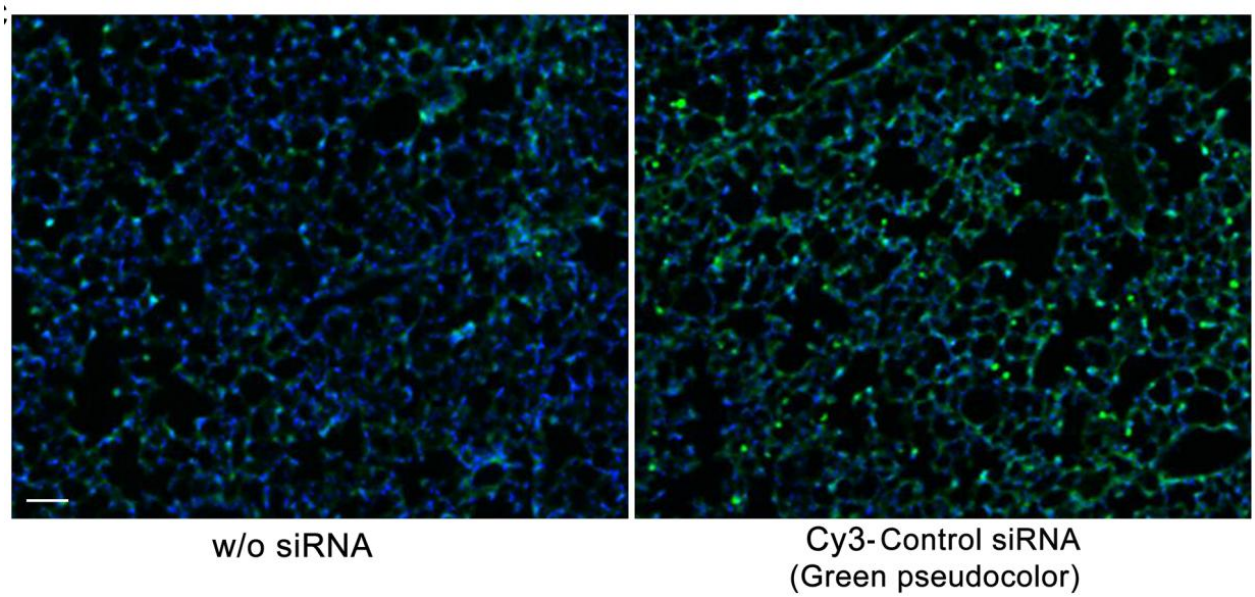

Figure 53. Efficiency of intra-tracheal delivery of siRNA. Lung immunofluorescence in WT animals that received either normal saline or Cy3 conjugated siRNA targeting siLuciferase (control siRNA). SiRNA fluorescence intensity is depicted using green pseudocolor (magnification 200x). Scale bar is representative of 50μM.

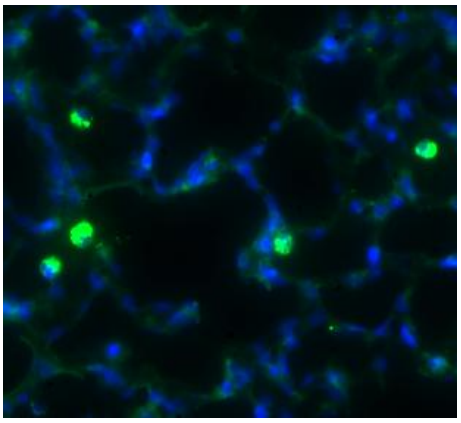

Figure 54. Efficiency of intra-tracheal delivery of siRNA.
Lung immunofluorescence in WT animals that received either normal saline or Cy3 conjugated siRNA targeting siLuciferase (control siRNA). SiRNA fluorescence intensity is depicted using green pseudocolor (magnification 400x).

The percentage of alveolar macrophages that received the siRNA was assessed by flow cytometry analysis 12h, 48h and 72hours after administration of Cy3 labeled siRNA targeting *Luciferase* (Figure 55). The effectiveness of GAPDH mRNA suppression in alveolar macrophages was also assessed by mRNA analysis via qPCR, 12h and 48h after siGADPH administration (Figure 56).

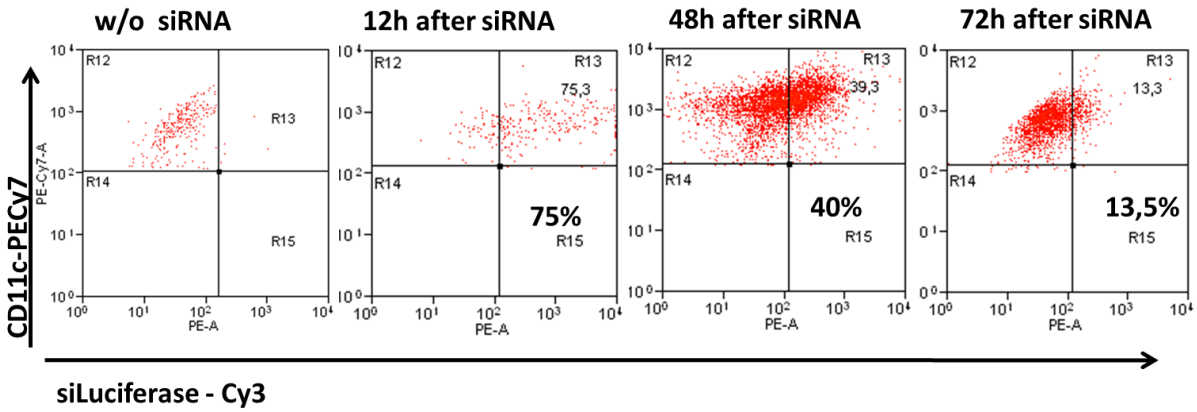

Figure 55. The percentage of alveolar macrophages that received the Cy3 labeled siRNA targeting *Luciferase,* assessed by flow cytometry analysis 12h, 48h and 72hours after administration.

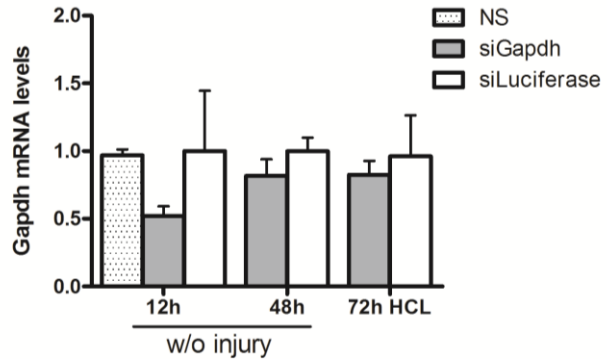

Figure 56. The effectiveness of GAPDH mRNA suppression in alveolar macrophages was also assessed by mRNA analysis via qPCR, 12h and 48h after siGADPH administration.

In vivo administration of siAkt2 and miR146a

To further confirm that inhibition of Akt2 and induction of miR-146a inhibit M1 activation of alveolar macrophages *in vivo*, acid-treated WT mice received intratracheally siAkt2, miR-146a mimic or miR-146a inhibitor to modulate Akt2 or miR-146a expression respectively. Transfection efficiency was confirmed by assessing total lung mRNA levels of Akt2, TRAF6 and IRAK1 (Figure 57) and miR-146a miRNA levels (Figure 57).

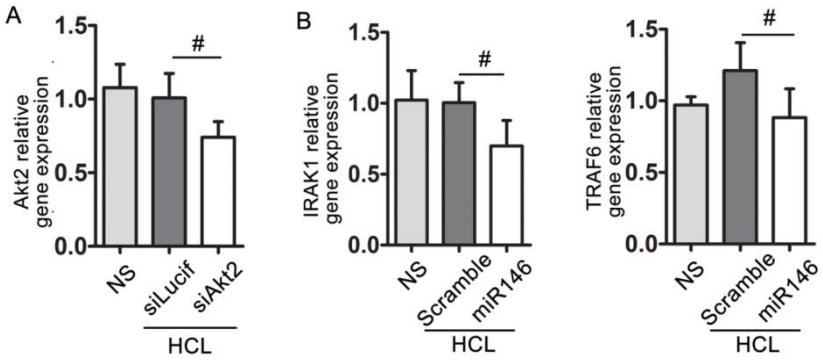

Figure 57. Efficiency of intra-tracheal delivery of siAkt2 and miR-146a. mRNA levels of (A) Akt2 and (B) IRAK1 and TRAF6 (miR-146a targets) are depicted in total lung lysates from WT animals that were treated intra-tracheally with siAkt2 and miR-146a respectively. Mean ± SD is depicted of n=4-6 wells per group. NS: normal saline. #: Akt2-/- vs. WT; #p<0.05

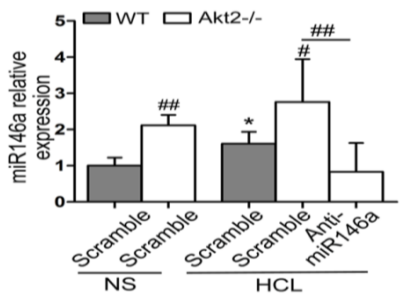

Figure 58. MiR146a relative expression in total lung lysates of WT and Akt2-/- animals treated with scramble RNA or miR146a inhibitor (anti-miR146a). N=6-8 animals per group or n=4-6 wells per group. *: acid- vs. NS-treated; *p<0.05. #: Akt2-/- vs. WT; #p<0.05, ##p<0.01.

Since iNOS is the major marker of M1 activated macrophages, we evaluated the effect of siAkt2, miR-146a mimic or miR-146a inhibitor administration in iNOS expression. Accordingly, iNOS was significantly suppressed in alveolar macrophages of mice treated with siAkt2 or miR-146a compared to those treated with scrambled-RNA (Figure 59), suggesting that *in vivo* modulation of Akt2 or miR-146a could effectively suppress aseptic lung inflammation induced by acid aspiration. Moreover, administration of miR-146a inhibitor in Akt2-/- mice resulted in partial reversal of iNOS suppression in those mice (Figure 60) suggesting that miR-146a induction is, at least in part, responsible for the protected phenotype of Akt2-/- mice. Overall, these findings suggest that induction of M2 macrophages either by inhibition of Akt2 or induction of miR-146a may be protective against aseptic lung injury.

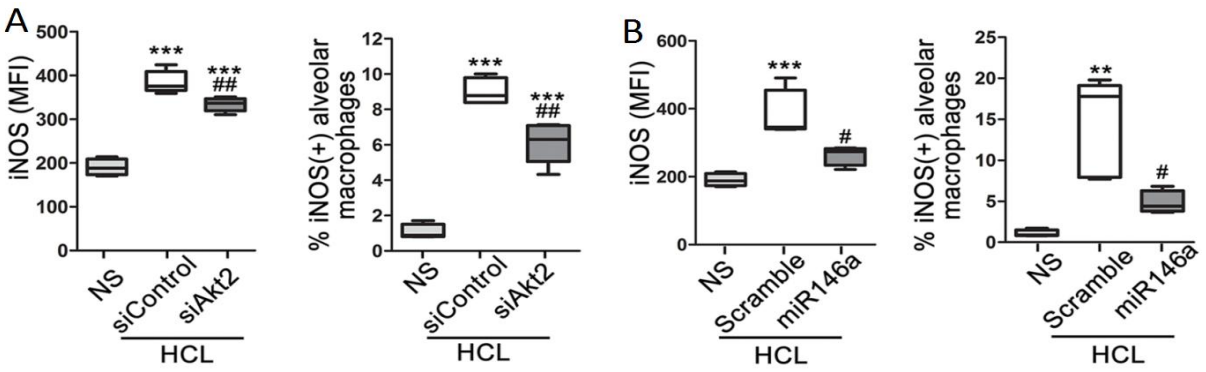

Figure 59. MiR-146a modulates macrophage activation in WT and Akt2-/- macrophages. iNOS protein expression (MFI) and percentage of iNOS positive macrophages were measured in WT mice with acid-induced lung injury that were treated *in vivo* with (A), siRNA for Akt2 (B) or miR146a mimic. MFI: Mean fluorescence intensity of cells gated for CD11c. NS: normal saline. N=5-8 mice per group. Bar graphs represent mean ± SD. Box Plot: box shows 5-95 percentiles, line at median and whiskers at min-max. *: acid- vs. NS-treated; *p<0.05, **p<0.01, ***p<0.001. #: Akt2-/- vs. WT; #p<0.05, ##p<0.01.

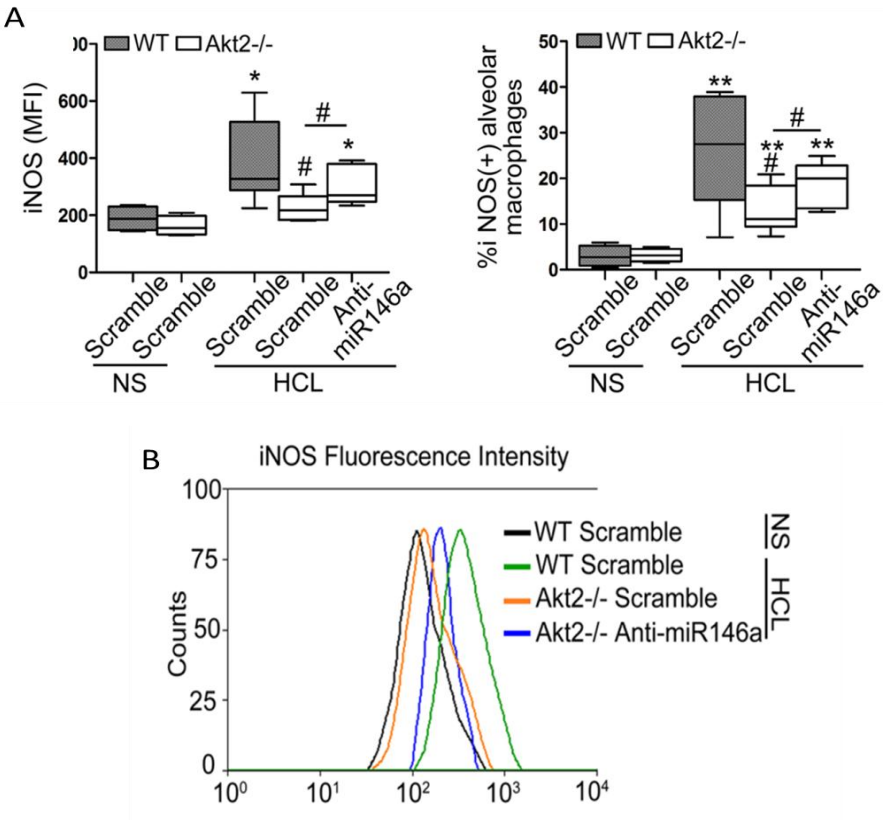

Figure 60. MiR-146a inhibition partially reverses iNOS suppression in Akt2-/- mice. (A) iNOS protein expression (MFI) and percentage of iNOS + macrophages were measured in WT mice with acid-induced lung injury that were treated *in vivo* with miR-146a inhibitor (Anti-miR146a). (B) Representative images of iNOS fluorescence intensity (measured by flow cytometry, MFI) after normal saline (NS) or acid exposure in alveolar macrophages (CD11+ cells) of WT and Akt2-/- animals treated with scramble RNA or miR146a inhibitor (anti-miR146a). MFI: of cells gated for CD11c. NS: normal saline. N=5-6 mice per group. Box Plot: box shows 5-95 percentiles, line at median and whiskers at min-max. *: acid- vs. NS-treated; *p<0.05, **p<0.01. #: Akt2-/- vs. WT; #p<0.05.

The effect of Akt2 depletion in a septic lung injury model

Since aspiration-induced lung injury is frequently accompanied by presence of pathogens such as bacteria, we investigated whether Akt2 depletion, and therefore M2 macrophage polarization, affects the response to live bacteria. For this purpose we inoculated WT or Akt2-/- mice with *Pseudomonas aeruginosa* ($2x10^7$ bacteria per mouse). Lung inspiratory capacity and protein concentration in BALF was similar between WT and Akt2-/- mice (Figure 61), while bacterial load (CFUs/ml in BALF) was significantly higher in Akt2-/- mice compared to WT mice 12hours after inoculation (Figure 61). Infiltration of macrophages and neutrophils as well as iNOS expression was less profound in Akt2-/- mice compared to WT (Figure 63). Macrophages from Akt2-/- mice retained their M2 prone phenotype in septic ALI and expressing more Arg1 compared to WT (Figure 63). However, IL-6 and TNFα concentration in the BALF did not differ between Akt2-/- and WT mice (Figure 63), but IL-6 and TNFα levels appeared significantly reduced in Akt2-/- mice compared to WT when normalized to P. aeruginosa CFUs (Figure 63), suggesting that the increase of these cytokines may be due to the increased bacterial load. Histological analysis of lung tissue upon P. aeruginosa infection revealed that both WT and Akt2-/- lung sections have severe distortion of normal lung architecture, due to presence of dense interstitial and alveolar inflammatory infiltrate composed mainly of neutrophils, macrophages and lymphocytes (Figure 62). However, the parenchymal damage was slightly less severe in Akt2-/- compared to WT mice, since they demonstrated less parenchymal consolidation and better preservation of alveoli probably due to diminished lung inflammation (Figure 62). Overall, these findings suggest that while ablation of Akt2 and M2 polarization of macrophages protects from aseptic lung injury it compromises the response of macrophages to live bacteria.

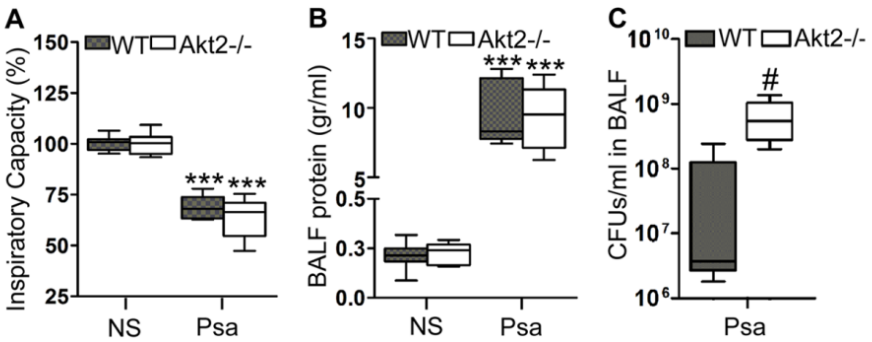

Figure 61. P. aeruginosa induced lung injury and inflammation in Akt2-/- mice. IC (A), protein concentration (B), and bacterial load (CFU/ml) (C) in BALF from WT and Akt2-/- mice at 12 h after P. aeruginosa inoculation (Psa). n = 6 mice/ group. In box-and-whisker plots, box shows 5–95 percentiles, horizontal line represents median, and whiskers represent minimum and maximum. *p , 0.05, **p , 0.01, ***p , 0.001, acid treatment versus NS treatment. #p , 0.05, ### p , 0.001, Akt22/2 versus WT.

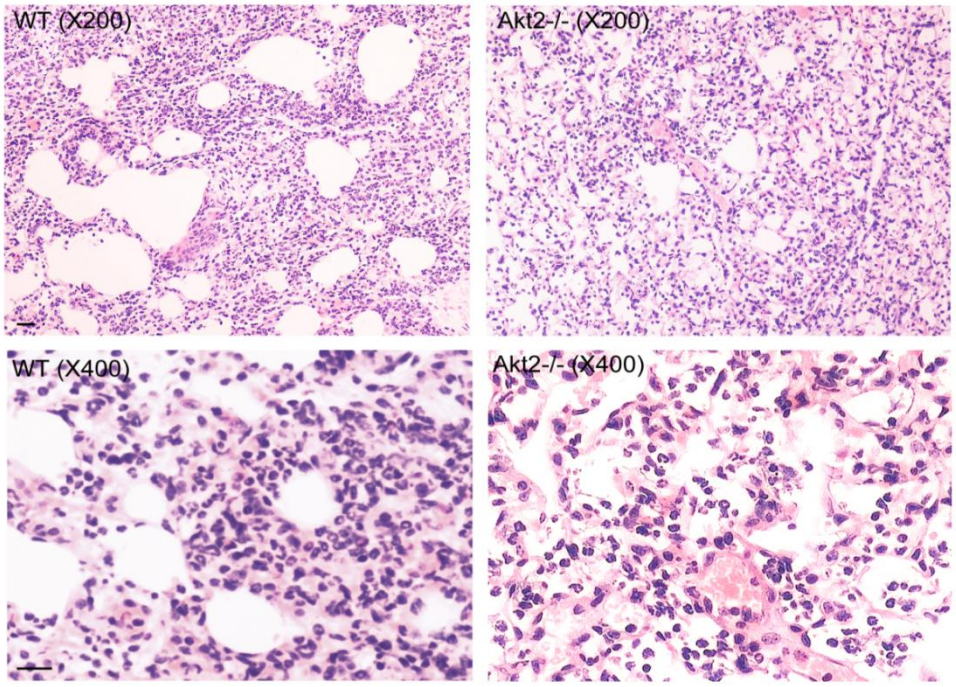

Figure 62. P. aeruginosa induced lung injury in Akt2-/- mice. Histological analysis of lung tissue sections of WT and Akt2-/- mice after P. aeruginosa pneumonia (H&E stain) shows severe distortion of lung architecture in both sections as the result of the presence of dense interstitial and alveolar inflammatory infiltrates. Akt2-/- mice demonstrate slightly better preservation of alveoli and less parenchymal consolidation. Scale bars, 50 mm. n = 6 mice/ group.

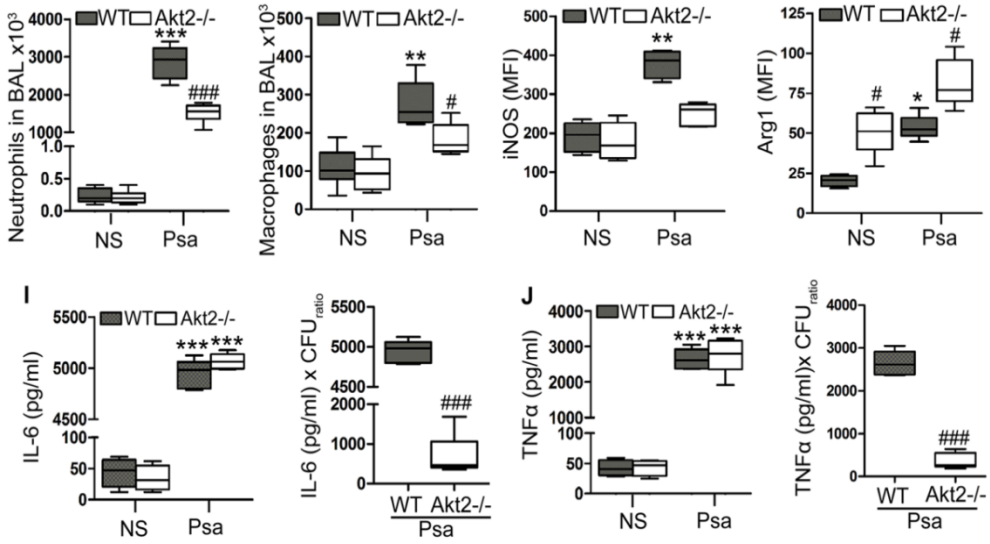

Figure 63. P. aeruginosa induced lung inflammation in Akt2-/- mice. Neutrophil and macrophage cell numbers in BALF from WT and Akt2-/- mice after P. aeruginosa infection (Psa). Protein levels of iNOS and Arg-1 in alveolar macrophages (CD11c+ cells) of WT and Akt2-/- mice with P. aeruginosa lung infection assessed by flow cytometry and expressed as mean fluorescence intensity (MFI). Levels of IL-6 and TNF-a in BALF of WT and Akt2-/- mice at 12 h after P. aeruginosa inoculation. IL-6 and TNF-a levels are also shown normalized to bacterial load in BALF. N = 6 mice/ group. In box-and-whisker plots, box shows 5–95 percentiles, horizontal line represents median, and whiskers represent minimum and maximum. *p , 0.05, **p , 0.01, ***p , 0.001, acid treatment versus NS treatment. #p , 0.05, ### p , 0.001, Akt2-/- versus WT.

PART TWO

M2 MACROPHAGE ACTIVATION DETERIORATES THE OUTCOME OF HYPOXIA INDUCED PULMONARY ARTERIAL HYPERTENSION

Main Findings

In order to characterize the inflammatory response and the macrophage activation phenotype in pulmonary arterial hypertension, as well as the mechanisms by which heme oxygenase-1, an anti-inflammatory enzyme, is protective in HPH, we generated bitransgenic mice that overexpress human heme oxygenase-1 under doxycycline control in an inducible, lung-specific manner and we applied hypoxia as a stimulus for PAH development.

Hypoxic exposure of mice in the absence of doxycycline resulted in early transient accumulation of monocytes/macrophages in the bronchoalveolar lavage that was ameliorated in doxycycline treated mice. Alveolar macrophages acquired an alternatively activated phenotype (M2) as soon as 4 days in response to hypoxia, characterized by the expression of found in inflammatory zone-1, arginase-1, and chitinase-3-like-3. Mice exposed to hypoxia developed pulmonary hypertension after 3weeks of hypoxic exposure; they showed an elevated right ventricular systolic pressure, the Fulton Index and thickened medial wall thickness .

A brief 2-day pulse of doxycycline delayed, but did not prevent, the peak of hypoxic inflammation and macrophage activation, and could not protect against HPH. In contrast, a 7-day doxycycline treatment sustained high heme oxygenase-1 levels during the entire period of hypoxic inflammation, inhibited macrophage accumulation and activation, induced macrophage interleukin-10 expression, and prevented the development of HPH. Supernatants from hypoxic M2 macrophages promoted the proliferation of pulmonary artery smooth muscle cells *in vitro*, whereas treatment with carbon monoxide, a heme oxygenase-1 enzymatic product, abrogated this effect. Early recruitment and alternative activation of macrophages in hypoxic lungs are critical for the later development of HPH. Heme oxygenase-1 may confer protection from HPH by effectively modifying the macrophage activation state in hypoxia.

Lung-Specific, Inducible Expression of Human Heme Oxygenase-1

Based on the design of the bitransgenic model (designated CC77; Figure 65), the hHO-1 transgene is under the control of both doxycycline and the Clara cell secretory protein promoter and therefore is inducibly expressed in the lung epithelium (Figure 65). HO-1 expression has been extensively assessed in the absence and presence of dox. HO-1 mRNA

was upregulated more than 20-fold upon 1mg/ml dox administration (Figure 65), and responded to dox treatment in a dose-dependent and time-dependent manner (Figure 65, 66). Upon withdrawal of dox, human HO-1 mRNA expression progressively falls and is undetected by 5 days (Figure 65). Semiquantitative polymerase chain reaction analysis on total lung RNA with hHO1-specific primers indicates that hHO-1 levels were upregulated with doxycycline treatment in a dose-dependent manner while they remained undetectable in the absence of doxycycline, in comparison with positive control mice (SHO-1 line that constitutively express HO-1 in the lung) and negative control mice (FVB wild type) (Figure 66). Also, after two days of dox administration, the inducible levels of hHO-1 transgene expression were comparable to those previously described in the SHO1 transgenic line that constitutively expresses hHO-1 in lung epithelial cells (Figure 66B). Protein levels of HO-1 were also profoundly elevated in dox-treated CC77 mice but not in the CCTA mice (Figure 66C) Control experiments were performed by treating mice of the parent line (CCTA), that harbor the tetracycline transactivator but not the human HO-1 transgene (Figure 66B), with dox to eliminate any potential effect of dox itself, independently of HO-1.

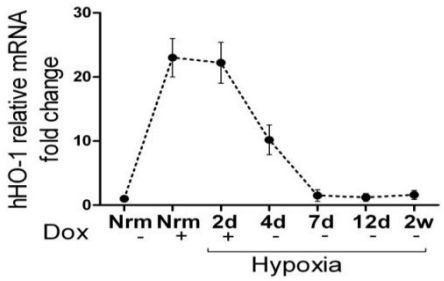

Figure 64. Characterization of the bitrangenic mouse line with inducible expression of HO-1. qPCR analysis of normoxic and hypoxic animals with or without dox. In dox treated mice, dox was removed the day 2 of hypoxia and HO-1 levels returned to baseline 5 days thereafter.

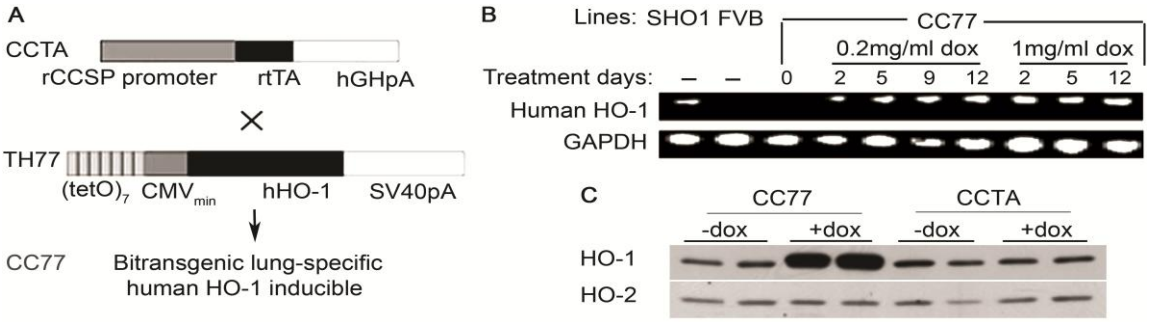

Figure 65. Lung-specific, dox-regulated expression of hHO-1. A, Bitransgenic mice were generated by crossing lines CCTA and TH77. CCTA harbours the reverse tetracycline transactivator (rtTA) under the control of the 2.3kb rat CCSP (Clara Cells Secretory Protein) promoter. TH77 harbours a human HO-1 (hHO-1) transgene under the control of 7copies of the tet operator linked to a minimal CMV promoter. B, Bitransgenic mice (CC77) were treated with 0.2 mg/ml or 1 mg/ml dox in the drinking water for 2 to 12 days and semi-quantitative PCR analysis on total lung RNA for hHO1 and the housekeeping gene, GADPH is depicted. SHO1: transgenics constitutively expressing hHO-1 in lung epithelium, and FVB: wild-type, served as positive and negative controls, respectively. The primers do not amplify endogenous murine HO-1 transcripts. C, Western Blot analysis of both endogenous and human HO-1 in total lung extracts of CC77 and CCTA mice. HO-2 was used as an internal control.

Sustained Induction of Heme Oxygenase-1 Prevents Hypoxia-Induced Pulmonary Hypertension

The development of PAH in our model was assessed by the measurement of right ventricular systolic pressure, the Fulton Index, and the medial wall thickness index. The Fulton Index, the ratio of right ventricle weight to left ventricle plus septum weight, represents a hallmark of right ventricular hypertrophy resulting from increased right ventricle pressure afterload. The medial wall thickness index was estimated from the histological sections of pulmonary arterioles stained with a - smooth muscle actin. Right ventricular systolic pressure, the Fulton Index, and the medial wall thickness index were significantly elevated as early as 7 days of hypoxia in both bitransgenics (CC77) and controls (CCTA) (Figure 67A through 67C). Doxycycline administration for the entire course of hypoxia prevented the increase in right ventricular systolic pressure, the Fulton Index, and the medial wall thickness index in the bitransgenic mice but not in the controls (Figure 67). Immunostaining of pulmonary arterioles for a-smooth muscle actin revealed thickened and remodeled medial vascular walls in lung sections of hypoxic mice. This pathology was absent in hypoxic mice treated with doxycycline (Figure 67D).

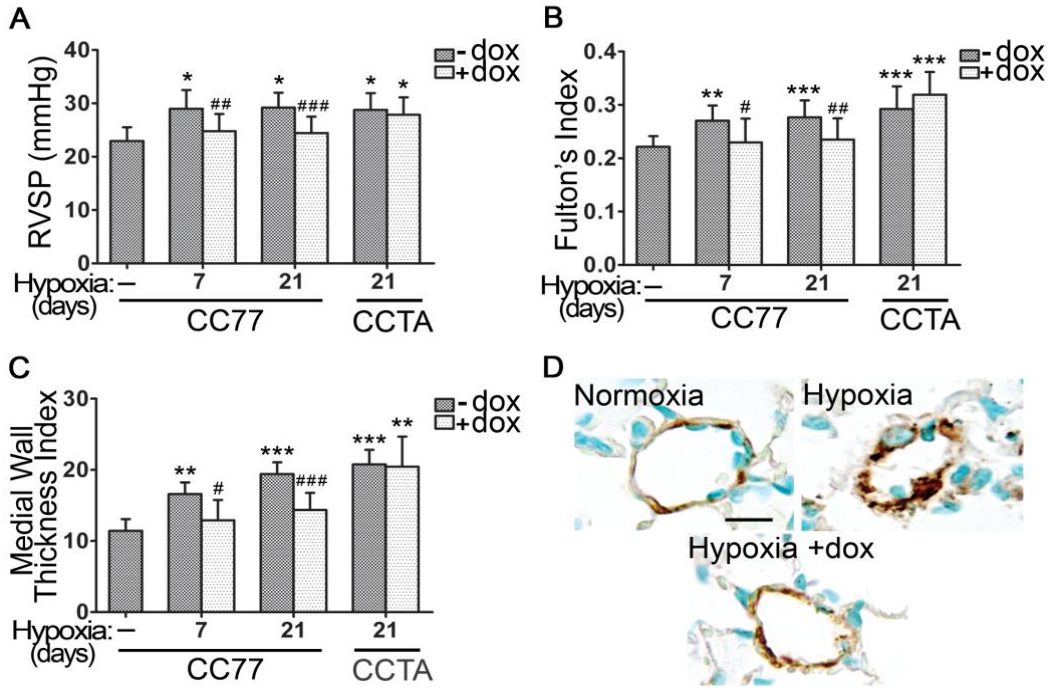

Figure 67. Sustained Expression of HO-1 Prevents HPH. [A] Right Ventricular Systolic Pressure (RVSP), [B] Fulton's Index, and [C] Medial Wall Thickness Index were determined at the indicated times of hypoxic exposure, in the presence or absence of 1 mg/ml dox in the drinking water of CC77 and CCTA mice. [D] Representative images of vascular remodeling in lung sections of mice exposed to hypoxia for 21 days and stained for alpha-smooth muscle actin (α-SMA). CC77: bitransgenic mice (CCSP-rtTA x TH77). CCTA: transgenic mice lacking HO-1 (CCSP-rtTA). Numbers represent mean +/-SD, n≥6 per group. Scale bar is representative of 25 μm *: relative to normoxia; *p<0.05, **p<0.01, ***p<0.001. #: relative to hypoxia –dox; #p<0.05, ##p<0.01, ###p<0.001

Hypoxia Induces Monocyte/Macrophage Infiltration and Lung Cytokine Production That Is Ameliorated by Heme Oxygenase-1 and its Enzymatic Product, Carbon Monoxide

To track the inflammatory response at the initial stages of hypoxic exposure and before the development of hypertension, animals were exposed to hypoxia, and a temporal profile of the cell content in BALF was performed. More than 95% of the isolated BALF cells were CD45-positive leukocytes (Figure 68A). These cells expressing the macrophage-specific cell surface antigens F4/80 and CD11c remained the predominant population (>98%) regardless of hypoxic exposure or doxycycline treatment (Figure 68B, C). Under these conditions, only a subtle increase in BALF neutrophils and T lymphocytes was observed (Figure 69).

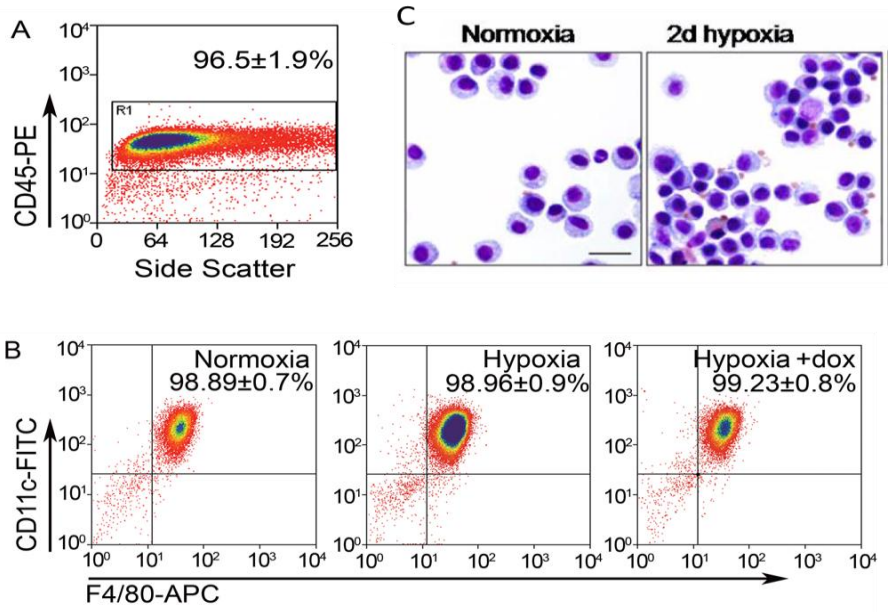

Figure 68. Analysis of BAL cell content in hypoxic mice. [A] Flow cytometric analysis of CD45 (+) leukocytes isolated from BAL that demonstrate expression of CD11c and F4/80 macrophage markers (≈98%). [B] More than 95% of the cells isolated (gated for Side and Forward Scatter) were CD45 (+), i.e. white blood cells.

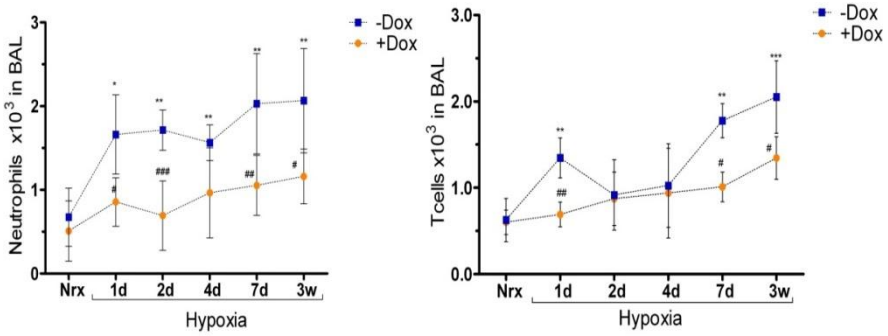

Figure 69. **Infiltration of Neutrophils and T cells in bronchoalveolar lavage of hypoxic mice. Effect of HO-1.** Bitransgenic mice were exposed to hypoxia for the indicated time periods. **A**, Neutrophil numbers (Lyc/G-1+) in the BAL of normoxic (Nrx) and hypoxic mice in the absence (-) or presence (+) of 1 mg/ml dox **B**, T lymphocytes (CD3+) gradually accumulated in small numbers during the course of hypoxia in the untreated mice (Numbers represent mean +/-SD, n=5-6 animals per time point or treatment group) *relatively to nrx:*p<0.05,**p<0.01,***p<0.001. #relatively to hyp(-dox):#p<0.05,##p<0.01,###p<0.001.

Upon commencing the hypoxic exposure, the numbers of monocytes/macrophages were significantly increased in the BALF of control hypoxic mice, reaching a peak at 2 days of hypoxia and dropping significantly by 7 days but remaining slightly elevated compared with normoxic animals (Figure 70). Doxycycline administration had a suppressive effect on the accumulation of cells at all time intervals investigated (Figure 70). Doxycycline treatment of the control mice (CCTA) had no impact on monocyte/macrophage accumulation, establishing that inhibition of cell infiltrate is due specifically to HO-1 overexpression and is not an artifact of doxycycline treatment (Figure 70).

To identify the specific enzymatic product of HO-1, CO, and/or biliverdin that is responsible for suppressing the peak of inflammation at 2 days of hypoxia, we exposed animals to intermittent inhalation of CO (250 ppm for 1 hour twice a day) and/or biliverdin injections (50 umol/kg IP twice a day). Intraperitoneal PBS injections served as control. Inhaled CO or CO plus biliverdin, but not biliverdin alone, was effective in inhibiting the inflammatory cell infiltrate in the BALF at levels comparable to doxycycline treatment (Figure 70). Dox treatment in the control mice had no impact on monocyte/macrophage accumulation indicating that independently of dox, inhibition of cell infiltrate is due to HO-1 overexpression (Figure 70).

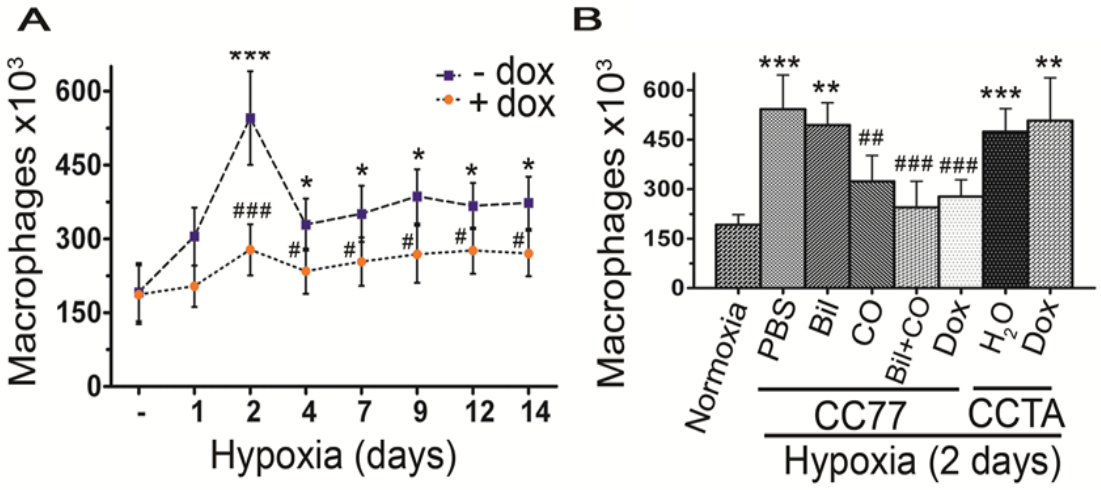

.

Figure 70. Hypoxia induces early monocyte/macrophage infiltration in the lungs that is ameliorated by HO-1. A peak of accumulation of monocytes/macrophages ($CD11c^+$, $F4/80^+$) is depicted over time in the BAL of hypoxic mice in the absence (-) or presence (+) of 1 mg/ml dox in the drinking water. [C] Dox treatment suppressed the hypoxia-induced macrophage accumulation in the BAL of CC77 mice but not in the CCTA controls. The effect of the different end products of HO-1 on macrophage accumulation, Biliverdin i.p (Bil), inhaled carbon monoxide (CO), and both Bil and CO is also shown*: relative to normoxia; *p<0.05, **p<0.01, ***p<0.001. #: relative to hypoxia –dox; #p<0.05, ##p<0.01, ###p<0.001

In addition to the accumulation of macrophages, several cytokines/chemokines were also upregulated in the BAL of hypoxic mice (Figure 71). In as early as two and four days of hypoxia, upregulation of fibroblast growth factor (FGF)β, IL-1β, macrophage inflammatory

protein (MIP)1α, IL-17 and IL-2 as well as of Th2-related cytokines, IL-13 and IL-4, was observed (Figure 71). The Th1-related cytokines, IL-12, TNF-α, and INF-γ, remained unaffected or were undetectable (Figure 71). Dox administration effectively suppressed FGFβ, IL-1β, MIP-1α and IL-2 at both, two days and four days of hypoxia, and suppressed IL-17, IL-13, and IL-4 only after four days of continuous administration (Figure 71).

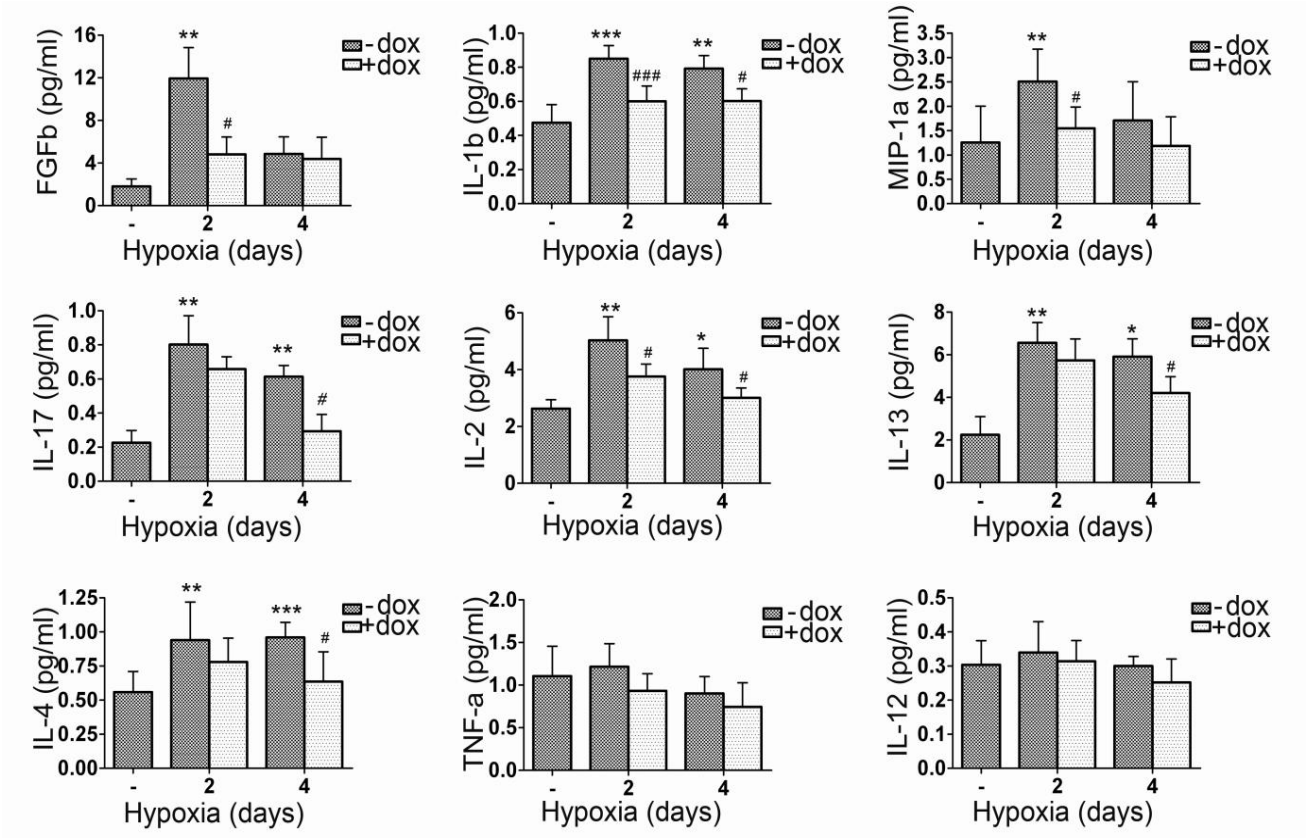

Figure 71. Chemokine and cytokine profile in the BAL fluid of hypoxic mice. Chemokine/cytokine profile in the BAL fluid of mice exposed in hypoxia for two and four days in the absence (-) or presence (+) of dox. Upregulation of FGFβ, IL-1β, MIP-1α, IL-13, IL-4, IL-17 and IL-2 in hypoxia and the suppressive effect of HO-1 expression (+dox). Th1 related cytokines, TNF-α and IL-12, were not upregulated in hypoxia as compared to normoxic mice. (Numbers represent mean +/-SD, with a minimum of 6 animals per time point or treatment group). *: relative to normoxia; *p<0.05, **p<0.01, ***p<0.001. #:relative to hypoxia –dox; #p<0.05, ##p<0.01, ###p<0.001

Cytospin preparation of BAL isolated macrophages revealed a striking alteration of macrophage morphology in cytospin preparations of BAL isolated macrophages was observed at four days of hypoxia, characterized by cytoplasmic enlargement in a population of hypoxic cells. This phenotype is consistent with activation and it was not detected in any of the macrophages isolated from dox-treated mice (Figure 3D).

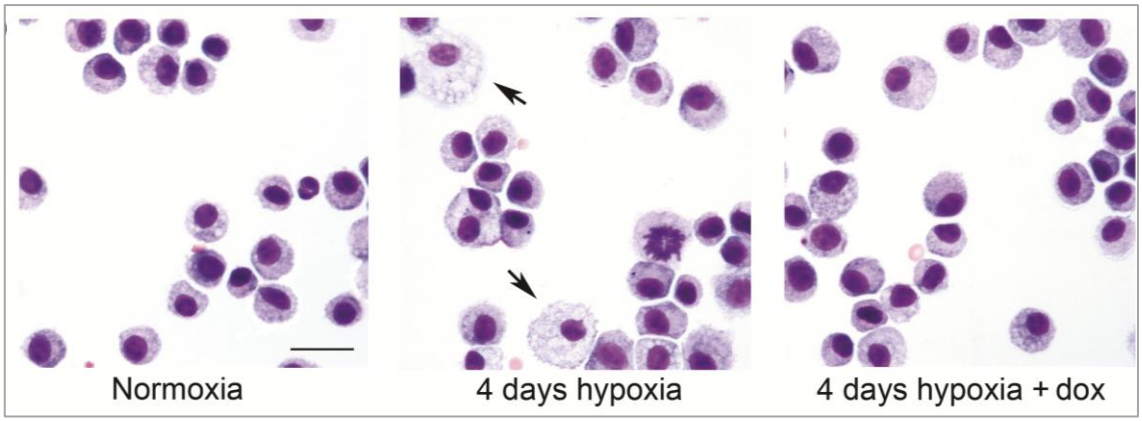

Figure 72. Morphologic alteration of a population of BAL isolated macrophages is observed within four days of hypoxia in untreated mice, a phenotype absent in dox-treated mice. Numbers represent mean +/-SD, n≥6 mice per group. Scale bar is representative of 25um.

Hypoxia Induces Alternative Activation of Macrophages: Suppressive Effect of Heme Oxygenase-1

The observation that macrophage morphology was altered in response to hypoxia led us to further investigate the potential activation state of hypoxic macrophages.

Quantitative polymerase chain reaction analysis of BALF-isolated alveolar macrophages from CC77 bitransgenic mice revealed an induction of well-defined markers of M2 macrophages in hypoxic mice, including Arg1, Fizz1, Ym1 (Figure 73), and mannose receptor, C type lectin-1 (data not shown). The peak expression occurred at 4 days of hypoxia and remained upregulated for at least 14 days. In addition, Fizz1 was secreted in the BALF of hypoxic mice (Figure 73). In contrast, there was no change in the mRNA levels of markers of M1 macrophage phenotype such as inducible nitric oxide synthase, TNF-a, and IL-12b (IL-12p40) or the costimulatory molecules, CD80/86, essential in the process of antigen presentation (Figure 74). Urea production, indicative of arginase activity, was also upregulated in *in vivo* hypoxic alveolar macrophages (Figure 73); this increase in enzymatic activity was due to Arg1 because Arg1 mRNA levels were induced 9.1+/- 3.4-fold after 4 days of hypoxic exposure, whereas Arg2 mRNA levels were 0.6 +/-0.1 of their normoxic value at this time point. Inducible nitric oxide synthase activity, as assessed by nitrite and nitrate production in the BALF, remained unchanged (Figure 73). Doxycycline administration effectively suppressed all markers of alternative activation (Figure 73A through 73C), whereas these markers were not suppressed in the CCTA line treated with doxycycline (Figure 73B, C and Figure 75).

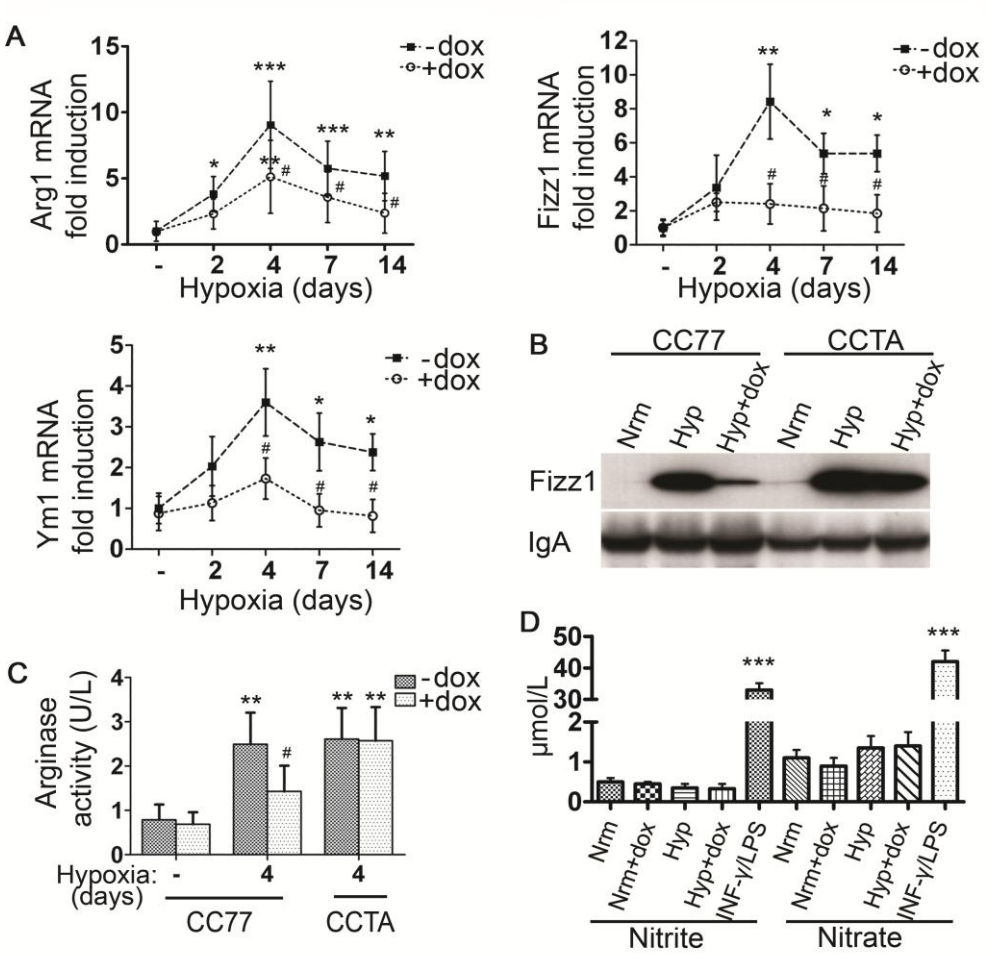

Figure 73. Hypoxia induces alternatively-activated macrophages: the suppressive effect of HO-1. [A] qPCR analysis of hypoxic alveolar macrophage mRNA isolated from bitrangenic mice (CC77) revealed increased Fizz1, Arg1 and Ym1 levels that were suppressed with dox, but Arg2 remained unchanged. [B] Fizz1 immunoblot of BAL fluid from four days normoxic and hypoxic mice +/-dox. IgA served as internal control. CC77: bitransgenic mice (CCSP-rtTA x TH77). CCTA: transgenic mice lacking HO-1 (CCSP-rtTA). [C] Arginase-1 activity (U/L) was assessed by urea formation in normoxic and hypoxic animals. [D] iNOS activity was estimated by the levels of nitrite and nitrate in the BAL fluid of hypoxic mice. Supernatants from RAW 264.7 macrophages stimulated with 100 µg/ml LPS E.coli and 100 U/ml INF-γ for 48 hours served as positive controls. Mean ± SD is depicted of n≥6 mice per group *: relative to normoxia; *p<0.05, **p<0.01, ***p<0.001. $^{\#}$: relative to hypoxia –dox; $^{\#}$p<0.05, $^{\#\#}$p<0.01, $^{\#\#\#}$p<0.001.

Immunofluorescent staining confirmed the localization of Fizz1 and the absence of inducible nitric oxide synthase in the cytoplasm of hypoxic macrophages (Figure 5B and 5C). Flow cytometry analysis also revealed that 10.8 ± 2.7% (35.5±8.9x10^3, mean±SD) of the macrophages was Fizz1 positive, whereas in the presence of doxycycline, this number was reduced to 2.17 ± 0.6% (5.1±1.4x10^3, mean±SD; *P*<0.01; Figure 76). Immunofluorescent staining of *in vivo* isolated macrophages indicated positive cytoplasmic staining of galectin-3 (Figure 77), Fizz1 (Figure76) and Ym1 (Figure 77) after 4 days of hypoxia. Mice treated with dox had reduced staining per cell and reduced number of positive cells per field. The macrophages were negative for the marker of classical activation (M1), inducible nitric oxide

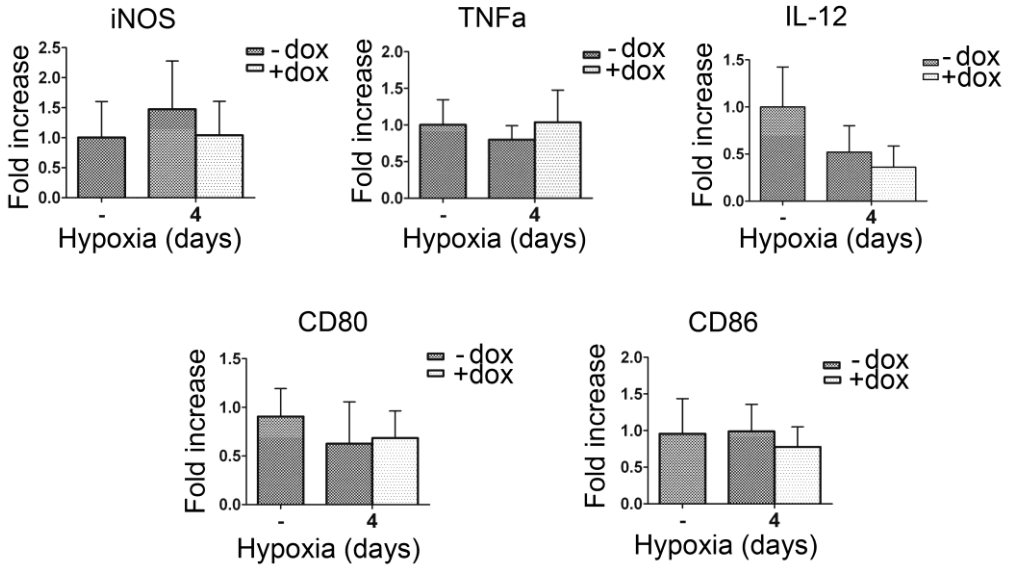

Figure 74. M1 markers expression levels in hypoxic alveolar macrophages. [A] The levels of M1 markers such as iNOS, TNFa, IL-12, CD80 and CD86 were assessed in alveolar macrophages of mice exposed to hypoxia for four days with or without dox treatment.

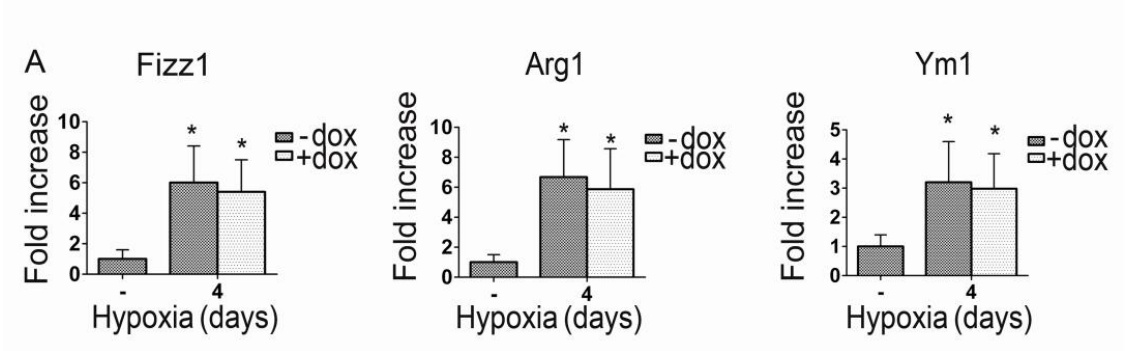

Figure 75. The anti-inflammatory effects of dox-treated mice are HO-1 dependent. The CCTA transgenic line that harbors the tetracycline transactivator but not the human HO-1 transgene was used to eliminate potential biologic effects of dox itself. Markers of alternative activation, Fizz1, Ym1, and MR, were not suppressed in the CCTA line treated with dox. *: relative to normoxia; *p<0.05.

synthase (iNOS) (Figure 76). Only primary macrophages stimulated *in vitro* for 48 hours with INF-γ and LPS in order to prime them towards a M1 phenotype, were profoundly positive for iNOS (Figure 76).

Apart from the slight elevation of the Th2 cytokines IL-13 and IL-4 in the BALF of hypoxic mice, we investigated the potential presence of other noncanonical inducers of M2 polarization. Thus, we assessed the mRNA levels of CCL2 and IL-6 in total lung extracts by quantitative polymerase chain reaction. CCL2 and IL-6 mRNA was robustly upregulated soon after hypoxic exposure but was significantly suppressed in the presence of doxycycline (Figure 78). In the CCTA control line lacking the HO-1 transgene, doxycycline treatment did not suppress CCL2 and IL-6 levels (Figure 78) in the under hypoxic conditions (0.5% O_2) also

manifested the M2 phenotype with increased levels online-only Data Supplement). Interestingly, primary alveolar macrophages cultured *in vitro* of Ym1, but not IL-12 and TNF-a (Figure 79), suggesting that M2 polarization induced by hypoxia is a cell autonomous phenomenon.

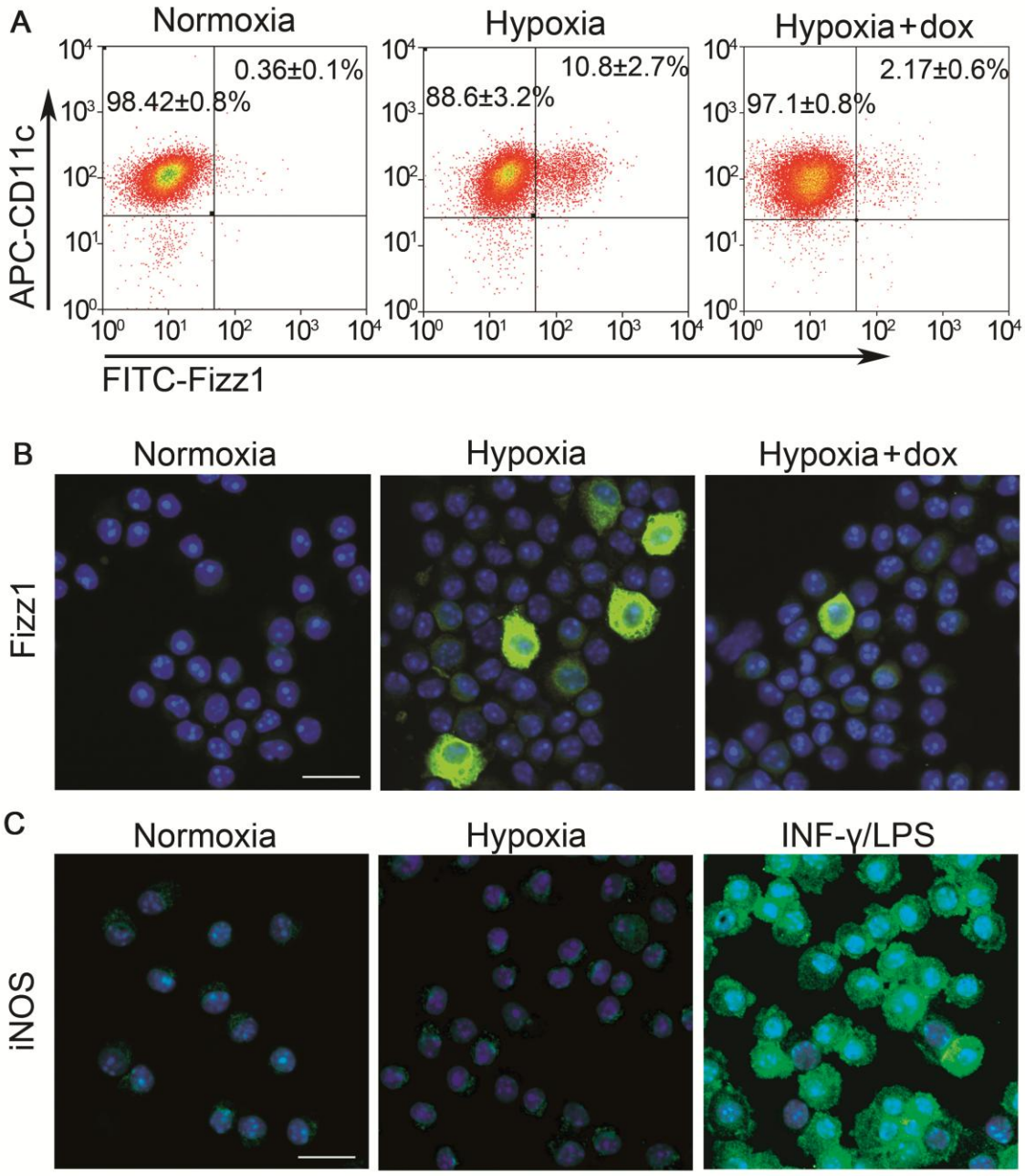

Figure 76. M2 and M1 expression profile of hypoxic alveolar macrophages. Representative images of Fizz1 expression in alveolar macrophages from normoxic mice or mice exposed to hypoxia in the absence or presence of dox were assessed by [A] Flow cytometry and [B] Immunofluorescence (FITC). [C] iNOS (FITC) staining in alveolar macrophages. Primary alveolar macrophages stimulated with 100 μg/ml LPS E.coli and 100 U/ml INF-γ for 48 hours served as positive controls. Nuclei were counterstained with DAPI. Scale bar is representative of 25 μm.

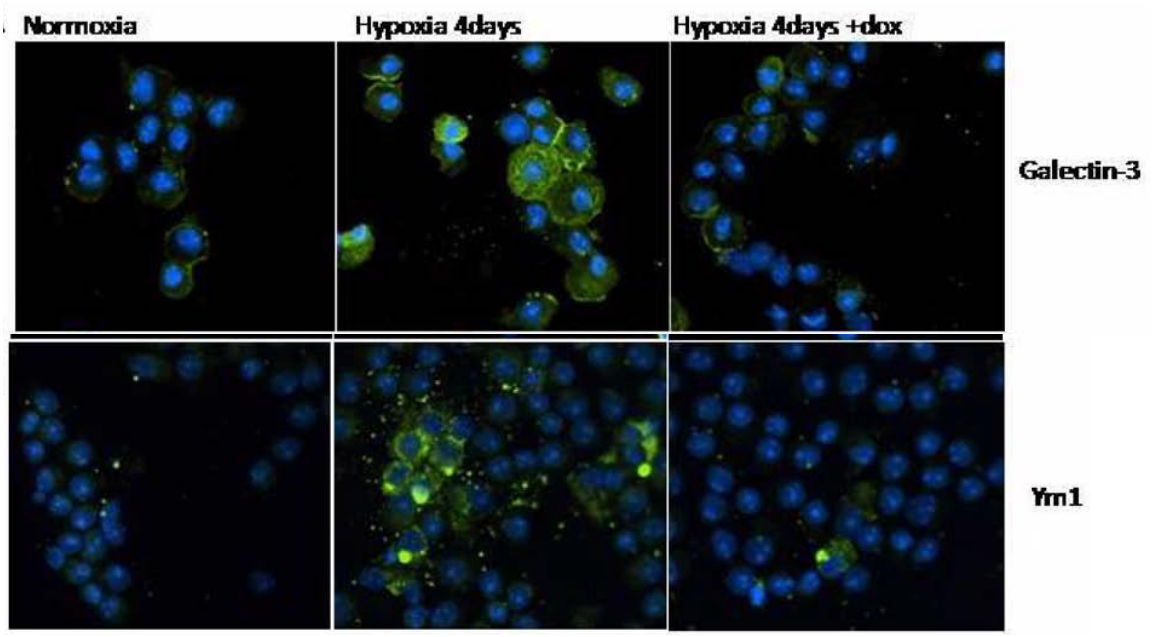

Figure 77. *In vivo* M2 and M1 expression profile of hypoxic alveolar macrophages. Representative immunofluorescent images of *in vivo* isolated alveolar macrophages from mice exposed to hypoxia in the absence or presence (+dox) of dox in the drinking water. Cytoplasmic localization of galectin-3 (FITC) and Ym1 (FITC) is depicted. Nuclei were counterstained with DAPI.

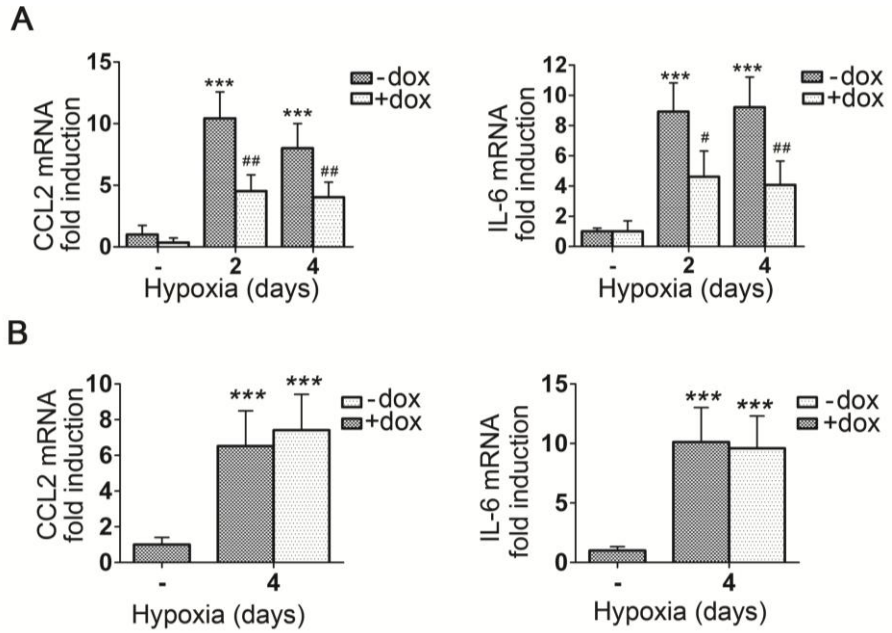

Figure 78. CCL2 and IL-6 levels in hypoxic lungs [A] Increased mRNA levels of CCL2 and IL-6 in total hypoxic lung extracts were suppressed in dox-treated mice. [B] CCL2 and IL-6 levels were not suppressed in hypoxic CCTA control mice. Numbers represent mean +/-SD, with a minimum of 6 mice per group. *: relative to normoxia, ***p<0.001. $^{\#}$: relative to hypoxia–dox; $^{\#}$p<0.05, $^{\#\#}$p<0.01, $^{\#\#\#}$p<0.001

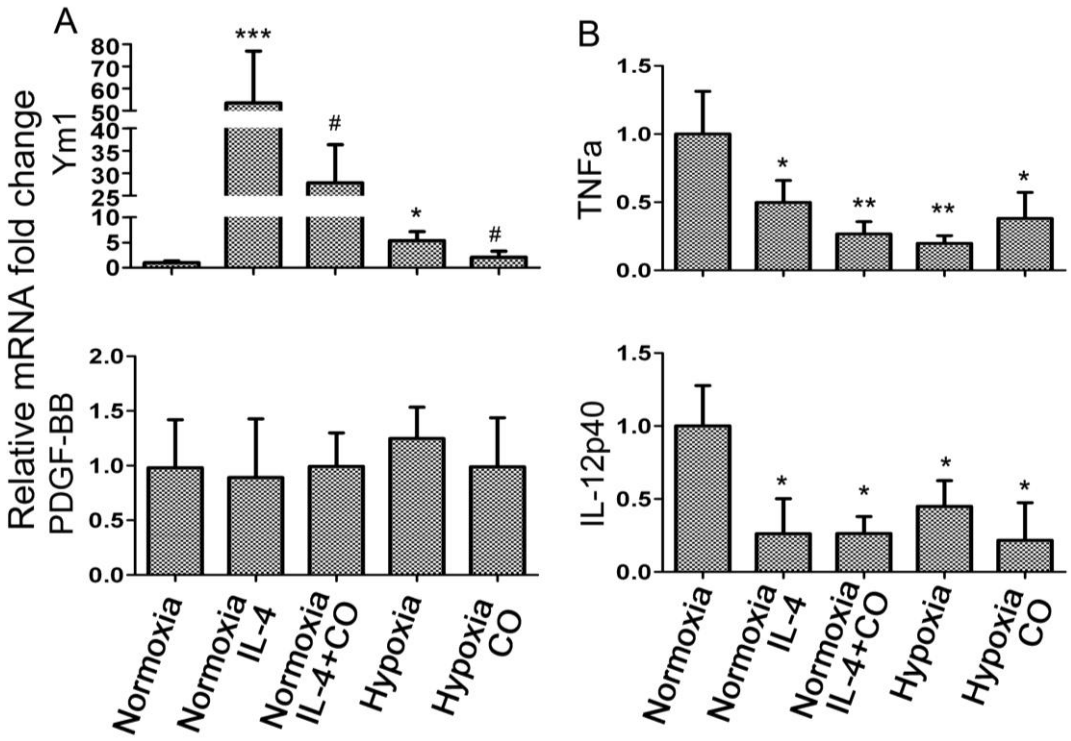

Figure 79. Cytokine and growth factor profile of in vitro stimulated primary alveolar macrophages. [A] The relative mRNA levels of the M2 markers, Arg1 and Ym1 but not the growth factor PDGF-BB, were upregulated in macrophages stimulated with 20 ng/ml IL-4 or 0.5% hypoxia and suppressed upon CO treatment. [B] The mRNA levels of M1 specific markers, TNF-α and IL-12b40 subunit, were downregulated in macrophages stimulated with 20 ng/ml IL-4 or 0.5% hypoxia with or without CO. Numbers represent mean +/-SD, at least 5 mice per group. *: relative to normoxia; *p<0.05, **p<0.01, ***p<0.001. #: relative to hypoxia or normoxia + IL-4; #p<0.05.

Heme Oxygenase-1 Promotes the Expression of Interleukin-10 in Alveolar Macrophages

In an effort to further evaluate the effect of HO-1 on macrophage phenotype, mRNA and protein levels of IL-10, a well-documented anti-inflammatory mediator, were directly assessed in freshly isolated alveolar macrophages. Interleukin-10 was significantly elevated in alveolar macrophages derived from hypoxic mice treated with doxycycline (Figure 80). Doxycycline treatment in the CCTA line failed to upregulate IL-10 (Figure 81), establishing that the observed effect is HO-1 dependent. Furthermore, the number of macrophages expressing IL-10 (CD11c+, IL-10+) under hypoxia was assessed by flow cytometry to be increased four - to nine -fold with doxycycline treatment, comprising approximately slightly 10% of the total macrophage population in BALF (data not shown).

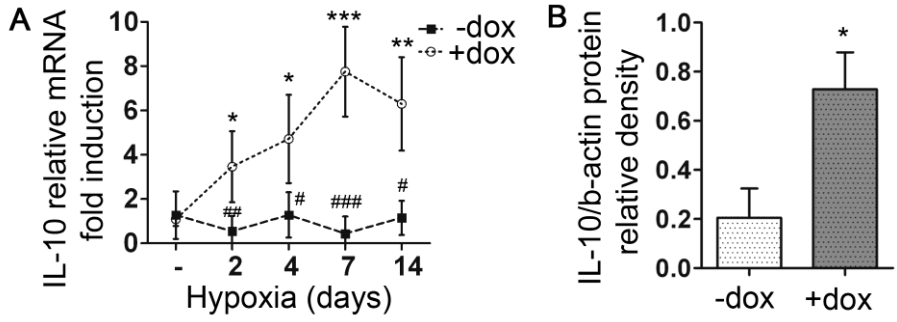

Figure 80. HO-1 induction promotes the expression of IL-10 in alveolar macrophages. Alveolar macrophages were isolated from animals exposed to hypoxia for the indicated times, and IL-10 expression was assessed by [A] qPCR analysis on total macrophage RNA. and [B] densitometric analysis of IL-10 protein levels normalized with b-actin levels at 7 days of hypoxic exposure. Numbers represent mean +/-SD, n≥5 mice per group *: relative to normoxia; *p<0.05, **p<0.01, ***p<0.001. #: relative to hypoxia +dox; #p<0.05, ##p<0.01, ###p<0.001.

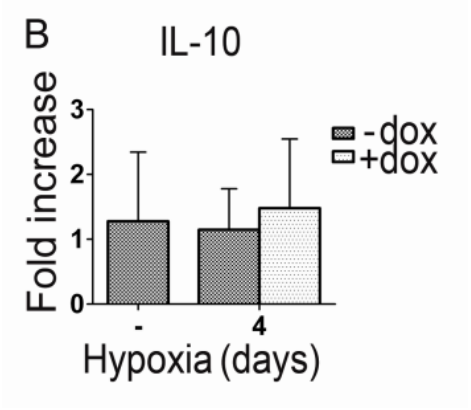

Figure 81. The anti-inflammatory effects of dox-treated mice are HO-1 dependent. The CCTA transgenic line that harbors the tetracycline transactivator but not the human HO-1 transgene was used to eliminate potential biologic effects of dox itself. The anti-inflammatory mediator, IL-10, failed to be upregulated in the dox treated CCTA animals that lacked the HO-1 transgene. *: relative to normoxia; *p<0.05.

Early Monocyte/Macrophage Accumulation Is Critical for the Later Development of Pulmonary Hypertension

To determine whether this early inflammatory response is essential for the later development of HPH and whether inducible expression of HO-1 at defined intervals during this process modulates the disease, we exposed the bitransgenic mice to doxycycline for various time periods. In addition to control animals exposed to hypoxia for 3 weeks in the absence of doxycycline, 1 group of littermates received doxycycline continuously for 3 weeks, and in 2 other groups, doxycycline was removed from the drinking water at 2 or 7 days of hypoxia. In all groups, animals remained in hypoxia for the entire 3-week period. On removal of doxycycline, hHO-1 mRNA levels returned to baseline within 3 days (Figure 82A and 82B, Groups in Methods session).

A short 2-day pulse of doxycycline at the onset of hypoxia caused a delay in the peak of macrophage recruitment in the BALF from 2 to 7 days, a time when HO-1 levels were reduced to baseline (Figure 82A). In the same group of animals, development of pulmonary hypertension, as assessed by right ventricular systolic pressure, the Fulton Index, the medial

wall thickness index, and histology of vascular remodeling, was not prevented (Figure 82C-F). In the case of a more prolonged, yet still transient, administration of doxycycline for 7 days, there was no macrophage influx even when HO-1 had reached baseline low levels, and pulmonary hypertension was completely prevented at 3 weeks (Figure 82B through 82F).

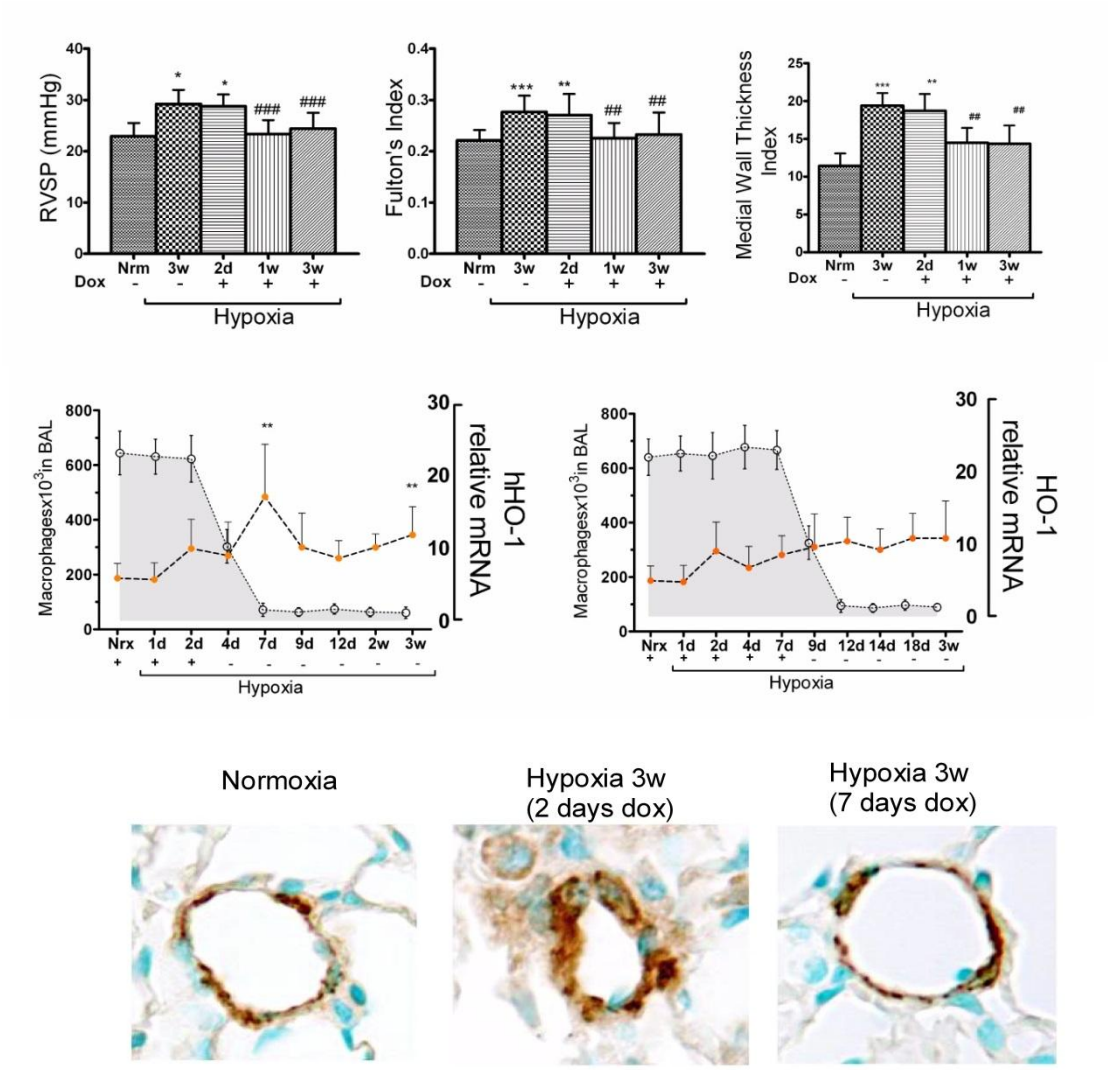

Figure 82. Early monocyte/macrophage accumulation is critical for the later development of pulmonary hypertension. HO-1 was transiently over-expressed in hypoxic mouse lung. [A] Dox administered at days -2 to +2 of hypoxic exposure (2d) delays but does not prevent the peak of macrophage accumulation when HO-1 levels return to baseline. [B] Dox administered at days -2 to +7 of hypoxic exposure (7d) prevents the peak of macrophage accumulation even twelve days later, long after HO-1 levels have returned to baseline. Dashed lines: alveolar macrophage number; dotted lines and shaded area: hHO-1 mRNA levels in the lung. [C] RVSP, [D] FI, and [E] MWTI were elevated in mice that received the two-day pulse but not in mice that received the seven-day pulse of dox. [F] Representative immunostaining for α-SMA of lung sections from mice exposed to hypoxia for 21 days who had previously received dox either for two days or seven days, in comparison with normoxia. Numbers represent mean +/-SD, n≥6 animals per group *: relative to normoxia; *p<0.05, **p<0.01, ***p<0.001. $^{\#}$: relative to hypoxia –dox; $^{\#\#}$p<0.01, $^{\#\#\#}$p<0.001.

Alternative Macrophage Activation Is Associated With the Development of Hypoxia-Induced Pulmonary Hypertension *in Vivo*

In agreement with macrophage numbers, M2 markers followed a similar pattern (Figure 83A). In the group in which doxycycline was removed after 2 days of hypoxic exposure and HPH was not prevented, mRNA levels of Fizz1, Arg1, and Ym1 increased 4 days after HO-1 levels had fallen to baseline (Figure 83A). However, in the group that received doxycycline for the first 7 days of hypoxia and the later development of hypertension was prevented, levels of Fizz1, Arg1, and Ym1 remained suppressed for all time periods examined (Figure 83B). Interestingly, in only the 7-day doxycycline treatment group, the anti-inflammatory marker IL-10 remained sustainably elevated above baseline (Figure 83A and 83B).

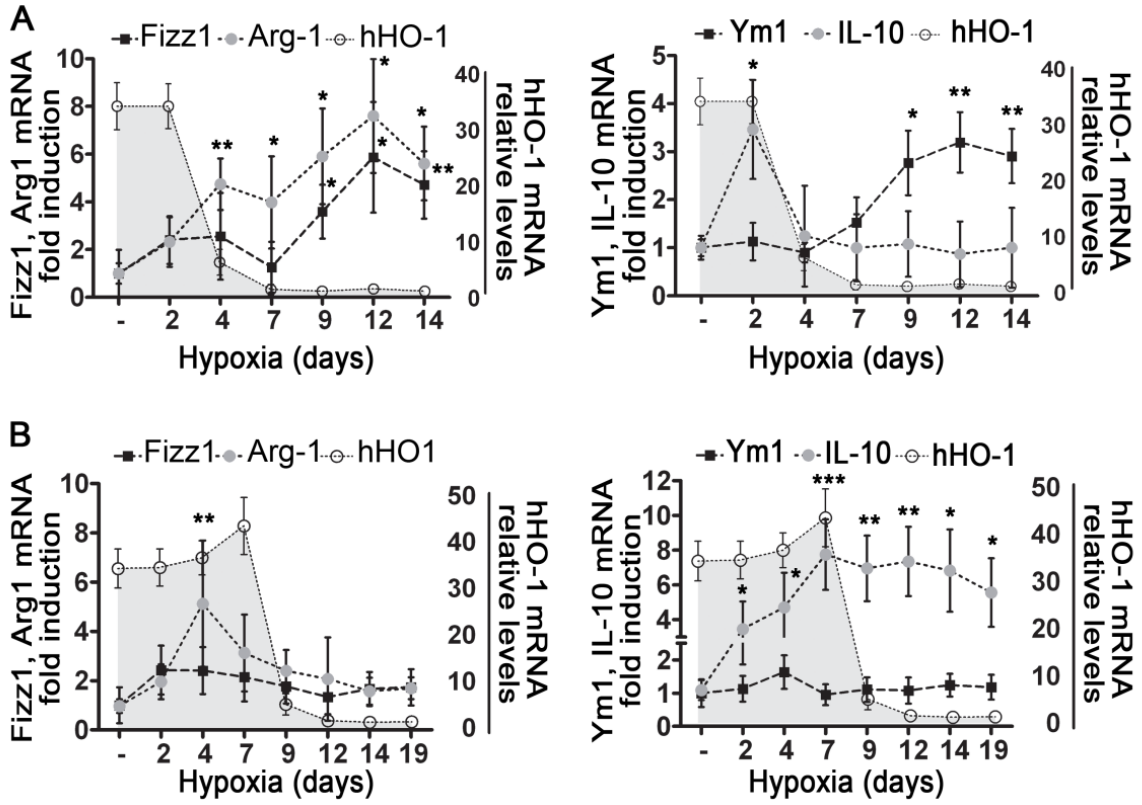

Figure 83. The role of macrophage activation profile in the development of pulmonary hypertension. [A] After a two-day pulse of dox and four days after HO-1 dropped to baseline, a pattern of alternative macrophage activation ensues (increased expression of Fizz-1, Arg1, Ym1), whereas IL-10 levels remained low. [B] After a seven-day pulse with dox, even when HO-1 levels return to baseline, high IL-10 expression persists. Shaded areas represent levels of hHO-1 transgene expression. Numbers represent mean +/-SD, n≥6 animals or wells per group. *: relative to normoxia; *p<0.05, **p<0.01, ***p<0.001.

Alternative Macrophage Activation Enhances Pulmonary Artery Smooth Muscle Cell Proliferation *in Vitro*

Interleukin-10 mRNA levels were also upregulated in primary alveolar macrophages cultured *in vitro* under hypoxic conditions (0.5% O_2) and treated with CO (500ppm; Figure 84). This suggests that CO release on HO-1 induction in this system is the trigger for IL-10 induction in macrophages. Supernatants of primary alveolar macrophages that were cultured *in vitro* under hypoxic conditions (0.5% oxygen) or normoxic macrophages treated with IL-4 (20 ng/mL) had high levels of Fizz1 and low levels of IL-10, and were able to stimulate pulmonary artery smooth muscle cell proliferation (Figure 84). However, supernatants from CO-treated hypoxic macrophages had reduced levels of Fizz1 and elevated IL-10 and had no proliferative effect on pulmonary artery smooth muscle cells (Figure 84).

Exogenous administration of IL-10 on pulmonary artery smooth muscle cells treated with hypoxic macrophage supernatants had no direct suppressive effect on their proliferation (Figure 85). Arg1, Fizz1, and Ym1 mRNA was upregulated in both IL-4– and hypoxia-stimulated macrophages, whereas neither platelet derived growth factor-BB nor the M1 specific markers IL-12 and TNF-α were affected (Figure 85, and data not shown). CO treatment suppressed the upregulation of the above M2 markers in both the IL-4– and hypoxia-stimulated macrophages (Figure 84 and data not shown).

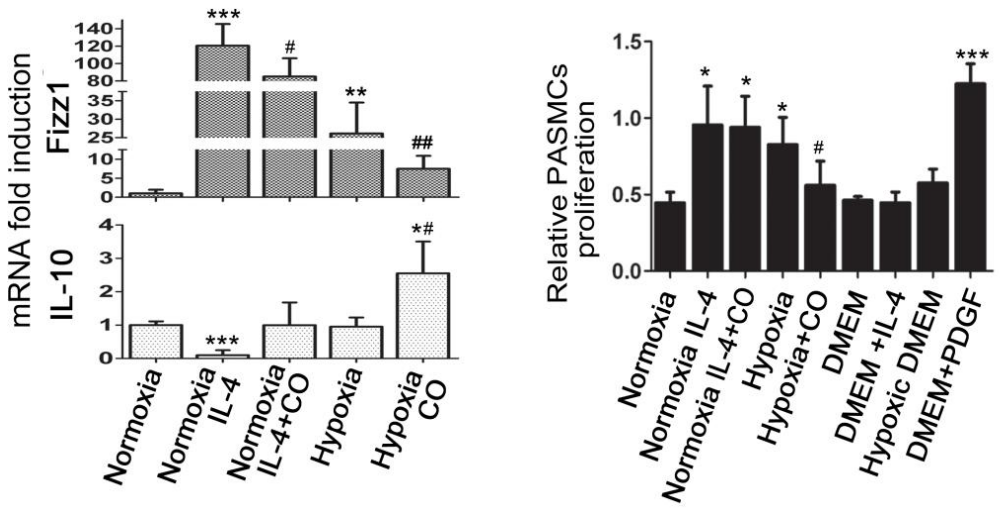

Figure 84. The role of macrophage activation profile in PASMS proliferation. [C] Fizz1 and IL-10 mRNA levels are shown in primary alveolar macrophages exposed to hypoxia or IL-4 (20 ng/ml) with or without CO. [D] Effect of the macrophage supernatants from different macrophage treatments depicted in subpanel C, on PASMC proliferation. PDGF-BB (10 ng/ml) treatment on PASMCs was used as a positive control and cell culture medium (DMEM) or medium calibrated in 0,5% oxygen for 48 hours (hypoxic DMEM) as negative controls. Numbers represent mean +/-SD, n≥6 animals or wells per group. *: relative to normoxia; *p<0.05, **p<0.01, ***p<0.001.

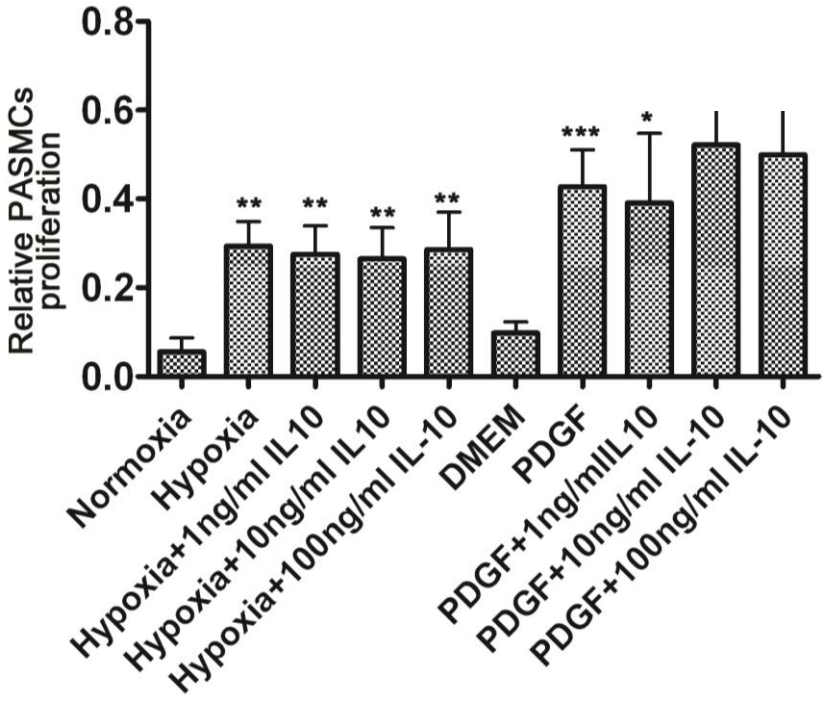

Figure 85. Effect of IL-10 on PASMCs proliferation. Addition of various concentration of mouse recombinant IL-10 (1ng/ml, 10ng/ml and 100ng/ml) on PASMCs treated with either supernatant from hypoxic macrophages or with 25ng/ml PDGF-BB had no suppressive effect on PASMCs proliferation.

DISCUSSION

Discussion

In the present thesis, the role of innate immunity and macrophage activation in two models of lung disease has been investigated. The alternative activation of alveolar macrophages had contradictory results in two different models of lung injury; it resulted in amelioration of lung inflammation in a model of acute lung injury while it was critical for the development of chronic lung inflammation and pulmonary arterial hypertension caused by hypoxia. Furthermore, molecular mechanisms by which an M1 to M2 switch or M2 suppression can take place *in vivo* have been investigated.

Part 1: Akt2 deficiency and M2 activation protects from ALI

In the present study we show that in the mouse model of aseptic lung injury, macrophages exhibit first a pro-inflammatory M1 phenotype followed by an M2 anti-inflammatory phenotype. Genetic ablation of Akt2, which promotes early M2-type activation and abrogates M1 activation via miR-146a induction, ameliorates acid-induced lung injury. However, Akt2 ablation resulted in increased bacterial load in a model of a septic lung inflammation caused by Pseudomonas aeruginosa lung infection.

ARDS, the devastating clinical syndrome of acute respiratory failure characterized by lung inflammation and alveolar barrier dysfunction, is a major cause of morbidity and mortality in intensive care unit. Although pneumonia and sepsis are the most common causes of ARDS, several aseptic conditions are associated with ARDS, such as acute pancreatitis, burns, near drowning, multiple trauma, and inhalation injury (136). Having no effective treatments available, there is urgent need to understand, and subsequently modulate, the pathogenesis of lung inflammation in ARDS.

To investigate the inflammatory response in ALI, we utilize a broadly used mouse model of ALI, hydrochloric acid (HCL)-aspiration ALI (133, 169), that simulates human lung injury due to gastric acid aspiration. Low pH in the lung causes a burn –type injury in type I alveolar epithelial cells and endothelial cells that enable us to recapitulate the characteristics of the disease (133), but it can also orchestrate an aseptic lung inflammatory response that resembles the pathology of many other lung diseases (133). We also verify some of our results in acid-induced ALI in another widely used model of aseptic ALI, the ventilation induced lung injury (VILI).

In our model of ALI, we demonstrate that Akt2 ablation protects mice from the severe manifestations of the disease. Akt2 deficient mice present with a less severe compromise of lung compliance and pulmonary edema and reduced lung inflammation upon acid aspiration and upon mechanical ventilation. Activation of the PI3K/Akt pathway has been demonstrated to play a significant role in septic and aseptic models of ALI (401-403) and furthermore, in accordance with our findings, inhibition of this pathway has been reported to protect from ALI (401-403). Up to now only one report has studied the role of individual Akt isoforms in the development of ALI; it has been reported that overexpression of a constitutively active Akt1 transgene ameliorated the endothelial barrier dysfunction in a mouse model of VILI (404).

The role or M2 macrophages in the pathogenesis of ALI

It is well established that macrophages play a central role in the pathogenesis of ARDS (169, 178, 179, 200). Most of the studies in animal models have examined the role of macrophages in LPS-induced lung injury, a model that resembles septic ARDS (47, 182, 208). Herein we utilized the model of acid-induced lung injury, a model of aseptic ARDS (133). We report here, in accordance with previous reports, that alveolar macrophages acquire a classical activation phenotype in the acute phase of aseptic ALI. We were also able to discriminate, based on the mRNA levels of markers of M1 and M2 activation, the onset of resolving phase of inflammation where suppression of iNOS and predominance of Arg1, Fizz1 and Ym1 expression takes place in the natural course of disease. In this phase, overexpression of M2 genes define the presence of alternatively activated macrophages that exert an immunosuppressive role.

In a recent study from our group, Akt2-/- peritoneal macrophages were found to be M2 prone and to protect from the generation of DSS induced colitis (49). In this study, we extent our previous findings in alveolar macrophages as well, since we found that alveolar macrophages from Akt2-/- mice demonstrate an M2 activation phenotype and we demonstrate a protective effect of those cells in lung pathology. We show that prevention of M1 development early in the acute phase of the disease by blocking TLR4 signaling activation and by substitution with M2 macrophages resulted in a better outcome of ALI.

However, a drawback of this study is that Akt2 deficiency is not macrophage specific in our mice and thus only a correlation among the presence of M2 and the prevention of ALI can be made. But, the major role of iNOS-expressing macrophages has been well demonstrated in previous studies, where macrophage depletion in WT mice and reconstitution with iNOS-/- macrophages led to significant amelioration from acid-aspiration

and other models of ALI (31, 169, 178, 179, 200, 201, 205-208). To overcome this obstacle and to elucidate whether or not M2 macrophages can confer protection from ALI we performed macrophage depletion experiments in WT and Akt2-/- mice in mice where alveolar macrophages have been depleted, we transferred WT or Akt2-/- alveolar macrophages, 1hour prior to HCL administration. We found that WT mice that received Akt2-/- macrophages exhibited reduced iNOS expression and improved inspiratory capacity compared to WT mice that received WT cells. And they had no difference in neutrophilic infiltration suggesting that M2 macrophages are critical for protection in ALI. Akt2-/- animals with ALI that received WT macrophages had a trend to exhibit more iNOS positive macrophages (although non-significantly) and reduced inspiratory capacity, compared to Akt2-/- animals that received Akt2-/- macrophages. The fact that we could not see a clear difference in the case of Akt2-/- mice can be possibly attributed to the fact that alveolar macrophage depletion was not complete (approximately 85%) and the remaining M2 macrophages in Akt2-/- mice were sufficient to interfere with the results.

Thus, based to these reports, the feature of Akt2-/- mice to promote reprogramming of macrophages from M1 to M2 state by blocking M1 activation and by promoting Arginase-1 overexpression, an enzyme that antagonizes iNOS, should be of outmost importance in the prevention from ALI.

In accordance with our findings, apart from M1 macrophages, it was been shown by other groups that the presence of M2 alveolar macrophages has been also noticed in the resolving phases in several models of ALI (7, 45). They appear after the acute phase and in the recovery phase of ALI (7, 45, 46). In fact, both populations of M1 and M2 alveolar macrophages exist in the same time in the lung and their equilibrium will determine the type or response. But also M1 macrophages upon the proper environment can be transformed to M2 (7). However, in the above studies only the presence of M2 macrophages was noticed and the role of M2 macrophages in the outcome of ALI was not clarified. In another report, it was shown that stem cell conditioned medium induced M2 polarization and suppressed lung inflammation in the model of LPS-induced lung injury (47), however no molecular mechanism of M2 induction was suggested. In our study, Akt2 deficient mice exhibited an ameliorated M1 response and an accelerated M2 activation resulting in significant protection from lung injury, suggesting that early induction of M2 macrophages, via Akt2 depletion, confer protection in the aseptic lung injury model. Our findings extend the existing evidence regarding the role of M2 macrophages in ALI; early induction of M2 in the course of disease can ameliorate lung inflammation and injury.

After the publication of the results of this study, subsequent studies supported the role of M2 macrophages in ALI. In an endotoxemic murine model of lung inflammation, M2 macrophage depletion resulted in neutrophil accumulation, upregulation of lung cytokines and exaggeration of lung injury (405). Also, β2 adrenergic receptor activation promoted M2

macrophage activation, inhibited M1 activation and resulted in amelioration of lung injury and increased survival in a model of LPS induced ALI (406). Resolvin D1 has potent anti-inflammatory and resolving effects in a murine model of cigarette smoke-induced lung inflammation, mainly via the induction of alternatively activated (M2) macrophages (407). Finally, another study reported that administration of the antisense oligonucleotide targeting miR-155 in a murine model of LPS induced ALI induced upregulation of c/EBPβ, promotion of IL-10 secretion and M2-like phenotype of macrophages and resulted in reduced lung inflammation and enhanced recovery (111).

The role of miR-155

We further sought to investigate the mechanisms involved in regulation of macrophage activation phenotype by Akt2 in this lung injury model. Activation of the PI3K/Akt pathway has been demonstrated to mediate anti-inflammatory effects in macrophages (49, 68, 95, 96). The anti-inflammatory actions of the PI3K/Akt pathway are differentially controlled by the two Akt isoforms, Akt1 and Akt2, which also regulate the activation phenotype of macrophages (49). Hence, ablation of Akt2 suppresses LPS responses promoting an M2 anti-inflammatory phenotype while ablation of Akt1 renders macrophages hyper-responsive to LPS and M1-prone (49).

To investigate potential regulatory pathways that regulate macrophage activation in ALI and play a role in Akt2 protection we sought to investigate the regulation of several microRNAs in ALI. The involvement of miRNAs in the pathogenesis of ALI has been previously reported (215, 408-410). Specifically, it has been found that high tidal volume ventilation resulted in up-regulation of several miRNAs in the lung such as miR-21, miR-155 and let-7 and that regulation of their expression could ameliorate disease severity (215). Akt kinase isoforms have been also previously reported to regulate macrophage phenotype via the modulation of miRNA levels (49, 68, 80, 95).

We have recently reported that miR155 up-regulation upon endotoxin induced sepsis was found to exacerbate M1 activation and iNOS induction, and miR-155 suppression by Akt2-/- peritoneal macrophages was crucial for the protective effects of Akt2 ablation in blocking M1 phenotype (49). Also miR-155 has been found to be important in the pathogenesis of LPS-induced lung injury (111). MiR-155 has not been involved in M1 inhibition but in promotion of M2 phenotype. Antisense oligonucleotide treatment enhances the recovery of acute lung injury through the induction of IL-10-secreting M2-like macrophages (111). Indeed, overexpression of miR-155 is capable to re-program anti-inflammatory M2 macrophages to pro-inflammatory M1 macrophages (109).

In this study, although we found that miR-155 expression is lower in Akt2-/- macrophages than in WT ones, we did not detected miR-155 up-regulation upon acid aspiration. This could be attributed to the different nature of inflammation which is sterile –aseptic in our case in contrast with the reports in endotoxin induced inflammation. Thus, miR-155 did not contribute to M1 priming in our model and furthermore, miR-155 suppression in Akt2 deficiency was not responsible for blocking M1 activation but only in promoting M2 state via C/EBPβ. These findings suggest that in this aseptic model a distinct mechanism regulates macrophage activation.

The role of miR-125b and its target IRF4

MiR-125b is another pro-inflammatory miRNA that was recently reported to play major role in M1 macrophage activation (98, 114). Enforced expression of miR-125b drives macrophages to M1 activation, whereas anti–miR-125b treatment decreases CD80 surface expression (115). MiR-125b can also sustain pro-inflammatory cell activation by targeting the transcription factor IFN regulatory factor IRF4 (116). IRF4 is known to promote alternative macrophage activation and also IRF-4 competes with IRF-5 for MyD88 interaction (77).

To investigate the involvement of miR-125b in the regulation of M1 phenotype in our model of aseptic lung injury, we measured miR-125b levels in alveolar macrophages from WT and Akt2-/- mice exposed to acid. We found that there was a mild non- significant increase in expression of miR-125b. These results suggest that miR-125b does not participate in the initial M1 activation of alveolar macrophages in aseptic lung injury.

We also examined the levels of IRF4 in alveolar macrophages from WT and Akt2-/- animals exposed to acid, since IRF4 is target of mir-125b and a positive regulator of M2 activation (116). The expression of IRF4 in naïve Akt2-/- alveolar macrophages was higher compared to WT both at basal levels and 12 hours post acid-aspiration. However, this upregulation was not correlated with miR-125b levels and was not confirmed in protein level.

TLR signaling and miR-146a

Various signaling pathways have been reported to regulate macrophage activation among which is STAT1/STAT6, SOCS2/SOCS3, TLR4 and IRF5/IRF4. Specifically, TLR4 signaling plays a central role in macrophage activation in both septic and aseptic inflammation including ARDS (209, 402, 411-415), and is critical in the pathogenesis of disease (200, 209, 415). TLR4 signaling was been found to be activated in aseptic acute lung injury and inflammation,

mutation or defect of which abrogated the generation of ALI (209, 412-414). In hydrochloric acid-induced ALI, TLR4 signaling in lung macrophages has been also demonstrated to be critical in the pathogenesis of disease (200, 209, 415).

Stimulation of TLR4 can trigger the activation of two downstream signaling pathways: MyD88-dependent or TRIF-dependent pathways (416). In the classical pathway, MyD88 recruits IL-1R-associated kinase (IRAK)-1 and TRAF6 leading to activation of NF-kB (416). TRIF pathway signaling, through IKK-3, leads to the activation of IRF3 and the expression of IFN-inducible genes (411, 416). It has been shown that TRAF6 binds to TRIF though TRAF6-binding motifs and is involved in TRIF-mediated activation of NF-kB *in vitro* (417). IRF5, although it is mainly known to be involved downstream MyD88 (411), it has been also found to be involved in TRIF-mediated response and thus to be activated by both MyD88 and TRIF (418). In acid-aspiration ALI, TLR4-TRIF-TRAF6 signaling in lung macrophages has been shown to determine the susceptibility to acute lung failure *in vivo* (200). In another study, in an aseptic model of ALI, TRIF and MyD88 deficiency fully and partially attenuated lung injury respectively (413). Both TRAF6 and IRF5 lead to NF-kB activation, but specifically IRF5 has been reported to be important regulator of iNOS and IL-12p40 expression, and thus M1 polarization (31, 66, 411, 418-420).

Apart from TLR4 signaling, interferon-γ signaling and the downstream STAT-1 phosphorylation is crucial for M1 activation. However, it has been recently found that two major cell signaling pathways regulate the activity of STATs: the canonical pathway elicited by cytokine receptors and JAKs and the non-canonical pathway triggered by TLRs, interleukin-1 receptor, tumor necrosis factor receptor and Fc-receptor for immunoglobulins (FcR) (397, 398). It has shown that multiple TLRs, such as TLR2 and TLR4, cross –talk with JAK/STAT pathway and induce Ser727 phosphorylation of STAT1, which is dependent on MyD88 and TRIF signaling, but independent of interferon (IFN) signaling (398). Furthermore, it was recently shown that TRAF6 is the major mediator of TLR-STAT1 cross talk; STAT1 interacts with tumor necrosis factor (TNF) receptor-associated factor-6 (TRAF6), and translocates to the nucleus (397). Thus STAT1, a major regulation of M1 activation, is also crucial for TLR and TRAF6 induced macrophage activation (397, 398).

In this study, we found that up-regulation of TRAF6, IRF5 and STAT1, signaling proteins downstream TLR as described above, takes place in WT macrophages upon acid aspiration. Interestingly, we found significant downregulation of TRAF6, IRAK1, IRF5 and STAT1 levels in Akt2-/- alveolar and peritoneal macrophages compared to WT. Based on our previous report in peritoneal macrophages (49), TLR4 expression is the same among WT and Akt2-/- peritoneal macrophages and thus this finding is not attributed to reduced TLR4 activation in Akt2-/- cells. Further identification of the signaling proteins that promote macrophage activation downstream TLR4 signaling was beyond the scope of this study.

Based on our findings that several components of TLR pathway were suppressed in Akt2 deficient macrophages, we sought to characterize the molecular mechanism responsible for this observation. According to the evidence present in the introductory part regarding the regulation of macrophage activation and TLR signaling reported so far, miR-146a has been identified as an LPS-induced miRNA, in an NF-kB dependent way, with the potential to target the 3' UTR of TRAF6 and IRAK1 mRNA (399, 400) and thus to suppress the expression of NF-κB target genes and TLR signaling (120, 421-423). Also IRF-5 and STAT-1 have been reported to be targets of miR-146a (119, 422).

Here, we demonstrate that Akt2 deficiency results in significant up-regulation of miR-146a, which is critical for its protective role in suppressing M1 state. MiR-146a transfection in WT macrophages was also able to inhibit iNOS induction and miR-146a suppression in Akt2-/- mice resulted in upregulation of iNOS expression. MiR-146 application on WT macrophages was able to inhibit iNOS induction. Although there are numerous reports that miR146 blocks NF-kB target genes via blockage of TLR signaling, to the authors' knowledge this is the first report that links miR-146 application with iNOS suppression in macrophages. iNOS inhibition by miR-146 has been previously showed in two reports in lymphocytes and renal cells respectively (424, 425).

It is of interest that introduction of miR-146a in WT macrophages induced expression of the transcription factor c/EBPβ, a master regulator of M2 polarization, indicating that miR-146a induction can promote alternative macrophage activation. However, inhibition of miR-146 in Akt2-/- M2 prone macrophages does not lead to reduction in M2 markers, suggesting that miR146a is sufficient but not necessary for the induction of M2 phenotype and there are additional molecules regulated by Akt2 that maintain M2 activation, such as miR-155.

Up to know, miR-146a has not been implicated in macrophage activation phenotypes per se. MiR-146a is an LPS-induced miRNA, well known to play a critical role in macrophage responses (120). MiR-146a is considered anti-inflammatory miRNA that mutes immune activation initiated by TLR4 by targeting the 3'UTR of TRAF6, IRAK1 and IRF5 mRNAs (399, 400) and suppressing TLR4-induced NF-kB regulated gene expression (120, 421-423). Mice with a targeted deletion of the miR-146a locus were found to be hypersensitive to bacterial challenge. They produce excessive amounts of pro-inflammatory cytokines in response to LPS and succumb to septic shock faster than the wild type littermates (117). Furthermore, aged knockout mice develop tumors in their secondary lymphoid organs and undergo myeloproliferation, suggesting that miR-146a regulates proliferation in immune cells (117, 118). MiR-146a deficient mice also display severe tissue inflammation, increased basal cytokine production, as well as elevated titers of autoantibodies—all classical signs of autoimmunity (117). Yet, the role of miR-146a macrophage activation phenotype and aseptic inflammation has not been investigated.

In agreement with our findings, miR-146a has been found to be upregulated in alternative activated macrophages. Microarray analysis of miRNA expression profiles of bone marrow-derived macrophages (BMDMs) with two distinct polarizing conditions, classical macrophage activation 'M1' and alternative activation 'M2', revealed that among others miR-146a was downregulated in M1 compared with M2 (426). Also, miR-146a has been found elevated in tolerant "M2-like" macrophages (120, 427) Importantly, tolerance induction requires miR-146a upregulation, and the transfection of miR-146a is sufficient to induce endotoxin tolerance even in the absence of LPS-priming (120). However, in another study it was found that miR-146a-5p was downregulated upon IL-4 treatment in macrophages (98). Downmodulation of this miRNA in IL-4–stimulated macrophages could enhance TLR signaling and thus this finding seems counterintuitive. However, reduced levels of miR-146a-5p did not occur until very late after IL-4 stimulation and long-term pre-incubation of macrophages with IL-4 has previously been shown to potentiate production of pro-inflammatory cytokines after secondary stimulation with LPS (98).

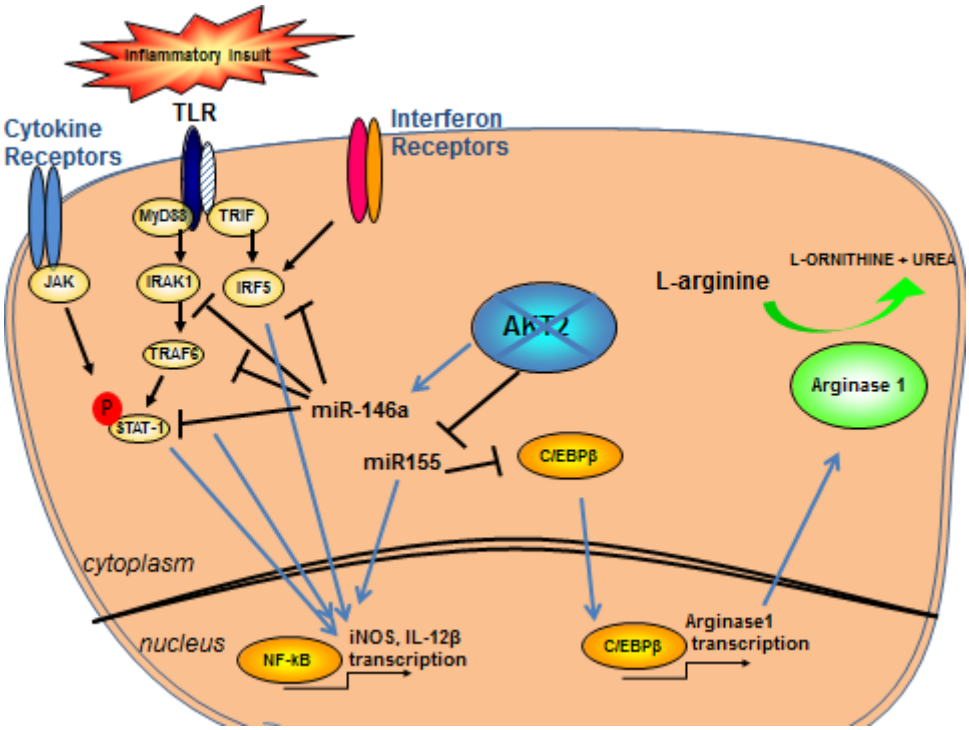

Figure 86. Proposed mechanism of modulation of macrophage activation in Akt2 deficient alveolar macrophages.

In vivo modulation of macrophage phenotype

Finally, we show that pulmonary macrophage polarization phenotype can be modulated *in vivo* by targeting locally Akt2 or miR-146a expression. Intratracheal administration of siRNA against Akt2 or of a miR-146a mimic in WT mice exposed to acid-induced lung injury resulted in a significant suppression of iNOS in alveolar macrophages. Since it is well established that suppression of iNOS, and subsequent inhibition of M1 activation as well as induction of M2 (47) can confer protection in ARDS, identification of molecules that promote this mechanism *in vivo* is of outmost importance (169, 178, 205-208). In agreement with our findings a recent study reported that miR-146a upregulation could suppress inflammatory mediators and ameliorates LPS induced-ALI model suggesting that miR-146a may be therapeutically targeted as a mean to repress inflammatory response following ALI (217).

M2 role in septic inflammatory conditions

Akt2 suppression was found protective in a model of aseptic lung injury. However, Akt2 suppression and M2 macrophages impair the innate immune response against live bacteria such as P. aeruginosa. This observation limits the use of M2 induction for the protection from gastric acid aspiration-induced lung injury. Simultaneous treatment with antibiotics may overcome such limitation in a clinical setting.

Part 2: The role of M2 macrophages in Pulmonary Hypertension

In the present study, we report that hypoxia activates *in vivo* gene expression in alveolar macrophages towards an alternative pathway that precedes the development of pulmonary hypertension and appears to play a critical role in the pathogenesis of disease. Overexpression of HO-1 induced a switch in macrophage polarity toward an increased IL-10 production and this effect was associated with protection from HPH.

Macrophage activation in hypoxia

Hypoxia is an important and common cause of cell injury and death as it impinges on aerobic mitochondrial oxidative respiration resulting in partial depletion of ATP with all the consequences of altered protein synthesis and membrane homeostasis. In our bitransgenic mouse model, hypoxia caused pulmonary hypertension with prominent vascular remodeling as well as a lung inflammatory response, characterized by macrophage accumulation and acquisition of an alternative activation state of the alveolar macrophages.

In our study, hypoxia resulted in alveolar inflammation that consisted predominantly of macrophages. These findings correlate with the fact that macrophages tend to accumulate in poorly vascularized, hypoxic sites, where considerable tissue damage may have occurred (125). Also, high macrophage numbers have been reported in avascular and necrotic sites carcinomas (428), hypoxic areas of dermal wounds (429, 430), and avascular locations of atherosclerotic plaques (431). Macrophages predominate in these areas, they consist of approximately 80-90% of innate immune cells as it was also found in our study (248). Our findings, in accordance with previous studies in HPH, highlighted the predominant role of the monocyte/macrophage lineage in modulating vascular remodeling (248).

Studies have suggested that hypoxia alters the phenotype of macrophages in a way that promotes these lesions. However, the genes up-regulated by macrophages in such hypoxic tissues are poorly characterized (125). Activation of macrophages is a key event in the inflammatory cascade in the lung and defines a functional state characterized by extrusion of pseudopodia and an increase in cell size and membrane ruffling (3). In our study, enlargement of macrophage diameter was the main observation that led us to further investigate macrophage activation phenotype.

Activated macrophages can be distinguished into classically activated (induced by IL-12 and INF-γ, expressing iNOS and TNF-a and contribute to host defence) (40, 41) and alternatively activated (induced by IL-4 or IL-13, and expressing arginase-1, mannose receptor CD206, Fizz-1, Ym-1, galectin-3 and MMP-9) (40, 41, 44, 432-435). Alternatively activated macrophages have been implicated in the pathology of various chronic diseases (54, 123, 436-439).

We found that hypoxia *in vivo* and *in vitro* polarized the population of alveolar macrophages toward the M2 phenotype. Alveolar macrophages isolated from hypoxic mice, expressed markers of M2 activation, including Fizz1, Ym1, CD206, arginase-1 and galectin-3 and were negative for markers of classical activation. Also alveolar macrophages exposed to hypoxia *ex vivo*, also upregulated M2 markers. This observation correlates with the cytokine profile of the BAL fluid of hypoxic mice and mRNA analysis of total lung: predominance of cytokines that promote M2 phenotype (CCL2, IL-6, IL-4, IL-13) and absence of cytokines that drive M1 activation (IL-12, TNF-a, INF-γ). The cell autonomous M2 polarization in *in vitro* hypoxic conditions, the upregulation *in vivo* of mRNA levels of 2 recently recognized noncanonical inducers of M2 polarization, CCL2 and IL-6, and the increased IL-13 and IL-4 cytokine levels in the BALF of hypoxic mice support the M2-like activation in our hypoxic model.

Hypoxic microenvironment is also a hallmark feature of tumors, and similar to the hypoxic macrophages in our model, the tumor-associated macrophages exhibit an M2-like phenotype. Macrophages are recruited to hypoxic tumor areas of tumors and polarized them towards a pro-angiogenic M2 phenotype (440). Furthermore, Fizz1, an M2-specific marker, is a hypoxia-inducible molecule, also designated hypoxia-induced mitogenic factor (441-443). Upregulated arginase-1 expression has been also observed in cultured anoxic macrophages (444). Moreover, it was been shown that hypoxia mediates impairment of mitochondrial respiratory chain in macrophages and inhibits their bactericidal activity, resembling by this way alternatively activated macrophages (445).

Furthermore, the pathway by which hypoxia promotes M2 polarization has been investigated. Specifically, it has been reported that hypoxia and HIF-1a activation leads to M2 macrophages via the activation of AKT/mTOR pathway and the production of lactic acid and succinate. Lactic acid produced by tumour cells, as a by-product of aerobic or anaerobic glycolysis, has a critical function in signalling, through inducing the expression of vascular endothelial growth factor and the M2-like polarization of tumour-associated macrophages. Furthermore, we demonstrate that this effect of lactic acid is mediated by hypoxia-inducible factor 1α (HIF1α) (446-448).

However, our results are not in agreement with two previous reports that found TNF-a upregulation (449) and IL-12 and INF-γ production (450) in macrophages of hypoxic rats and mice respectively. We believe that our *in vivo* studies most closely approximate the disease physiology, since the first study was performed *in vitro,* using isolated rat alveolar macrophages in a sepsis-induced hypoxia model, and the second study involved not alveolar but peritoneal macrophages cultured under hypoxic conditions. In such studies, the reductionist approach obviously deprives the macrophages from tissue-specific microenvironmental signal, and it is difficult to place in perspective the physiological relevance of such simplistic models.

M2 macrophages and pulmonary hypertension

In the present study, we report that hypoxia activates *in vivo* gene expression in alveolar macrophages towards an alternative pathway. Since macrophage numbers and markers of alternative activation correlate with the development of HPH, these cells play a significant role in the later development of hypertension. Our finding that the presence of M2 macrophages is associated with the development of HPH *in vivo* and pulmonary artery smooth muscle cell proliferation *in vitro* suggests that these polarized trophic macrophages may play a significant role in the later development of pulmonary hypertension.

Our results are in agreement with recent studies in pulmonary hypertension not only in hypoxic exposure but in other systems as well. Specifically, CCL2 a potent inducer of M2, was recent found to play an important role in patients with idiopathic PAH (314). Another inducer of M2, IL-6, has been implicated to induce pulmonary arterial remodeling and hypertension (451). A Th2 immune response, which is characterized mainly by IL-4 and IL-13 production, had been also recently reported to provoke pulmonary vascular remodeling in monocrotaline-induced PH model in rats (228, 452).

After the publication of the results of this study, many other reported supported the role of M2 activation in PAH. Interestingly, in a recent report that evaluated the role of Akt isoforms in the development of hypoxia induced pulmonary hypertension it was shown that in comparison to the wild-type (WT) littermates, $Akt1^{-/-}$ mice were protected against the development and progression of pulmonary vascular remodeling and chronic hypoxia-induced PH, while $Akt2^{-/-}$ mice did not demonstrate any significant protection against the development of HPH (453). Based on our findings in the first part of this study that Akt1 deficient mice exhibit M1 macrophage activation while Akt2 deficient mice exhibit an M2 response, the results of this study are also in agreement with our results; mice with Akt2 deficiency that host M2 activated macrophages did not demonstrate any significant protection against the development of HPH. Finally, increased expression of markers of alternative macrophage activation has been found in patients with systemic sclerosis associated pulmonary arterial hypertension (454). Also, infection with the parasite Schistosoma mansoni resulted in PAH and remodeling of pulmonary arteries (455).

The role of M2 related mediators in the development of PAH

- Arginase-1

Among the M2 -related mediators, arginase and Fizz1 appear to play a major role in the development of PAH. The activity of arginase I, which reduces NO synthesis by competing

with iNOS for the substrate L-arginine, has been also found to be increased in endothelial cells of PAH patients (456). Indeed, enhanced polyamine and L-proline synthesis caused by Arg1 has been shown to contribute to vascular damage and remodeling, and elevated Arg1 in lungs of hypoxic mice has been associated with increased severity of PAH (457, 458). Arginase-1 is induced by numerous pathologic stimuli and contributes to vascular cell dysfunction and vessel wall remodeling in several diseases (459, 460). Clinical and experimental studies have documented increases in the expression and/or activity of arginase I in blood vessels following arterial injury and in pulmonary and arterial hypertension, aging, and atherosclerosis (459). Single-nucleotide polymorphisms in arginase-1 gene have been associated with decreased risk of pulmonary hypertension in bronchopulmonary dysplasia (461). Significantly, pharmacological inhibition or genetic ablation of arginase in animals ameliorates abnormalities in vascular cells and normalizes blood vessel architecture and function in all of these pathological states (459, 460). The detrimental effect of arginase in vascular remodeling is attributable to its ability to stimulate vascular smooth muscle cell and endothelial cell proliferation, and collagen deposition by promoting the synthesis of polyamines and l-proline, respectively (459). Moreover, the proliferative, fibrotic, and inflammatory actions of arginase in the vasculature are further amplified by its capacity to inhibit nitric oxide (NO) synthesis by competing with NO synthase for substrate, L-arginine (459).

- Fizz1

Fizz1 has been recently reported to have mitogenic, angiogenic, and vasoconstrictive properties that are associated with pulmonary vascular remodeling (441, 462). Its human homolog, resistin-like molecule b, has also been detected in patients with scleroderma-associated pulmonary hypertension (463). Fizz-1 (also known as HIMF: hypoxia induced mitogenic factor), that derives from lung parenchyma has been reported to be a mitogen for smooth muscle cells, has been recently found to promote smooth muscle cell proliferation (464) and to contribute to the development of hypoxia induced pulmonary hypertension (465). Also Fizz1 induces the release of endothelin -1 from endothelial cells causing significant increases in pulmonary vascular smooth muscle cell proliferation (466). Knockdown of Fizz1/HIMF partially blocked increases in mean pulmonary artery pressure, pulmonary vascular resistance, right heart hypertrophy, and vascular remodeling caused by chronic hypoxia (467). Fizz1/HIMF-gene transfer into the lungs of rats using a HIMF-expressing adeno-associated virus (AAV) caused development of PH similar to that of chronic hypoxia. The findings suggest that HIMF represents a critical cytokine-like growth factor in the development of PH (467, 468).

These reports are consistent with the fact that Fizz1 expression pattern in response to absence or presence of HO-1 was found to correlate with the development of pulmonary hypertension. Apart from the mitogenic and angiogenic effects, Fizz1 has been reported to contribute to the activation of vascular inflammation by inducing endothelial cells apoptosis in the lung (466). It has been recently demonstrated that hypoxia-induced mitogenic factor (HIMF/FIZZ1/RELMa) is chemotactic to murine bone marrow cells *in vitro* and involved in pulmonary vascular remodeling *in vivo* (469, 470).

To the best of our knowledge, this is the first study to propose a link between alternatively activated macrophages and the development of HPH. One potential mechanism of action of alternatively activated macrophages may be upregulation of Arginase-1 and the secretion of Fizz1, the overexpression of which have been reported to lead to PAH as described above. Further studies are required to determine the specific mediators from the secretome of M2 macrophages that may be contributing factors in the signaling cascade leading to HPH.

The role of Heme Oxygenase-1

HO-1 overexpression provoked a robust anti-inflammatory effect. It could suppress macrophage accumulation, alternative activation and cytokine production in the lungs and prevent the subsequent development of pulmonary hypertension. Carbon monoxide appeared to be the key HO-1 effector inhibiting macrophage accumulation in the BALF and suppressing the expression of M2 markers *in vitro*. This observation is in agreement with previous reports, where the anti-inflammatory effect of CO has been demonstrated (346, 347, 349, 471, 472). Furthermore, CO has been indicated by our group and others to prevent or reverse the development of pulmonary vascular remodeling and HPH (367, 473, 474).

It is well known that endogenous HO-1 is upregulated in hypoxia, as a compensatory mechanism, but since it's a transient upregulation, is not adequate to prevent the hypoxia-induced inflammation and HPH (246). The transient effects of hypoxia are mediated by the smooth muscle cells via the increased expression of HO-1 resulting in increased CO production. Increased CO levels inhibit smooth muscle cell growth in an autocrine manner and inhibit the endothelial expression of ET-1 and PDGF-B, thereby inhibiting smooth muscle cell contractility and proliferation in a paracrine manner (245). Exogenous CO administration is protective in PAH and can reverse the disease in animal models of PAH (359). However, under prolonged periods of hypoxia, HO-1 and CO production is not sustained and thus the endothelial cell pathway predominates, leading to active and sustained vasoconstriction with structural remodeling of the pulmonary vasculature (245).

Only longer enhancement of HO-1 expression can be protective in HPH (246). For this reason, we were not surprised that 2 days administration dox and thus HO-1 upregulation actually postponed inflammation and did not protect from the development of hypertension. Interestingly, dox administration for 7 days, covering the entire period of hypoxia-induced inflammation, was adequate to suppress the inflammatory response in a way that it did not relapse even 2 weeks after the return of the HO-1 to the baseline levels. Since the switch in macrophage phenotype occurs in the 1st week of hypoxia, we hypothesize the enhancement of HO-1 during this critical period may act as a pivot to shift the balance of immune response from pro-inflammatory towards immunosuppressive microenvironment. Actually, recent studies strongly support the hypothesis that HO-1 expression mediate potent anti-inflammatory effects in monocytes and macrophages (475) probably by preventing these cells from inducing tissue injury and modulating the immune response (351, 476-479). Furthermore, HO-1 has been demonstrated to exert protection in several models of disease by the induction of a regulatory T cell population (479-481). Thus, enhancement of HO-1 may not be necessary for the whole course of hypoxia but may need to take place in an adequate period of time in order to induce and establish anti-inflammatory cascades. Based on this model, a sustained expression of HO-1 leading to increased CO levels could prevent or reduce the development of hypoxic pulmonary hypertension *in vivo* (245). Therapies aimed at enhancing and sustaining CO production for longer periods may prevent the proliferative cellular responses and minimize injury secondary to hypoxia (245).

Furthermore, lung HO-1 overexpression upregulated IL-10 in hypoxic macrophages and increased the number of IL-10–expressing alveolar macrophages in the BALF. Because CO could upregulate IL-10 in the *in vitro* cultured hypoxic macrophages, it seems to be a major effector molecule of HO-1 immunomodulation. The macrophages in HO-1 bitrangenic mice exposed to hypoxia for a long period of time have a unique phenotype characterized by upregulation of IL-10 and downregulation of Fizz1 and Arg1 compared with macrophages exposed to hypoxia alone. Based on the latest categorization of M2 macrophages described in the introductory part, hypoxic macrophages resemble the IL-4 stimulated macrophages while macrophages under HO-1 and CO production most closely resemble macrophages activated by IL-10, glucocorticosteroids or immune complexes.

In agreement with our findings, several lines of evidence suggest that HO-1 expression is related to interleukin-10 (IL-10) signaling and vice versa (338, 482). HO-1 and CO modulate IL- 10 production through the activation of p38 MAPK (483). Previous reports have described that lipopolysaccharide (LPS) stimulation induces IL-10 production in human monocytes and mouse macrophages (482). The inductions were significantly abrogated in the presence of the HO inhibitor, zinc protoporphyrin IX. In contrast, cobalt protoporphyrin IX, which is the HO-1 inducer, enhanced LPS-induced IL-10 production (482). HO-1 and exogenous CO have

previously been reported to increase IL-10 expression in macrophages *in vivo* and *in vitro* (185, 354, 355, 363, 484). This positive feedback circuit between HO-1 and IL-10 has been shown to be functional, which might amplify the anti-inflammatory effects of HO-1 in monocyte/macrophage (485). The latter idea is supported by our results based on which IL-10 remained elevated even 2 weeks after HO-1 expression returned to baseline levels. These findings point to a switch in immunoregulation triggered by HO-1 during an early critical period, and whose presence was no longer essential, at least for the subsequent 2 weeks of hypoxia.

After the publication of this study, many other studies reported that HO-1 upregulation in macrophages renders them M2-like and anti-inflammatory. Weis and colleagues demonstrated that apoptotic cells polarized macrophages toward M2 phenotype, and that HO-1 induced by apoptotic cells is closely involved in the polarization (486). However, the expression levels of M1 and M2 markers were not measured in this study (486). In other reports, adiponectin was found to promote M2 macrophage activation via HO-1 induction (42). Hemin administration, that induces HO-1, has been shown to reduce the pro-inflammatory macrophage M1 phenotype, and to enhance the M2 phenotype that dampens inflammation (487, 488). Isolated peritoneal macrophages from Bach1-deficient mice that highly overexpress HO-1 manifested M2 macrophage markers such as Arg1, Mrc1, Fizz1, and Ym1 (489).

In our model we found that Fizz1 is downregulated in alveolar macrophages in mice with HO-1 overexpression in Clara cells. But the alveolar macrophages in HO-1 bitrangenic mice still belong to M2 macrophage categorization based on the latest proposed M2 nomenclature. The main characteristic of macrophages in hypoxic HO-1 trangenic mice is reduced Fizz1 expression and enhanced IL-10 expression compared to hypoxic alveolar macrophages in WT mice. If we had compared macrophages from HO-1 transgenic mice with classically M1 macrophages we may have found relatively lower levels of Fizz1 in the latter. In our model we don't have M1 activation at all, and we actually compare two different populations of alternative activated macrophages. We should also point out that our model holds a major difference with the aforementioned studies. In all the studies that HO-1 promoted M2 macrophage activation, HO-1 was induced in macrophages. In our system, HO-1 upregulation takes place only in epithelial cells and not in macrophages, thus the effect that we see in macrophage phenotype is mostly paracrine in nature, mainly promoted via CO release. By this way, we don't have the antioxidant benefits of HO-1 induction into the cells as well as other effects independent of HO-1 products that may also account for HO-1 protection.

The effect of IL-10 expressing macrophages in pulmonary vascular remodeling

In our study we show a correlation among IL-10 expressing macrophages and protection from HPH. In accordance with this finding, elevated IL-10 levels have been also associated with protection from HPH, and IL-10 expression has been reported to protect from monocrotaline-induced PAH in rats (316).

We show that macrophages were the source of IL-10, but it remains unclear whether they are also a target of this cytokine. Because IL-10 is a pleiotropic cytokine, it may act in an autocrine and paracrine manner to affect many different cell types besides macrophages. However, IL-10 did not have direct anti-proliferative effects on pulmonary artery smooth muscle cells in our *in vitro* model, indicating that HO-1 and CO may also have anti-inflammatory functions independently of IL-10, or that IL-10 expression may indirectly ameliorate remodeling via suppression of pro-inflammatory pathways that promote smooth muscle cell proliferation. Further studies are required to decipher the role of IL-10 pathway in the protection from HPH development and the mechanism of sustained protection from HPH conferred by a transient immunomodulatory event.

In summary, this study poses a correlation among monocyte/macrophage recruitment and alternative activation with the later development of pulmonary hypertension. However, we haven't characterized how exactly M2s promote vascular remodeling and more experiments are required to figure out which factor from the secretome of M2 is the most crucial for the promotion of disease.

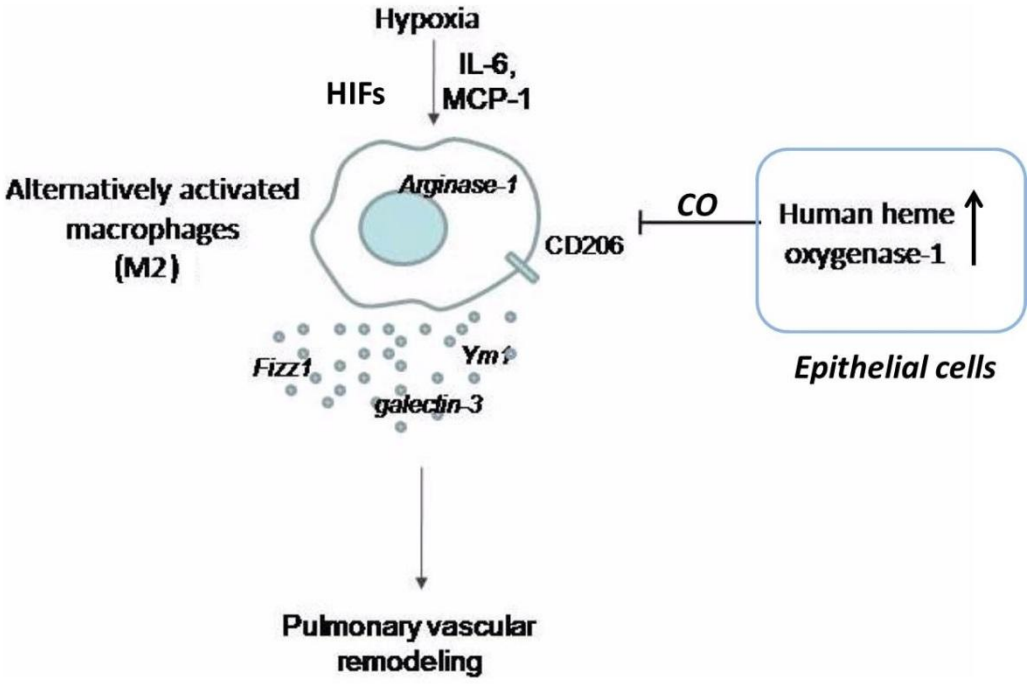

Figure 87. Proposed mechanism by which hypoxia drives alternative activation of the alveolar macrophages, the secretome of which contribute to the development of hypoxic pulmonary hypertension.

Special considerations

In the present study significant results regarding the role of macrophage activation and molecular mechanisms to regulate this activation have been presented. However, there are several limitations of this study.

Part 1

First, in the model of acute lung injury, a great amount of data was collected using conditional Akt2 -/- mice and not macrophage specific Akt2 deficient mice. Thus, additional effects of Akt2 deficiency in other cell types that may also contribute in protection from ALI in the *in vivo* system cannot be excluded.

Indeed, it has been found that Akt2 inhibition interferes with chemotaxis of immune cells. Inhibition of Akt2 using siRNA inhibited monocyte/macrophage cell line migration in response to M-CSF due to defects in actin polymerization (490). Also, Akt2 deficiency affects neutrophilic chemotaxis in sites of inflammation (491). Lack of Akt2 also results in reduced production of superoxide (O_2^-) and reduced neutrophil degranulation in response to chemoattractants (491). A defect in neutrophilic chemotaxis in Akt2-/- mice was also evident in our results with macrophage depletion and reconstitution experiments; Akt2-/- mice had a reduced neutrophilic response compared to WT mice regardless the macrophage population transferred, WT or Akt2-/-, meaning that neutrophilic chemotaxis is inherently defective in Akt2-/- mice and it is not dependent on macrophage activation state.

However, we managed to overcome this issue by performing macrophage depletion and reconstitution experiments. We found that WT mice that received Akt2-/- macrophages exhibited reduced iNOS expression and improved inspiratory capacity compared to WT mice that received WT cells. Also, these two groups of mice had no difference in neutrophilic infiltration suggesting that M2 macrophages are critical for protection in ALI in our model and neutrophilic response was not so important.

In the same model, another drawback was the method of siRNA delivery and miRNA delivery used. Naked siRNAs and miRNAs have been used intra-nasally or intra-tracheally in high doses in the literature and exhibited a weak but significant knowndown of target genes that resulted in a biological effect (215, 384-386, 492). Although it was effective, very high amount of siRNA/miRNA was required to achieve an effect and this approach increases the possibility of toxicity and off-target effects. Due to its large molecular weight and polyanionic nature (negative phosphate charges), naked siRNA does not easily cross the cell membrane, and thus delivery systems are required to facilitate its access to its intracellular sites of action (493). Thus delivery systems can be used to favorably alter the pharmacokinetics of naked siRNA and reduce the dosing requirements so as to minimize toxicity and possibly off-

target effects and immune stimulation, both of which are often dose dependent. The siRNA delivery strategies described so far include conjugation to polyethylene glycol (PEGylation) or formation of complexes with lipids or polymers and incorporation in viral vectors, each of them characterized by specific benefits and disadvantages (493). However, the scope of this study was not to test the efficiency of a delivery method in the lung but to evaluate the biologic effect of an RNAi approach. This effect was achieved with naked siRNA and miRNA delivery in our system. Further research is required to determine the most efficient method for siRNA and miRNA delivery in the lungs.

Another limitation of this study was that we evaluated the effect of siRNA/miRNA delivery on macrophage and neutrophil accumulation in the BAL fluid as well as on the protein levels in BAL, however, we did not assessed whether introduction of RNAi affected interferon –α, interferon –γ and TLR signaling in macrophages. However, the siRNA molecule targeting *Akt2* and *Luciferase* that we utilized had undergone chemical modifications that enhanced its biological stability and reduced its recognition by immune system, thus eliminating immune response activation.

Finally, in our model of ALI, we attribute STAT1 activation in TLR4 –STAT1 cross-talk via TRAF6 without testing interferon gamma signaling in our model. We cannot exclude that apart from TLR signaling, interferon signaling may also be responsible for M1 activation in ALI.

Part 2

In the second part of the study, we evaluate the role of M2 macrophages in the development of PAH and we pose a correlation among the M2 activation and the development of disease. We utilize HO-1 bitrangenic mice that overexpress HO-1 in Clara cells and release CO in lung microenvironment to switch on and off inflammatory response and macrophage activation phenotype. We prove that CO administration can modulate macrophage phenotype. However, we cannot exclude that HO-1 induction and CO release have pleiotropic protective effects in other cells in the lung such as endothelial and smooth muscle cells that may also contribute in their protective role in PAH.

Herein we propose that one of the mechanisms of HO-1 protection in PAH is by suppression of mitogenic and angiogenic factors released by alternative activated macrophages. If we aimed to pose a causative link among M2 response and PAH, we should have performed macrophage depletion and reconstitution experiments with M2 macrophages and then determine the outcome of PAH.

CONCLUSIONS

Conclusion

In summary, this study demonstrates the different properties of alternatively activated macrophages in two different models of lung disease; their protective role in ARDS and their harmful role in pulmonary hypertension. In this report we also identify molecular ways ny which a switch to macrophage phenotype can take place in vivo, via Akt2 silencing, miR-146a induction and HO-1/CO upregulation.

In this study we found that macrophages are activated in a different way based on their environmental stimuli. We reported that molecules such as Akt2 deficiency, miR-146a and hypoxic stimulus can promote M2 polarization of alveolar macrophages. The mechanism by which this is achieved is not clear yet. Subsequent reports have indicated that hypoxia alters macrophage phenotype via alteration of macrophage metabolism (lactic acid production, mTOR activation). Also, akt2 deficiency also alters macrophage metabolism (mTOR activation and impaired insulin signaling). Thus, a common mechanism may be the case in these two different systems, the metabolic pathway.

The results of this study will substantially add to our understanding of how functionally different populations of activated macrophages contribute to the pathogenesis of ALI and PAH. Studies have shown significant amelioration of both inflammation and pulmonary edema with macrophage depletion. However, macrophage depletion is not a feasible approach in clinical practice; macrophages are essential for bacteria elimination and tissue healing, thus precluding macrophage depletion as a therapeutic option (212, 386). Experimental treatments proposed for ALI such as anti-inflammatory treatment with IL-10 have shown promise in deactivating these cells as a means of inhibiting cytokine production. At this time, there is certainly no evidence that immunosuppression is effective in ARDS and PAH, except perhaps in isolated cases of PAH related to certain connective tissue diseases, such as lupus and mixed connective tissue disease. Of the current available treatments for PAH and ARDS, none specifically targets inflammation (308).

In our study, we suggest that only a subset of macrophages, the M1 activated in ALI and M2 activated in PAH contribute to the pathology of disease and thus efforts should be made for the specific elimination or inactivation of those cells and not to the whole population of macrophages in the lung. Therefore, methods that modulate macrophage activation *in vivo* state are more than promising in promoting resolution of inflammation and tissue healing. In this study we examine methods to induce a phenotype switch to M2 *in vivo* as a therapeutic strategy for ALI. It appears that oligonucleotide – based treatments that utilize RNAi mediated suppression of gene expression by siRNA and miRNA and inhibition of microRNA function by antimiR oligonucleotides are good candidates for this purpose (212, 386). Based on the findings of this study and many reports of the literature, it is expected that, with limited adverse effects on healthy cells, these targeted therapies would reactivate pathways

in diseased cells that are necessary for normal development and impede pathways that drive the disease. Based on these findings, Akt2 and miR-146a appear as promising therapeutic targets for aseptic ARDS and HO-1 induction of M2 inactivation for PAH.

In order to reduce the prevalence and improve the outcome of patients with acute respiratory distress syndrome and pulmonary hypertension, future experiments need to be directed at determining the factors that recruit and activate inflammatory cells in the lung and vessel wall so as to ultimately design specific therapies to turn the process off.

Future Prospects

Based on the findings of this study, several questions are raised and further experiments can be done that will enrich our knowledge on macrophage activation and on the pathogenesis of ARDS and PH.

First, in the present study we don't shown how Akt2 deficiency regulates miRNA levels such as miR-155 and miR-146a. Akt2 signals in the cell via phosphorylation of specific proteins, thus miRNA regulation is probably an indirect effect. Also, we did not explain in the current study how HO-1/CO upregulation in epithelial cells suppresses M2 polarization. It maybe via CO regulation of gene expression of via an anti-inflammatory and antioxidant function of HO-1 in general. Further experiments will clarify these questions and will increase our understanding on macrophage activation signaling pathways.

In case of ARDS, it will be interesting to test macrophage activation phenotype in other animal models such as hyperoxia induced lung injury. Also further experiments are required to identify the optimal delivery system in the lung for miRNAs and siRNAS.

In case of PAH, the presence of M2 macrophages need to be verified in other models of PH – independent of hypoxia to clarify whether M2 activation is a unique characteristic of hypoxic tissueor or it is a common mechanism in other forms of PAH as well. Next, further research is required in PAH to identify molecules that can block M2 activation and Fizz1 excretion in vivo and to test the effectiveness of these molecules on the outcome of experimental PH.

REFERENCES

References

1. Robbins SL, Kumar V. Robbins and cotran pathologic basis of disease. Philadelphia, PA: Saunders/Elsevier; 2010.
2. Wheeler DS, Wong HR, Shanley TP. The respiratory tract in pediatric critical illness and injury. London: Springer; 2009.
3. Fishman AP, Elias JA. Fishman's pulmonary diseases and disorders. New York: McGraw-Hill, Medical Pub. Division; 2008.
4. West JB. Respiratory physiology--the essentials. Baltimore: Williams & Wilkins; 1995.
5. West JB. Pulmonary pathophysiology : The essentials. Baltimore: Williams & Wilkins; 1998.
6. Murray JF, Mason RJ. Murray and nadel's textbook of respiratory medicine. Philadelphia: Saunders/Elsevier; 2010.
7. Herold S, Mayer K, Lohmeyer J. Acute lung injury: How macrophages orchestrate resolution of inflammation and tissue repair. *Front Immunol* 2011;2:65.
8. Harris RS. Pressure-volume curves of the respiratory system. *Respir Care* 2005;50:78-98; discussion 98-79.
9. Beghetti M, Berger RM. The challenges in paediatric pulmonary arterial hypertension. *Eur Respir Rev* 2014;23:498-504.
10. Rabinovitch M. Molecular pathogenesis of pulmonary arterial hypertension. *J Clin Invest* 2012;122:4306-4313.
11. Bals R, Hiemstra PS. Innate immunity in the lung: How epithelial cells fight against respiratory pathogens. *Eur Respir J* 2004;23:327-333.
12. Chen K, Kolls JK. T cell-mediated host immune defenses in the lung. *Annu Rev Immunol* 2013;31:605-633.
13. Lee YG, Lee J, Byeon SE, Yoo DS, Kim MH, Lee SY, Cho JY. Functional role of akt in macrophage-mediated innate immunity. *Front Biosci (Landmark Ed)* 2011;16:517-530.
14. Thepen T, Kraal G, Holt PG. The role of alveolar macrophages in regulation of lung inflammation. *Ann N Y Acad Sci* 1994;725:200-206.
15. von Garnier C, Nicod LP. Immunology taught by lung dendritic cells. *Swiss Med Wkly* 2009;139:186-192.
16. Hammad H, Lambrecht BN. Dendritic cells and airway epithelial cells at the interface between innate and adaptive immune responses. *Allergy* 2011;66:579-587.
17. Misharin AV, Morales-Nebreda L, Mutlu GM, Budinger GR, Perlman H. Flow cytometric analysis of macrophages and dendritic cell subsets in the mouse lung. *Am J Respir Cell Mol Biol* 2013;49:503-510.
18. Guilliams M, Lambrecht BN, Hammad H. Division of labor between lung dendritic cells and macrophages in the defense against pulmonary infections. *Mucosal Immunol* 2013;6:464-473.
19. Sozzani S, Vermi W, Del Prete A, Facchetti F. Trafficking properties of plasmacytoid dendritic cells in health and disease. *Trends Immunol* 2010;31:270-277.
20. Erjefalt JS. Mast cells in human airways: The culprit? *Eur Respir Rev* 2014;23:299-307.
21. Paul WE. Fundamental immunology. Philadelphia: Wolters Kluwer Health/Lippincott Williams & Wilkins; 2013.

22. Zaynagetdinov R, Sherrill TP, Kendall PL, Segal BH, Weller KP, Tighe RM, Blackwell TS. Identification of myeloid cell subsets in murine lungs using flow cytometry. *Am J Respir Cell Mol Biol* 2013;49:180-189.
23. Mestas J, Hughes CC. Of mice and not men: Differences between mouse and human immunology. *J Immunol* 2004;172:2731-2738.
24. Condon TV, Sawyer RT, Fenton MJ, Riches DW. Lung dendritic cells at the innate-adaptive immune interface. *J Leukoc Biol* 2011;90:883-895.
25. Hajishengallis G, Lambris JD. Microbial manipulation of receptor crosstalk in innate immunity. *Nat Rev Immunol* 2011;11:187-200.
26. Takeuchi O, Akira S. Pattern recognition receptors and inflammation. *Cell* 2010;140:805-820.
27. Foster SL, Medzhitov R. Gene-specific control of the tlr-induced inflammatory response. *Clin Immunol* 2009;130:7-15.
28. Kobayashi KS, Flavell RA. Shielding the double-edged sword: Negative regulation of the innate immune system. *J Leukoc Biol* 2004;75:428-433.
29. Quinn SR, O'Neill LA. A trio of microrna that control toll-like receptor signalling. *Int Immunol* 2011;23:421-425.
30. Kondo T, Kawai T, Akira S. Dissecting negative regulation of toll-like receptor signaling. *Trends Immunol* 2012;33:449-458.
31. Lawrence T, Natoli G. Transcriptional regulation of macrophage polarization: Enabling diversity with identity. *Nat Rev Immunol* 2011;11:750-761.
32. Sheedy FJ, Palsson-McDermott E, Hennessy EJ, Martin C, O'Leary JJ, Ruan Q, Johnson DS, Chen Y, O'Neill LA. Negative regulation of tlr4 via targeting of the proinflammatory tumor suppressor pdcd4 by the microrna mir-21. *Nat Immunol* 2010;11:141-147.
33. Alber A, Howie SE, Wallace WA, Hirani N. The role of macrophages in healing the wounded lung. *Int J Exp Pathol* 2012;93:243-251.
34. Chen CJ, Kono H, Golenbock D, Reed G, Akira S, Rock KL. Identification of a key pathway required for the sterile inflammatory response triggered by dying cells. *Nature medicine* 2007;13:851-856.
35. Nathan C. Metchnikoff's legacy in 2008. *Nature immunology* 2008;9:695-698.
36. Hashimoto D, Chow A, Noizat C, Teo P, Beasley MB, Leboeuf M, Becker CD, See P, Price J, Lucas D, Greter M, Mortha A, Boyer SW, Forsberg EC, Tanaka M, van Rooijen N, Garcia-Sastre A, Stanley ER, Ginhoux F, Frenette PS, Merad M. Tissue-resident macrophages self-maintain locally throughout adult life with minimal contribution from circulating monocytes. *Immunity* 2013;38:792-804.
37. Hussell T, Bell TJ. Alveolar macrophages: Plasticity in a tissue-specific context. *Nat Rev Immunol* 2014;14:81-93.
38. Westphalen K, Gusarova GA, Islam MN, Subramanian M, Cohen TS, Prince AS, Bhattacharya J. Sessile alveolar macrophages communicate with alveolar epithelium to modulate immunity. *Nature* 2014;506:503-506.
39. Mosser DM, Edwards JP. Exploring the full spectrum of macrophage activation. *Nat Rev Immunol* 2008;8:958-969.
40. Mosser DM, Edwards JP. Exploring the full spectrum of macrophage activation. *Nature reviews* 2008;8:958-969.
41. Edwards JP, Zhang X, Frauwirth KA, Mosser DM. Biochemical and functional characterization of three activated macrophage populations. *Journal of leukocyte biology* 2006;80:1298-1307.

42. Lovren F, Pan Y, Quan A, Szmitko PE, Singh KK, Shukla PC, Gupta M, Chan L, Al-Omran M, Teoh H, Verma S. Adiponectin primes human monocytes into alternative anti-inflammatory m2 macrophages. *Am J Physiol Heart Circ Physiol* 2010;299:H656-663.
43. Haschemi A, Kosma P, Gille L, Evans CR, Burant CF, Starkl P, Knapp B, Haas R, Schmid JA, Jandl C, Amir S, Lubec G, Park J, Esterbauer H, Bilban M, Brizuela L, Pospisilik JA, Otterbein LE, Wagner O. The sedoheptulose kinase carkl directs macrophage polarization through control of glucose metabolism. *Cell Metab* 2012;15:813-826.
44. Gordon S. Alternative activation of macrophages. *Nature reviews* 2003;3:23-35.
45. Johnston LK, Rims CR, Gill SE, McGuire JK, Manicone AM. Pulmonary macrophage subpopulations in the induction and resolution of acute lung injury. *Am J Respir Cell Mol Biol* 2012;47:417-426.
46. Gea-Sorli S, Guillamat R, Serrano-Mollar A, Closa D. Activation of lung macrophage subpopulations in experimental acute pancreatitis. *J Pathol* 2011;223:417-424.
47. Ionescu L, Byrne RN, van Haaften T, Vadivel A, Alphonse RS, Rey-Parra GJ, Weissmann G, Hall A, Eaton F, Thebaud B. Stem cell conditioned medium improves acute lung injury in mice: In vivo evidence for stem cell paracrine action. *Am J Physiol Lung Cell Mol Physiol* 2012;303:L967-977.
48. Gordon S, Martinez FO. Alternative activation of macrophages: Mechanism and functions. *Immunity* 2010;32:593-604.
49. Arranz A, Doxaki C, Vergadi E, Martinez de la Torre Y, Vaporidi K, Lagoudaki ED, Ieronymaki E, Androulidaki A, Venihaki M, Margioris AN, Stathopoulos EN, Tsichlis PN, Tsatsanis C. Akt1 and akt2 protein kinases differentially contribute to macrophage polarization. *Proc Natl Acad Sci U S A* 2012;109:9517-9522.
50. Boorsma CE, Draijer C, Melgert BN. Macrophage heterogeneity in respiratory diseases. *Mediators Inflamm* 2013;2013:769214.
51. Mantovani A, Sica A, Sozzani S, Allavena P, Vecchi A, Locati M. The chemokine system in diverse forms of macrophage activation and polarization. *Trends in immunology* 2004;25:677-686.
52. Murray PJ, Allen JE, Biswas SK, Fisher EA, Gilroy DW, Goerdt S, Gordon S, Hamilton JA, Ivashkiv LB, Lawrence T, Locati M, Mantovani A, Martinez FO, Mege JL, Mosser DM, Natoli G, Saeij JP, Schultze JL, Shirey KA, Sica A, Suttles J, Udalova I, van Ginderachter JA, Vogel SN, Wynn TA. Macrophage activation and polarization: Nomenclature and experimental guidelines. *Immunity* 2014;41:14-20.
53. Fairweather D, Cihakova D. Alternatively activated macrophages in infection and autoimmunity. *Journal of autoimmunity* 2009;33:222-230.
54. Kurowska-Stolarska M, Stolarski B, Kewin P, Murphy G, Corrigan CJ, Ying S, Pitman N, Mirchandani A, Rana B, van Rooijen N, Shepherd M, McSharry C, McInnes IB, Xu D, Liew FY. Il-33 amplifies the polarization of alternatively activated macrophages that contribute to airway inflammation. *J Immunol* 2009;183:6469-6477.
55. Lucas M, Zhang X, Prasanna V, Mosser DM. Erk activation following macrophage fcgammar ligation leads to chromatin modifications at the il-10 locus. *J Immunol* 2005;175:469-477.
56. Martinez FO, Sica A, Mantovani A, Locati M. Macrophage activation and polarization. *Front Biosci* 2008;13:453-461.
57. Biswas SK, Lopez-Collazo E. Endotoxin tolerance: New mechanisms, molecules and clinical significance. *Trends Immunol* 2009;30:475-487.

58. del Fresno C, Garcia-Rio F, Gomez-Pina V, Soares-Schanoski A, Fernandez-Ruiz I, Jurado T, Kajiji T, Shu C, Marin E, Gutierrez del Arroyo A, Prados C, Arnalich F, Fuentes-Prior P, Biswas SK, Lopez-Collazo E. Potent phagocytic activity with impaired antigen presentation identifying lipopolysaccharide-tolerant human monocytes: Demonstration in isolated monocytes from cystic fibrosis patients. *J Immunol* 2009;182:6494-6507.
59. Pena OM, Pistolic J, Raj D, Fjell CD, Hancock RE. Endotoxin tolerance represents a distinctive state of alternative polarization (m2) in human mononuclear cells. *J Immunol* 2011;186:7243-7254.
60. Murray PJ, Wynn TA. Protective and pathogenic functions of macrophage subsets. *Nat Rev Immunol* 2011;11:723-737.
61. de las Casas-Engel M, Dominguez-Soto A, Sierra-Filardi E, Bragado R, Nieto C, Puig-Kroger A, Samaniego R, Loza M, Corcuera MT, Gomez-Aguado F, Bustos M, Sanchez-Mateos P, Corbi AL. Serotonin skews human macrophage polarization through htr2b and htr7. *J Immunol* 2013;190:2301-2310.
62. Martinez FO, Helming L, Gordon S. Alternative activation of macrophages: An immunologic functional perspective. *Annu Rev Immunol* 2009;27:451-483.
63. Martinez FO. Regulators of macrophage activation. *Eur J Immunol* 2011;41:1531-1534.
64. Whyte CS, Bishop ET, Ruckerl D, Gaspar-Pereira S, Barker RN, Allen JE, Rees AJ, Wilson HM. Suppressor of cytokine signaling (socs)1 is a key determinant of differential macrophage activation and function. *J Leukoc Biol* 2011;90:845-854.
65. Guiducci C, Ghirelli C, Marloie-Provost MA, Matray T, Coffman RL, Liu YJ, Barrat FJ, Soumelis V. Pi3k is critical for the nuclear translocation of irf-7 and type i ifn production by human plasmacytoid predendritic cells in response to tlr activation. *The Journal of experimental medicine* 2008;205:315-322.
66. Honda K, Taniguchi T. Irfs: Master regulators of signalling by toll-like receptors and cytosolic pattern-recognition receptors. *Nat Rev Immunol* 2006;6:644-658.
67. Spence S, Fitzsimons A, Boyd CR, Kessler J, Fitzgerald D, Elliott J, Gabhann JN, Smith S, Sica A, Hams E, Saunders SP, Jefferies CA, Fallon PG, McAuley DF, Kissenpfennig A, Johnston JA. Suppressors of cytokine signaling 2 and 3 diametrically control macrophage polarization. *Immunity* 2013;38:66-78.
68. Androulidaki A, Iliopoulos D, Arranz A, Doxaki C, Schworer S, Zacharioudaki V, Margioris AN, Tsichlis PN, Tsatsanis C. The kinase akt1 controls macrophage response to lipopolysaccharide by regulating microrna s. *Immunity* 2009;31:220-231.
69. Porta C, Rimoldi M, Raes G, Brys L, Ghezzi P, Di Liberto D, Dieli F, Ghisletti S, Natoli G, De Baetselier P, Mantovani A, Sica A. Tolerance and m2 (alternative) macrophage polarization are related processes orchestrated by p50 nuclear factor kappab. *Proc Natl Acad Sci U S A* 2009;106:14978-14983.
70. Satoh T, Takeuchi O, Vandenbon A, Yasuda K, Tanaka Y, Kumagai Y, Miyake T, Matsushita K, Okazaki T, Saitoh T, Honma K, Matsuyama T, Yui K, Tsujimura T, Standley DM, Nakanishi K, Nakai K, Akira S. The jmjd3-irf4 axis regulates m2 macrophage polarization and host responses against helminth infection. *Nature immunology*.
71. Odegaard JI, Ricardo-Gonzalez RR, Goforth MH, Morel CR, Subramanian V, Mukundan L, Red Eagle A, Vats D, Brombacher F, Ferrante AW, Chawla A. Macrophage-specific ppargamma controls alternative activation and improves insulin resistance. *Nature* 2007;447:1116-1120.

72. Ruffell D, Mourkioti F, Gambardella A, Kirstetter P, Lopez RG, Rosenthal N, Nerlov C. A creb-c/ebpbeta cascade induces m2 macrophage-specific gene expression and promotes muscle injury repair. *Proc Natl Acad Sci U S A* 2009;106:17475-17480.
73. Liu YC, Zou XB, Chai YF, Yao YM. Macrophage polarization in inflammatory diseases. *Int J Biol Sci* 2014;10:520-529.
74. MacKinnon AC, Farnworth SL, Hodkinson PS, Henderson NC, Atkinson KM, Leffler H, Nilsson UJ, Haslett C, Forbes SJ, Sethi T. Regulation of alternative macrophage activation by galectin-3. *J Immunol* 2008;180:2650-2658.
75. Fong CH, Bebien M, Didierlaurent A, Nebauer R, Hussell T, Broide D, Karin M, Lawrence T. An antiinflammatory role for ikkbeta through the inhibition of "classical" macrophage activation. *J Exp Med* 2008;205:1269-1276.
76. Satoh T, Takeuchi O, Vandenbon A, Yasuda K, Tanaka Y, Kumagai Y, Miyake T, Matsushita K, Okazaki T, Saitoh T, Honma K, Matsuyama T, Yui K, Tsujimura T, Standley DM, Nakanishi K, Nakai K, Akira S. The jmjd3-irf4 axis regulates m2 macrophage polarization and host responses against helminth infection. *Nat Immunol* 2010;11:936-944.
77. Negishi H, Ohba Y, Yanai H, Takaoka A, Honma K, Yui K, Matsuyama T, Taniguchi T, Honda K. Negative regulation of toll-like-receptor signaling by irf-4. *Proc Natl Acad Sci U S A* 2005;102:15989-15994.
78. Fukao T, Koyasu S. Pi3k and negative regulation of tlr signaling. *Trends Immunol* 2003;24:358-363.
79. Franke TF, Yang SI, Chan TO, Datta K, Kazlauskas A, Morrison DK, Kaplan DR, Tsichlis PN. The protein kinase encoded by the akt proto-oncogene is a target of the pdgf-activated phosphatidylinositol 3-kinase. *Cell* 1995;81:727-736.
80. Iliopoulos D, Polytarchou C, Hatziapostolou M, Kottakis F, Maroulakou IG, Struhl K, Tsichlis PN. Microrna differentially regulated by akt isoforms control emt and stem cell renewal in cancer cells. *Sci Signal* 2009;2:ra62.
81. Peng XD, Xu PZ, Chen ML, Hahn-Windgassen A, Skeen J, Jacobs J, Sundararajan D, Chen WS, Crawford SE, Coleman KG, Hay N. Dwarfism, impaired skin development, skeletal muscle atrophy, delayed bone development, and impeded adipogenesis in mice lacking akt1 and akt2. *Genes Dev* 2003;17:1352-1365.
82. Cho H, Mu J, Kim JK, Thorvaldsen JL, Chu Q, Crenshaw EB, 3rd, Kaestner KH, Bartolomei MS, Shulman GI, Birnbaum MJ. Insulin resistance and a diabetes mellitus-like syndrome in mice lacking the protein kinase akt2 (pkb beta). *Science* 2001;292:1728-1731.
83. Tschopp O, Yang ZZ, Brodbeck D, Dummler BA, Hemmings-Mieszczak M, Watanabe T, Michaelis T, Frahm J, Hemmings BA. Essential role of protein kinase b gamma (pkb gamma/akt3) in postnatal brain development but not in glucose homeostasis. *Development* 2005;132:2943-2954.
84. Gonzalez E, McGraw TE. The akt kinases: Isoform specificity in metabolism and cancer. *Cell Cycle* 2009;8:2502-2508.
85. Staal SP. Molecular cloning of the akt oncogene and its human homologues akt1 and akt2: Amplification of akt1 in a primary human gastric adenocarcinoma. *Proc Natl Acad Sci U S A* 1987;84:5034-5037.
86. Cheng JQ, Godwin AK, Bellacosa A, Taguchi T, Franke TF, Hamilton TC, Tsichlis PN, Testa JR. Akt2, a putative oncogene encoding a member of a subfamily of protein-serine/threonine kinases, is amplified in human ovarian carcinomas. *Proc Natl Acad Sci U S A* 1992;89:9267-9271.

87. Pearl LH, Barford D. Regulation of protein kinases in insulin, growth factor and wnt signalling. *Curr Opin Struct Biol* 2002;12:761-767.
88. Sale EM, Sale GJ. Protein kinase b: Signalling roles and therapeutic targeting. *Cell Mol Life Sci* 2008;65:113-127.
89. Song G, Ouyang G, Bao S. The activation of akt/pkb signaling pathway and cell survival. *J Cell Mol Med* 2005;9:59-71.
90. Mitsuuchi Y, Johnson SW, Moonblatt S, Testa JR. Translocation and activation of akt2 in response to stimulation by insulin. *J Cell Biochem* 1998;70:433-441.
91. Naiki T, Saijou E, Miyaoka Y, Sekine K, Miyajima A. Trb2, a mouse tribbles ortholog, suppresses adipocyte differentiation by inhibiting akt and c/ebpbeta. *J Biol Chem* 2007;282:24075-24082.
92. Sasaoka T, Wada T, Fukui K, Murakami S, Ishihara H, Suzuki R, Tobe K, Kadowaki T, Kobayashi M. Sh2-containing inositol phosphatase 2 predominantly regulates akt2, and not akt1, phosphorylation at the plasma membrane in response to insulin in 3t3-l1 adipocytes. *J Biol Chem* 2004;279:14835-14843.
93. Ono H, Katagiri H, Funaki M, Anai M, Inukai K, Fukushima Y, Sakoda H, Ogihara T, Onishi Y, Fujishiro M, Kikuchi M, Oka Y, Asano T. Regulation of phosphoinositide metabolism, akt phosphorylation, and glucose transport by pten (phosphatase and tensin homolog deleted on chromosome 10) in 3t3-l1 adipocytes. *Mol Endocrinol* 2001;15:1411-1422.
94. Marone R, Cmiljanovic V, Giese B, Wymann MP. Targeting phosphoinositide 3-kinase: Moving towards therapy. *Biochim Biophys Acta* 2008;1784:159-185.
95. Lee YG, Lee J, Byeon SE, Yoo DS, Kim MH, Lee SY, Cho JY. Functional role of akt in macrophage-mediated innate immunity. *Front Biosci* 2011;16:517-530.
96. Fukao T, Koyasu S. Pi3k and negative regulation of tlr signaling. *Trends Immunol.* 2003;24:358-363.
97. Kuijl C, Savage ND, Marsman M, Tuin AW, Janssen L, Egan DA, Ketema M, van den Nieuwendijk R, van den Eeden SJ, Geluk A, Poot A, van der Marel G, Beijersbergen RL, Overkleeft H, Ottenhoff TH, Neefjes J. Intracellular bacterial growth is controlled by a kinase network around pkb/akt1. *Nature* 2007;450:725-730.
98. Ruckerl D, Jenkins SJ, Laqtom NN, Gallagher IJ, Sutherland TE, Duncan S, Buck AH, Allen JE. Induction of il-4ralpha-dependent micrornas identifies pi3k/akt signaling as essential for il-4-driven murine macrophage proliferation in vivo. *Blood* 2012;120:2307-2316.
99. O'Connell RM, Chaudhuri AA, Rao DS, Baltimore D. Inositol phosphatase ship1 is a primary target of mir-155. *Proc Natl Acad Sci U S A* 2009.
100. He M, Xu Z, Ding T, Kuang DM, Zheng L. Microrna-155 regulates inflammatory cytokine production in tumor-associated macrophages via targeting c/ebpbeta. *Cellular & molecular immunology* 2009;6:343-352.
101. Alexander WS, Starr R, Fenner JE, Scott CL, Handman E, Sprigg NS, Corbin JE, Cornish AL, Darwiche R, Owczarek CM, Kay TW, Nicola NA, Hertzog PJ, Metcalf D, Hilton DJ. Socs1 is a critical inhibitor of interferon gamma signaling and prevents the potentially fatal neonatal actions of this cytokine. *Cell* 1999;98:597-608.
102. Rauh MJ, Ho V, Pereira C, Sham A, Sly LM, Lam V, Huxham L, Minchinton AI, Mui A, Krystal G. Ship represses the generation of alternatively activated macrophages. *Immunity* 2005;23:361-374.
103. El Kasmi KC, Qualls JE, Pesce JT, Smith AM, Thompson RW, Henao-Tamayo M, Basaraba RJ, Konig T, Schleicher U, Koo MS, Kaplan G, Fitzgerald KA, Tuomanen EI, Orme IM, Kanneganti TD, Bogdan C, Wynn TA, Murray PJ. Toll-like receptor-induced arginase 1 in

macrophages thwarts effective immunity against intracellular pathogens. *Nature immunology* 2008;9:1399-1406.
104. Gray MJ, Poljakovic M, Kepka-Lenhart D, Morris SM, Jr. Induction of arginase i transcription by il-4 requires a composite DNA response element for stat6 and c/ebpbeta. *Gene* 2005;353:98-106.
105. Bartel DP. Micrornas: Genomics, biogenesis, mechanism, and function. *Cell* 2004;116:281-297.
106. Luers AJ, Loudig OD, Berman JW. Micrornas are expressed and processed by human primary macrophages. *Cell Immunol* 2010;263:1-8.
107. Martinez-Nunez RT, Louafi F, Sanchez-Elsner T. The interleukin 13 (il-13) pathway in human macrophages is modulated by microrna-155 via direct targeting of interleukin 13 receptor alpha1 (il13ralpha1). *J Biol Chem* 2011;286:1786-1794.
108. Bala S, Marcos M, Kodys K, Csak T, Catalano D, Mandrekar P, Szabo G. Up-regulation of microrna-155 in macrophages contributes to increased tumor necrosis factor {alpha} (tnf{alpha}) production via increased mrna half-life in alcoholic liver disease. *J Biol Chem* 2011;286:1436-1444.
109. Cai X, Yin Y, Li N, Zhu D, Zhang J, Zhang CY, Zen K. Re-polarization of tumor-associated macrophages to pro-inflammatory m1 macrophages by microrna-155. *J Mol Cell Biol* 2012;4:341-343.
110. McCoy CE, Sheedy FJ, Qualls JE, Doyle SL, Quinn SR, Murray PJ, O'Neill LA. Il-10 inhibits mir-155 induction by toll-like receptors. *J Biol Chem* 2010;285:20492-20498.
111. Guo Z, Wen Z, Qin A, Zhou Y, Liao Z, Liu Z, Liang Y, Ren T, Xu L. Antisense oligonucleotide treatment enhances the recovery of acute lung injury through il-10-secreting m2-like macrophage-induced expansion of cd4+ regulatory t cells. *J Immunol* 2013;190:4337-4348.
112. Graff JW, Dickson AM, Clay G, McCaffrey AP, Wilson ME. Identifying functional micrornas in macrophages with polarized phenotypes. *J Biol Chem* 2012;287:21816-21825.
113. Squadrito ML, Etzrodt M, De Palma M, Pittet MJ. Microrna-mediated control of macrophages and its implications for cancer. *Trends Immunol* 2013;34:350-359.
114. Squadrito ML, Pucci F, Magri L, Moi D, Gilfillan GD, Ranghetti A, Casazza A, Mazzone M, Lyle R, Naldini L, De Palma M. Mir-511-3p modulates genetic programs of tumor-associated macrophages. *Cell Rep* 2012;1:141-154.
115. Chaudhuri AA, So AY, Sinha N, Gibson WS, Taganov KD, O'Connell RM, Baltimore D. Microrna-125b potentiates macrophage activation. *J Immunol* 2011;187:5062-5068.
116. So AY, Sookram R, Chaudhuri AA, Minisandram A, Cheng D, Xie C, Lim EL, Flores YG, Jiang S, Kim JT, Keown C, Ramakrishnan P, Baltimore D. Dual mechanisms by which mir-125b represses irf4 to induce myeloid and b-cell leukemias. *Blood* 2014;124:1502-1512.
117. Boldin MP, Taganov KD, Rao DS, Yang L, Zhao JL, Kalwani M, Garcia-Flores Y, Luong M, Devrekanli A, Xu J, Sun G, Tay J, Linsley PS, Baltimore D. Mir-146a is a significant brake on autoimmunity, myeloproliferation, and cancer in mice. *J Exp Med* 2011;208:1189-1201.
118. Zhao JL, Rao DS, Boldin MP, Taganov KD, O'Connell RM, Baltimore D. Nf-kappab dysregulation in microrna-146a-deficient mice drives the development of myeloid malignancies. *Proc Natl Acad Sci U S A* 2011;108:9184-9189.
119. Lu LF, Boldin MP, Chaudhry A, Lin LL, Taganov KD, Hanada T, Yoshimura A, Baltimore D, Rudensky AY. Function of mir-146a in controlling treg cell-mediated regulation of th1 responses. *Cell* 2010;142:914-929.

120. Nahid MA, Pauley KM, Satoh M, Chan EK. Mir-146a is critical for endotoxin-induced tolerance: Implication in innate immunity. *J Biol Chem* 2009;284:34590-34599.
121. Veremeyko T, Siddiqui S, Sotnikov I, Yung A, Ponomarev ED. Il-4/il-13-dependent and independent expression of mir-124 and its contribution to m2 phenotype of monocytic cells in normal conditions and during allergic inflammation. *PLoS One* 2013;8:e81774.
122. Zhuang G, Meng C, Guo X, Cheruku PS, Shi L, Xu H, Li H, Wang G, Evans AR, Safe S, Wu C, Zhou B. A novel regulator of macrophage activation: Mir-223 in obesity-associated adipose tissue inflammation. *Circulation* 2012;125:2892-2903.
123. Shaykhiev R, Krause A, Salit J, Strulovici-Barel Y, Harvey BG, O'Connor TP, Crystal RG. Smoking-dependent reprogramming of alveolar macrophage polarization: Implication for pathogenesis of chronic obstructive pulmonary disease. *J Immunol* 2009;183:2867-2883.
124. Varin A, Mukhopadhyay S, Herbein G, Gordon S. Alternative activation of macrophages by il-4 impairs phagocytosis of pathogens but potentiates microbial-induced signalling and cytokine secretion. *Blood* 2010;115:353-362.
125. Lewis C, Murdoch C. Macrophage responses to hypoxia: Implications for tumor progression and anti-cancer therapies. *The American journal of pathology* 2005;167:627-635.
126. Murdoch C, Lewis CE. Macrophage migration and gene expression in response to tumor hypoxia. *International journal of cancer* 2005;117:701-708.
127. Hunter MM, Wang A, Parhar KS, Johnston MJ, Van Rooijen N, Beck PL, McKay DM. In vitro-derived alternatively activated macrophages reduce colonic inflammation in mice. *Gastroenterology* 2010;138:1395-1405.
128. Weisser SB, Brugger HK, Voglmaier NS, McLarren KW, van Rooijen N, Sly LM. Ship-deficient, alternatively activated macrophages protect mice during dss-induced colitis. *J Leukoc Biol* 2011;90:483-492.
129. Porta C, Rimoldi M, Raes G, Brys L, Ghezzi P, Di Liberto D, Dieli F, Ghisletti S, Natoli G, De Baetselier P, Mantovani A, Sica A. Tolerance and m2 (alternative) macrophage polarization are related processes orchestrated by p50 nuclear factor kappab. *Proceedings of the National Academy of Sciences of the United States of America* 2009;106:14978-14983.
130. Ranieri VM, Rubenfeld GD, Thompson BT, Ferguson ND, Caldwell E, Fan E, Camporota L, Slutsky AS. Acute respiratory distress syndrome: The berlin definition. *Jama* 2012;307:2526-2533.
131. Matute-Bello G, Downey G, Moore BB, Groshong SD, Matthay MA, Slutsky AS, Kuebler WM. An official american thoracic society workshop report: Features and measurements of experimental acute lung injury in animals. *Am J Respir Cell Mol Biol* 2011;44:725-738.
132. Hernu R, Wallet F, Thiolliere F, Martin O, Richard JC, Schmitt Z, Wallon G, Delannoy B, Rimmele T, Demaret C, Magnin C, Vallin H, Lepape A, Baboi L, Argaud L, Piriou V, Allaouchiche B, Aubrun F, Bastien O, Lehot JJ, Ayzac L, Guerin C. An attempt to validate the modification of the american-european consensus definition of acute lung injury/acute respiratory distress syndrome by the berlin definition in a university hospital. *Intensive Care Med* 2013;39:2161-2170.
133. Matute-Bello G, Frevert CW, Martin TR. Animal models of acute lung injury. *Am J Physiol Lung Cell Mol Physiol* 2008;295:L379-399.
134. Vlahakis NE, Hubmayr RD. Cellular stress failure in ventilator-injured lungs. *Am J Respir Crit Care Med* 2005;171:1328-1342.

135. Herold S, Gabrielli NM, Vadasz I. Novel concepts of acute lung injury and alveolar-capillary barrier dysfunction. *Am J Physiol Lung Cell Mol Physiol* 2013;305:L665-681.
136. Ware LB, Matthay MA. The acute respiratory distress syndrome. *N Engl J Med* 2000;342:1334-1349.
137. Matthay MA. Resolution of pulmonary edema. Thirty years of progress. *Am J Respir Crit Care Med* 2014;189:1301-1308.
138. Smith LS, Zimmerman JJ, Martin TR. Mechanisms of acute respiratory distress syndrome in children and adults: A review and suggestions for future research. *Pediatr Crit Care Med* 2013;14:631-643.
139. Ventilation with lower tidal volumes as compared with traditional tidal volumes for acute lung injury and the acute respiratory distress syndrome. The acute respiratory distress syndrome network. *N Engl J Med* 2000;342:1301-1308.
140. dos Santos CC, Slutsky AS. Protective ventilation of patients with acute respiratory distress syndrome. *Crit Care* 2004;8:145-147.
141. Gomella TL, Cunningham MD, Eyal FG. Neonatology : Management, procedures, on-call problems, diseases, and drugs. New York: McGraw-Hill Medical; 2009.
142. Vlahakis NE, Hubmayr RD. Response of alveolar cells to mechanical stress. *Curr Opin Crit Care* 2003;9:2-8.
143. Wakabayashi K, Wilson MR, Tatham KC, O'Dea KP, Takata M. Volutrauma, but not atelectrauma, induces systemic cytokine production by lung-marginated monocytes. *Crit Care Med* 2014;42:e49-57.
144. Vlahakis NE, Schroeder MA, Limper AH, Hubmayr RD. Stretch induces cytokine release by alveolar epithelial cells in vitro. *Am J Physiol* 1999;277:L167-173.
145. Uhlig S, Ranieri M, Slutsky AS. Biotrauma hypothesis of ventilator-induced lung injury. *Am J Respir Crit Care Med* 2004;169:314-315; author reply 315.
146. Taylor KR, Trowbridge JM, Rudisill JA, Termeer CC, Simon JC, Gallo RL. Hyaluronan fragments stimulate endothelial recognition of injury through tlr4. *J Biol Chem* 2004;279:17079-17084.
147. Vanderbilt JN, Mager EM, Allen L, Sawa T, Wiener-Kronish J, Gonzalez R, Dobbs LG. Cxc chemokines and their receptors are expressed in type ii cells and upregulated following lung injury. *Am J Respir Cell Mol Biol* 2003;29:661-668.
148. Wilson MR, Choudhury S, Goddard ME, O'Dea KP, Nicholson AG, Takata M. High tidal volume upregulates intrapulmonary cytokines in an in vivo mouse model of ventilator-induced lung injury. *J Appl Physiol (1985)* 2003;95:1385-1393.
149. Lionetti V, Recchia FA, Ranieri VM. Overview of ventilator-induced lung injury mechanisms. *Curr Opin Crit Care* 2005;11:82-86.
150. Imai Y, Parodo J, Kajikawa O, de Perrot M, Fischer S, Edwards V, Cutz E, Liu M, Keshavjee S, Martin TR, Marshall JC, Ranieri VM, Slutsky AS. Injurious mechanical ventilation and end-organ epithelial cell apoptosis and organ dysfunction in an experimental model of acute respiratory distress syndrome. *Jama* 2003;289:2104-2112.
151. Tremblay LN, Slutsky AS. Ventilator-induced lung injury: From the bench to the bedside. *Intensive Care Med* 2006;32:24-33.
152. Santschi M, Randolph AG, Rimensberger PC, Jouvet P. Mechanical ventilation strategies in children with acute lung injury: A survey on stated practice pattern*. *Pediatr Crit Care Med* 2013;14:e332-337.
153. Saddy F, Sutherasan Y, Rocco PR, Pelosi P. Ventilator-associated lung injury during assisted mechanical ventilation. *Semin Respir Crit Care Med* 2014;35:409-417.

154. Vaporidi K, Voloudakis G, Priniannakis G, Kondili E, Koutsopoulos A, Tsatsanis C, Georgopoulos D. Effects of respiratory rate on ventilator-induced lung injury at a constant paco2 in a mouse model of normal lung. *Crit Care Med* 2008;36:1277-1283.
155. Halbertsma FJ, Vaneker M, Pickkers P, Snijdelaar DG, van Egmond J, Scheffer GJ, van der Hoeven HG. Hypercapnic acidosis attenuates the pulmonary innate immune response in ventilated healthy mice. *Crit Care Med* 2008;36:2403-2406.
156. Brochard LJ. Tidal volume during acute lung injury: Let the patient choose? *Intensive Care Med* 2009;35:1830-1832.
157. Contreras M, Masterson C, Laffey JG. Permissive hypercapnia: What to remember. *Curr Opin Anaesthesiol* 2014.
158. Lang JD, Figueroa M, Sanders KD, Aslan M, Liu Y, Chumley P, Freeman BA. Hypercapnia via reduced rate and tidal volume contributes to lipopolysaccharide-induced lung injury. *Am J Respir Crit Care Med* 2005;171:147-157.
159. Liu Y, Chacko BK, Ricksecker A, Shingarev R, Andrews E, Patel RP, Lang JD, Jr. Modulatory effects of hypercapnia on in vitro and in vivo pulmonary endothelial-neutrophil adhesive responses during inflammation. *Cytokine* 2008;44:108-117.
160. Ortiz-Diaz E, Festic E, Gajic O, Levitt JE. Emerging pharmacological therapies for prevention and early treatment of acute lung injury. *Semin Respir Crit Care Med* 2013;34:448-458.
161. Uhlig C, Silva PL, Ornellas D, Santos RS, Miranda PJ, Spieth PM, Kiss T, Kasper M, Wiedemann B, Koch T, Morales MM, Pelosi P, de Abreu MG, Rocco PR. The effects of salbutamol on epithelial ion channels depend on the etiology of acute respiratory distress syndrome but not the route of administration. *Respir Res* 2014;15:56.
162. Meduri GU, Headley AS, Golden E, Carson SJ, Umberger RA, Kelso T, Tolley EA. Effect of prolonged methylprednisolone therapy in unresolving acute respiratory distress syndrome: A randomized controlled trial. *Jama* 1998;280:159-165.
163. Steinberg KP, Hudson LD, Goodman RB, Hough CL, Lanken PN, Hyzy R, Thompson BT, Ancukiewicz M. Efficacy and safety of corticosteroids for persistent acute respiratory distress syndrome. *N Engl J Med* 2006;354:1671-1684.
164. Lowrey LD, Anderson M, Calhoun J, Edmonds H, Flint LM. Failure of corticosteroid therapy for experimental acid aspiration. *J Surg Res* 1982;32:168-172.
165. Bernard GR, Luce JM, Sprung CL, Rinaldo JE, Tate RM, Sibbald WJ, Kariman K, Higgins S, Bradley R, Metz CA, et al. High-dose corticosteroids in patients with the adult respiratory distress syndrome. *N Engl J Med* 1987;317:1565-1570.
166. Bone RC, Fisher CJ, Jr., Clemmer TP, Slotman GJ, Metz CA. Early methylprednisolone treatment for septic syndrome and the adult respiratory distress syndrome. *Chest* 1987;92:1032-1036.
167. Young MP, Manning HL, Wilson DL, Mette SA, Riker RR, Leiter JC, Liu SK, Bates JT, Parsons PE. Ventilation of patients with acute lung injury and acute respiratory distress syndrome: Has new evidence changed clinical practice? *Crit Care Med* 2004;32:1260-1265.
168. Barton SK, Moss TJ, Hooper SB, Crossley KJ, Gill AW, Kluckow M, Zahra V, Wong FY, Pichler G, Galinsky R, Miller SL, Tolcos M, Polglase GR. Protective ventilation of preterm lambs exposed to acute chorioamnionitis does not reduce ventilation-induced lung or brain injury. *PLoS One* 2014;9:e112402.
169. Kudoh I, Miyazaki H, Ohara M, Fukushima J, Tazawa T, Yamada H. Activation of alveolar macrophages in acid-injured lung in rats: Different effects of pentoxifylline on tumor necrosis factor-alpha and nitric oxide production. *Crit Care Med* 2001;29:1621-1625.

170. Suresh Kumar V, Sadikot RT, Purcell JE, Malik AB, Liu Y. Pseudomonas aeruginosa induced lung injury model. *J Vis Exp* 2014.
171. Knight PR, Davidson BA, Nader ND, Helinski JD, Marschke CJ, Russo TA, Hutson AD, Notter RH, Holm BA. Progressive, severe lung injury secondary to the interaction of insults in gastric aspiration. *Exp Lung Res* 2004;30:535-557.
172. Chen Q, Luo AA, Qiu H, Han B, Ko BH, Slutsky AS, Zhang H. Monocyte interaction accelerates hcl-induced lung epithelial remodeling. *BMC Pulm Med* 2014;14:135.
173. Protti A, Cressoni M, Santini A, Langer T, Mietto C, Febres D, Chierichetti M, Coppola S, Conte G, Gatti S, Leopardi O, Masson S, Lombardi L, Lazzerini M, Rampoldi E, Cadringher P, Gattinoni L. Lung stress and strain during mechanical ventilation: Any safe threshold? *Am J Respir Crit Care Med* 2011;183:1354-1362.
174. Sawa T. The molecular mechanism of acute lung injury caused by pseudomonas aeruginosa: From bacterial pathogenesis to host response. *J Intensive Care* 2014;2:10.
175. Ranieri VM, Suter PM, Tortorella C, De Tullio R, Dayer JM, Brienza A, Bruno F, Slutsky AS. Effect of mechanical ventilation on inflammatory mediators in patients with acute respiratory distress syndrome: A randomized controlled trial. *JAMA : the journal of the American Medical Association* 1999;282:54-61.
176. Frank JA, Matthay MA. Science review: Mechanisms of ventilator-induced injury. *Crit. Care* 2003;7:233-241.
177. Frank JA, Pittet JF, Lee H, Godzich M, Matthay MA. High tidal volume ventilation induces nos2 and impairs camp- dependent air space fluid clearance. *Am J Physiol Lung Cell Mol Physiol* 2003;284:L791-798.
178. Frank JA, Wray CM, McAuley DF, Schwendener R, Matthay MA. Alveolar macrophages contribute to alveolar barrier dysfunction in ventilator-induced lung injury. *Am J Physiol Lung Cell Mol Physiol* 2006;291:L1191-1198.
179. Eyal FG, Hamm CR, Parker JC. Reduction in alveolar macrophages attenuates acute ventilator induced lung injury in rats. *Intensive Care Med* 2007;33:1212-1218.
180. Ning Q, Wang X. Role of rel a and ikappab of nuclear factor kappab in the release of interleukin-8 by cyclic mechanical strain in human alveolar type ii epithelial cells a549. *Respirology* 2007;12:792-798.
181. Fanelli V, Puntorieri V, Assenzio B, Martin EL, Elia V, Bosco M, Delsedime L, Del Sorbo L, Ferrari A, Italiano S, Ghigo A, Slutsky AS, Hirsch E, Ranieri VM. Pulmonary-derived phosphoinositide 3-kinase gamma (pi3kgamma) contributes to ventilator-induced lung injury and edema. *Intensive Care Med* 2010;36:1935-1945.
182. Dhaliwal K, Scholefield E, Ferenbach D, Gibbons M, Duffin R, Dorward DA, Morris AC, Humphries D, MacKinnon A, Wilkinson TS, Wallace WA, van Rooijen N, Mack M, Rossi AG, Davidson DJ, Hirani N, Hughes J, Haslett C, Simpson AJ. Monocytes control second-phase neutrophil emigration in established lipopolysaccharide-induced murine lung injury. *Am J Respir Crit Care Med* 2012;186:514-524.
183. Vaporidi K, Francis RC, Bloch KD, Zapol WM. Nitric oxide synthase 3 contributes to ventilator-induced lung injury. *Am J Physiol Lung Cell Mol Physiol* 2010;299:L150-159.
184. Goldman G, Welbourn R, Kobzik L, Valeri CR, Shepro D, Hechtman HB. Tumor necrosis factor-alpha mediates acid aspiration-induced systemic organ injury. *Ann. Surg.* 1990;212:513-519; discussion 519-520.
185. Dolinay T, Szilasi M, Liu M, Choi AM. Inhaled carbon monoxide confers antiinflammatory effects against ventilator-induced lung injury. *Am J Respir Crit Care Med* 2004;170:613-620.

186. Hoegl S, Bachmann M, Scheiermann P, Goren I, Hofstetter C, Pfeilschifter J, Zwissler B, Muhl H. Protective properties of inhaled il-22 in a model of ventilator-induced lung injury. *Am. J. Respir. Cell Mol. Biol.* 2011;44:369-376.
187. Frank JA, Pittet JF, Wray C, Matthay MA. Protection from experimental ventilator-induced acute lung injury by il-1 receptor blockade. *Thorax* 2008;63:147-153.
188. Vincent JL, Zambon M. Why do patients who have acute lung injury/acute respiratory distress syndrome die from multiple organ dysfunction syndrome? Implications for management. *Clin Chest Med* 2006;27:725-731; abstract x-xi.
189. Hoegl S, Boost KA, Czerwonka H, Dolfen A, Scheiermann P, Muhl H, Zwissler B, Hofstetter C. Inhaled il-10 reduces biotrauma and mortality in a model of ventilator-induced lung injury. *Respir Med* 2009;103:463-470.
190. Li HD, Zhang QX, Mao Z, Xu XJ, Li NY, Zhang H. Exogenous interleukin-10 attenuates hyperoxia-induced acute lung injury in mice. *Exp Physiol* 2014.
191. Shyamsundar M, McAuley DF, Ingram RJ, Gibson DS, O'Kane D, McKeown ST, Edwards A, Taggart C, Elborn JS, Calfee CS, Matthay MA, O'Kane CM. Keratinocyte growth factor promotes epithelial survival and resolution in a human model of lung injury. *Am J Respir Crit Care Med* 2014;189:1520-1529.
192. Wang L, Zhao L, Lv J, Yin Q, Liang X, Chu Y, He R. Blt1-dependent alveolar recruitment of cd4(+)cd25(+) foxp3(+) regulatory t cells is important for resolution of acute lung injury. *Am J Respir Crit Care Med* 2012;186:989-998.
193. Sun J, Han ZB, Liao W, Yang SG, Yang Z, Yu J, Meng L, Wu R, Han ZC. Intrapulmonary delivery of human umbilical cord mesenchymal stem cells attenuates acute lung injury by expanding cd4+cd25+ forkhead boxp3 (foxp3)+ regulatory t cells and balancing anti- and pro-inflammatory factors. *Cell Physiol Biochem* 2011;27:587-596.
194. Song H, Zhou Y, Li G, Bai J. Regulatory t cells contribute to the recovery of acute lung injury by upregulating tim-3. *Inflammation* 2014.
195. D'Alessio FR, Tsushima K, Aggarwal NR, West EE, Willett MH, Britos MF, Pipeling MR, Brower RG, Tuder RM, McDyer JF, King LS. Cd4+cd25+foxp3+ tregs resolve experimental lung injury in mice and are present in humans with acute lung injury. *J Clin Invest* 2009;119:2898-2913.
196. Chen J, Li C, Gao X, Liang Z, Yu L, Li Y, Xiao X, Chen L. Keratinocyte growth factor gene delivery via mesenchymal stem cells protects against lipopolysaccharide-induced acute lung injury in mice. *PLoS One* 2013;8:e83303.
197. Tong L, Bi J, Zhu X, Wang G, Liu J, Rong L, Wang Q, Xu N, Zhong M, Zhu D, Song Y, Bai C. Keratinocyte growth factor-2 is protective in lipopolysaccharide-induced acute lung injury in rats. *Respir Physiol Neurobiol* 2014;201:7-14.
198. Bi J, Tong L, Zhu X, Yang D, Bai C, Song Y, She J. Keratinocyte growth factor-2 intratracheal instillation significantly attenuates ventilator-induced lung injury in rats. *J Cell Mol Med* 2014;18:1226-1235.
199. Adamzik M, Broll J, Steinmann J, Westendorf AM, Rehfeld I, Kreissig C, Peters J. An increased alveolar cd4 + cd25 + foxp3 + t-regulatory cell ratio in acute respiratory distress syndrome is associated with increased 30-day mortality. *Intensive Care Med* 2013;39:1743-1751.
200. Imai Y, Kuba K, Neely GG, Yaghubian-Malhami R, Perkmann T, van Loo G, Ermolaeva M, Veldhuizen R, Leung YH, Wang H, Liu H, Sun Y, Pasparakis M, Kopf M, Mech C, Bavari S, Peiris JS, Slutsky AS, Akira S, Hultqvist M, Holmdahl R, Nicholls J, Jiang C, Binder CJ, Penninger

JM. Identification of oxidative stress and toll-like receptor 4 signaling as a key pathway of acute lung injury. *Cell* 2008;133:235-249.
201. Beck-Schimmer B, Rosenberger DS, Neff SB, Jamnicki M, Suter D, Fuhrer T, Schwendener R, Booy C, Reyes L, Pasch T, Schimmer RC. Pulmonary aspiration: New therapeutic approaches in the experimental model. *Anesthesiology* 2005;103:556-566.
202. Aggarwal NR, King LS, D'Alessio FR. Diverse macrophage populations mediate acute lung inflammation and resolution. *Am J Physiol Lung Cell Mol Physiol* 2014;306:L709-725.
203. Janssen WJ, Barthel L, Muldrow A, Oberley-Deegan RE, Kearns MT, Jakubzick C, Henson PM. Fas determines differential fates of resident and recruited macrophages during resolution of acute lung injury. *Am J Respir Crit Care Med* 2011;184:547-560.
204. Gordon S. Alternative activation of macrophages. *Nat Rev Immunol* 2003;3:23-35.
205. Jian MY, Koizumi T, Kubo K. Effects of nitric oxide synthase inhibitor on acid aspiration-induced lung injury in rats. *Pulm Pharmacol Ther* 2005;18:33-39.
206. Peng X, Abdulnour RE, Sammani S, Ma SF, Han EJ, Hasan EJ, Tuder R, Garcia JG, Hassoun PM. Inducible nitric oxide synthase contributes to ventilator-induced lung injury. *Am J Respir Crit Care Med* 2005;172:470-479.
207. Liu R, Hotta Y, Graveline AR, Evgenov OV, Buys ES, Bloch KD, Ichinose F, Zapol WM. Congenital nos2 deficiency prevents impairment of hypoxic pulmonary vasoconstriction in murine ventilator-induced lung injury. *Am J Physiol Lung Cell Mol Physiol* 2007;293:L1300-1305.
208. Farley KS, Wang LF, Razavi HM, Law C, Rohan M, McCormack DG, Mehta S. Effects of macrophage inducible nitric oxide synthase in murine septic lung injury. *Am J Physiol Lung Cell Mol Physiol* 2006;290:L1164-1172.
209. Prakash A, Mesa KR, Wilhelmsen K, Xu F, Dodd-o JM, Hellman J. Alveolar macrophages and toll-like receptor 4 mediate ventilated lung ischemia reperfusion injury in mice. *Anesthesiology* 2012;117:822-835.
210. He Z, Chen X, Wang S, Zou Z. Toll-like receptor 4 monoclonal antibody attenuates lipopolysaccharide-induced acute lung injury in mice. *Exp Ther Med* 2014;8:871-876.
211. Boyle AJ, McNamee JJ, McAuley DF. Biological therapies in the acute respiratory distress syndrome. *Expert Opin Biol Ther* 2014;14:969-981.
212. Stenvang J, Petri A, Lindow M, Obad S, Kauppinen S. Inhibition of microrna function by antimir oligonucleotides. *Silence* 2012;3:1.
213. Hassan T, McKiernan PJ, McElvaney NG, Cryan SA, Greene CM. Therapeutic modulation of mirna for the treatment of proinflammatory lung diseases. *Expert Rev Anti Infect Ther* 2012;10:359-368.
214. Huang C, Xiao X, Chintagari NR, Breshears M, Wang Y, Liu L. Microrna and mrna expression profiling in rat acute respiratory distress syndrome. *BMC Med Genomics* 2014;7:46.
215. Vaporidi K, Vergadi E, Kaniaris E, Hatziapostolou M, Lagoudaki E, Georgopoulos D, Zapol WM, Bloch KD, Iliopoulos D. Pulmonary microrna profiling in a mouse model of ventilator-induced lung injury. *Am J Physiol Lung Cell Mol Physiol* 2012;303:L199-207.
216. Cai ZG, Zhang SM, Zhang Y, Zhou YY, Wu HB, Xu XP. Micrornas are dynamically regulated and play an important role in lps-induced lung injury. *Can J Physiol Pharmacol* 2012;90:37-43.
217. Zeng Z, Gong H, Li Y, Jie K, Ding C, Shao Q, Liu F, Zhan Y, Nie C, Zhu W, Qian K. Upregulation of mir-146a contributes to the suppression of inflammatory responses in lps-induced acute lung injury. *Exp Lung Res* 2013;39:275-282.

218. Maron-Gutierrez T, Laffey JG, Pelosi P, Rocco PR. Cell-based therapies for the acute respiratory distress syndrome. *Curr Opin Crit Care* 2014;20:122-131.
219. Hayes M, Curley G, Ansari B, Laffey JG. Clinical review: Stem cell therapies for acute lung injury/acute respiratory distress syndrome - hope or hype? *Crit Care* 2012;16:205.
220. Yang JX, Zhang N, Wang HW, Gao P, Yang QP, Wen QP. Cxcr4 overexpression in mesenchymal stem cells facilitates treatment of acute lung injury in rats. *J Biol Chem* 2014.
221. Sdrimas K, Kourembanas S. Msc microvesicles for the treatment of lung disease: A new paradigm for cell-free therapy. *Antioxid Redox Signal* 2014;21:1905-1915.
222. Walter J, Ware LB, Matthay MA. Mesenchymal stem cells: Mechanisms of potential therapeutic benefit in ards and sepsis. *Lancet Respir Med* 2014;2:1016-1026.
223. Shu YS, Tao W, Miao QB, Zhu YB, Yang YF. Improvement of ventilation-induced lung injury in a rodent model by inhibition of inhibitory kappab kinase. *J Trauma Acute Care Surg* 2014;76:1417-1424.
224. Hu R, Chen ZF, Yan J, Li QF, Huang Y, Xu H, Zhang X, Jiang H. Complement c5a exacerbates acute lung injury induced through autophagy-mediated alveolar macrophage apoptosis. *Cell Death Dis* 2014;5:e1330.
225. Wen Z, Fan L, Li Y, Zou Z, Scott MJ, Xiao G, Li S, Billiar TR, Wilson MA, Shi X, Fan J. Neutrophils counteract autophagy-mediated anti-inflammatory mechanisms in alveolar macrophage: Role in posthemorrhagic shock acute lung inflammation. *J Immunol* 2014;193:4623-4633.
226. Badesch DB, Champion HC, Sanchez MA, Hoeper MM, Loyd JE, Manes A, McGoon M, Naeije R, Olschewski H, Oudiz RJ, Torbicki A. Diagnosis and assessment of pulmonary arterial hypertension. *Journal of the American College of Cardiology* 2009;54:S55-66.
227. Idrees MM, Saleemi S, Azem MA, Aldammas S, Alhazmi M, Khan J, Gari A, Aldabbagh M, Sakkijha H, Aldalaan A, Alnajashi K, Alhabeeb W, Nizami I, Kouatli A, Chehab M, Tamimi O, Banjar H, Kashour T, Lopes A, Minai O, Hassoun P, Pasha Q, Mayer E, Butrous G, Bhagavathula S, Ghio S, Swiston J, Boueiz A, Tonelli A, Levy RD, Hoeper M. Saudi guidelines on the diagnosis and treatment of pulmonary hypertension: 2014 updates. *Ann Thorac Med* 2014;9:S1-S15.
228. Groth A, Vrugt B, Brock M, Speich R, Ulrich S, Huber LC. Inflammatory cytokines in pulmonary hypertension. *Respir Res* 2014;15:47.
229. Simonneau G, Gatzoulis MA, Adatia I, Celermajer D, Denton C, Ghofrani A, Gomez Sanchez MA, Krishna Kumar R, Landzberg M, Machado RF, Olschewski H, Robbins IM, Souza R. Updated clinical classification of pulmonary hypertension. *J Am Coll Cardiol* 2013;62:D34-41.
230. Hoeper MM. Definition, classification, and epidemiology of pulmonary arterial hypertension. *Semin Respir Crit Care Med* 2009;30:369-375.
231. Mandras SA, Gilkin RJ, Jr., Pruett JA, Raspa S. Pulmonary arterial hhypertension: Progress and challenges in the modern treatment era. *Am J Manag Care* 2014;20:s191-199.
232. Waxman AB, Zamanian RT. Pulmonary arterial hypertension: New insights into the optimal role of current and emerging prostacyclin therapies. *Am J Cardiol* 2013;111:1A-16A; quiz 17A-19A.
233. Morrell NW, Adnot S, Archer SL, Dupuis J, Jones PL, MacLean MR, McMurtry IF, Stenmark KR, Thistlethwaite PA, Weissmann N, Yuan JX, Weir EK. Cellular and molecular basis of pulmonary arterial hypertension. *Journal of the American College of Cardiology* 2009;54:S20-31.

234. Archer S, Rich S. Primary pulmonary hypertension: A vascular biology and translational research "work in progress". *Circulation* 2000;102:2781-2791.
235. Michelakis ED, Wilkins MR, Rabinovitch M. Emerging concepts and translational priorities in pulmonary arterial hypertension. *Circulation* 2008;118:1486-1495.
236. Puthiyachirakkal M, Mhanna MJ. Pathophysiology, management, and outcome of persistent pulmonary hypertension of the newborn: A clinical review. *Front Pediatr* 2013;1:23.
237. Runo JR, Loyd JE. Primary pulmonary hypertension. *Lancet* 2003;361:1533-1544.
238. Meloche J, Pflieger A, Vaillancourt M, Graydon C, Provencher S, Bonnet S. Mirnas in pah: Biomarker, therapeutic target or both? *Drug Discov Today* 2014;19:1264-1269.
239. Seferian A, Simonneau G. Therapies for pulmonary arterial hypertension: Where are we today, where do we go tomorrow? *Eur Respir Rev* 2013;22:217-226.
240. Galie N, Torbicki A, Barst R, Dartevelle P, Haworth S, Higenbottam T, Olschewski H, Peacock A, Pietra G, Rubin LJ, Simonneau G, Priori SG, Garcia MA, Blanc JJ, Budaj A, Cowie M, Dean V, Deckers J, Burgos EF, Lekakis J, Lindahl B, Mazzotta G, McGregor K, Morais J, Oto A, Smiseth OA, Barbera JA, Gibbs S, Hoeper M, Humbert M, Naeije R, Pepke-Zaba J. Guidelines on diagnosis and treatment of pulmonary arterial hypertension. The task force on diagnosis and treatment of pulmonary arterial hypertension of the european society of cardiology. *Eur Heart J* 2004;25:2243-2278.
241. Cavasin MA, Demos-Davies KM, Schuetze KB, Blakeslee WW, Stratton MS, Tuder RM, McKinsey TA. Reversal of severe angioproliferative pulmonary arterial hypertension and right ventricular hypertrophy by combined phosphodiesterase-5 and endothelin receptor inhibition. *J Transl Med* 2014;12:314.
242. van Berkel S, Binkhorst M, van Heijst AF, Wijnen MH, Liem KD. Adapted ecmo criteria for newborns with persistent pulmonary hypertension after inhaled nitric oxide and/or high-frequency oscillatory ventilation. *Intensive Care Med* 2013;39:1113-1120.
243. James AT, Bee C, Corcoran JD, McNamara PJ, Franklin O, El-Khuffash AF. Treatment of premature infants with pulmonary hypertension and right ventricular dysfunction with milrinone: A case series. *J Perinatol* 2014.
244. Zamanian RT, Kudelko KT, Sung YK, de Jesus Perez V, Liu J, Spiekerkoetter E. Current clinical management of pulmonary arterial hypertension. *Circ Res* 2014;115:131-147.
245. Kourembanas S, Morita T, Christou H, Liu Y, Koike H, Brodsky D, Arthur V, Mitsial SA. Hypoxic responses of vascular cells. *Chest* 1998;114:25S-28S.
246. Christou H, Morita T, Hsieh CM, Koike H, Arkonac B, Perrella MA, Kourembanas S. Prevention of hypoxia-induced pulmonary hypertension by enhancement of endogenous heme oxygenase-1 in the rat. *Circulation research* 2000;86:1224-1229.
247. Stenmark KR, Meyrick B, Galie N, Mooi WJ, McMurtry IF. Animal models of pulmonary arterial hypertension the hope for etiologic discovery and pharmacologic cure. *American journal of physiology* 2009.
248. Stenmark KR, Meyrick B, Galie N, Mooi WJ, McMurtry IF. Animal models of pulmonary arterial hypertension: The hope for etiological discovery and pharmacological cure. *Am J Physiol Lung Cell Mol Physiol* 2009;297:L1013-1032.
249. Das M, Fessel J, Tang H, West J. A process-based review of mouse models of pulmonary hypertension. *Pulm Circ* 2012;2:415-433.
250. Rothman AM, Chico TJ, Lawrie A. Microrna in pulmonary vascular disease. *Prog Mol Biol Transl Sci* 2014;124:43-63.

251. Taylor CT. Mitochondria and cellular oxygen sensing in the hif pathway. *The Biochemical journal* 2008;409:19-26.
252. Gorlach A, Bonello S. The cross-talk between nf-kappab and hif-1: Further evidence for a significant liaison. *The Biochemical journal* 2008;412:e17-19.
253. Fraisl P, Aragones J, Carmeliet P. Inhibition of oxygen sensors as a therapeutic strategy for ischaemic and inflammatory disease. *Nat Rev Drug Discov* 2009;8:139-152.
254. Cummins EP, Berra E, Comerford KM, Ginouves A, Fitzgerald KT, Seeballuck F, Godson C, Nielsen JE, Moynagh P, Pouyssegur J, Taylor CT. Prolyl hydroxylase-1 negatively regulates ikappab kinase-beta, giving insight into hypoxia-induced nfkappab activity. *Proc Natl Acad Sci U S A* 2006;103:18154-18159.
255. BelAiba RS, Djordjevic T, Bonello S, Flugel D, Hess J, Kietzmann T, Gorlach A. Redox-sensitive regulation of the hif pathway under non-hypoxic conditions in pulmonary artery smooth muscle cells. *Biological chemistry* 2004;385:249-257.
256. Burke DL, Frid MG, Kunrath CL, Karoor V, Anwar A, Wagner BD, Strassheim D, Stenmark KR. Sustained hypoxia promotes the development of a pulmonary artery-specific chronic inflammatory microenvironment. *Am J Physiol Lung Cell Mol Physiol* 2009;297:L238-250.
257. Crosswhite P, Sun Z. Molecular mechanisms of pulmonary arterial remodeling. *Mol Med* 2014;20:191-201.
258. Budhiraja R, Tuder RM, Hassoun PM. Endothelial dysfunction in pulmonary hypertension. *Circulation* 2004;109:159-165.
259. Humbert M, Montani D, Perros F, Dorfmuller P, Adnot S, Eddahibi S. Endothelial cell dysfunction and cross talk between endothelium and smooth muscle cells in pulmonary arterial hypertension. *Vascular pharmacology* 2008;49:113-118.
260. Christman BW, McPherson CD, Newman JH, King GA, Bernard GR, Groves BM, Loyd JE. An imbalance between the excretion of thromboxane and prostacyclin metabolites in pulmonary hypertension. *The New England journal of medicine* 1992;327:70-75.
261. Angelini DJ, Su Q, Yamaji-Kegan K, Fan C, Skinner JT, Poloczek A, El-Haddad H, Cheadle C, Johns RA. Hypoxia-induced mitogenic factor (himf/fizz1/relmalpha) in chronic hypoxia- and antigen-mediated pulmonary vascular remodeling. *Respir Res* 2013;14:1.
262. Kim FY, Barnes EA, Ying L, Chen C, Lee L, Alvira CM, Cornfield DN. Pulmonary artery smooth muscle cell endothelin-1 expression modulates the pulmonary vascular response to chronic hypoxia. *Am J Physiol Lung Cell Mol Physiol* 2014:ajplung 00253 02014.
263. Kourembanas S, Marsden PA, McQuillan LP, Faller DV. Hypoxia induces endothelin gene expression and secretion in cultured human endothelium. *J Clin Invest* 1991;88:1054-1057.
264. Michelakis ED. Spatio-temporal diversity of apoptosis within the vascular wall in pulmonary arterial hypertension: Heterogeneous bmp signaling may have therapeutic implications. *Circulation research* 2006;98:172-175.
265. Welsh DJ, Harnett M, MacLean M, Peacock AJ. Proliferation and signaling in fibroblasts: Role of 5-hydroxytryptamine2a receptor and transporter. *American journal of respiratory and critical care medicine* 2004;170:252-259.
266. McLaughlin VV, Archer SL, Badesch DB, Barst RJ, Farber HW, Lindner JR, Mathier MA, McGoon MD, Park MH, Rosenson RS, Rubin LJ, Tapson VF, Varga J, Harrington RA, Anderson JL, Bates ER, Bridges CR, Eisenberg MJ, Ferrari VA, Grines CL, Hlatky MA, Jacobs AK, Kaul S, Lichtenberg RC, Lindner JR, Moliterno DJ, Mukherjee D, Pohost GM, Rosenson RS, Schofield RS, Shubrooks SJ, Stein JH, Tracy CM, Weitz HH, Wesley DJ. Accf/aha 2009 expert consensus

document on pulmonary hypertension: A report of the american college of cardiology foundation task force on expert consensus documents and the american heart association: Developed in collaboration with the american college of chest physicians, american thoracic society, inc., and the pulmonary hypertension association. *Circulation* 2009;119:2250-2294.
267. Stenmark KR, Fagan KA, Frid MG. Hypoxia-induced pulmonary vascular remodeling: Cellular and molecular mechanisms. *Circ Res* 2006;99:675-691.
268. Frid MG, Li M, Gnanasekharan M, Burke DL, Fragoso M, Strassheim D, Sylman JL, Stenmark KR. Sustained hypoxia leads to the emergence of cells with enhanced growth, migratory, and promitogenic potentials within the distal pulmonary artery wall. *Am J Physiol Lung Cell Mol Physiol* 2009;297:L1059-1072.
269. Ricard N, Tu L, Le Hiress M, Huertas A, Phan C, Thuillet R, Sattler C, Fadel E, Seferian A, Montani D, Dorfmuller P, Humbert M, Guignabert C. Increased pericyte coverage mediated by endothelial-derived fibroblast growth factor-2 and interleukin-6 is a source of smooth muscle-like cells in pulmonary hypertension. *Circulation* 2014;129:1586-1597.
270. Arciniegas E, Frid MG, Douglas IS, Stenmark KR. Perspectives on endothelial-to-mesenchymal transition: Potential contribution to vascular remodeling in chronic pulmonary hypertension. *Am J Physiol Lung Cell Mol Physiol* 2007;293:L1-8.
271. Wojciak-Stothard B, Tsang LY, Paleolog E, Hall SM, Haworth SG. Rac1 and rhoa as regulators of endothelial phenotype and barrier function in hypoxia-induced neonatal pulmonary hypertension. *American journal of physiology* 2006;290:L1173-1182.
272. de Jesus Perez V, Yuan K, Alastalo TP, Spiekerkoetter E, Rabinovitch M. Targeting the wnt signaling pathways in pulmonary arterial hypertension. *Drug Discov Today* 2014;19:1270-1276.
273. MacLean MR, Herve P, Eddahibi S, Adnot S. 5-hydroxytryptamine and the pulmonary circulation: Receptors, transporters and relevance to pulmonary arterial hypertension. *British journal of pharmacology* 2000;131:161-168.
274. Sullivan CC, Du L, Chu D, Cho AJ, Kido M, Wolf PL, Jamieson SW, Thistlethwaite PA. Induction of pulmonary hypertension by an angiopoietin 1/tie2/serotonin pathway. *Proceedings of the National Academy of Sciences of the United States of America* 2003;100:12331-12336.
275. Dewachter L, Adnot S, Fadel E, Humbert M, Maitre B, Barlier-Mur AM, Simonneau G, Hamon M, Naeije R, Eddahibi S. Angiopoietin/tie2 pathway influences smooth muscle hyperplasia in idiopathic pulmonary hypertension. *American journal of respiratory and critical care medicine* 2006;174:1025-1033.
276. Bonnet S, Michelakis ED, Porter CJ, Andrade-Navarro MA, Thebaud B, Bonnet S, Haromy A, Harry G, Moudgil R, McMurtry MS, Weir EK, Archer SL. An abnormal mitochondrial-hypoxia inducible factor-1alpha-kv channel pathway disrupts oxygen sensing and triggers pulmonary arterial hypertension in fawn hooded rats: Similarities to human pulmonary arterial hypertension. *Circulation* 2006;113:2630-2641.
277. Olschewski A, Papp R, Nagaraj C, Olschewski H. Ion channels and transporters as therapeutic targets in the pulmonary circulation. *Pharmacol Ther* 2014;144:349-368.
278. Saco TV, Parthasarathy PT, Cho Y, Lockey RF, Kolliputi N. Role of epigenetics in pulmonary hypertension. *Am J Physiol Cell Physiol* 2014;306:C1101-1105.
279. Rowan SC, McLoughlin P. Hypoxic pulmonary hypertension: The paradigm is changing. *Exp Physiol* 2014;99:837-838.
280. Huang JB, Liang J, Zhao XF, Wu WS, Zhang F. Epigenetics: Novel mechanism of pulmonary hypertension. *Lung* 2013;191:601-610.

281. Wei C, Henderson H, Spradley C, Li L, Kim IK, Kumar S, Hong N, Arroliga AC, Gupta S. Circulating mirnas as potential marker for pulmonary hypertension. *PLoS One* 2013;8:e64396.
282. Zhou G, Chen T, Raj JU. Micrornas in pulmonary hypertension. *Am J Respir Cell Mol Biol* 2014.
283. Meloche J, Paulin R, Provencher S, Bonnet S. Therapeutic potential of microrna modulation in pulmonary arterial hypertension. *Curr Vasc Pharmacol* 2013.
284. Kang K, Peng X, Zhang X, Wang Y, Zhang L, Gao L, Weng T, Zhang H, Ramchandran R, Raj JU, Gou D, Liu L. Microrna-124 suppresses the transactivation of nuclear factor of activated t cells by targeting multiple genes and inhibits the proliferation of pulmonary artery smooth muscle cells. *J Biol Chem* 2013;288:25414-25427.
285. Li S, Ran Y, Zhang D, Chen J, Zhu D. Microrna-138 plays a role in hypoxic pulmonary vascular remodelling by targeting mst1. *Biochem J* 2013;452:281-291.
286. Kim J, Kang Y, Kojima Y, Lighthouse JK, Hu X, Aldred MA, McLean DL, Park H, Comhair SA, Greif DM, Erzurum SC, Chun HJ. An endothelial apelin-fgf link mediated by mir-424 and mir-503 is disrupted in pulmonary arterial hypertension. *Nat Med* 2013;19:74-82.
287. Wang D, Zhang H, Li M, Frid MG, Flockton AR, McKeon BA, Yeager ME, Fini MA, Morrell NW, Pullamsetti SS, Velegala S, Seeger W, McKinsey TA, Sucharov CC, Stenmark KR. Microrna-124 controls the proliferative, migratory, and inflammatory phenotype of pulmonary vascular fibroblasts. *Circ Res* 2014;114:67-78.
288. Li SS, Ran YJ, Zhang DD, Li SZ, Zhu D. Microrna-190 regulates hypoxic pulmonary vasoconstriction by targeting a voltage-gated k(+) channel in arterial smooth muscle cells. *J Cell Biochem* 2014;115:1196-1205.
289. Li C, Mpollo MS, Gonsalves CS, Tahara SM, Malik P, Kalra VK. Peroxisome proliferator-activated receptor-alpha-mediated transcription of mir-199a2 attenuates endothelin-1 expression via hypoxia-inducible factor-1alpha. *J Biol Chem* 2014;289:36031-36047.
290. Lane KB, Machado RD, Pauciulo MW, Thomson JR, Phillips JA, 3rd, Loyd JE, Nichols WC, Trembath RC. Heterozygous germline mutations in bmpr2, encoding a tgf-beta receptor, cause familial primary pulmonary hypertension. *Nature genetics* 2000;26:81-84.
291. Deng Z, Morse JH, Slager SL, Cuervo N, Moore KJ, Venetos G, Kalachikov S, Cayanis E, Fischer SG, Barst RJ, Hodge SE, Knowles JA. Familial primary pulmonary hypertension (gene pph1) is caused by mutations in the bone morphogenetic protein receptor-ii gene. *American journal of human genetics* 2000;67:737-744.
292. Thomson JR, Machado RD, Pauciulo MW, Morgan NV, Humbert M, Elliott GC, Ward K, Yacoub M, Mikhail G, Rogers P, Newman J, Wheeler L, Higenbottam T, Gibbs JS, Egan J, Crozier A, Peacock A, Allcock R, Corris P, Loyd JE, Trembath RC, Nichols WC. Sporadic primary pulmonary hypertension is associated with germline mutations of the gene encoding bmpr-ii, a receptor member of the tgf-beta family. *Journal of medical genetics* 2000;37:741-745.
293. Machado RD, Eickelberg O, Elliott CG, Geraci MW, Hanaoka M, Loyd JE, Newman JH, Phillips JA, 3rd, Soubrier F, Trembath RC, Chung WK. Genetics and genomics of pulmonary arterial hypertension. *Journal of the American College of Cardiology* 2009;54:S32-42.
294. Newman JH, Wheeler L, Lane KB, Loyd E, Gaddipati R, Phillips JA, 3rd, Loyd JE. Mutation in the gene for bone morphogenetic protein receptor ii as a cause of primary pulmonary hypertension in a large kindred. *The New England journal of medicine* 2001;345:319-324.
295. Machado RD, Pauciulo MW, Thomson JR, Lane KB, Morgan NV, Wheeler L, Phillips JA, 3rd, Newman J, Williams D, Galie N, Manes A, McNeil K, Yacoub M, Mikhail G, Rogers P,

Corris P, Humbert M, Donnai D, Martensson G, Tranebjaerg L, Loyd JE, Trembath RC, Nichols WC. Bmpr2 haploinsufficiency as the inherited molecular mechanism for primary pulmonary hypertension. *American journal of human genetics* 2001;68:92-102.
296. Thomson J, Machado R, Pauciulo M, Morgan N, Yacoub M, Corris P, McNeil K, Loyd J, Nichols W, Trembath R. Familial and sporadic primary pulmonary hypertension is caused by bmpr2 gene mutations resulting in haploinsufficiency of the bone morphogenetic protein tuype ii receptor. *J Heart Lung Transplant* 2001;20:149.
297. Pasha Q. Saudi guidelines on the diagnosis and treatment of pulmonary hypertension: Genetics of pulmonary hypertension. *Ann Thorac Med* 2014;9:S16-20.
298. Chida A, Shintani M, Matsushita Y, Sato H, Eitoku T, Nakayama T, Furutani Y, Hayama E, Kawamura Y, Inai K, Ohtsuki S, Saji T, Nonoyama S, Nakanishi T. Mutations of notch3 in childhood pulmonary arterial hypertension. *Mol Genet Genomic Med* 2014;2:229-239.
299. Soubrier F, Chung WK, Machado R, Grunig E, Aldred M, Geraci M, Loyd JE, Elliott CG, Trembath RC, Newman JH, Humbert M. Genetics and genomics of pulmonary arterial hypertension. *J Am Coll Cardiol* 2013;62:D13-21.
300. West J, Austin E, Fessel JP, Loyd J, Hamid R. Rescuing the bmpr2 signaling axis in pulmonary arterial hypertension. *Drug Discov Today* 2014;19:1241-1245.
301. Ma L, Roman-Campos D, Austin ED, Eyries M, Sampson KS, Soubrier F, Germain M, Tregouet DA, Borczuk A, Rosenzweig EB, Girerd B, Montani D, Humbert M, Loyd JE, Kass RS, Chung WK. A novel channelopathy in pulmonary arterial hypertension. *N Engl J Med* 2013;369:351-361.
302. Best DH, Austin ED, Chung WK, Elliott CG. Genetics of pulmonary hypertension. *Curr Opin Cardiol* 2014;29:520-527.
303. Saji T. Update on pediatric pulmonary arterial hypertension. Differences and similarities to adult disease. *Circ J* 2013;77:2639-2650.
304. Minamino T, Christou H, Hsieh CM, Liu Y, Dhawan V, Abraham NG, Perrella MA, Mitsialis SA, Kourembanas S. Targeted expression of heme oxygenase-1 prevents the pulmonary inflammatory and vascular responses to hypoxia. *Proceedings of the National Academy of Sciences of the United States of America* 2001;98:8798-8803.
305. Balabanian K, Foussat A, Dorfmuller P, Durand-Gasselin I, Capel F, Bouchet-Delbos L, Portier A, Marfaing-Koka A, Krzysiek R, Rimaniol AC, Simonneau G, Emilie D, Humbert M. Cx(3)c chemokine fractalkine in pulmonary arterial hypertension. *American journal of respiratory and critical care medicine* 2002;165:1419-1425.
306. Dorfmuller P, Zarka V, Durand-Gasselin I, Monti G, Balabanian K, Garcia G, Capron F, Coulomb-Lhermine A, Marfaing-Koka A, Simonneau G, Emilie D, Humbert M. Chemokine rantes in severe pulmonary arterial hypertension. *American journal of respiratory and critical care medicine* 2002;165:534-539.
307. Li J, Rao J, Liu Y, Cao Y, Zhang Y, Zhang Q, Zhu D. 15-lipoxygenase promotes chronic hypoxia-induced pulmonary artery inflammation via positive interaction with nuclear factor-kappab. *Arterioscler Thromb Vasc Biol* 2013;33:971-979.
308. Hassoun PM. Inflammation in pulmonary arterial hypertension: Is it time to quell the fire? *Eur Respir J* 2014;43:685-688.
309. Humbert M, Monti G, Brenot F, Sitbon O, Portier A, Grangeot-Keros L, Duroux P, Galanaud P, Simonneau G, Emilie D. Increased interleukin-1 and interleukin-6 serum concentrations in severe primary pulmonary hypertension. *American journal of respiratory and critical care medicine* 1995;151:1628-1631.

310. Isern RA, Yaneva M, Weiner E, Parke A, Rothfield N, Dantzker D, Rich S, Arnett FC. Autoantibodies in patients with primary pulmonary hypertension: Association with anti-ku. *The American journal of medicine* 1992;93:307-312.
311. Hall S, Brogan P, Haworth SG, Klein N. Contribution of inflammation to the pathology of idiopathic pulmonary arterial hypertension in children. *Thorax* 2009;64:778-783.
312. Fartoukh M, Emilie D, Le Gall C, Monti G, Simonneau G, Humbert M. Chemokine macrophage inflammatory protein-1alpha mrna expression in lung biopsy specimens of primary pulmonary hypertension. *Chest* 1998;114:50S-51S.
313. Sakamaki F, Kyotani S, Nagaya N, Sato N, Oya H, Satoh T, Nakanishi N. Increased plasma p-selectin and decreased thrombomodulin in pulmonary arterial hypertension were improved by continuous prostacyclin therapy. *Circulation* 2000;102:2720-2725.
314. Sanchez O, Marcos E, Perros F, Fadel E, Tu L, Humbert M, Dartevelle P, Simonneau G, Adnot S, Eddahibi S. Role of endothelium-derived cc chemokine ligand 2 in idiopathic pulmonary arterial hypertension. *American journal of respiratory and critical care medicine* 2007;176:1041-1047.
315. Yue TL, Wang X, Sung CP, Olson B, McKenna PJ, Gu JL, Feuerstein GZ. Interleukin-8. A mitogen and chemoattractant for vascular smooth muscle cells. *Circulation research* 1994;75:1-7.
316. Ito T, Okada T, Miyashita H, Nomoto T, Nonaka-Sarukawa M, Uchibori R, Maeda Y, Urabe M, Mizukami H, Kume A, Takahashi M, Ikeda U, Shimada K, Ozawa K. Interleukin-10 expression mediated by an adeno-associated virus vector prevents monocrotaline-induced pulmonary arterial hypertension in rats. *Circ Res* 2007;101:734-741.
317. Price LC, Wort SJ, Perros F, Dorfmuller P, Huertas A, Montani D, Cohen-Kaminsky S, Humbert M. Inflammation in pulmonary arterial hypertension. *Chest* 2012;141:210-221.
318. Tuder RM, Groves B, Badesch DB, Voelkel NF. Exuberant endothelial cell growth and elements of inflammation are present in plexiform lesions of pulmonary hypertension. *The American journal of pathology* 1994;144:275-285.
319. Pinto RF, Higuchi Mde L, Aiello VD. Decreased numbers of t-lymphocytes and predominance of recently recruited macrophages in the walls of peripheral pulmonary arteries from 26 patients with pulmonary hypertension secondary to congenital cardiac shunts. *Cardiovasc Pathol* 2004;13:268-275.
320. Perros F, Dorfmuller P, Souza R, Durand-Gasselin I, Mussot S, Mazmanian M, Herve P, Emilie D, Simonneau G, Humbert M. Dendritic cell recruitment in lesions of human and experimental pulmonary hypertension. *Eur Respir J* 2007;29:462-468.
321. Hautefort A, Girerd B, Montani D, Cohen Kaminsky S, Price L, Lambrecht BN, Humbert M, Perros F. Th17 polarization in pulmonary arterial hypertension. *Chest* 2014.
322. Gaowa S, Zhou W, Yu L, Zhou X, Liao K, Yang K, Lu Z, Jiang H, Chen X. Effect of th17 and treg axis disorder on outcomes of pulmonary arterial hypertension in connective tissue diseases. *Mediators Inflamm* 2014;2014:247372.
323. Chu Y, Xiangli X, Xiao W. Regulatory t cells protect against hypoxia-induced pulmonary arterial hypertension in mice. *Mol Med Rep* 2014.
324. Hayashida K, Fujita J, Miyake Y, Kawada H, Ando K, Ogawa S, Fukuda K. Bone marrow-derived cells contribute to pulmonary vascular remodeling in hypoxia-induced pulmonary hypertension. *Chest* 2005;127:1793-1798.
325. Burke DL, Frid MG, Kunrath CL, Karoor V, Anwar A, Wagner BD, Strassheim D, Stenmark KR. Sustained hypoxia promotes the development of a pulmonary artery-specific

chronic inflammatory microenvironment. *American journal of physiology* 2009;297:L238-250.
326. Stenmark KR, Fagan KA, Frid MG. Hypoxia-induced pulmonary vascular remodeling: Cellular and molecular mechanisms. *Circulation research* 2006;99:675-691.
327. Frid MG, Brunetti JA, Burke DL, Carpenter TC, Davie NJ, Reeves JT, Roedersheimer MT, van Rooijen N, Stenmark KR. Hypoxia-induced pulmonary vascular remodeling requires recruitment of circulating mesenchymal precursors of a monocyte/macrophage lineage. *The American journal of pathology* 2006;168:659-669.
328. Price LC, Caramori G, Perros F, Meng C, Gambaryan N, Dorfmuller P, Montani D, Casolari P, Zhu J, Dimopoulos K, Shao D, Girerd B, Mumby S, Proudfoot A, Griffiths M, Papi A, Humbert M, Adcock IM, Wort SJ. Nuclear factor kappa-b is activated in the pulmonary vessels of patients with end-stage idiopathic pulmonary arterial hypertension. *PLoS One* 2013;8:e75415.
329. Lewis C, Murdoch C. Macrophage responses to hypoxia: Implications for tumor progression and anti-cancer therapies. *Am J Pathol* 2005;167:627-635.
330. Zampetaki A, Mitsialis SA, Pfeilschifter J, Kourembanas S. Hypoxia induces macrophage inflammatory protein-2 (mip-2) gene expression in murine macrophages via nf-kappab: The prominent role of p42/ p44 and pi3 kinase pathways. *Faseb J* 2004;18:1090-1092.
331. Wen H, Ting JP. Agitation by suffocation: How hypoxia activates innate immunity via the warburg effect. *Cell Metab* 2013;17:814-815.
332. Stenmark KR, Bouchey D, Nemenoff R, Dempsey EC, Das M. Hypoxia-induced pulmonary vascular remodeling: Contribution of the adventitial fibroblasts. *Physiol Res* 2000;49:503-517.
333. Chao J, Wood JG, Gonzalez NC. Alveolar hypoxia, alveolar macrophages, and systemic inflammation. *Respir Res* 2009;10:54.
334. Gonzalez NC, Allen J, Blanco VG, Schmidt EJ, van Rooijen N, Wood JG. Alveolar macrophages are necessary for the systemic inflammation of acute alveolar hypoxia. *J Appl Physiol (1985)* 2007;103:1386-1394.
335. Loboda A, Jazwa A, Grochot-Przeczek A, Rutkowski AJ, Cisowski J, Agarwal A, Jozkowicz A, Dulak J. Heme oxygenase-1 and the vascular bed: From molecular mechanisms to therapeutic opportunities. *Antioxidants & redox signaling* 2008;10:1767-1812.
336. Leopold JA, Loscalzo J. Oxidative enzymopathies and vascular disease. *Arteriosclerosis, thrombosis, and vascular biology* 2005;25:1332-1340.
337. Otterbein LE, Soares MP, Yamashita K, Bach FH. Heme oxygenase-1: Unleashing the protective properties of heme. *Trends in immunology* 2003;24:449-455.
338. Ryter SW, Kim HP, Nakahira K, Zuckerbraun BS, Morse D, Choi AM. Protective functions of heme oxygenase-1 and carbon monoxide in the respiratory system. *Antioxid Redox Signal* 2007;9:2157-2173.
339. Baranano DE, Rao M, Ferris CD, Snyder SH. Biliverdin reductase: A major physiologic cytoprotectant. *Proceedings of the National Academy of Sciences of the United States of America* 2002;99:16093-16098.
340. Abraham NG, Drummond G. Cd163-mediated hemoglobin-heme uptake activates macrophage ho-1, providing an antiinflammatory function. *Circ Res* 2006;99:911-914.
341. Yet SF, Perrella MA, Layne MD, Hsieh CM, Maemura K, Kobzik L, Wiesel P, Christou H, Kourembanas S, Lee ME. Hypoxia induces severe right ventricular dilatation and infarction in heme oxygenase-1 null mice. *The Journal of clinical investigation* 1999;103:R23-29.

342. Morita T, Mitsialis SA, Koike H, Liu Y, Kourembanas S. Carbon monoxide controls the proliferation of hypoxic vascular smooth muscle cells. *J Biol Chem* 1997;272:32804-32809.
343. Ryter SW, Otterbein LE, Morse D, Choi AM. Heme oxygenase/carbon monoxide signaling pathways: Regulation and functional significance. *Mol Cell Biochem* 2002;234-235:249-263.
344. Morita T, Perrella MA, Lee ME, Kourembanas S. Smooth muscle cell-derived carbon monoxide is a regulator of vascular cgmp. *Proc Natl Acad Sci U S A* 1995;92:1475-1479.
345. Yamashita K, McDaid J, Ollinger R, Tsui TY, Berberat PO, Usheva A, Csizmadia E, Smith RN, Soares MP, Bach FH. Biliverdin, a natural product of heme catabolism, induces tolerance to cardiac allografts. *Faseb J* 2004;18:765-767.
346. Hoetzel A, Dolinay T, Vallbracht S, Zhang Y, Kim HP, Ifedigbo E, Alber S, Kaynar AM, Schmidt R, Ryter SW, Choi AM. Carbon monoxide protects against ventilator-induced lung injury via ppar-gamma and inhibition of egr-1. *American journal of respiratory and critical care medicine* 2008;177:1223-1232.
347. Dolinay T, Szilasi M, Liu M, Choi AM. Inhaled carbon monoxide confers antiinflammatory effects against ventilator-induced lung injury. *American journal of respiratory and critical care medicine* 2004;170:613-620.
348. Yachie A, Niida Y, Wada T, Igarashi N, Kaneda H, Toma T, Ohta K, Kasahara Y, Koizumi S. Oxidative stress causes enhanced endothelial cell injury in human heme oxygenase-1 deficiency. *The Journal of clinical investigation* 1999;103:129-135.
349. Otterbein LE, Bach FH, Alam J, Soares M, Tao Lu H, Wysk M, Davis RJ, Flavell RA, Choi AM. Carbon monoxide has anti-inflammatory effects involving the mitogen-activated protein kinase pathway. *Nature medicine* 2000;6:422-428.
350. Willis D, Moore AR, Frederick R, Willoughby DA. Heme oxygenase: A novel target for the modulation of the inflammatory response. *Nat Med* 1996;2:87-90.
351. Tzima S, Victoratos P, Kranidioti K, Alexiou M, Kollias G. Myeloid heme oxygenase-1 regulates innate immunity and autoimmunity by modulating ifn-beta production. *The Journal of experimental medicine* 2009;206:1167-1179.
352. Zampetaki A, Minamino T, Mitsialis SA, Kourembanas S. Effect of heme oxygenase-1 overexpression in two models of lung inflammation. *Exp Biol Med (Maywood)* 2003;228:442-446.
353. Seldon MP, Silva G, Pejanovic N, Larsen R, Gregoire IP, Filipe J, Anrather J, Soares MP. Heme oxygenase-1 inhibits the expression of adhesion molecules associated with endothelial cell activation via inhibition of nf-kappab rela phosphorylation at serine 276. *J Immunol* 2007;179:7840-7851.
354. Inoue S, Suzuki M, Nagashima Y, Suzuki S, Hashiba T, Tsuburai T, Ikehara K, Matsuse T, Ishigatsubo Y. Transfer of heme oxygenase 1 cdna by a replication-deficient adenovirus enhances interleukin 10 production from alveolar macrophages that attenuates lipopolysaccharide-induced acute lung injury in mice. *Hum Gene Ther* 2001;12:967-979.
355. Xia ZW, Xu LQ, Zhong WW, Wei JJ, Li NL, Shao J, Li YZ, Yu SC, Zhang ZL. Heme oxygenase-1 attenuates ovalbumin-induced airway inflammation by up-regulation of foxp3 t-regulatory cells, interleukin-10, and membrane-bound transforming growth factor- 1. *Am J Pathol* 2007;171:1904-1914.
356. Ma JL, Yang PY, Rui YC, Lu L, Kang H, Zhang J. Hemin modulates cytokine expressions in macrophage-derived foam cells via heme oxygenase-1 induction. *J Pharmacol Sci* 2007;103:261-266.

357. Tzima S, Victoratos P, Kranidioti K, Alexiou M, Kollias G. Myeloid heme oxygenase-1 regulates innate immunity and autoimmunity by modulating ifn-beta production. *J Exp Med* 2009;206:1167-1179.
358. George JF, Braun A, Brusko TM, Joseph R, Bolisetty S, Wasserfall CH, Atkinson MA, Agarwal A, Kapturczak MH. Suppression by cd4+cd25+ regulatory t cells is dependent on expression of heme oxygenase-1 in antigen-presenting cells. *Am J Pathol* 2008;173:154-160.
359. Zuckerbraun BS, Chin BY, Wegiel B, Billiar TR, Czsimadia E, Rao J, Shimoda L, Ifedigbo E, Kanno S, Otterbein LE. Carbon monoxide reverses established pulmonary hypertension. *J Exp Med* 2006;203:2109-2119.
360. Morita T, Mitsialis SA, Koike H, Liu Y, Kourembanas S. Carbon monoxide controls the proliferation of hypoxic vascular smooth muscle cells. *J Biol Chem* 1997;272:32804-32809.
361. Hoetzel A, Dolinay T, Vallbracht S, Zhang Y, Kim HP, Ifedigbo E, Alber S, Kaynar AM, Schmidt R, Ryter SW, Choi AM. Carbon monoxide protects against ventilator-induced lung injury via ppar-gamma and inhibition of egr-1. *Am J Respir Crit Care Med* 2008;177:1223-1232.
362. Nemzek JA, Fry C, Abatan O. Low-dose carbon monoxide treatment attenuates early pulmonary neutrophil recruitment after acid aspiration. *Am J Physiol Lung Cell Mol Physiol* 2008;294:L644-653.
363. Otterbein LE, Bach FH, Alam J, Soares M, Tao Lu H, Wysk M, Davis RJ, Flavell RA, Choi AM. Carbon monoxide has anti-inflammatory effects involving the mitogen-activated protein kinase pathway. *Nat Med* 2000;6:422-428.
364. Otterbein LE, Otterbein SL, Ifedigbo E, Liu F, Morse DE, Fearns C, Ulevitch RJ, Knickelbein R, Flavell RA, Choi AM. Mkk3 mitogen-activated protein kinase pathway mediates carbon monoxide-induced protection against oxidant-induced lung injury. *Am J Pathol* 2003;163:2555-2563.
365. Anyanwu AC, Bentley JK, Popova AP, Malas O, Alghanem H, Goldsmith AM, Hershenson MB, Pinsky DJ. Suppression of inflammatory cell trafficking and alveolar simplification by the heme oxygenase-1 product carbon monoxide. *Am J Physiol Lung Cell Mol Physiol* 2014;306:L749-763.
366. Nakahira K, Kim HP, Geng XH, Nakao A, Wang X, Murase N, Drain PF, Sasidhar M, Nabel EG, Takahashi T, Lukacs NW, Ryter SW, Morita K, Choi AM. Carbon monoxide differentially inhibits tlr signaling pathways by regulating ros-induced trafficking of tlrs to lipid rafts. *J Exp Med* 2006;203:2377-2389.
367. Vitali SH, Mitsialis SA, Liang OD, Liu X, Fernandez-Gonzalez A, Christou H, Wu X, McGowan FX, Kourembanas S. Divergent cardiopulmonary actions of heme oxygenase enzymatic products in chronic hypoxia. *PLoS One* 2009;4:e5978.
368. Sarady-Andrews JK, Liu F, Gallo D, Nakao A, Overhaus M, Ollinger R, Choi AM, Otterbein LE. Biliverdin administration protects against endotoxin-induced acute lung injury in rats. *American journal of physiology* 2005;289:L1131-1137.
369. Sarady-Andrews JK, Liu F, Gallo D, Nakao A, Overhaus M, Ollinger R, Choi AM, Otterbein LE. Biliverdin administration protects against endotoxin-induced acute lung injury in rats. *Am J Physiol Lung Cell Mol Physiol* 2005;289:L1131-1137.
370. El Chami H, Hassoun PM. Inflammatory mechanisms in the pathogenesis of pulmonary arterial hypertension. *Compr Physiol* 2011;1:1929-1941.
371. Luo L, Lin T, Zheng S, Xie Z, Chen M, Lian G, Xu C, Wang H, Xie L. Adipose-derived stem cells attenuate pulmonary arterial hypertension and ameliorate pulmonary arterial

remodeling in monocrotaline-induced pulmonary hypertensive rats. *Clin Exp Hypertens* 2014:1-8.
372. Lanzola E, Farha S, Erzurum SC, Asosingh K. Bone marrow-derived vascular modulatory cells in pulmonary arterial hypertension. *Pulm Circ* 2013;3:781-791.
373. Yang JX, Pan YY, Zhao YY, Wang XX. Endothelial progenitor cell-based therapy for pulmonary arterial hypertension. *Cell Transplant* 2013;22:1325-1336.
374. Liang OD, Mitsialis SA, Chang MS, Vergadi E, Lee C, Aslam M, Fernandez-Gonzalez A, Liu X, Baveja R, Kourembanas S. Mesenchymal stromal cells expressing heme oxygenase-1 reverse pulmonary hypertension. *Stem Cells* 2011;29:99-107.
375. Lee C, Mitsialis SA, Aslam M, Vitali SH, Vergadi E, Konstantinou G, Sdrimas K, Fernandez-Gonzalez A, Kourembanas S. Exosomes mediate the cytoprotective action of mesenchymal stromal cells on hypoxia-induced pulmonary hypertension. *Circulation* 2012;126:2601-2611.
376. Kourembanas S. Exosomes: Vehicles of intercellular signaling, biomarkers, and vectors of cell therapy. *Annu Rev Physiol* 2014.
377. Foster WS, Suen CM, Stewart DJ. Regenerative cell and tissue-based therapies for pulmonary arterial hypertension. *Can J Cardiol* 2014;30:1350-1360.
378. Jais X, Launay D, Yaici A, Le Pavec J, Tcherakian C, Sitbon O, Simonneau G, Humbert M. Immunosuppressive therapy in lupus- and mixed connective tissue disease-associated pulmonary arterial hypertension: A retrospective analysis of twenty-three cases. *Arthritis Rheum* 2008;58:521-531.
379. Perl AK, Tichelaar JW, Whitsett JA. Conditional gene expression in the respiratory epithelium of the mouse. *Transgenic Res.* 2002;11:21-29.
380. Van Rooijen N, Sanders A. Liposome mediated depletion of macrophages: Mechanism of action, preparation of liposomes and applications. *J Immunol Methods* 1994;174:83-93.
381. van Rooijen N, van Kesteren-Hendrikx E. "In vivo" depletion of macrophages by liposome-mediated "suicide". *Methods Enzymol* 2003;373:3-16.
382. Judge AD, Robbins M, Tavakoli I, Levi J, Hu L, Fronda A, Ambegia E, McClintock K, MacLachlan I. Confirming the rnai-mediated mechanism of action of sirna-based cancer therapeutics in mice. *J Clin Invest* 2009;119:661-673.
383. Robbins M, Judge A, MacLachlan I. Sirna and innate immunity. *Oligonucleotides* 2009;19:89-102.
384. Zhang X, Shan P, Jiang D, Noble PW, Abraham NG, Kappas A, Lee PJ. Small interfering rna targeting heme oxygenase-1 enhances ischemia-reperfusion-induced lung apoptosis. *J Biol Chem* 2004;279:10677-10684.
385. Alvarez R, Elbashir S, Borland T, Toudjarska I, Hadwiger P, John M, Roehl I, Morskaya SS, Martinello R, Kahn J, Van Ranst M, Tripp RA, DeVincenzo JP, Pandey R, Maier M, Nechev L, Manoharan M, Kotelianski V, Meyers R. Rna interference-mediated silencing of the respiratory syncytial virus nucleocapsid defines a potent antiviral strategy. *Antimicrob Agents Chemother* 2009;53:3952-3962.
386. Gutbier B, Kube SM, Reppe K, Santel A, Lange C, Kaufmann J, Suttorp N, Witzenrath M. Rnai-mediated suppression of constitutive pulmonary gene expression by small interfering rna in mice. *Pulm Pharmacol Ther* 2010;23:334-344.
387. Yamashita K, McDaid J, Ollinger R, Tsui TY, Berberat PO, Usheva A, Csizmadia E, Smith RN, Soares MP, Bach FH. Biliverdin, a natural product of heme catabolism, induces tolerance

to cardiac allografts. *FASEB journal : official publication of the Federation of American Societies for Experimental Biology* 2004;18:765-767.
388. Reinhard C, Eder G, Fuchs H, Ziesenis A, Heyder J, Schulz H. Inbred strain variation in lung function. *Mammalian genome : official journal of the International Mammalian Genome Society* 2002;13:429-437.
389. Jones R, Jacobson M, Steudel W. Alpha-smooth-muscle actin and microvascular precursor smooth-muscle cells in pulmonary hypertension. *American journal of respiratory cell and molecular biology* 1999;20:582-594.
390. Kimura I, Moritani Y, Tanizaki Y. Basophils in bronchial asthma with reference to reagin-type allergy. *Clin. Allergy* 1973;3:195-202.
391. Pfaffl MW. A new mathematical model for relative quantification in real-time rt-pcr. *Nucleic Acids Res.* 2001;29:e45.
392. Kimura I, Moritani Y, Tanizaki Y. Basophils in bronchial asthma with reference to reagin-type allergy. *Clin Allergy* 1973;3:195-202.
393. Khazen W, M'Bika J P, Tomkiewicz C, Benelli C, Chany C, Achour A, Forest C. Expression of macrophage-selective markers in human and rodent adipocytes. *FEBS Lett* 2005;579:5631-5634.
394. van Rijt LS, Kuipers H, Vos N, Hijdra D, Hoogsteden HC, Lambrecht BN. A rapid flow cytometric method for determining the cellular composition of bronchoalveolar lavage fluid cells in mouse models of asthma. *J Immunol Methods* 2004;288:111-121.
395. Shirey KA, Cole LE, Keegan AD, Vogel SN. Francisella tularensis live vaccine strain induces macrophage alternative activation as a survival mechanism. *J Immunol* 2008;181:4159-4167.
396. Corraliza IM, Campo ML, Soler G, Modolell M. Determination of arginase activity in macrophages: A micromethod. *J Immunol Methods* 1994;174:231-235.
397. Luu K, Greenhill CJ, Majoros A, Decker T, Jenkins BJ, Mansell A. Stat1 plays a role in tlr signal transduction and inflammatory responses. *Immunol Cell Biol* 2014;92:761-769.
398. Rhee SH, Jones BW, Toshchakov V, Vogel SN, Fenton MJ. Toll-like receptors 2 and 4 activate stat1 serine phosphorylation by distinct mechanisms in macrophages. *J Biol Chem* 2003;278:22506-22512.
399. Williams AE, Perry MM, Moschos SA, Larner-Svensson HM, Lindsay MA. Role of mirna-146a in the regulation of the innate immune response and cancer. *Biochem Soc Trans* 2008;36:1211-1215.
400. Taganov KD, Boldin MP, Chang KJ, Baltimore D. Nf-kappab-dependent induction of microrna mir-146, an inhibitor targeted to signaling proteins of innate immune responses. *Proc. Natl. Acad. Sci. U. S. A.* 2006;103:12481-12486.
401. Li LF, Liu YY, Yang CT, Chien Y, Twu NF, Wang ML, Wang CY, Huang CC, Kao KC, Hsu HS, Wu CW, Chiou SH. Improvement of ventilator-induced lung injury by ips cell-derived conditioned medium via inhibition of pi3k/akt pathway and ip-10-dependent paracrine regulation. *Biomaterials* 2013;34:78-91.
402. He Z, Gao Y, Deng Y, Li W, Chen Y, Xing S, Zhao X, Ding J, Wang X. Lipopolysaccharide induces lung fibroblast proliferation through toll-like receptor 4 signaling and the phosphoinositide3-kinase-akt pathway. *PLoS One* 2012;7:e35926.
403. Faller S, Strosing KM, Ryter SW, Buerkle H, Loop T, Schmidt R, Hoetzel A. The volatile anesthetic isoflurane prevents ventilator-induced lung injury via phosphoinositide 3-kinase/akt signaling in mice. *Anesth Analg* 2012;114:747-756.

404. Meyer NJ, Huang Y, Singleton PA, Sammani S, Moitra J, Evenoski CL, Husain AN, Mitra S, Moreno-Vinasco L, Jacobson JR, Lussier YA, Garcia JG. Gadd45a is a novel candidate gene in inflammatory lung injury via influences on akt signaling. *FASEB J* 2009;23:1325-1337.
405. Kambara K, Ohashi W, Tomita K, Takashina M, Fujisaka S, Hayashi R, Mori H, Tobe K, Hattori Y. In vivo depletion of cd206(+) m2 macrophages exaggerates lung injury in endotoxemic mice. *Am J Pathol* 2015;185:162-171.
406. Grailer JJ, Haggadone MD, Sarma JV, Zetoune FS, Ward PA. Induction of m2 regulatory macrophages through the beta2-adrenergic receptor with protection during endotoxemia and acute lung injury. *J Innate Immun* 2014;6:607-618.
407. Hsiao HM, Sapinoro RE, Thatcher TH, Croasdell A, Levy EP, Fulton RA, Olsen KC, Pollock SJ, Serhan CN, Phipps RP, Sime PJ. A novel anti-inflammatory and pro-resolving role for resolvin d1 in acute cigarette smoke-induced lung inflammation. *PLoS One* 2013;8:e58258.
408. Zhou T, Garcia JG, Zhang W. Integrating micrornas into a system biology approach to acute lung injury. *Transl Res* 2011;157:180-190.
409. Xie T, Liang J, Liu N, Wang Q, Li Y, Noble PW, Jiang D. Microrna-127 inhibits lung inflammation by targeting igg fcgamma receptor i. *J Immunol* 2012;188:2437-2444.
410. Yehya N, Yerrapureddy A, Tobias J, Margulies SS. Microrna modulate alveolar epithelial response to cyclic stretch. *BMC Genomics* 2012;13:154.
411. Takaoka A, Yanai H, Kondo S, Duncan G, Negishi H, Mizutani T, Kano S, Honda K, Ohba Y, Mak TW, Taniguchi T. Integral role of irf-5 in the gene induction programme activated by toll-like receptors. *Nature* 2005;434:243-249.
412. Connor AJ, Laskin JD, Laskin DL. Ozone-induced lung injury and sterile inflammation. Role of toll-like receptor 4. *Exp. Mol. Pathol.* 2012;92:229-235.
413. Reino DC, Pisarenko V, Palange D, Doucet D, Bonitz RP, Lu Q, Colorado I, Sheth SU, Chandler B, Kannan KB, Ramanathan M, Xu da Z, Deitch EA, Feinman R. Trauma hemorrhagic shock-induced lung injury involves a gut-lymph-induced tlr4 pathway in mice. *PLoS One* 2011;6:e14829.
414. Krzyzaniak M, Cheadle G, Peterson C, Loomis W, Putnam J, Wolf P, Baird A, Eliceiri B, Bansal V, Coimbra R. Burn-induced acute lung injury requires a functional toll-like receptor 4. *Shock* 2011;36:24-29.
415. Hilberath JN, Carlo T, Pfeffer MA, Croze RH, Hastrup F, Levy BD. Resolution of toll-like receptor 4-mediated acute lung injury is linked to eicosanoids and suppressor of cytokine signaling 3. *FASEB journal : official publication of the Federation of American Societies for Experimental Biology* 2011;25:1827-1835.
416. Akira S, Uematsu S, Takeuchi O. Pathogen recognition and innate immunity. *Cell* 2006;124:783-801.
417. Sato S, Sugiyama M, Yamamoto M, Watanabe Y, Kawai T, Takeda K, Akira S. Toll/il-1 receptor domain-containing adaptor inducing ifn-beta (trif) associates with tnf receptor-associated factor 6 and tank-binding kinase 1, and activates two distinct transcription factors, nf-kappa b and ifn-regulatory factor-3, in the toll-like receptor signaling. *J Immunol* 2003;171:4304-4310.
418. Ouyang X, Negishi H, Takeda R, Fujita Y, Taniguchi T, Honda K. Cooperation between myd88 and trif pathways in tlr synergy via irf5 activation. *Biochem Biophys Res Commun* 2007;354:1045-1051.
419. Paun A, Bankoti R, Joshi T, Pitha PM, Stager S. Critical role of irf-5 in the development of t helper 1 responses to leishmania donovani infection. *PLoS Pathog* 2011;7:e1001246.

420. Krausgruber T, Blazek K, Smallie T, Alzabin S, Lockstone H, Sahgal N, Hussell T, Feldmann M, Udalova IA. Irf5 promotes inflammatory macrophage polarization and th1-th17 responses. *Nat Immunol* 2011;12:231-238.
421. Hou J, Wang P, Lin L, Liu X, Ma F, An H, Wang Z, Cao X. Microrna-146a feedback inhibits rig-i-dependent type i ifn production in macrophages by targeting traf6, irak1, and irak2. *J Immunol* 2009;183:2150-2158.
422. Tang Y, Luo X, Cui H, Ni X, Yuan M, Guo Y, Huang X, Zhou H, de Vries N, Tak PP, Chen S, Shen N. Microrna-146a contributes to abnormal activation of the type i interferon pathway in human lupus by targeting the key signaling proteins. *Arthritis Rheum* 2009;60:1065-1075.
423. O'Connell RM, Rao DS, Baltimore D. Microrna regulation of inflammatory responses. *Annu Rev Immunol* 2012;30:295-312.
424. Dai R, Phillips RA, Zhang Y, Khan D, Crasta O, Ahmed SA. Suppression of lps-induced interferon-gamma and nitric oxide in splenic lymphocytes by select estrogen-regulated microrna: A novel mechanism of immune modulation. *Blood* 2008;112:4591-4597.
425. Perske C, Lahat N, Sheffy Levin S, Bitterman H, Hemmerlein B, Rahat MA. Loss of inducible nitric oxide synthase expression in the mouse renal cell carcinoma cell line renca is mediated by microrna mir-146a. *Am J Pathol* 2010;177:2046-2054.
426. Zhang Y, Zhang M, Zhong M, Suo Q, Lv K. Expression profiles of mirnas in polarized macrophages. *Int J Mol Med* 2013;31:797-802.
427. El Gazzar M, Church A, Liu T, McCall CE. Microrna-146a regulates both transcription silencing and translation disruption of tnf-alpha during tlr4-induced gene reprogramming. *J Leukoc Biol* 2011;90:509-519.
428. Leek RD, Lewis CE, Whitehouse R, Greenall M, Clarke J, Harris AL. Association of macrophage infiltration with angiogenesis and prognosis in invasive breast carcinoma. *Cancer research* 1996;56:4625-4629.
429. Remensnyder JP, Majno G. Oxygen gradients in healing wounds. *The American journal of pathology* 1968;52:301-323.
430. Hunt TK, Knighton DR, Thakral KK, Goodson WH, 3rd, Andrews WS. Studies on inflammation and wound healing: Angiogenesis and collagen synthesis stimulated in vivo by resident and activated wound macrophages. *Surgery* 1984;96:48-54.
431. Igarashi M, Takeda Y, Mori S, Ishibashi N, Komatsu E, Takahashi K, Fuse T, Yamamura M, Sugiyama Y, Saito Y. Bayw6228 suppresses accumulation of macrophages in balloon-induced intimal thickening of rabbit carotid artery. *Atherosclerosis* 1997;128:251-254.
432. Raes G, Noel W, Beschin A, Brys L, de Baetselier P, Hassanzadeh GH. Fizz1 and ym as tools to discriminate between differentially activated macrophages. *Dev Immunol* 2002;9:151-159.
433. Raes G, De Baetselier P, Noel W, Beschin A, Brombacher F, Hassanzadeh Gh G. Differential expression of fizz1 and ym1 in alternatively versus classically activated macrophages. *Journal of leukocyte biology* 2002;71:597-602.
434. Martinez FO, Helming L, Gordon S. Alternative activation of macrophages: An immunologic functional perspective. *Annual review of immunology* 2009;27:451-483.
435. MacKinnon AC, Farnworth SL, Hodkinson PS, Henderson NC, Atkinson KM, Leffler H, Nilsson UJ, Haslett C, Forbes SJ, Sethi T. Regulation of alternative macrophage activation by galectin-3. *J Immunol* 2008;180:2650-2658.
436. Frisancho-Kiss S, Coronado MJ, Frisancho JA, Lau VM, Rose NR, Klein SL, Fairweather D. Gonadectomy of male balb/c mice increases tim-3(+) alternatively activated m2

macrophages, tim-3(+) t cells, th2 cells and treg in the heart during acute coxsackievirus-induced myocarditis. *Brain, behavior, and immunity* 2009;23:649-657.
437. Liu T, Jin H, Ullenbruch M, Hu B, Hashimoto N, Moore B, McKenzie A, Lukacs NW, Phan SH. Regulation of found in inflammatory zone 1 expression in bleomycin-induced lung fibrosis: Role of il-4/il-13 and mediation via stat-6. *J Immunol* 2004;173:3425-3431.
438. Wang H, Peters T, Kess D, Sindrilaru A, Oreshkova T, Van Rooijen N, Stratis A, Renkl AC, Sunderkotter C, Wlaschek M, Haase I, Scharffetter-Kochanek K. Activated macrophages are essential in a murine model for t cell-mediated chronic psoriasiform skin inflammation. *The Journal of clinical investigation* 2006;116:2105-2114.
439. Henderson NC, Mackinnon AC, Farnworth SL, Kipari T, Haslett C, Iredale JP, Liu FT, Hughes J, Sethi T. Galectin-3 expression and secretion links macrophages to the promotion of renal fibrosis. *The American journal of pathology* 2008;172:288-298.
440. Tripathi C, Tewari BN, Kanchan RK, Baghel KS, Nautiyal N, Shrivastava R, Kaur H, Bhatt ML, Bhadauria S. Macrophages are recruited to hypoxic tumor areas and acquire a pro-angiogenic m2-polarized phenotype via hypoxic cancer cell derived cytokines oncostatin m and eotaxin. *Oncotarget* 2014;5:5350-5368.
441. Teng X, Li D, Champion HC, Johns RA. Fizz1/relmalpha, a novel hypoxia-induced mitogenic factor in lung with vasoconstrictive and angiogenic properties. *Circ Res* 2003;92:1065-1067.
442. Leeper-Woodford SK, Detmer K. Acute hypoxia increases alveolar macrophage tumor necrosis factor activity and alters nf-kappab expression. *Am J Physiol* 1999;276:L909-916.
443. Acosta-Iborra B, Elorza A, Olazabal IM, Martin-Cofreces NB, Martin-Puig S, Miro M, Calzada MJ, Aragones J, Sanchez-Madrid F, Landazuri MO. Macrophage oxygen sensing modulates antigen presentation and phagocytic functions involving ifn-gamma production through the hif-1 alpha transcription factor. *J Immunol* 2009;182:3155-3164.
444. Albina JE, Henry WL, Jr., Mastrofrancesco B, Martin BA, Reichner JS. Macrophage activation by culture in an anoxic environment. *J Immunol* 1995;155:4391-4396.
445. Wiese M, Gerlach RG, Popp I, Matuszak J, Mahapatro M, Castiglione K, Chakravortty D, Willam C, Hensel M, Bogdan C, Jantsch J. Hypoxia-mediated impairment of the mitochondrial respiratory chain inhibits the bactericidal activity of macrophages. *Infect Immun* 2012;80:1455-1466.
446. Colegio OR, Chu NQ, Szabo AL, Chu T, Rhebergen AM, Jairam V, Cyrus N, Brokowski CE, Eisenbarth SC, Phillips GM, Cline GW, Phillips AJ, Medzhitov R. Functional polarization of tumour-associated macrophages by tumour-derived lactic acid. *Nature* 2014;513:559-563.
447. Cheng SC, Quintin J, Cramer RA, Shepardson KM, Saeed S, Kumar V, Giamarellos-Bourboulis EJ, Martens JH, Rao NA, Aghajanirefah A, Manjeri GR, Li Y, Ifrim DC, Arts RJ, van der Veer BM, Deen PM, Logie C, O'Neill LA, Willems P, van de Veerdonk FL, van der Meer JW, Ng A, Joosten LA, Wijmenga C, Stunnenberg HG, Xavier RJ, Netea MG. Mtor- and hif-1alpha-mediated aerobic glycolysis as metabolic basis for trained immunity. *Science* 2014;345:1250684.
448. Palsson-McDermott EM, Curtis AM, Goel G, Lauterbach MA, Sheedy FJ, Gleeson LE, van den Bosch MW, Quinn SR, Domingo-Fernandez R, Johnston DG, Jiang JK, Israelsen WJ, Keane J, Thomas C, Clish C, Vanden Heiden M, Xavier RJ, O'Neill LA. Pyruvate kinase m2 regulates hif-1alpha activity and il-1beta induction and is a critical determinant of the warburg effect in lps-activated macrophages. *Cell Metab* 2015;21:65-80.

449. Leeper-Woodford SK, Detmer K. Acute hypoxia increases alveolar macrophage tumor necrosis factor activity and alters nf-kappab expression. *The American journal of physiology* 1999;276:L909-916.
450. Acosta-Iborra B, Elorza A, Olazabal IM, Martin-Cofreces NB, Martin-Puig S, Miro M, Calzada MJ, Aragones J, Sanchez-Madrid F, Landazuri MO. Macrophage oxygen sensing modulates antigen presentation and phagocytic functions involving ifn-gamma production through the hif-1 alpha transcription factor. *J Immunol* 2009;182:3155-3164.
451. Steiner MK, Syrkina OL, Kolliputi N, Mark EJ, Hales CA, Waxman AB. Interleukin-6 overexpression induces pulmonary hypertension. *Circulation research* 2009;104:236-244, 228p following 244.
452. Daley E, Emson C, Guignabert C, de Waal Malefyt R, Louten J, Kurup VP, Hogaboam C, Taraseviciene-Stewart L, Voelkel NF, Rabinovitch M, Grunig E, Grunig G. Pulmonary arterial remodeling induced by a th2 immune response. *The Journal of experimental medicine* 2008;205:361-372.
453. Tang H, Chen J, Fraidenburg DR, Song S, Sysol JR, Drennan AR, Offermanns S, Ye RD, Bonini MG, Minshall RD, Garcia JG, Machado RF, Makino A, Yuan JX. Deficiency of akt1, but not akt2, attenuates the development of pulmonary hypertension. *Am J Physiol Lung Cell Mol Physiol* 2015;308:L208-220.
454. Christmann RB, Hayes E, Pendergrass S, Padilla C, Farina G, Affandi AJ, Whitfield ML, Farber HW, Lafyatis R. Interferon and alternative activation of monocyte/macrophages in systemic sclerosis-associated pulmonary arterial hypertension. *Arthritis Rheum* 2011;63:1718-1728.
455. Kolosionek E, King J, Rollinson D, Schermuly RT, Grimminger F, Graham BB, Morrell N, Butrous G. Schistosomiasis causes remodeling of pulmonary vessels in the lung in a heterogeneous localized manner: Detailed study. *Pulm Circ* 2013;3:356-362.
456. Xu W, Kaneko FT, Zheng S, Comhair SA, Janocha AJ, Goggans T, Thunnissen FB, Farver C, Hazen SL, Jennings C, Dweik RA, Arroliga AC, Erzurum SC. Increased arginase ii and decreased no synthesis in endothelial cells of patients with pulmonary arterial hypertension. *Faseb J* 2004;18:1746-1748.
457. Durante W, Liao L, Reyna SV, Peyton KJ, Schafer AI. Transforming growth factor-beta(1) stimulates l-arginine transport and metabolism in vascular smooth muscle cells: Role in polyamine and collagen synthesis. *Circulation* 2001;103:1121-1127.
458. Jin Y, Calvert TJ, Chen B, Chicoine LG, Joshi M, Bauer JA, Liu Y, Nelin LD. Mice deficient in mkp-1 develop more severe pulmonary hypertension and greater lung protein levels of arginase in response to chronic hypoxia. *Am J Physiol Heart Circ Physiol* 2010;298:H1518-1528.
459. Durante W. Role of arginase in vessel wall remodeling. *Front Immunol* 2013;4:111.
460. Nara A, Nagai H, Shintani-Ishida K, Ogura S, Shimosawa T, Kuwahira I, Shirai M, Yoshida KI. Pulmonary arterial hypertension in rats due to age-related arginase activation in intermittent hypoxia. *Am J Respir Cell Mol Biol* 2014.
461. Trittmann JK, Nelin LD, Zmuda EJ, Gastier-Foster JM, Chen B, Backes CH, Frick J, Vaynshtok P, Vieland VJ, Klebanoff MA. Arginase i gene single-nucleotide polymorphism is associated with decreased risk of pulmonary hypertension in bronchopulmonary dysplasia. *Acta Paediatr* 2014;103:e439-443.
462. Yamaji-Kegan K, Su Q, Angelini DJ, Champion HC, Johns RA. Hypoxia-induced mitogenic factor has proangiogenic and proinflammatory effects in the lung via vegf and vegf receptor-2. *Am J Physiol Lung Cell Mol Physiol* 2006;291:L1159-1168.

463. Angelini DJ, Su Q, Yamaji-Kegan K, Fan C, Teng X, Hassoun PM, Yang SC, Champion HC, Tuder RM, Johns RA. Resistin-like molecule-beta in scleroderma-associated pulmonary hypertension. *Am J Respir Cell Mol Biol* 2009;41:553-561.
464. Teng X, Li D, Champion HC, Johns RA. Fizz1/relmalpha, a novel hypoxia-induced mitogenic factor in lung with vasoconstrictive and angiogenic properties. *Circulation research* 2003;92:1065-1067.
465. Angelini DJ, Su Q, Yamaji-Kegan K, Fan C, Skinner JT, Champion HC, Crow MT, Johns RA. Hypoxia-induced mitogenic factor (himf/fizz1/relmalpha) induces the vascular and hemodynamic changes of pulmonary hypertension. *American journal of physiology* 2009;296:L582-593.
466. Yamaji-Kegan K, Takimoto E, Zhang A, Weiner NC, Meuchel LW, Berger AE, Cheadle C, Johns RA. Hypoxia-induced mitogenic factor (fizz1/relmalpha) induces endothelial cell apoptosis and subsequent interleukin-4-dependent pulmonary hypertension. *Am J Physiol Lung Cell Mol Physiol* 2014;306:L1090-1103.
467. Angelini DJ, Su Q, Yamaji-Kegan K, Fan C, Skinner JT, Champion HC, Crow MT, Johns RA. Hypoxia-induced mitogenic factor (himf/fizz1/relmalpha) induces the vascular and hemodynamic changes of pulmonary hypertension. *Am J Physiol Lung Cell Mol Physiol* 2009;296:L582-593.
468. Steppan CM, Brown EJ, Wright CM, Bhat S, Banerjee RR, Dai CY, Enders GH, Silberg DG, Wen X, Wu GD, Lazar MA. A family of tissue-specific resistin-like molecules. *Proc Natl Acad Sci U S A* 2001;98:502-506.
469. Liu T, Jin H, Ullenbruch M, Hu B, Hashimoto N, Moore B, McKenzie A, Lukacs NW, Phan SH. Regulation of found in inflammatory zone 1 expression in bleomycin-induced lung fibrosis: Role of il-4/il-13 and mediation via stat-6. *J Immunol* 2004;173:3425-3431.
470. Angelini DJ, Su Q, Kolosova IA, Fan C, Skinner JT, Yamaji-Kegan K, Collector M, Sharkis SJ, Johns RA. Hypoxia-induced mitogenic factor (himf/fizz1/relm alpha) recruits bone marrow-derived cells to the murine pulmonary vasculature. *PLoS One* 2010;5:e11251.
471. Otterbein LE, Mantell LL, Choi AM. Carbon monoxide provides protection against hyperoxic lung injury. *The American journal of physiology* 1999;276:L688-694.
472. Sarady JK, Otterbein SL, Liu F, Otterbein LE, Choi AM. Carbon monoxide modulates endotoxin-induced production of granulocyte macrophage colony-stimulating factor in macrophages. *American journal of respiratory cell and molecular biology* 2002;27:739-745.
473. Zuckerbraun BS, Chin BY, Wegiel B, Billiar TR, Czsimadia E, Rao J, Shimoda L, Ifedigbo E, Kanno S, Otterbein LE. Carbon monoxide reverses established pulmonary hypertension. *The Journal of experimental medicine* 2006;203:2109-2119.
474. Vitali SH, Mitsialis SA, Christou H, Fernandez-Gonzalez A, Liu X, Kourembanas S. Mechanisms of heme oxygenase-1-mediated cardiac and pulmonary vascular protection in chronic hypoxia: Roles of carbon monoxide and bilirubin. *Chest* 2005;128:578S-579S.
475. Lee TS, Chau LY. Heme oxygenase-1 mediates the anti-inflammatory effect of interleukin-10 in mice. *Nature medicine* 2002;8:240-246.
476. Weis N, Weigert A, von Knethen A, Brune B. Heme oxygenase-1 contributes to an alternative macrophage activation profile induced by apoptotic cell supernatants. *Molecular biology of the cell* 2009;20:1280-1288.
477. Devey L, Ferenbach D, Mohr E, Sangster K, Bellamy CO, Hughes J, Wigmore SJ. Tissue-resident macrophages protect the liver from ischemia reperfusion injury via a heme oxygenase-1-dependent mechanism. *Mol Ther* 2009;17:65-72.

478. Sica A, Bronte V. Altered macrophage differentiation and immune dysfunction in tumor development. *The Journal of clinical investigation* 2007;117:1155-1166.
479. George JF, Braun A, Brusko TM, Joseph R, Bolisetty S, Wasserfall CH, Atkinson MA, Agarwal A, Kapturczak MH. Suppression by cd4+cd25+ regulatory t cells is dependent on expression of heme oxygenase-1 in antigen-presenting cells. *The American journal of pathology* 2008;173:154-160.
480. Xia ZW, Zhong WW, Xu LQ, Sun JL, Shen QX, Wang JG, Shao J, Li YZ, Yu SC. Heme oxygenase-1-mediated cd4+cd25high regulatory t cells suppress allergic airway inflammation. *J Immunol* 2006;177:5936-5945.
481. Xia ZW, Xu LQ, Zhong WW, Wei JJ, Li NL, Shao J, Li YZ, Yu SC, Zhang ZL. Heme oxygenase-1 attenuates ovalbumin-induced airway inflammation by up-regulation of foxp3 t-regulatory cells, interleukin-10, and membrane-bound transforming growth factor- 1. *The American journal of pathology* 2007;171:1904-1914.
482. Lee TS, Chau LY. Heme oxygenase-1 mediates the anti-inflammatory effect of interleukin-10 in mice. *Nat Med* 2002;8:240-246.
483. Drechsler Y, Dolganiuc A, Norkina O, Romics L, Li W, Kodys K, Bach FH, Mandrekar P, Szabo G. Heme oxygenase-1 mediates the anti-inflammatory effects of acute alcohol on il-10 induction involving p38 mapk activation in monocytes. *J Immunol* 2006;177:2592-2600.
484. Sierra-Filardi E, Vega MA, Sanchez-Mateos P, Corbi AL, Puig-Kroger A. Heme oxygenase-1 expression in m-csf-polarized m2 macrophages contributes to lps-induced il-10 release. *Immunobiology* 2010;215:788-795.
485. Naito Y, Takagi T, Higashimura Y. Heme oxygenase-1 and anti-inflammatory m2 macrophages. *Arch Biochem Biophys* 2014;564:83-88.
486. Weis N, Weigert A, von Knethen A, Brune B. Heme oxygenase-1 contributes to an alternative macrophage activation profile induced by apoptotic cell supernatants. *Mol Biol Cell* 2009;20:1280-1288.
487. Jadhav A, Tiwari S, Lee P, Ndisang JF. The heme oxygenase system selectively enhances the anti-inflammatory macrophage-m2 phenotype, reduces pericardial adiposity, and ameliorated cardiac injury in diabetic cardiomyopathy in zucker diabetic fatty rats. *J Pharmacol Exp Ther* 2013;345:239-249.
488. Tu TH, Joe Y, Choi HS, Chung HT, Yu R. Induction of heme oxygenase-1 with hemin reduces obesity-induced adipose tissue inflammation via adipose macrophage phenotype switching. *Mediators Inflamm* 2014;2014:290708.
489. Harusato A, Naito Y, Takagi T, Uchiyama K, Mizushima K, Hirai Y, Higashimura Y, Katada K, Handa O, Ishikawa T, Yagi N, Kokura S, Ichikawa H, Muto A, Igarashi K, Yoshikawa T. Btb and cnc homolog 1 (bach1) deficiency ameliorates tnbs colitis in mice: Role of m2 macrophages and heme oxygenase-1. *Inflamm Bowel Dis* 2013;19:740-753.
490. Zhang B, Ma Y, Guo H, Sun B, Niu R, Ying G, Zhang N. Akt2 is required for macrophage chemotaxis. *Eur J Immunol* 2009;39:894-901.
491. Chen J, Tang H, Hay N, Xu J, Ye RD. Akt isoforms differentially regulate neutrophil functions. *Blood* 2010;115:4237-4246.
492. DeVincenzo J, Lambkin-Williams R, Wilkinson T, Cehelsky J, Nochur S, Walsh E, Meyers R, Gollob J, Vaishnaw A. A randomized, double-blind, placebo-controlled study of an rnai-based therapy directed against respiratory syncytial virus. *Proc Natl Acad Sci U S A* 2010;107:8800-8805.
493. Akhtar S, Benter IF. Nonviral delivery of synthetic sirnas in vivo. *J Clin Invest* 2007;117:3623-3632.

PUBLICATIONS

Early Macrophage Recruitment and Alternative Activation Are Critical for the Later Development of Hypoxia-Induced Pulmonary Hypertension

Eleni Vergadi, Mun Seog Chang, Changjin Lee, Olin D. Liang, Xianlan Liu, Angeles Fernandez-Gonzalez, S. Alex Mitsialis and Stella Kourembanas

Circulation. 2011;123:1986-1995; originally published online April 25, 2011;
doi: 10.1161/CIRCULATIONAHA.110.978627
Circulation is published by the American Heart Association, 7272 Greenville Avenue, Dallas, TX 75231

Print ISSN: 0009-7322. Online ISSN: 1524-4539

Early Macrophage Recruitment and Alternative Activation Are Critical for the Later Development of Hypoxia-Induced Pulmonary Hypertension

Eleni Vergadi, MD*; Mun Seog Chang, PhD*; Changjin Lee, PhD; Olin D. Liang, PhD; Xianlan Liu, MS; Angeles Fernandez-Gonzalez, PhD; S. Alex Mitsialis, PhD†; Stella Kourembanas, MD†

Background—Lung inflammation precedes the development of hypoxia-induced pulmonary hypertension (HPH); however, its role in the pathogenesis of HPH is poorly understood. We sought to characterize the hypoxic inflammatory response and to elucidate its role in the development of HPH. We also aimed to investigate the mechanisms by which heme oxygenase-1, an anti-inflammatory enzyme, is protective in HPH.

Methods and Results—We generated bitransgenic mice that overexpress human heme oxygenase-1 under doxycycline control in an inducible, lung-specific manner. Hypoxic exposure of mice in the absence of doxycycline resulted in early transient accumulation of monocytes/macrophages in the bronchoalveolar lavage. Alveolar macrophages acquired an alternatively activated phenotype (M2) in response to hypoxia, characterized by the expression of found in inflammatory zone-1, arginase-1, and chitinase-3-like-3. A brief 2-day pulse of doxycycline delayed, but did not prevent, the peak of hypoxic inflammation, and could not protect against HPH. In contrast, a 7-day doxycycline treatment sustained high heme oxygenase-1 levels during the entire period of hypoxic inflammation, inhibited macrophage accumulation and activation, induced macrophage interleukin-10 expression, and prevented the development of HPH. Supernatants from hypoxic M2 macrophages promoted the proliferation of pulmonary artery smooth muscle cells, whereas treatment with carbon monoxide, a heme oxygenase-1 enzymatic product, abrogated this effect.

Conclusions—Early recruitment and alternative activation of macrophages in hypoxic lungs are critical for the later development of HPH. Heme oxygenase-1 may confer protection from HPH by effectively modifying the macrophage activation state in hypoxia. **(*Circulation*. 2011;123:1986-1995.)**

Key Words: heme oxygenase-1 ■ hypertension, pulmonary ■ hypoxia ■ macrophage activation ■ inflammation

Pulmonary arterial hypertension (PAH) is a devastating disease characterized by vasoconstriction and vascular wall remodeling with resultant right ventricular hypertrophy and eventual failure. Despite significant progress in this field, the mechanisms underlying the development of PAH are still obscure. Recently, in an increasing number of studies, lung inflammation has been implicated as a potential maladaptation underlying the development of PAH. Infiltrates of leukocytes and inflammatory mediators have been detected in patients with PAH,[1–3] and have been reported to contribute to pulmonary vascular remodeling in animal models of disease.[4–6] Tissue hypoxia, a well-known stimulus for pulmonary hypertension, has also been demonstrated by our group and others to induce an inflammatory response that precedes the development of hypoxia-induced pulmonary hypertension (HPH).[7–9]

Clinical Perspective on p 1995

Among the inflammatory cells implicated in PAH, those of the monocyte/macrophage lineage have been correlated with disease more often.[1,2,8–10] However, macrophages efficiently respond to environmental signals with remarkable plasticity and undergo different forms of polarized activation that can be roughly categorized as classically activated (M1), alternatively activated (M2), and anti-inflammatory (regulatory) macrophages.[11,12] Classically activated macrophages are effector phagocytes activated by interferon-γ and tumor necrosis factor (TNF-α). They produce inducible nitric oxide synthase and interleukin (IL)-12 and exhibit enhanced microbicidal or tumoricidal capacity.[11] On the other hand, M2-polarized macrophages are activated mostly by IL-4 or IL-13, and, as recently discovered, by CCL2 and IL-6,[13] and they

Received July 21, 2010; accepted February 24, 2011.

From the Division of Newborn Medicine, Children's Hospital Boston, Harvard Medical School, Boston, MA (E.V., M.S.C., C.L., O.D.L., X.L., A.F.-G., S.A.M., S.K.); and Department of Prescriptionology, College of Oriental Medicine, Kyung Hee University, Seoul, Korea (M.S.C.).

Guest Editor for this article was Jeffrey R. Bender, MD.

*Drs Vergadi and Chang contributed equally to this article.

†Drs Mitsialis and Kourembanas contributed equally to this article as senior authors.

The online-only Data Supplement is available with this article at http://circ.ahajournals.org/cgi/content/full/CIRCULATIONAHA.110.978627/DC1.

Correspondence to Stella Kourembanas, Division of Newborn Medicine, Children's Hospital Boston, 300 Longwood Ave, Boston, MA 02115. E-mail stella.kourembanas@childrens.harvard.edu

Circulation **is available at http://circ.ahajournals.org** **DOI: 10.1161/CIRCULATIONAHA.110.978627**

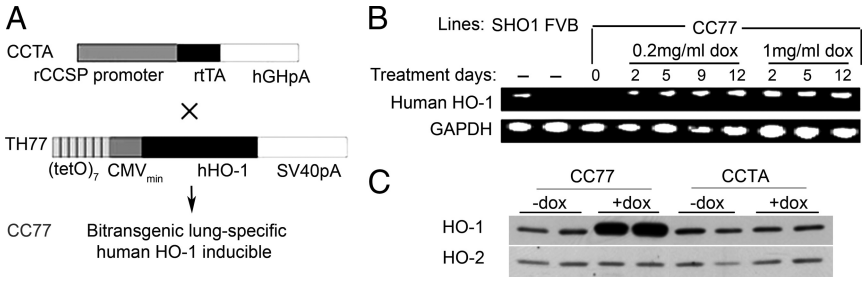

Figure 1. Lung-specific, doxycycline (dox)-regulated expression of human heme oxygenase-1 (HO-1). **A,** Bitransgenic mice were generated by crossing lines CCTA and TH77. CCTA harbors the reverse tetracycline transactivator (rtTA) under the control of the 2.3-kb rat Clara cells secretory protein (CCSP) promoter. TH77 harbors a human HO-1 (hHO-1) transgene under the control of 7 copies of the tet operator linked to a minimal cytomegalovirus (CMV) promoter. **B,** Bitransgenic mice (CC77) were treated with 0.2 or 1 mg/mL dox in the drinking water for 2 to 12 days, and semiquantitative polymerase chain reaction analysis on total lung RNA for hHO1 and the housekeeping gene, GADPH, is depicted. The SHO1 (transgenics constitutively expressing hHO-1 in lung epithelium) and FVB (wild-type) mouse strains served as positive and negative controls, respectively. The primers used target a divergent region on HO-1 mRNA and do not amplify endogenous murine HO-1 transcripts. **C,** Western Blot analysis of HO-1 protein in total lung extracts of CC77 and CCTA mice. Note that the antibody used detects both the dox-regulated human HO-1 and the endogenous murine HO-1. Heme oxygenase-2 (HO-2) was used as an internal control.

express arginase-1 (Arg-1), found in inflammatory zone-1 (Fizz1), chitinase-3-like-3 (Ym1), and mannose receptor, C type lectin-1.[11,12,14] M2 macrophages have been implicated in the pathogenesis of lung and other disorders via their ability to promote trophic, profibrotic, and angiogenic functions.[15,16] The major characteristic of the third population, regulatory macrophages, is the production of high IL-10 and low IL-12 levels and the promotion of immunosuppression.[11,14] In the case of PAH, the activation state of the recruited macrophages and their contribution to disease has remained unclear until now.

Heme oxygenase-1 (HO-1) is a major antioxidant and cytoprotective enzyme that catalyzes the degradation of heme to 3 enzymatic end products: carbon monoxide (CO), free Fe^{2+}, and biliverdin.[17] Heme oxygenase-1 and its enzymatic product, CO, have been reported by our group and others to be protective in HPH.[7,18–20] This protection, up to now, has been attributed mainly to the relaxation of vascular tone and inhibition of vascular smooth muscle cell proliferation by CO.[21] However, it has been demonstrated that HO-1[7,17,22,23] and CO[24,25] have potent anti-inflammatory properties, some of which may be exerted via the upregulation of the anti-inflammatory cytokine IL-10.[25,26] Moreover, HO-1–deficient mice develop a chronic oxidative inflammatory state that progresses with age[27] and have a maladaptive response to hypoxia with right ventricular dilation, fibrosis, and inflammation.[18,28] Therefore, we hypothesized that immunomodulation is a key mechanism of HO-1 protection in PAH.

To characterize in detail the lung inflammatory response caused by hypoxia, to assess its role in pulmonary hypertension, and to investigate the protective properties of HO-1 in this context, we generated a bitransgenic mouse model with doxycycline-inducible, lung-specific expression of HO-1. We report here that hypoxic exposure in the absence of doxycycline provoked a significant monocyte/macrophage accumulation in the bronchoalveolar lavage fluid (BALF) that manifested a phenotype consistent with alternative activation, with upregulated expression of Fizz1, Arg1, Ym1, and mannose receptor, C type lectin-1. Heme oxygenase-1 overexpression by doxycycline treatment inhibited hypoxic macrophage recruitment and activation and resulted in upregulation of IL-10 in macrophages. Supernatants from hypoxic cultures of M2 macrophages promoted proliferation of pulmonary artery smooth muscle cells, whereas CO treatment abrogated this effect. By modulating the timing and duration of HO-1 expression with doxycycline, we were able to either delay or suppress lung inflammation and macrophage activation and, in the latter case, abolish HPH.

Methods

Bitransgenic mice were generated by crossing Balb/c transgenic mice that harbor the tetracycline transcriptional activator (tetON system) under the control of the Clara cell secretory protein promoter with FVB transgenic mice that carry the human HO-1 (hHO-1) transgene under the control of the tetracycline response element (Figure 1A). Expression of hHO-1 in the lung was achieved by the addition of 1 mg/mL doxycycline to the drinking water. The CCTA mouse line that lacks the hHO-1 transgene was treated with doxycycline and served as control to eliminate any potential effects imparted by doxycycline itself independently of hHO-1. All animal procedures were approved by the Children's Hospital Boston Animal Care and Use Committee. An expanded Methods section is available in the online-only Data Supplement.

Statistical Analysis

All values are expressed as mean±SD. Comparison of results between different groups was performed by 1-way ANOVA or Mann-Whitney *U* test when appropriate with GraphPad InStat (GraphPad Software, San Diego, CA). Values of $P<0.05$ were considered significant.

Results

Lung-Specific, Inducible Expression of Human Heme Oxygenase-1

Based on the design of the bitransgenic model (designated CC77; Figure 1A), the hHO-1 transgene is under the control of both doxycycline and the Clara cell secretory protein promoter and therefore is inducibly expressed in the lung epithelium. Semiquantitative polymerase chain reaction analysis on total lung RNA with hHO1-specific primers indicates that hHO-1 levels were upregulated with doxycycline treat-

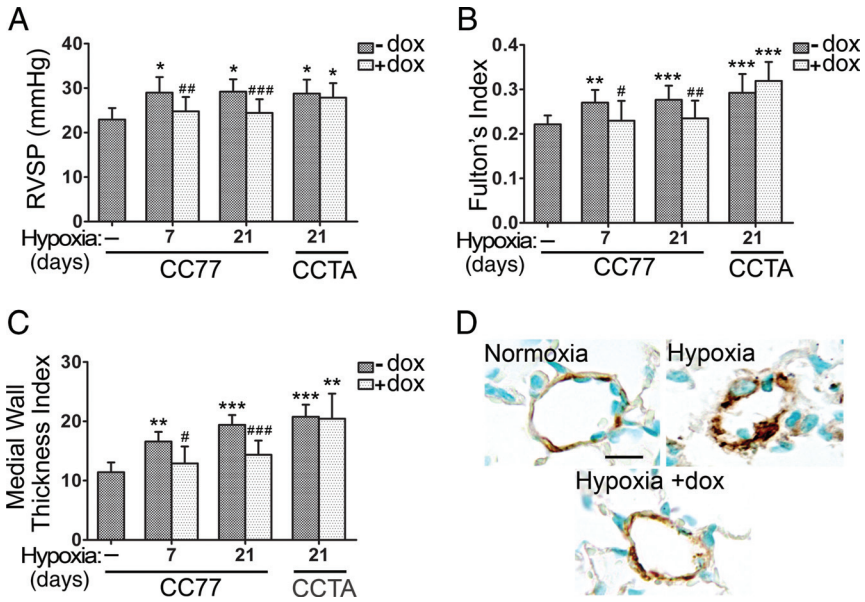

Figure 2. Sustained expression of heme oxygenase-1 (HO-1) prevents hypoxia-induced pulmonary hypertension. Right ventricular systolic pressure (RVSP; **A**), the Fulton Index (**B**), and the medial wall thickness index (**C**) were determined at the indicated times of hypoxic exposure in the presence or absence of 1 mg/mL doxycycline (dox) in the drinking water of CC77 and CCTA mice. **D,** Representative images of vascular remodeling in lung sections of mice exposed to hypoxia for 21 days and stained for α-smooth muscle actin. CC77 mice are bitransgenic mice (Clara cell secretory protein–reverse tetracycline transactivator [CCSP-rtTA]×TH77). CCTA mice are transgenic mice lacking HO-1 (CCSP-rtTA). Numbers represent mean±SD; n≥6 per group. Scale bar=25 μm. *P<0.05, **P<0.01, ***P<0.001 relative to normoxia; #P<0.05, ##P<0.01, ###P<0.001 relative to hypoxia-dox.

ment in a dose-dependent manner but remained undetectable in the absence of doxycycline (Figure 1B). Using an antibody that detects both human and murine HO-1, we detected profoundly elevated protein levels of HO-1 in the lungs of doxycycline-treated CC77 mice but not in CCTA mice (Figure 1C).

Sustained Induction of Heme Oxygenase-1 Prevents Hypoxia-Induced Pulmonary Hypertension

The development of PAH in our model was assessed by the measurement of right ventricular systolic pressure, the Fulton Index, and the medial wall thickness index. The Fulton Index, the ratio of right ventricle weight to left ventricle plus septum weight, represents a hallmark of right ventricular hypertrophy resulting from increased right ventricle pressure afterload. The medial wall thickness index was estimated from the histological sections of pulmonary arterioles stained with α-smooth muscle actin. Right ventricular systolic pressure, the Fulton Index, and the medial wall thickness index were significantly elevated as early as 7 days of hypoxia in both bitransgenics (CC77) and controls (CCTA) (Figure 2A through 2C). Doxycycline administration for the entire course of hypoxia prevented the increase in right ventricular systolic pressure, the Fulton Index, and the medial wall thickness index in the bitransgenic mice but not in the controls (Figure 2).

Immunostaining of pulmonary arterioles for α-smooth muscle actin revealed thickened and remodeled medial vascular walls in lung sections of hypoxic mice. This pathology was absent in hypoxic mice treated with doxycycline (Figure 2D).

Hypoxia Induces Monocyte/Macrophage Infiltration and Lung Cytokine Production That Is Ameliorated by Heme Oxygenase-1 and its Enzymatic Product, Carbon Monoxide

To track the inflammatory response at the initial stages of hypoxic exposure and before the development of hypertension, animals were exposed to hypoxia, and a temporal profile of the cell content in BALF was performed. More than 95% of the isolated BALF cells were CD45-positive leukocytes (Figure IA in the online-only Data Supplement). The cells expressing the macrophage-specific cell surface antigens F4/80 and CD11c remained the predominant population (>98%) regardless of hypoxic exposure or doxycycline treatment (Figure IB in the online-only Data Supplement and Figure 3A). Under these conditions, only a subtle increase in BALF neutrophils and T lymphocytes was observed (data not shown). When hypoxic exposure was begun, the numbers of monocytes/macrophages were significantly increased in the BALF of control hypoxic mice, reaching a peak at 2 days of hypoxia and dropping significantly by 7 days but remaining slightly elevated compared with normoxic animals (Figure 3B). Doxycycline administration had a suppressive effect on the accumulation of cells at all time intervals investigated (Figure 3B). Doxycycline treatment of the control mice (CCTA) had no impact on monocyte/macrophage accumulation, establishing that inhibition of cell infiltrate is due specifically to HO-1 overexpression and is not an artifact of doxycycline treatment (Figure 3C).

To identify the specific enzymatic product of HO-1, CO, and/or biliverdin that is responsible for suppressing the peak of inflammation at 2 days of hypoxia, we exposed animals to intermittent inhalation of CO (250 ppm for 1 hour twice a day) and/or biliverdin injections (50 μmol/kg IP twice a day). Intraperitoneal PBS injections served as control. Inhaled CO or CO plus biliverdin, but not biliverdin alone, was effective in inhibiting the inflammatory cell infiltrate in the BALF at levels comparable to doxycycline treatment (Figure 3C).

In addition to the accumulation of macrophages, several cytokines/chemokines were upregulated in the BALF of hypoxic mice (Figure II in the online-only Data Supplement). In as early as 2 and 4 days of hypoxia, upregulation of fibroblast growth factor β, IL-1β, macrophage inflammatory

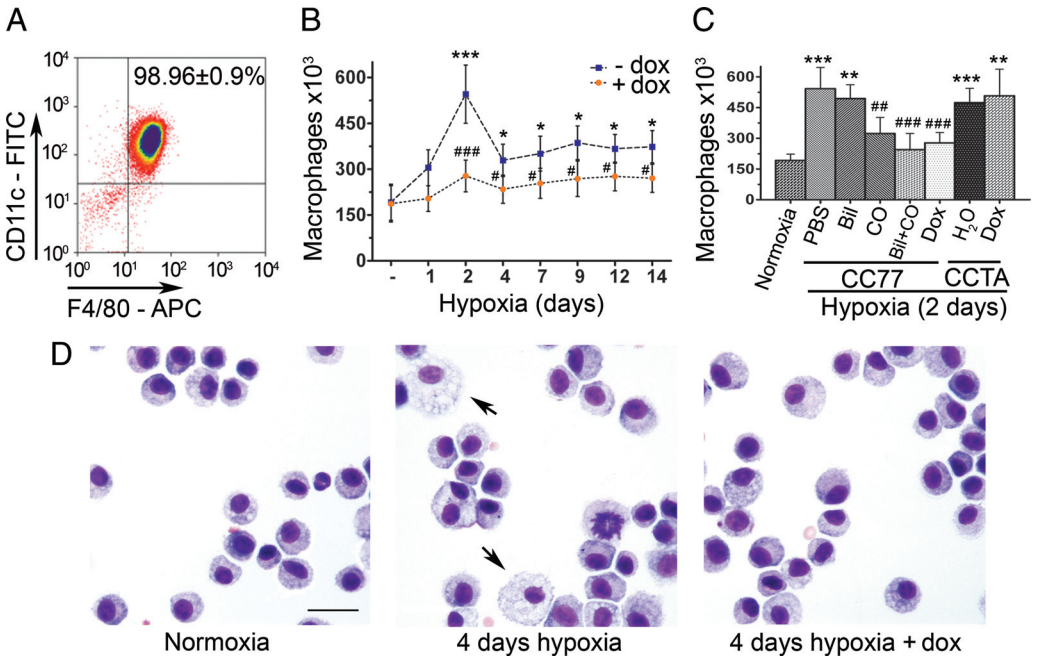

Figure 3. Hypoxia induces early monocyte/macrophage infiltration in the lungs that is ameliorated by heme oxygenase-1 (HO-1). **A,** Flow cytometric analysis of $CD45^+$ leukocytes isolated from bronchoalveolar lavage fluid (BALF) demonstrates expression of CD11c and F4/80 macrophage markers (≈98%). **B,** Accumulation of monocytes/macrophages ($CD11c^+$, $F4/80^+$) is depicted over time in the BALF of hypoxic mice in the absence (−) or presence (+) of 1 mg/mL doxycycline (dox) in the drinking water. **C,** Doxycycline treatment suppressed the hypoxia-induced 2-day peak of macrophage accumulation in the BALF of CC77 mice but not in the CCTA controls. The effect of the HO-1 products (intraperitoneal biliverdin [Bil], inhaled CO, and Bil+CO combined) on macrophage accumulation is also shown. **D,** Morphological alteration of a population of BALF-isolated macrophages is observed within 4 days of hypoxia in untreated mice, a phenotype absent in dox-treated mice. Numbers represent mean±SD; n ≥6 mice per group. Scale bar=25 μm. *$P<0.05$, **$P<0.01$, ***$P<0.001$ relative to normoxia; #$P<0.05$, ##$P<0.01$, ###$P<0.001$ relative to hypoxia-dox.

protein-1α, IL-17, and IL-2, as well as of Th2-related cytokines IL-13 and IL-4, was observed. The Th1-related cytokines, IL-12, and TNF-α remained unaffected (Figure II in the online-only Data Supplement), and interferon-γ levels were undetectable (not shown). Doxycycline administration effectively suppressed fibroblast growth factor-β, IL-1β, macrophage inflammatory protein-1α, and IL-2 at both 2 and 4 days of hypoxia and suppressed IL-17, IL-13, and IL-4 only after 4 days of continuous administration (Figure II in the online-only Data Supplement).

Interestingly, a striking alteration of macrophage morphology in cytospin preparations of BALF-isolated macrophages was observed at 4 days of hypoxia, characterized by cytoplasmic enlargement in a population of cells. This phenotype is consistent with activation and was not detected in any of the macrophages isolated from doxycycline-treated mice (Figure 3D).

Hypoxia Induces Alternative Activation of Macrophages: Suppressive Effect of Heme Oxygenase-1

The observation that macrophage morphology was altered in response to hypoxia led us to further investigate the potential activation state of hypoxic macrophages. Quantitative polymerase chain reaction analysis of BALF-isolated alveolar macrophages from CC77 bitransgenic mice revealed an induction of well-defined markers of M2 macrophages in hypoxic mice, including Arg1, Fizz1, Ym1 (Figure 4A), and mannose receptor, C type lectin-1 (data not shown). The peak expression occurred at 4 days of hypoxia and remained upregulated for at least 14 days. In addition, Fizz1 was secreted in the BALF of hypoxic mice (Figure 4B). In contrast, there was no change in the mRNA levels of markers of M1 macrophage phenotype such as inducible nitric oxide synthase, TNF-α, and IL-12β (IL-12p40) or the costimulatory molecules, CD80/86, essential in the process of antigen presentation (Figure III in the online-only Data Supplement). Urea production, indicative of arginase activity, was also upregulated in in vivo hypoxic alveolar macrophages (Figure 4C); this increase in enzymatic activity was due to Arg1 because Arg1 mRNA levels were induced 9.1±3.4-fold after 4 days of hypoxic exposure, whereas Arg2 mRNA levels were 0.6±0.1 of their normoxic value at this time point. Inducible nitric oxide synthase activity, as assessed by nitrite and nitrate production in the BALF, remained unchanged (Figure 4D). Doxycycline administration effectively suppressed all markers of alternative activation (Figure 4A through 4C), whereas these markers were not suppressed in the CCTA line treated with doxycycline (Figure 4B and 4C and Figure IVA in the online-only Data Supplement). Immunostaining revealed that 10.8±2.7% ($35.5\pm8.9\times10^3$, mean±SD) of the macrophages were Fizz1 positive, whereas in the presence of doxycycline, this number was reduced to 2.17±0.6% ($5.1\pm1.4\times10^3$, mean± SD; $P<0.01$; Figure 5A). Immunofluorescent staining confirmed the localization of Fizz1 and the absence of inducible nitric oxide synthase in the cytoplasm of hypoxic macrophages (Figure 5B and 5C).

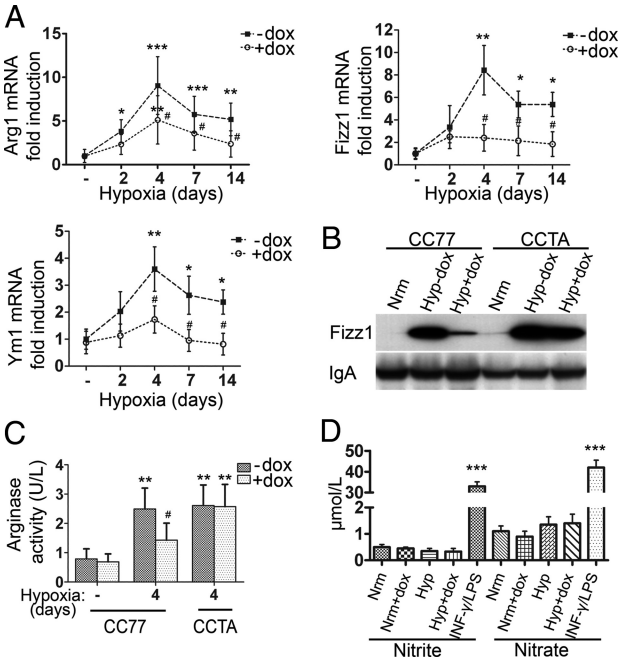

Figure 4. Hypoxia induces alternatively activated macrophages: the suppressive effect of heme oxygenase-1 (HO-1). **A,** Quantitative polymerase chain reaction analysis of hypoxic alveolar macrophage mRNA isolated from bitransgenic mice (CC77) revealed increased found in inflammatory zone-1 (Fizz1), arginase-1 (Arg1), and chitinase-3-like-3 (Ym1) levels that were suppressed with doxycycline (dox). **B,** Western blot analysis for Fizz1 on bronchoalveolar lavage fluid (BALF) from normoxic mice (Nrm) and mice exposed to hypoxia for 4 days−dox (Hyp-dox) or with dox treatment (Hyp+dox); IgA served as internal control. **C,** Arginase activity (U/L) was assessed by urea formation in alveolar macrophages from normoxic and hypoxic animals. **D,** Inducible nitric oxide synthase activity was estimated by the levels of nitrite and nitrate in the BALF of hypoxic mice. Supernatants from RAW 264.7 macrophages stimulated with 100 μg/mL lipopolysaccharide (LPS) *Escherichia coli* and 100 U/mL interferon-γ (INF-γ) for 48 hours served as positive controls. Mean±SD is depicted for n≥6 mice per group. *P<0.05, **P<0.01, ***P<0.001 relative to normoxia; #P<0.05, ##P<0.01, ###P<0.001 relative to hypoxia-dox.

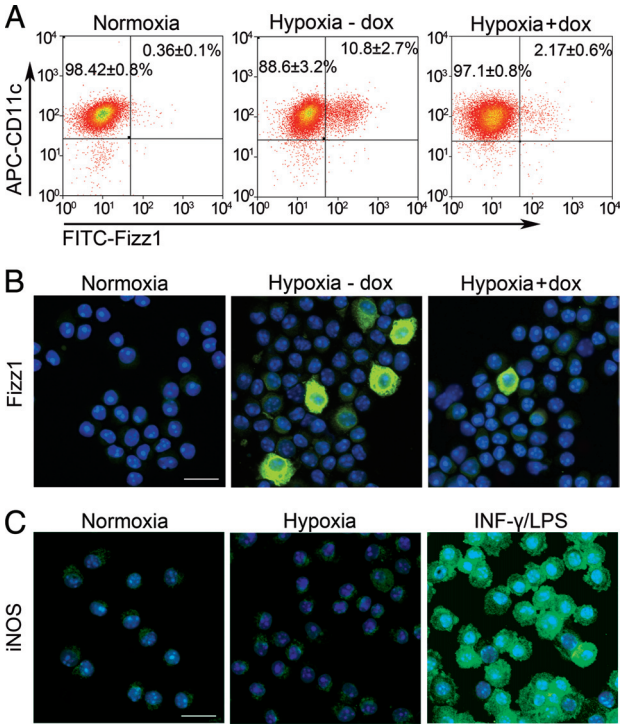

Figure 5. M2 and M1 expression profile of hypoxic alveolar macrophages. Found in inflammatory zone-1 (Fizz1) expression in alveolar macrophages from normoxic mice or mice exposed to hypoxia in the absence or presence of doxycycline (dox) was assessed by flow cytometry (**A**) and immunofluorescence (**B**; FITC). **C,** Inducible nitric oxide synthase (iNOS; FITC) staining in alveolar macrophages. Primary alveolar macrophages stimulated with 100 μg/mL lipopolysaccharide *Escherichia coli* and 100 U/mL interferon-γ (INF-γ) for 48 hours served as positive controls. Nuclei were counterstained with DAPI. Scale bar=25 μm.

Apart from the slight elevation of the Th2 cytokines IL-13 and IL-4 in the BALF of hypoxic mice, we investigated the potential presence of other noncanonical inducers of M2 polarization. Thus, we assessed the mRNA levels of CCL2 and IL-6 in total lung extracts by quantitative polymerase chain reaction. CCL2 and IL-6 mRNA was robustly upregulated soon after hypoxic exposure but was significantly suppressed in the presence of doxycycline (Figure VA in the online-only Data Supplement). In the CCTA control line lacking the HO-1 transgene, doxycycline treatment did not suppress CCL2 and IL-6 levels (Figure VB in the online-only Data Supplement). Interestingly, primary alveolar macrophages cultured in vitro under hypoxic conditions (0.5% O_2) also manifested the M2 phenotype with increased levels of Ym1, but not IL-12 and TNF-α (Figure VI in the online-only Data Supplement), suggesting that M2 polarization induced by hypoxia is a cell autonomous phenomenon.

Heme Oxygenase-1 Promotes the Expression of Interleukin-10 in Alveolar Macrophages

In an effort to further evaluate the effect of HO-1 on macrophage phenotype, mRNA and protein levels of IL-10, a well-documented anti-inflammatory mediator, were directly assessed in freshly isolated alveolar macrophages. Interleukin-10 was significantly elevated in alveolar macrophages derived from hypoxic mice treated with doxycycline (Figure 6). Doxycycline treatment in the CCTA line failed to upregulate IL-10 (Figure IVB in the online-only Data Supplement), establishing that the observed effect is HO-1 dependent. Furthermore, the number of regulatory macrophages expressing IL-10 (CD11c+, IL-10+) under hypoxia was assessed by flow cytometry to be increased 4- to 9-fold with doxycycline treatment, comprising slightly <10% of the total macrophage population in BALF (data not shown).

Early Monocyte/Macrophage Accumulation Is Critical for the Later Development of Pulmonary Hypertension

To determine whether this early inflammatory response is essential for the later development of HPH and whether inducible expression of HO-1 at defined intervals during this process modulates the disease, we exposed the bitransgenic mice to doxycycline for various time periods. In addition to

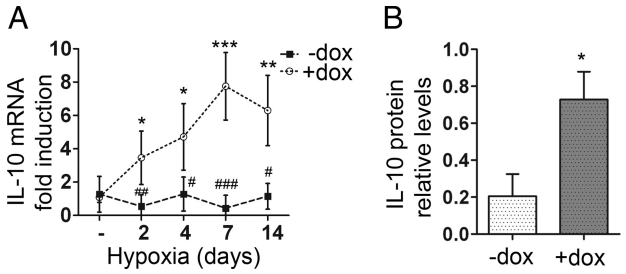

Figure 6. Heme oxygenase-1 induction promotes the expression of interleukin (IL)-10 in alveolar macrophages. Alveolar macrophages were isolated from animals exposed to hypoxia for the indicated times; IL-10 mRNA expression was assessed by quantitative polymerase chain reaction and IL-10 protein levels by Western blot followed by densitometric analysis. Relative IL-10 mRNA levels at the indicated time points (**A**) and IL-10 protein levels at day 7 of hypoxia (**B**) are shown normalized to β-actin. Numbers represent mean±SD; n≥5 mice per group. *P<0.05, **P<0.01, ***P<0.001 relative to normoxia; #P<0.05, ##P<0.01, ###P<0.001 relative to hypoxia+doxycycline (dox).

control animals exposed to hypoxia for 3 weeks in the absence of doxycycline, 1 group of littermates received doxycycline continuously for 3 weeks, and in 2 other groups, doxycycline was removed from the drinking water at 2 or 7 days of hypoxia. In all groups, animals remained in hypoxia for the entire 3-week period. On removal of doxycycline, hHO-1 mRNA levels returned to baseline within 3 days (Figure 7A and 7B).

A short 2-day pulse of doxycycline at the onset of hypoxia caused a delay in the peak of macrophage recruitment in the BALF from 2 to 7 days, a time when HO-1 levels were reduced to baseline (Figure 7A). In the same group of animals, development of pulmonary hypertension, as assessed by right ventricular systolic pressure, the Fulton Index, the medial wall thickness index, and histology of vascular remodeling, was not prevented (Figure 7C through 7F). In the case of a more prolonged, yet still transient, administration of doxycycline for 7 days, there was no macrophage influx even when HO-1 had reached baseline low levels, and pulmonary hypertension was completely prevented at 3 weeks (Figure 7B through 7F).

Alternative Macrophage Activation Is Associated With the Development of Hypoxia-Induced Pulmonary Hypertension In Vivo and Enhances Pulmonary Artery Smooth Muscle Cell Proliferation In Vitro

In agreement with macrophage numbers, M2 markers followed a similar pattern (Figure 8A). In the group in which doxycycline was removed after 2 days of hypoxic exposure and HPH was not prevented, mRNA levels of Fizz1, Arg1, and Ym1 increased 4 days after HO-1 levels had fallen to baseline (Figure 8A). However, in the group that received doxycycline for the first 7 days of hypoxia and the later development of hypertension was prevented, levels of Fizz1, Arg1, and Ym1 remained suppressed for all time periods examined (Figure 8B). Interestingly, in only the 7-day doxycycline treatment group, the anti-inflammatory marker IL-10 remained sustainably elevated above baseline (Figure 8A and 8B).

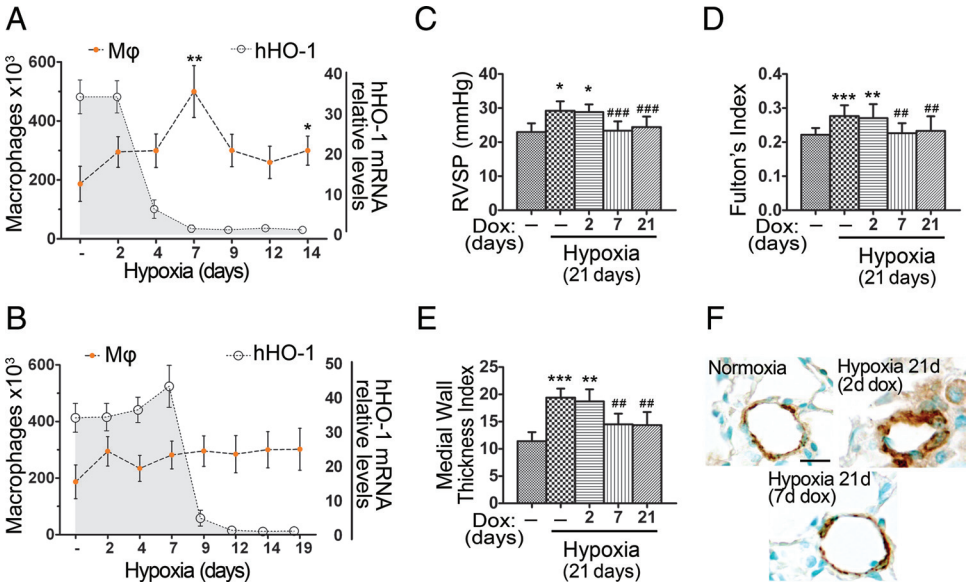

Figure 7. Early monocyte/macrophage accumulation is critical for the later development of hypoxia-induced pulmonary hypertension. Heme oxygenase-1 (HO-1) was transiently overexpressed in hypoxic mouse lung. **A,** Doxycycline (dox) administered at days −2 to 2 of hypoxic exposure (2 days) delays but does not prevent the peak of macrophage accumulation when HO-1 levels return to baseline. hHO-1 indicates human HO-1. **B,** Doxycycline administered at days −2 to 7 of hypoxic exposure (7 days) prevents the peak of macrophage accumulation for >12 days after HO-1 levels have returned to baseline. Mϕ indicates macrophage numbers. Right ventricular systolic pressure (RVSP; **C**), the Fulton Index (**D**), and medial wall thickness index (**E**) were elevated in mice that received the 2-day pulse but not in mice that received the 77-day pulse of dox. **F,** Representative immunostaining for α-smooth muscle actin of lung sections from mice exposed to hypoxia for 21 days that had previously received dox for either 2 or 7 days compared with normoxia. Numbers represent mean±SD; n≥6 animals per group. *P<0.05, **P<0.01, ***P<0.001 relative to normoxia; ##P<0.01, ###P<0.001 relative to hypoxia-dox.

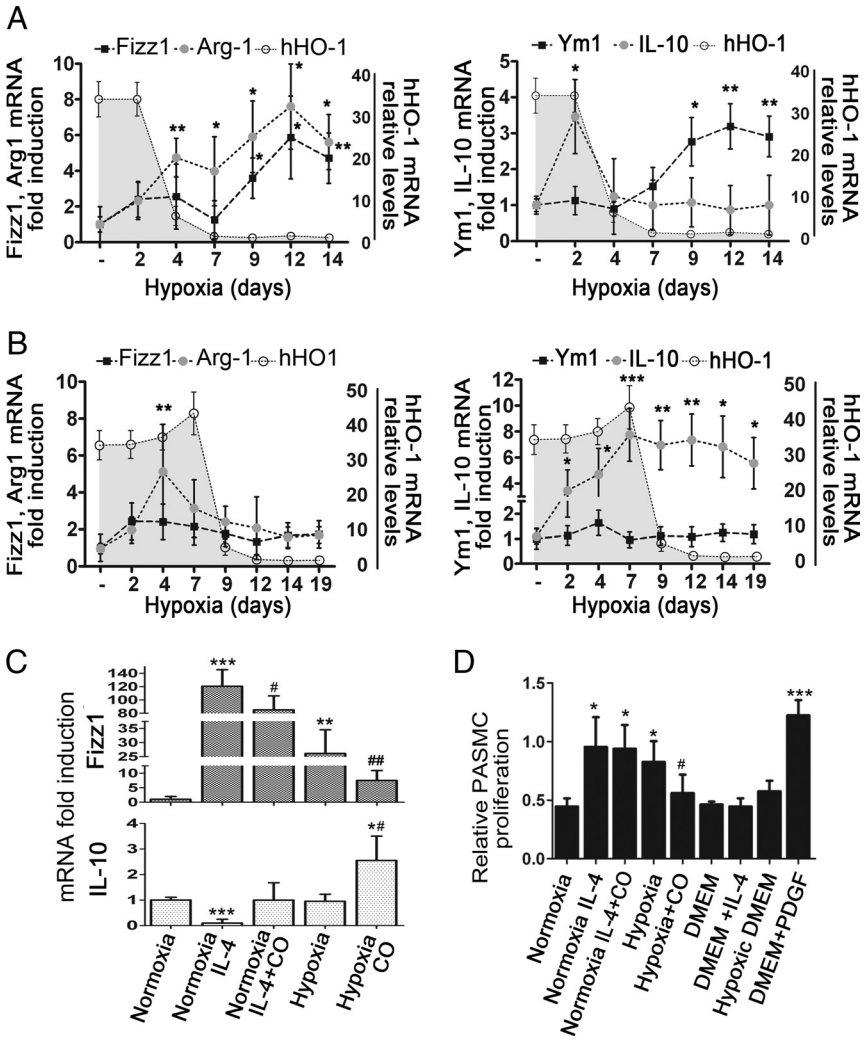

Figure 8. The role of macrophage activation profile in the development of hypoxia-induced pulmonary hypertension. **A,** After a 2-day pulse of doxycycline (dox) and 4 days after heme oxygenase-1 (HO-1) dropped to baseline, a pattern of alternative macrophage activation ensues (increased expression of found in inflammatory zone-1 [Fizz1], arginase-1 [Arg1], and chitinase-3-like-3 [Ym1]), whereas interleukin (IL)-10 levels remained low. **B,** After a 7-day pulse with dox, even when HO-1 levels return to baseline, high IL-10 expression persists. Shaded areas represent levels of human HO-1 (hHO-1) transgene expression. **C,** Fizz1 and IL-10 mRNA levels are shown in primary alveolar macrophages exposed to hypoxia or IL-4 (20 ng/mL) with or without carbon monoxide (CO). **D,** Effect of macrophage supernatants from different treatments on pulmonary artery smooth muscle cell proliferation. Platelet-derived growth factor-BB (PDGF-BB; 25 ng/mL) was used as positive control, and cell culture medium (Dulbecco modified Eagle medium [DMEM]) or medium exposed to 0.5% oxygen for 48 hours (hypoxic DMEM) was used as negative control. Numbers represent mean±SD; n≥6 animals or wells per group. *$P<0.05$, **$P<0.01$, ***$P<0.001$ relative to normoxia; #$P<0.05$, ##$P<0.01$ relative to hypoxia-dox.

Interleukin-10 mRNA levels were also upregulated in primary alveolar macrophages cultured in vitro under hypoxic conditions (0.5% O_2) and treated with CO (500 ppm; Figure 8C). This suggests that CO release on HO-1 induction in this system is the trigger for IL-10 induction in macrophages.

Supernatants of primary alveolar macrophages that were cultured in vitro under hypoxic conditions (0.5% oxygen) or normoxic macrophages treated with IL-4 (20 ng/mL) had high levels of Fizz1 and low levels of IL-10, and were able to stimulate pulmonary artery smooth muscle cell proliferation (Figure 8D). However, supernatants from CO-treated hypoxic macrophages had reduced levels of Fizz1 and elevated IL-10 and had no proliferative effect on pulmonary artery smooth muscle cells (Figure 8D). Exogenous administration of IL-10 on pulmonary artery smooth muscle cells treated with hypoxic macrophage supernatants had no direct suppressive effect on their proliferation (Figure VII in the online-only Data Supplement). Arg1, Fizz1, and Ym1 mRNA was upregulated in both IL-4– and hypoxia-stimulated macrophages, whereas neither platelet derived growth factor-BB nor the M1 specific markers IL-12 and TNF-α were affected (Figure 8C, Figure VI in the online-only Data Supplement, and data not shown). CO treatment suppressed the upregulation of the above M2 markers in both the IL-4– and hypoxia-stimulated macrophages (Figure 8C, Figure VI in the online-only Data Supplement, and data not shown).

Discussion

In our bitransgenic mouse model, we demonstrate that hypoxia provokes an accumulation of alternatively activated alveolar macrophages that precedes the development of pulmonary hypertension and appears to play a critical role in the pathogenesis of disease. Overexpression of HO-1 induced a switch in macrophage polarity toward an anti-inflammatory phenotype, and this effect was associated with protection from HPH.

Hypoxia resulted in alveolar inflammation that consisted predominantly of macrophages. These findings correlate with the fact that macrophages tend to accumulate in poorly vascularized areas with low oxygen tension,[29] and correlates with previous studies in HPH that highlighted the predominant role of the monocyte/macrophage lineage in modulating vascular remodeling.[8] Additionally, we found that hypoxia in vivo and in vitro polarized the population of alveolar macrophages toward the M2 phenotype. Hypoxic microenvironment is also a hallmark feature of tumors, and similar to the

hypoxic macrophages in our model, the tumor-associated macrophages exhibit an M2-like phenotype.[11,29] The cell-autonomous M2 polarization in in vitro hypoxic conditions, the upregulation in vivo of mRNA levels of 2 recently recognized noncanonical inducers of M2 polarization, CCL2 and IL-6,[13] and the increased IL-13 and IL-4 cytokine levels in the BALF of hypoxic mice support the M2-like activation in our hypoxic model. Furthermore, Fizz1, an M2-specific marker, is a hypoxia-inducible molecule, also designated hypoxia-induced mitogenic factor.[30] However, contrary to our findings, 2 previous studies reported upregulation of TNF-α,[31] IL-12, and interferon-γ[32] in hypoxic macrophages. We believe that our in vivo studies most closely approximate the disease physiology because the first of the 2 previous studies was performed only in vitro using isolated rat alveolar macrophages in a sepsis-induced hypoxia model and the second study was conducted on peritoneal macrophages.

Our finding that the presence of M2 macrophages is associated with the development of HPH in vivo and pulmonary artery smooth muscle cell proliferation in vitro suggests that these polarized trophic macrophages may play a significant role in the later development of pulmonary hypertension. Indeed, enhanced polyamine and L-proline synthesis caused by Arg1 has been shown to contribute to vascular damage and remodeling, and elevated Arg1 in lungs of hypoxic mice has been associated with increased severity of PAH.[33,34] Fizz1 has been recently reported to have mitogenic, angiogenic, and vasoconstrictive properties that are associated with pulmonary vascular remodeling.[5,30,35] Its human homolog, resistin-like molecule β, has also been detected in patients with scleroderma-associated pulmonary hypertension.[36] However, to the best of our knowledge, this is the first study to propose a link between alternatively activated macrophages and the development of HPH. One potential mechanism of action of alternatively activated macrophages may be the secretion of Fizz1, the overexpression of which has been reported to lead to PAH.[5] Further studies are required to determine the specific mediators from the secretome of M2 macrophages that may be contributing factors in the signaling cascade leading to HPH. In agreement with our findings, previous studies have shown that Th2 cytokines, as well as IL-6 and CCL2, induce M2 and have been implicated in human pulmonary disease and animal models of PAH.[3,6,37]

Overexpression of HO-1 in our bitransgenic model provoked a robust anti-inflammatory effect. It suppressed macrophage accumulation, M2 activation, and cytokine production in the lungs and prevented the subsequent development of pulmonary hypertension. Carbon monoxide appeared to be the key HO-1 effector inhibiting macrophage accumulation in the BALF and suppressing the expression of M2 markers in vitro. This observation is in agreement with previous studies in which HO-1 and CO were reported to have potent anti-inflammatory effects.[7,25]

Endogenous HO-1 is upregulated in hypoxia as a compensatory mechanism,[19] but its brief upregulation is not adequate to prevent hypoxia-induced inflammation and HPH, and only a more sustained enhancement of HO-1 expression can be protective in HPH.[7] For this reason, it is not surprising that a 2-day upregulation of HO-1 with doxycycline only postponed inflammation and did not protect from the development of HPH. Interestingly, HO-1 induction for 7 days, covering the entire period of hypoxia-induced inflammation, was sufficient to prevent the later development of HPH. Indeed, 7-day upregulation of HO-1 suppressed the inflammatory response even 2 weeks after the return of HO-1 to baseline levels, despite continuous hypoxia.

Because the switch in macrophage phenotype occurred within the first 4 days of hypoxia, we hypothesize that the enhancement of HO-1 during this critical period may act as a pivot to shift the balance of immune response from proinflammatory toward immunosuppressive. In support of this, lung HO-1 overexpression upregulated IL-10 in hypoxic macrophages and increased the number of IL-10–expressing regulatory macrophages in the BALF. Because CO could upregulate IL-10 in the in vitro cultured hypoxic macrophages, it seems to be a major effector molecule of HO-1 immunomodulation. In agreement with our findings, HO-1 and exogenous CO have previously been reported to increase IL-10 expression in macrophages in vivo and in vitro.[25,38–40]

Interestingly, IL-10 remained elevated even 2 weeks after HO-1 expression returned to baseline levels. These findings point to a switch in immunoregulation triggered by HO-1 during an early critical period, and whose presence was no longer essential, at least for the subsequent 2 weeks of hypoxia. Elevated IL-10 levels were also associated with protection from HPH, and IL-10 expression has been reported to protect from monocrotaline-induced PAH in rats.[4] We show that macrophages were the source of IL-10, but it remains unclear whether they are also a target of this cytokine. Because IL-10 is a pleiotrophic cytokine, it may act in an autocrine and paracrine manner to affect many different cell types besides macrophages. However, IL-10 did not have direct antiproliferative effects on pulmonary artery smooth muscle cells in our in vitro model, indicating that HO-1 and CO may also have anti-inflammatory functions independently of IL-10. Further studies are required to decipher the role of IL-10 pathway in the protection from HPH development and the mechanism of sustained protection from HPH conferred by a transient immunomodulatory event.

Conclusions

The present study demonstrates a link between macrophage accumulation and M2 activation and the promotion of HPH. On the basis of our findings, targeting the elimination or inactivation of this subset of macrophages may ameliorate the outcome of disease and improve the long-term prognosis of PAH. Importantly, M2 activation may serve as a biomarker to identify a therapeutic window for anti-inflammatory treatments and obviate the need for long-term therapies.

Acknowledgments

We thank Sarah Gately for her expert assistance in the preparation of the manuscript.

Sources of Funding

This work was supported by the National Institutes of Health grants RO1 HL 055454 and RO1 HL085446 (Drs Kourembanas and Mitsia-

lis). Dr Vergadi was supported in part by the Propontis Foundation (Athens, Greece) and the State Scholarships Foundation of Greece as a graduate student in the Graduate Program in Molecular Basis of Human Disease (University of Crete School of Medicine).

Disclosures

None.

References

1. Tuder RM, Groves B, Badesch DB, Voelkel NF. Exuberant endothelial cell growth and elements of inflammation are present in plexiform lesions of pulmonary hypertension. *Am J Pathol*. 1994;144:275–285.
2. Pinto RF, Higuchi Mde L, Aiello VD. Decreased numbers of T-lymphocytes and predominance of recently recruited macrophages in the walls of peripheral pulmonary arteries from 26 patients with pulmonary hypertension secondary to congenital cardiac shunts. *Cardiovasc Pathol*. 2004;13:268–275.
3. Sanchez O, Marcos E, Perros F, Fadel E, Tu L, Humbert M, Dartevelle P, Simonneau G, Adnot S, Eddahibi S. Role of endothelium-derived CC chemokine ligand 2 in idiopathic pulmonary arterial hypertension. *Am J Respir Crit Care Med*. 2007;176:1041–1047.
4. Ito T, Okada T, Miyashita H, Nomoto T, Nonaka-Sarukawa M, Uchibori R, Maeda Y, Urabe M, Mizukami H, Kume A, Takahashi M, Ikeda U, Shimada K, Ozawa K. Interleukin-10 expression mediated by an adeno-associated virus vector prevents monocrotaline-induced pulmonary arterial hypertension in rats. *Circ Res*. 2007;101:734–741.
5. Angelini DJ, Su Q, Yamaji-Kegan K, Fan C, Skinner JT, Champion HC, Crow MT, Johns RA. Hypoxia-induced mitogenic factor (HIMF/FIZZ1/RELMalpha) induces the vascular and hemodynamic changes of pulmonary hypertension. *Am J Physiol Lung Cell Mol Physiol*. 2009;296:L582–L593.
6. Steiner MK, Syrkina OL, Kolliputi N, Mark EJ, Hales CA, Waxman AB. Interleukin-6 overexpression induces pulmonary hypertension. *Circ Res*. 2009;104:236–244.
7. Minamino T, Christou H, Hsieh CM, Liu Y, Dhawan V, Abraham NG, Perrella MA, Mitsialis SA, Kourembanas S. Targeted expression of heme oxygenase-1 prevents the pulmonary inflammatory and vascular responses to hypoxia. *Proc Natl Acad Sci U S A*. 2001;98:8798–8803.
8. Frid MG, Brunetti JA, Burke DL, Carpenter TC, Davie NJ, Reeves JT, Roedersheimer MT, van Rooijen N, Stenmark KR. Hypoxia-induced pulmonary vascular remodeling requires recruitment of circulating mesenchymal precursors of a monocyte/macrophage lineage. *Am J Pathol*. 2006;168:659–669.
9. Hayashida K, Fujita J, Miyake Y, Kawada H, Ando K, Ogawa S, Fukuda K. Bone marrow-derived cells contribute to pulmonary vascular remodeling in hypoxia-induced pulmonary hypertension. *Chest*. 2005;127:1793–1798.
10. Sahara M, Sata M, Morita T, Nakamura K, Hirata Y, Nagai R. Diverse contribution of bone marrow-derived cells to vascular remodeling associated with pulmonary arterial hypertension and arterial neointimal formation. *Circulation*. 2007;115:509–517.
11. Mosser DM, Edwards JP. Exploring the full spectrum of macrophage activation. *Nat Rev Immunol*. 2008;8:958–969.
12. Edwards JP, Zhang X, Frauwirth KA, Mosser DM. Biochemical and functional characterization of three activated macrophage populations. *J Leukoc Biol*. 2006;80:1298–1307.
13. Roca H, Varsos ZS, Sud S, Craig MJ, Ying C, Pienta KJ. CCL2 and IL-6 promote survival of human CD11b+- peripheral blood mononuclear cells and induce M2-type macrophage polarization. *J Biol Chem*. 2009;284:34342–34354.
14. Gordon S, Martinez FO. Alternative activation of macrophages: mechanism and functions. *Immunity*. 2010;32:593–604.
15. Mora AL, Torres-Gonzalez E, Rojas M, Corredor C, Ritzenthaler J, Xu J, Roman J, Brigham K, Stecenko A. Activation of alveolar macrophages via the alternative pathway in herpesvirus-induced lung fibrosis. *Am J Respir Cell Mol Biol*. 2006;35:466–473.
16. Shaykhiev R, Krause A, Salit J, Strulovici-Barel Y, Harvey BG, O'Connor TP, Crystal RG. Smoking-dependent reprogramming of alveolar macrophage polarization: implication for pathogenesis of chronic obstructive pulmonary disease. *J Immunol*. 2009;183:2867–2883.
17. Willis D, Moore AR, Frederick R, Willoughby DA. Heme oxygenase: a novel target for the modulation of the inflammatory response. *Nat Med*. 1996;2:87–90.
18. Yet SF, Perrella MA, Layne MD, Hsieh CM, Maemura K, Kobzik L, Wiesel P, Christou H, Kourembanas S, Lee ME. Hypoxia induces severe right ventricular dilatation and infarction in heme oxygenase-1 null mice. *J Clin Invest*. 1999;103:R23–R29.
19. Christou H, Morita T, Hsieh CM, Koike H, Arkonac B, Perrella MA, Kourembanas S. Prevention of hypoxia-induced pulmonary hypertension by enhancement of endogenous heme oxygenase-1 in the rat. *Circ Res*. 2000;86:1224–1229.
20. Zuckerbraun BS, Chin BY, Wegiel B, Billiar TR, Czsimadia E, Rao J, Shimoda L, Ifedigbo E, Kanno S, Otterbein LE. Carbon monoxide reverses established pulmonary hypertension. *J Exp Med*. 2006;203:2109–2119.
21. Morita T, Mitsialis SA, Koike H, Liu Y, Kourembanas S. Carbon monoxide controls the proliferation of hypoxic vascular smooth muscle cells. *J Biol Chem*. 1997;272:32804–32809.
22. Wagener FA, Eggert A, Boerman OC, Oyen WJ, Verhofstad A, Abraham NG, Adema G, van Kooyk Y, de Witte T, Figdor CG. Heme is a potent inducer of inflammation in mice and is counteracted by heme oxygenase. *Blood*. 2001;98:1802–1811.
23. Tzima S, Victoratos P, Kranidioti K, Alexiou M, Kollias G. Myeloid heme oxygenase-1 regulates innate immunity and autoimmunity by modulating IFN-beta production. *J Exp Med*. 2009;206:1167–1179.
24. Lee TS, Chau LY. Heme oxygenase-1 mediates the anti-inflammatory effect of interleukin-10 in mice. *Nat Med*. 2002;8:240–246.
25. Otterbein LE, Bach FH, Alam J, Soares M, Tao Lu H, Wysk M, Davis RJ, Flavell RA, Choi AM. Carbon monoxide has anti-inflammatory effects involving the mitogen-activated protein kinase pathway. *Nat Med*. 2000;6:422–428.
26. Drechsler Y, Dolganiuc A, Norkina O, Romics L, Li W, Kodys K, Bach FH, Mandrekar P, Szabo G. Heme oxygenase-1 mediates the anti-inflammatory effects of acute alcohol on IL-10 induction involving p38 MAPK activation in monocytes. *J Immunol*. 2006;177:2592–2600.
27. Poss KD, Tonegawa S. Heme oxygenase 1 is required for mammalian iron reutilization. *Proc Natl Acad Sci U S A*. 1997;94:10919–10924.
28. Vitali SH, Mitsialis SA, Liang OD, Liu X, Fernandez-Gonzalez A, Christou H, Wu X, McGowan FX, Kourembanas S. Divergent cardiopulmonary actions of heme oxygenase enzymatic products in chronic hypoxia. *PLoS One*. 2009;4:e5978.
29. Lewis C, Murdoch C. Macrophage responses to hypoxia: implications for tumor progression and anti-cancer therapies. *Am J Pathol*. 2005;167:627–635.
30. Teng X, Li D, Champion HC, Johns RA. FIZZ1/RELMalpha, a novel hypoxia-induced mitogenic factor in lung with vasoconstrictive and angiogenic properties. *Circ Res*. 2003;92:1065–1067.
31. Leeper-Woodford SK, Detmer K. Acute hypoxia increases alveolar macrophage tumor necrosis factor activity and alters NF-kappaB expression. *Am J Physiol*. 1999;276:L909–L916.
32. Acosta-Iborra B, Elorza A, Olazabal IM, Martin-Cofreces NB, Martin-Puig S, Miro M, Calzada MJ, Aragones J, Sanchez-Madrid F, Landazuri MO. Macrophage oxygen sensing modulates antigen presentation and phagocytic functions involving IFN-gamma production through the HIF-1 alpha transcription factor. *J Immunol*. 2009;182:3155–3164.
33. Durante W, Liao L, Reyna SV, Peyton KJ, Schafer AI. Transforming growth factor-beta(1) stimulates L-arginine transport and metabolism in vascular smooth muscle cells: role in polyamine and collagen synthesis. *Circulation*. 2001;103:1121–1127.
34. Jin Y, Calvert TJ, Chen B, Chicoine LG, Joshi M, Bauer JA, Liu Y, Nelin LD. Mice deficient in Mkp-1 develop more severe pulmonary hypertension and greater lung protein levels of arginase in response to chronic hypoxia. *Am J Physiol Heart Circ Physiol*. 2010;298:H1518–H1528.
35. Yamaji-Kegan K, Su Q, Angelini DJ, Champion HC, Johns RA. Hypoxia-induced mitogenic factor has proangiogenic and proinflammatory effects in the lung via VEGF and VEGF receptor-2. *Am J Physiol Lung Cell Mol Physiol*. 2006;291:L1159–L1168.
36. Angelini DJ, Su Q, Yamaji-Kegan K, Fan C, Teng X, Hassoun PM, Yang SC, Champion HC, Tuder RM, Johns RA. Resistin-like molecule-beta in scleroderma-associated pulmonary hypertension. *Am J Respir Cell Mol Biol*. 2009;41:553–561.
37. Daley E, Emson C, Guignabert C, de Waal Malefyt R, Louten J, Kurup VP, Hogaboam C, Taraseviciene-Stewart L, Voelkel NF, Rabinovitch M,

Grunig E, Grunig G. Pulmonary arterial remodeling induced by a Th2 immune response. *J Exp Med*. 2008;205:361–372.
38. Inoue S, Suzuki M, Nagashima Y, Suzuki S, Hashiba T, Tsuburai T, Ikehara K, Matsuse T, Ishigatsubo Y. Transfer of heme oxygenase 1 cDNA by a replication-deficient adenovirus enhances interleukin 10 production from alveolar macrophages that attenuates lipopolysaccharide-induced acute lung injury in mice. *Hum Gene Ther*. 2001;12:967–979.
39. Xia ZW, Xu LQ, Zhong WW, Wei JJ, Li NL, Shao J, Li YZ, Yu SC, Zhang ZL. Heme oxygenase-1 attenuates ovalbumin-induced airway inflammation by up-regulation of foxp3 T-regulatory cells, interleukin-10, and membrane-bound transforming growth factor- 1. *Am J Pathol*. 2007;171:1904–1914.
40. Dolinay T, Szilasi M, Liu M, Choi AM. Inhaled carbon monoxide confers antiinflammatory effects against ventilator-induced lung injury. *Am J Respir Crit Care Med*. 2004;170:613–620.

CLINICAL PERSPECTIVE

Pulmonary arterial hypertension is a devastating disease with molecular and cellular underpinnings that remain poorly understood, despite substantial progress in the field. Recent studies from several groups, including ours, have documented an important role for inflammation in the development of pulmonary hypertension, but the specific inflammatory cell types and mediators leading to lung vascular remodeling have yet to be characterized. In this report, using a murine model of hypoxia-induced pulmonary hypertension, we show that hypoxia leads to early accumulation of macrophages in the lung that acquire an activated M2 phenotype characterized by overexpression found in inflammatory zone-1 and arginase-1. These M2 markers have been recognized as mitogenic, angiogenic, and profibrotic factors, and their induction by hypoxia in our model is associated with the later development of pulmonary arterial hypertension. Using transgenic mice with lung-specific, inducible expression of heme oxygenase-1, we demonstrated suppression of macrophage accumulation and M2 activation by hypoxia and a shift toward an anti-inflammatory macrophage phenotype that was associated with prevention of pulmonary arterial hypertension. Activated lung macrophages may thus be a significant source of mitogenic and trophic factors that contribute to the remodeling observed in pulmonary arterial hypertension. Importantly, M2 activation may serve as a biomarker of disease progression to identify a critical window for treatment aimed at promoting a switch toward the anti-inflammatory macrophage phenotype that, according to our findings, has antiproliferative and antihypertensive effects on the lung vasculature.

SUPPLEMENTAL MATERIAL

SUPPLEMENTAL MATERIAL

Supplemental Methods

Bitransgenic mice

Bitransgenic mice were generated by the crossing of Balb/c transgenic mice that harbor the reverse tetracycline transcriptional activator (rtTA, tetON system) under the control of the Clara Cell secreted protein (CCSP) promoter (CCTA line: a kind gift from Dr. J.A Whitsett)[1] with FVB transgenic mice that carry the human HO-1 transgene under the control of the tetracycline response element (TH77 line: CCSP-rTTA x TRE-hHO1). The latter was generated by microinjection of a $(TetO)_7$-CMV-human HO-1 transgene that consists of seven copies of the tet operator linked to a minimal CMV promoter, the human HO-1 cDNA, and SV40 polyadenylation signals. Animals were maintained in the pathogen-free Childrenôs Hospital Animal Care facility and all animal experiments were approved by the Childrenôs Hospital Boston Animal Care and Use Committee.

Hypoxic mouse model of PAH

Expression of human HO-1 in the lung was achieved by the addition of 1 mg/ml doxycycline (dox) (Sigma-Aldrich, Inc., St. Louis, MO) in the drinking water. After two days pretreatment with dox, animals were introduced to normobaric hypoxia (8.5% O_2) inside a chamber where oxygen was tightly regulated by an Oxycycler controller (Biospherix, Ltd., Lacona, NY). Nitrogen was automatically introduced as required to maintain the proper FiO_2 and ventilation was adjusted to keep CO_2 levels less than 8,000 ppm (0.8%). Ammonia was removed by charcoal filtration using an electric air purifier. Dox administration was either continued for the entire duration of the hypoxic exposure or terminated at two days or after seven days of hypoxia. Age and sex-matched littermates were exposed to identical conditions in hypoxia or normoxia and served as controls. The CCTA mouse line that lacks

the human HO-1 trangene, treated with dox, served as control to eliminate any potential effects imparted by dox itself, independent of human HO-1 expression.

CO treated mice inhaled the gas intermittently: 250 ppm for 1 hour prior to hypoxic exposure and then received 250 ppm for 1 hour twice daily, inside the hypoxic chamber for a total of 48 hours. A group of mice underwent i.p injections of 50 εmol/kg biliverdin IX hydrochloride (Frontier Scientific, Inc., Logan, UT) as previously reported,[2] prior to the onset of hypoxia and twice daily thereafter. Finally, a third group received both CO and biliverdin as above. Control mice were injected i.p with the same volume of PBS and inhaled room air or hypoxic air (8.5% O_2) without CO.

Hemodynamic and ventricular weight measurements

After hypoxic exposure at the indicated time periods, mice were anesthetized and hemodynamic and ventricular weight measurements were performed. Right ventricular systolic pressure (RVSP) was measured through a trans-thoracic route: a pressure transducer (ADI Instruments, Inc., Colorado Springs, CO) attached to a 23G needle was used and data were collected and analyzed using the PowerLab Software (ADI Instruments, Inc., Colorado Springs, CO).[3] Right ventricular (RV) hypertrophy was assessed by harvesting hearts, removing atria, dissecting the RV and deriving Fulton's Index, i.e the weight ratio of (right ventricle)/ (left ventricle and septum) [(RV)/(LV+S)].

Immunohistochemical analysis

Lungs were initially perfused with PBS through the right ventricle. The perfusion flow was kept at approximately 1ml/min by the use of a peristaltic pump with Platinum L/S 13 Masterflex silicone tubing. Lungs were then intratracheally inflated with 4% paraformaldehyde, fixed overnight at 4°C, then stored in 70% ethanol before embedding in paraffin. Lung tissue sections were deparaffinized and rehydrated. Immunohistochemical assessment of vascular remodeling was performed by staining for alpha-smooth muscle actin (anti-Ŭ-SMA antibody, Sigma-Aldrich, Inc., St. Louis, MO), a marker of smooth muscle

cells.[4] Endogenous peroxidase activity was inhibited with 3% H_2O_2 (Sigma- Aldrich, Inc., St. Louis, MO) in methanol. Next, the sections were incubated with a biotinylated horse anti-mouse IgG (Vector Laboratories, Inc., Burlingame, CA), treated with the avidinï biotin complex (Vectastain Elite ABC kit, Vector Laboratories, Inc., Burlingame, CA), and stained with 3,3ô diaminobenzidine substrate (KPL, Inc., Gaithersburg, MD). Slides were counterstained with 1% Methyl Green (Sigma-Aldrich, Inc., St. Louis, MO).

Morphometric analysis

Alveolar/distal pulmonary arterioles of 50-100 ε m in diameter, not associated with bronchi, from lung sections immunostained with Ŭ-SMA (as described above), were captured with light microscopy. At least 10 representative pulmonary arterioles were chosen from three different sections from each animal. Morphometric analysis of medial vessel wall thickness was performed using the software package Metamorph v.6.2r (Universal Imaging, Downingtown, PA). The entire vessel area including the lumen was identified as ñTotal Areaò and the area of brown-color (Ŭ- SMA stained) that represents the medial smooth muscular layer was labeled ñThreshold Areaò. Medial Wall Thickness Index was determined by using the quotient of Threshold Area x 100 over Total Area [(%Threshold Area x 100)/ total Area].

Isolation of alveolar macrophages

Animals were anesthetized with 2,2,2-tribromoethanol (avertin, Sigma-Aldrich, Inc., St. Louis, MO) after exposure for the indicated time periods in hypoxia. Bronchoalveolar lavage fluid (BALF) was obtained through intratracheal instillation of 4 x 0.85 ml PBS and filtered via a 35 ε m cell strainer to exclude contamination from epithelial cells that appeared in clusters. Red blood cells were lysed using ammonium chloride lysis buffer (Sigma-Aldrich, Inc., St. Louis, MO). More than ninety percent of the cells isolated this way appeared to be of the monocyte/macrophage lineage and this was confirmed by cell-specific markers in flow cytometry (below). Isolated cells were used for RNA extraction, flow cytometry, or immunocytochemistry.

Flow cytometry

Total white blood cell (WBC) counts of BALF isolated cells were accessed by hemocytometer counting using Kimura stain,[5] and reconfirmed by flow cytometry analysis [6] by the use of FITC-anti mouse CD45 antibody (BD Biosciences, Franklin Lakes, NJ) and flow cytometry absolute count standard beads (Bangs Laboratories, Fishers, IN). Differential WBC analysis was performed using APCï anti-mouse F4/80 (eBioscience, Inc., San Diego, CA), PE-anti-mouse Ly-6G/Ly-6C (BD Biosciences, Franklin Lakes, NJ), and Pacific Blue-anti-mouse CD3 (eBioscience, Inc., San Diego, CA) antibodies specific for macrophages, neutrophils, and T cells, respectively. Expression profile of BALF isolated alveolar macrophages was assessed by APC-anti mouse F4/80 (eBioscience, Inc., San Diego, CA),[7] FITC-anti-mouse CD11c, and PE-anti-mouse CD45 (BD Biosciences, Franklin Lakes, NJ) in separate analyses. Fizz1 expression was assessed by performing fixation with parafolmadelhyde, intracellular permeabilization and staining with primary rabbit anti-mouse-Fizz1 antibody (Abcam, Cambridge, MA) followed by secondary rabbit FITC-conjugated anti-rabbit antibody (BD Biosciences, Franklin Lakes, NJ). In order to evaluate the IL-10-expressing alveolar macrophages, BALF-isolated cells were incubated with Golgi inhibitor (monensin, BD Biosciences, Franklin Lakes, NJ) fixed and permeabilized, and stained with APC-conjugated monoclonal antibody against murine IL-10 (BD Biosciences, Franklin Lakes, NJ). The proper isotype controls were used in each case. The flow cytometry events were acquired in a MoFlo Legacy Cell Sorter (Beckman Coulter, Inc., Brea, CA) and analyzed with the use of Summit Software (Summit Software, Inc., Fort Wayne, IN).

Cytospin preparation and Immunocytochemistry

BAL was performed and the cell suspension was cytocentrifuged at 300g for 5 min using the Shandon Cytospin 4 (Thermo Fisher Scientific, Inc., Waltham, MA). Slides were air-dried overnight, stained with Hema stain set (Fisher Diagnostics, Middletown, VA), and evaluated

under light microscope. Immunocytochemistry for Fizz1 or iNOS was performed by immersion of the slides in 2% parafolmadehyde, incubation with blocking serum, followed by incubation at 4°C overnight with rabbit polyclonal anti-mouse-Fizz1 antibody (Abcam, Cambridge, MA), or rabbit polyclonal anti-mouse iNOS antibody (Santa Cruz Biotechnology, Inc., Santa Cruz, CA). Goat biotinylated anti-rabbit secondary antibody (Cell Signaling Technology, Inc., Boston, MA) and FITC-avidin conjugate (Vector Laboratories, Inc., Burlingame, CA) were further used. Primary alveolar macrophages stimulated with 100 εg/ml LPS *E.coli* and 100 U/ml INF-ɔ for 48 hours served as positive controls. Nuclei were counterstained with DAPI (Thermo Fisher Scientific, Inc., Waltham, MA) and samples were observed with fluorescent microscopy.

Quantitative PCR

RNA from total lung or from alveolar macrophages was isolated using the Qiagen RNAeasy mini and micro extraction kit, respectively (Qiagen, Hilden, Germany). One εg of total DNA-digested RNA was used for cDNA synthesis (Superscript III oligo dT primer kit, Invitrogen Corporation, Carlsbad, CA). The following primers were used in the PCR reaction: human HO-1; fwd: 5ô GCAGTCAGGCAGAGGGTGATA-3ǫ rev: 5ô AGCCTGGGAGCGGGTGTTGAG-3ǫ Ym1; fwd: 5ô GCAGAAGCTCTCCAGAAGCAATCCTG-3ǫrev: 5ôATTGGCCTGTCCTTAGCCCAACTG-3ǫ Fizz1; fwd: 5ôGCTGATGGTCCCAGTGAATAC-3ǫ rev: 5ôCCAGTAGCAGTCATCCCAGC-3ǫ Arginase-1; fwd: 5ôCAGAAGAATGGAAGAGTCAG-3ǫ rev: 5ô CAGATATGCAGGGAGTCACC-3ǫ Arginase-2; fwd: 5ôCACGGGCAAATTCCTTGCGTCC-3ǫ rev: 5ôGGTTGGCAAGGCCCACTGAACG-3ǫ Mannose Receptor, C type 1 (MR): fwd: 5ô TTTCCATCGAGACTGCTGC-3ǫ rev: 5ôACCAAAGCCACTTCCCTTC-3ǫ iNOS; fwd: 5ô TCCTGGAGGAAGTGGGCCGAAG-3ǫ rev: 5ôCCTCCACGGGCCCGGTACTC-3ǫ IL12b; fwd: 5ô GGAGGGGTGTAACCAGAAAGGTGC-3ǫ rev: 5ô CCTGCAGGGAACACATGCCCAC-3ǫ TNFa; fwd: 5ôGCCCACGTCGTAGCAAACCACC-3ǫ rev: 5ôCGGGGCAGCCTTGTCCCTTG-3ǫ CCL2 (MCP-1); fwd: 5ô

GGCTGGAGCATCCACGTGTTGG-3ô; rev: 5ôTTGGGGTCAGCACAGACCTCTCTC-3ô; IL-6; fwd: 5ôCAAAGCCAGAGTCCTTCAGAG-3ô; rev: 5ôCACTCCTTCTGTGACTCCAGC-3ô; IL-10; fwd: 5ô GCGCTGTCATCGATTTCTCCCCTG-3ô; rev: 5ô GGCCTTGTAGACACCTTGGTCTTGG-3ô; PDGF-BB: fwd: 5ô GGGAGCAGCGAGCCAAGACG-3ô; rev: 5ôTGCCCACACTCTTGCCGACG-3ô; CD80 (B7-1); fwd: 5ôGGGAAAAACCCCCAGAAG-3ô; rev: 5ô CCCGAAGGTAAGGCTGTTG-3ô; CD86; fwd: 5ô CAGCCTAGCAGGCCCAG-3ô; rev: 5ô GGCTCTCACTGCCTTCACTC-3ô Ribosomal Protein S9 (Rps9) with forward primer 5ôGCTAGACGAGAAGGATCCCC-3ôand reverse primer 5ô. CAGGCCCAGCTTAAAGACCT -3ôserved as housekeeping gene. Annealing was carried out at 60ęC for 30 sec, extension at 72ęC for 30 sec, and denaturation at 95ęC for 30 sec for 40 cycles. Analysis of the fold change was performed based on the Pfaffl method.[8]

BAL fluid cytokine profile

The BALF supernatant was analyzed using a multiplex mouse cytokine kit (FGFƀ, MIP-1Ŭ, IL-1ƀ, IL-17, IL-2, IL-13, IL-4, TNF-Ŭ, IL-12, INF-ɔ) (Invitrogen Corporation, Carlsbad, CA) in the Luminex 200Ê System (Luminex Corporation, Austin, TX). BALF supernatant samples from animals treated with either dox or regular water in normoxia versus two and four days in hypoxia were analyzed in duplicate. Standard Luminex protocol was followed as suggested by the manufacturer.

Western blot analysis

Protein concentration from BALF or total lung was determined by the Bradford assay. BALF samples were concentrated with 20% trichloroacetic acid (TCA, Sigma-Aldrich, Inc., St. Louis, MO) overnight, washed with ice-cold acetone and resuspended in SDS-containing loading dye. Twenty ɛg of protein was electrophoresed on 13.3% denaturing polyacrylamide gel prior to wet transfer to 0.2 ɛm PVDF membrane (Bio-Rad Laboratories, Hercules, CA). Briefly, after blocking with 5% bovine serum albumin (BSA) in phosphate buffered saline (pH 7.4) containing 0.1% Tween 20 (PBST) for an hour at room temperature, the membranes

were incubated with rabbit polyclonal anti-mouse Fizz1 antibody (Abcam, Cambridge, MA), rabbit polyclonal anti-human and anti-mouse HO-1 antibody (Enzo Life Sciences International, Inc., Plymouth Meeting, PA), rabbit polyclonal anti-mouse HO-2 antibody (Enzo Life Sciences International, Inc., Plymouth Meeting, PA) or goat polyclonal anti-mouse IgA Ab (Millipore, Billerica, MA) at 4°C overnight. The membranes were then incubated with 40 ng/ml of peroxidase-conjugated anti-rabbit or anti-goat secondary antibody (Santa Santa Cruz Biotechnology, Inc., Santa Cruz, CA), respectively, for 30 min at room temperature followed by reaction with Lumi-Light ECL substrate (Thermo Fisher Scientific, Inc., Waltham, MA).

For IL-10 detection in alveolar macrophages, cells were collected from BALF and centrifuged at 400g for 5 min. Cells were washed with PBS prior to lysis in 20 ul of RIPA buffer supplemented with protease inhibitor cocktail. Ten ug protein per lane was loaded on 13.3% polyacrylamide gel, wet transfer was performed at 200 mAmp for 2-3 hrs, followed by blocking with 2.5% BSA in PBST (0.1% Tween 20) for 30 min, and incubation with rat anti-mouse IL-10 antibody (Abcam, Cambridge, MA) overnight at 4°C with continuous shaking. Anti-mouse ɓ-actin monoclonal antibody (R&D Systems, Minneapolis, MN) was used as internal control and densitometric analysis was performed with the NIH ImageJ program.

Griess reaction and arginase activity assay

In the Griess reaction, nitrite and nitrate concentration in BALF supernatant were measured by the Total NO/Nitrite/Nitrate Assay (R&D Systems, Minneapolis, MN). Proteins were removed before analysis with ultrafiltration using 10,000 molecular weight (MW) cut-off filters (Amicon Ultra; Millipore, Billerica, MA). Supernatants from RAW 264.7 macrophages stimulated with 100 ɛg/ml LPS or 100 U/ml INF-ɔ for 48 hours served as positive controls.

Arginase activity in BALF-isolated alveolar macrophages was assessed utilizing the Quantichrom arginase assay kit (Bioassay Systems, Hayward, CA). Briefly, 10^5 cells per sample were harvested, washed, and lysed with 10 mM Tris.HCl (pH 7.4) containing 0.4%

(w/v) Triton X-100 and protease inhibitor cocktail (Complete; Roche Diagnostics, Mannheim, Germany). Cell lysate samples were analyzed for arginase activity in duplicate.

Primary alveolar macrophage culture

For cell culture experiments, BALF was obtained through intratracheal instillation of 5 x 1 ml Hankôs Balanced Salt Solution (without calcium and magnesium) supplemented with 10 mM EDTA and 1 mM HEPES and filtered twice via a 35 εm cell strainer to exclude contamination of epithelial cells. $3.5x10^5$ macrophages per well were seeded in 48-well tissue-culture plates in a volume of 0.25 ml macrophage complete medium (DMEM/10: Dulbeccoôs Modified Eagle Medium) (GIBCO, Invitrogen Corporation, Carlsbad, CA) supplemented with 10% (v/v) FBS, 10 mM L-glutamine, 100 IU/ml penicillin and 100 ug/ml streptomycin). Cells were incubated at 37°C for 4 hours and then their medium was replaced with serum-free DMEM prior to hypoxic exposure or IL-4 stimulation.

Macrophage activation and CO treatment

Macrophages were cultured for 48 hours at 0.5-1% O_2 (pO_2 in the media was 14-18 torr) in a hypoxic work station (in Vivo2, Ruskinn Technology, Ltd., Bridgend, UK) and/or Billups chambers that were flushed with a mix of 0.5% O_2 and 5% CO_2 (N_2 balance). Alternatively, macrophages were stimulated with 20 ng/ml murine recombinant interleukin-4 (IL-4) (R&D Systems, Minneapolis, MN) in order to be polarized towards M2.[9, 10] CO treatment was performed in Billups chambers that were flushed with a mix of 0.5% O_2, 5% CO_2, 500 ppm CO (N_2 balance). Cells were pretreated with CO for 1 hour in normoxia prior to hypoxic exposure. Cell viability was greater than 80% in all groups as assessed by trypan blue exclusion.

PASMC proliferation assay

Mouse primary pulmonary artery smooth muscle cells (PASMCs) were cultured ($2x10^3$ cells per well) in a volume of 100 µl of DMEM (GIBCO, Invitrogen Corporation, Carlsbad,

CA) supplemented with 10% FBS, 10 mM L-glutamine, 100 IU/ml penicillin and 100 µg/ml streptomycin, using 96-well tissue culture plates. Two days prior to proliferation assay, the medium was replaced with DMEM supplemented with 0.1% FBS, 10 mM L-glutamine, 100 IU/ml penicillin and 100 µg/ml streptomycin. Macrophage-conditioned media, diluted two-fold with fresh low-serum media, were then applied to PASMCs and the cultures were incubated for an additional three days. Cell proliferation was assessed by cell proliferation reagent WST-1 (Roche Diagnostics, Mannheim, Germany) by applying 10 µl of WST-1 reagent to each well and measuring OD_{440}-OD_{690} after two hours of incubation at 37^0C. Treatment of PASMCs with 25 ng/ml PDGF-BB served as a positive control. Fresh cell culture medium (DMEM) or medium equilibrated in 0.5% Oxygen for 48 hours were used as negative controls. Mouse recombinant IL-10 (R&D Systems, Minneapolis, MN) was used in the range of 1-100 ng/ml.

Supplemental Figures and Figure Legends

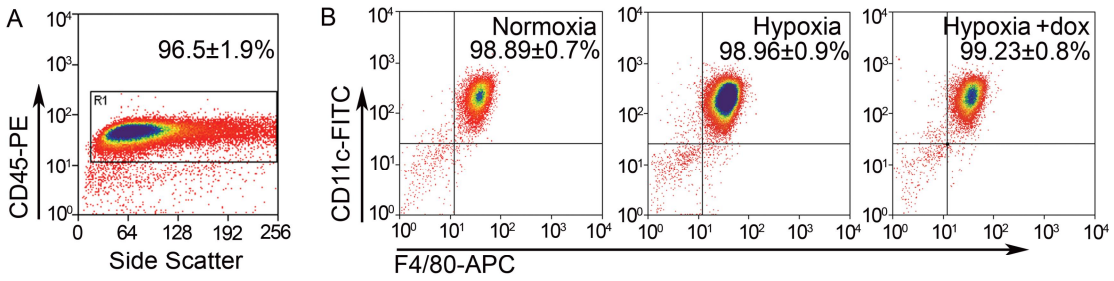

Vergadi et al, Figure S1

Supplemental Figure 1. Analysis of BALF cell content in hypoxic mice. [A] More than 95% of the cells isolated (gated for Side and Forward Scatter) were CD45(+), i.e white blood cells. [B] More than 98% of CD45 (+) cells expressed the macrophage cell surface antigens F4/80 and CD11c, irrespective of treatment.

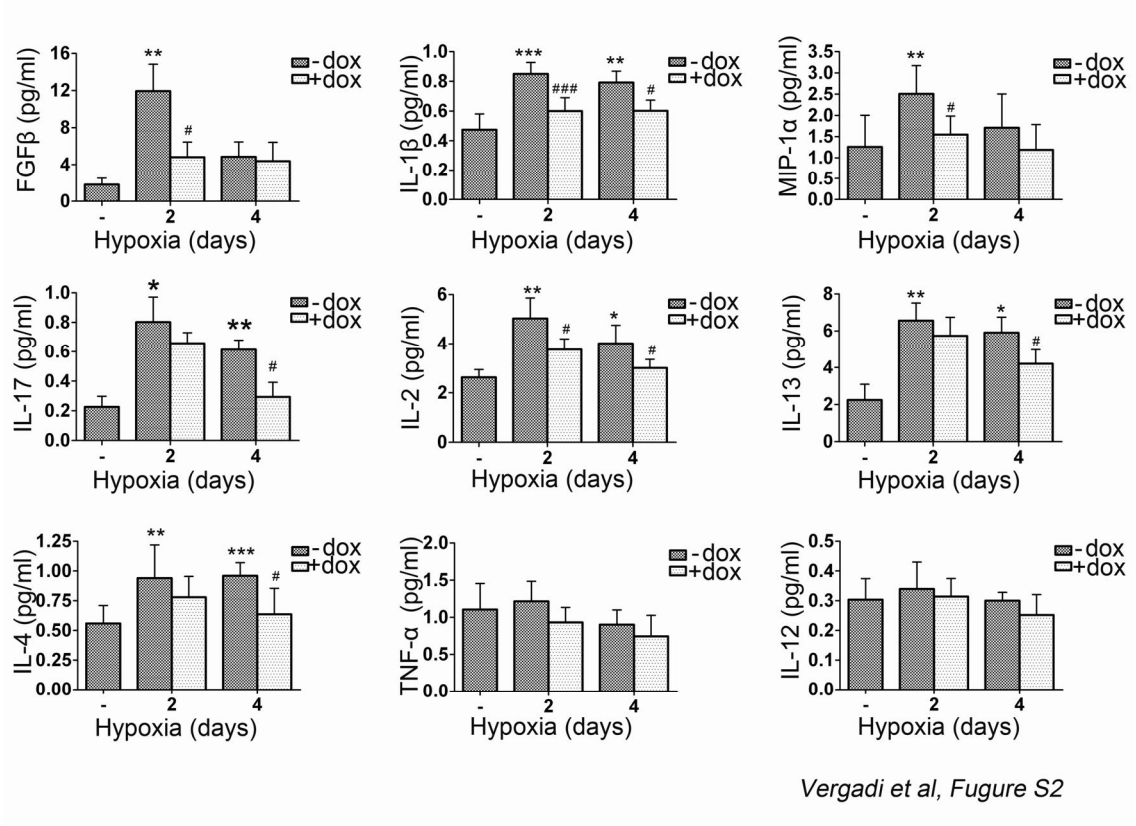

Supplemental Figure 2. Chemokine and cytokine profile in the BALF of hypoxic mice. Chemokine/cytokine profile in the BALF of mice exposed in hypoxia for two and four days in the absence (-) or presence (+) of dox. Upregulation of FGFb, IL-1b, MIP-1Ŭ, IL-13, IL-4, IL-17 and IL-2 in hypoxia and the suppressive effect of HO-1 expression (+dox). Note that the Th1 related cytokines, TNF-Ŭ and IL-12, were not upregulated in hypoxia as compared to normoxic mice. (Numbers represent mean +/-SD, with a minimum of 6 animals per time point or treatment group). *: relative to normoxia; *p<0.05, **p<0.01, ***p<0.001. #:relative to hypoxia ï dox; #p<0.05, ###p<0.001.

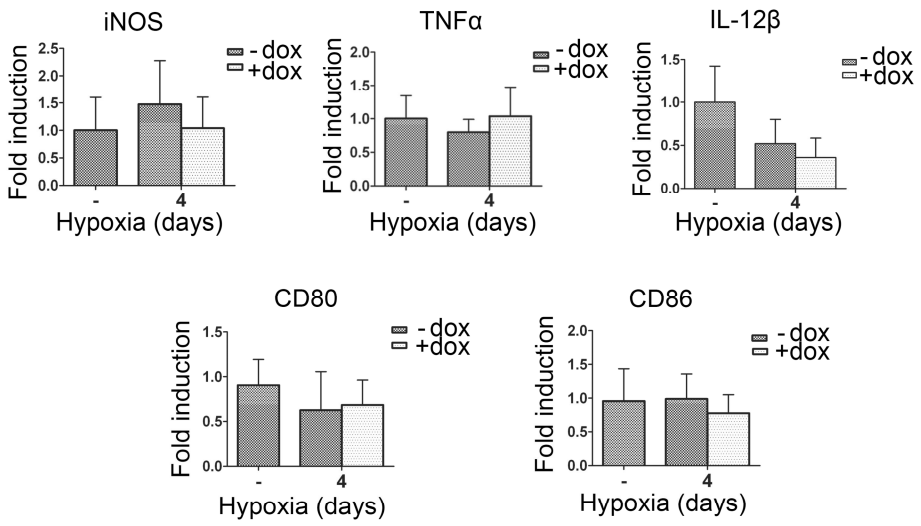

Vergadi et al, Figure S3

Supplemental Figure 3. Expression levels of M1 markers in hypoxic alveolar macrophages. mRNA levels of M1 markers, iNOS, TNFŭ, IL-12ƀ, CD80, and CD86, were assessed through qPCR in alveolar macrophages isolated from normoxic animals or animals exposed to hypoxia for four days with or without dox treatment. Values are shown relative to normoxia.

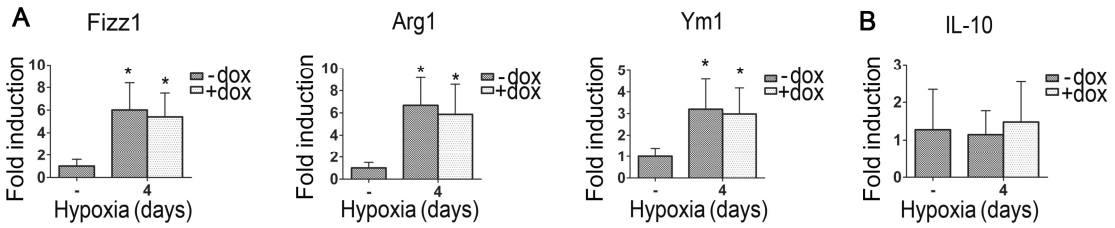

Supplemental Figure 4. The anti-inflammatory effects of dox-treatment are hHO-1 dependent. The CCTA transgenic line that harbors the tetracycline transactivator but lacks the human HO-1 transgene was used to assess potential biologic effects of dox treatment. [A] Markers of alternative activation, Fizz1, Arg1, and Ym1, were not suppressed in hypoxic CCTA animals treated with dox. [B] Concordantly, the anti-inflammatory mediator, IL-10, was not upregulated in dox-treated CCTA animals. *: relative to normoxia; *p<0.05.

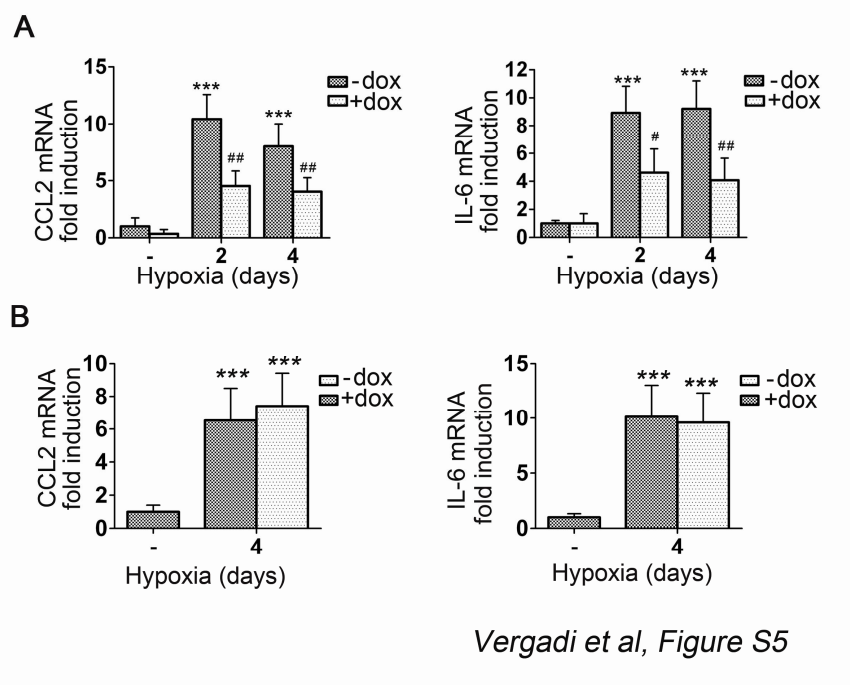

Supplemental Figure 5. Suppression of CCL2 and IL-6 levels in the hypoxic lung is HO-1 dependent [A] CC77 animals. The hypoxic induction of CCL2 and IL-6 mRNA levels in the lung was suppressed by dox treatment. [B] CCTA animals. CCL2 and IL-6 mRNA levels were not suppressed in hypoxic CCTA animals lacking the hHO-1 transgene. Numbers represent mean +/-SD, with a minimum of 6 mice per group. *: relative to normoxia, ***p<0.001. $^{\#}$:relative to hypoxiaï dox; $^{\#}$p<0.05, $^{\#\#}$p<0.01.

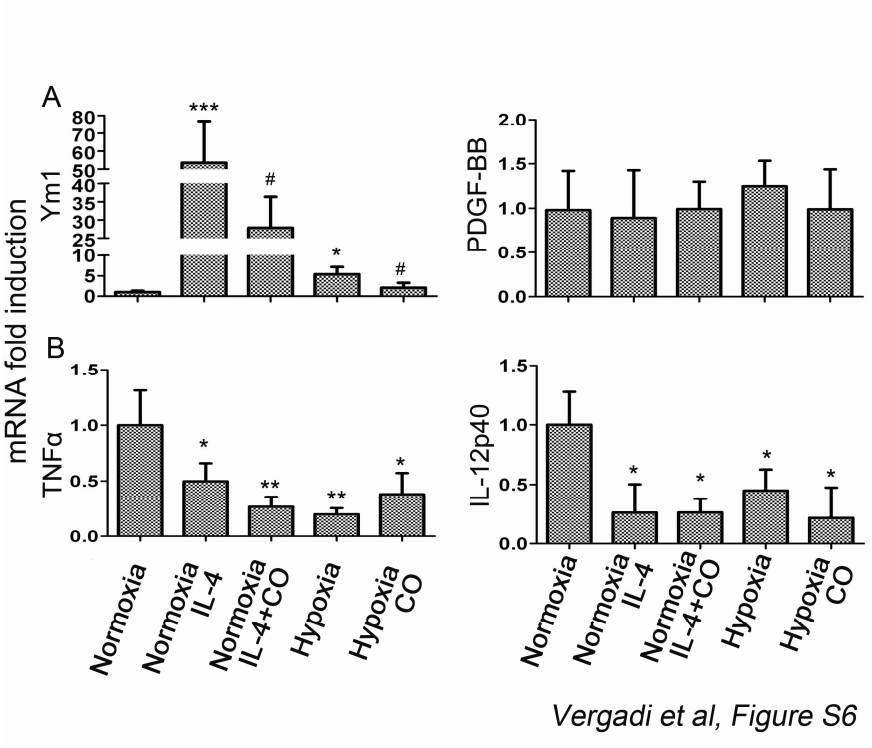

Supplemental Figure 6. Cytokine and growth factor profile of *in vitro* stimulated primary alveolar macrophages. [A] mRNA levels of the M2 marker, Ym1, but not the growth factor, PDGF-BB, were upregulated in primary alveolar macrophages stimulated with 20 ng/ml IL-4 or hypoxia (0.5% O_2) and suppressed upon CO treatment. [B] The mRNA levels of M1 specific markers, TNF-Ŭ and IL-12p40 subunit, were downregulated in alveolar macrophages stimulated with 20 ng/ml IL-4 or hypoxia (0.5% O_2) with or without 250 ppm CO. Numbers represent mean +/-SD, at least 5 mice donors per group. *: relative to normoxia; *p<0.05, **p<0.01, ***p<0.001. $^{\#}$:relative to hypoxia or normoxia + IL-4; $^{\#}$p<0.05.

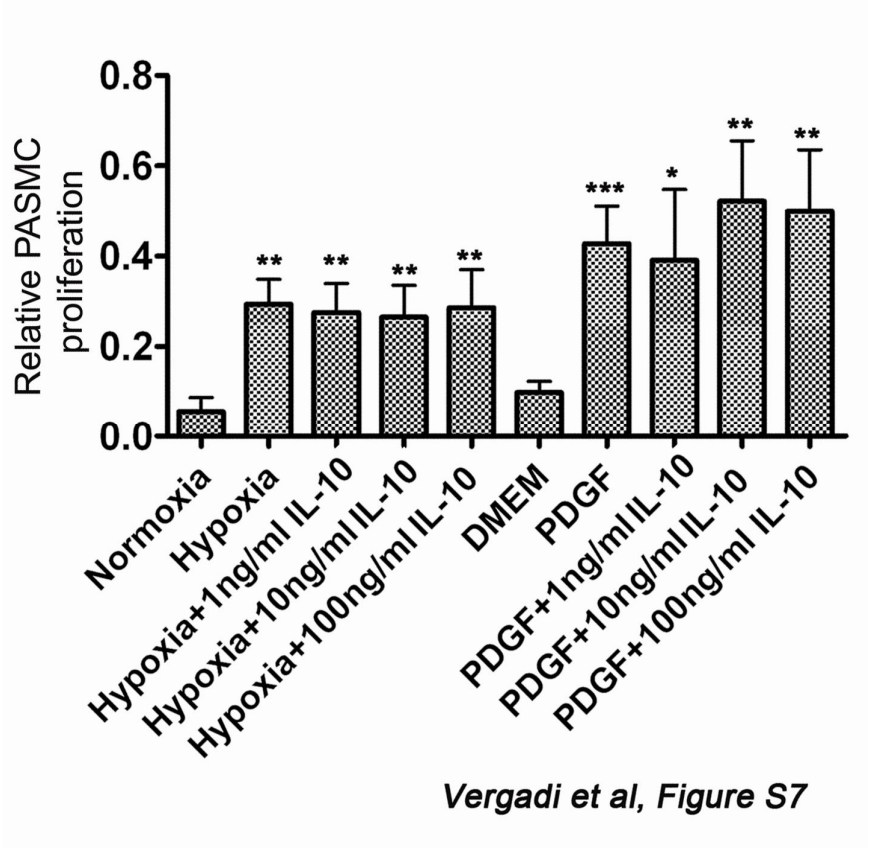

Supplemental Figure 7. IL-10 is not sufficient to block hypoxic macrophage-derived signals for PASMC proliferation. PASMC cultures were inclubated with media conditioned by either normoxic [Normoxia] or hypoxic [Hypoxia] alveolar macrophages in the presence or absence of IL-10 at the indicated final concentrations, and their proliferation rate assessed. Stimulation of PASMC proliferation by 25 ng/ml PDGF-BB served as a control. *: relative to normoxia; *p<0.05, **p<0.01, ***p<0.001.

Supplemental References

1. Perl AK, Tichelaar JW, Whitsett JA. Conditional gene expression in the respiratory epithelium of the mouse. *Transgenic Res.* 2002;11:21-29.
2. Yamashita K, McDaid J, Ollinger R, Tsui TY, Berberat PO, Usheva A, Csizmadia E, Smith RN, Soares MP, Bach FH. Biliverdin, a natural product of heme catabolism, induces tolerance to cardiac allografts. *FASEB J.* 2004;18:765-767.
3. Fagan KA, Fouty BW, Tyler RC, Morris KG, Jr., Hepler LK, Sato K, LeCras TD, Abman SH, Weinberger HD, Huang PL, McMurtry IF, Rodman DM. The pulmonary circulation of homozygous or heterozygous eNOS-null mice is hyperresponsive to mild hypoxia. *J Clin Invest.* 1999;103:291-299.
4. Jones R, Jacobson M, Steudel W. alpha-smooth-muscle actin and microvascular precursor smooth-muscle cells in pulmonary hypertension. *Am J Respir Cell Mol Biol.* 1999;20:582-594.
5. Kimura I, Moritani Y, Tanizaki Y. Basophils in bronchial asthma with reference to reagin-type allergy. *Clin Allergy.* 1973;3:195-202.
6. van Rijt LS, Kuipers H, Vos N, Hijdra D, Hoogsteden HC, Lambrecht BN. A rapid flow cytometric method for determining the cellular composition of bronchoalveolar lavage fluid cells in mouse models of asthma. *J Immunol Methods.* 2004;288:111-121.
7. Khazen W, M'Bika J P, Tomkiewicz C, Benelli C, Chany C, Achour A, Forest C. Expression of macrophage-selective markers in human and rodent adipocytes. *FEBS Lett.* 2005;579:5631-5634.
8. Pfaffl MW. A new mathematical model for relative quantification in real-time RT-PCR. *Nucleic Acids Res.* 2001;29:e45.
9. Classen A, Lloberas J, Celada A. Macrophage activation: classical versus alternative. *Methods Mol Biol.* 2009;531:29-43.
10. Mosser DM, Zhang X. Activation of murine macrophages. *Curr Protoc Immunol.* 2008;Chapter 14:Unit 14 12.

Akt2 Deficiency Protects from Acute Lung Injury via Alternative Macrophage Activation and miR-146a Induction in Mice

Eleni Vergadi, Katerina Vaporidi, Emmanuel E. Theodorakis, Christina Doxaki, Eleni Lagoudaki, Eleftheria Ieronymaki, Vassilia I. Alexaki, Mike Helms, Eumorfia Kondili, Birte Soennichsen, Efstathios N. Stathopoulos, Andrew N. Margioris, Dimitrios Georgopoulos and Christos Tsatsanis

J Immunol published online 25 November 2013
http://www.jimmunol.org/content/early/2013/11/25/jimmunol.1300959

The Journal of Immunology is published twice each month by The American Association of Immunologists, Inc., 9650 Rockville Pike, Bethesda, MD 20814-3994.

Print ISSN: 0022-1767 Online ISSN: 1550-6606.

Published November 25, 2013, doi:10.4049/jimmunol.1300959

Akt2 Deficiency Protects from Acute Lung Injury via Alternative Macrophage Activation and miR-146a Induction in Mice

Eleni Vergadi,*,† Katerina Vaporidi,† Emmanuel E. Theodorakis,*,† Christina Doxaki,* Eleni Lagoudaki,‡ Eleftheria Ieronymaki,* Vassilia I. Alexaki,* Mike Helms,§ Eumorfia Kondili,† Birte Soennichsen,§ Efstathios N. Stathopoulos,‡ Andrew N. Margioris,* Dimitrios Georgopoulos,† and Christos Tsatsanis*

Acute respiratory distress syndrome (ARDS) is a major cause of respiratory failure, with limited effective treatments available. Alveolar macrophages participate in the pathogenesis of ARDS. To investigate the role of macrophage activation in aseptic lung injury and identify molecular mediators with therapeutic potential, lung injury was induced in wild-type (WT) and Akt2$^{-/-}$ mice by hydrochloric acid aspiration. Acid-induced lung injury in WT mice was characterized by decreased lung compliance and increased protein and cytokine concentration in bronchoalveolar lavage fluid. Alveolar macrophages acquired a classical activation (M1) phenotype. Acid-induced lung injury was less severe in Akt2$^{-/-}$ mice compared with WT mice. Alveolar macrophages from acid-injured Akt2$^{-/-}$ mice demonstrated the alternative activation phenotype (M2). Although M2 polarization suppressed aseptic lung injury, it resulted in increased lung bacterial load when Akt2$^{-/-}$ mice were infected with *Pseudomonas aeruginosa*. miR-146a, an anti-inflammatory microRNA targeting TLR4 signaling, was induced during the late phase of lung injury in WT mice, whereas it was increased early in Akt2$^{-/-}$ mice. Indeed, miR-146a overexpression in WT macrophages suppressed LPS-induced inducible NO synthase (iNOS) and promoted M2 polarization, whereas miR-146a inhibition in Akt2$^{-/-}$ macrophages restored iNOS expression. Furthermore, miR-146a delivery or Akt2 silencing in WT mice exposed to acid resulted in suppression of iNOS in alveolar macrophages. In conclusion, Akt2 suppression and miR-146a induction promote the M2 macrophage phenotype, resulting in amelioration of acid-induced lung injury. In vivo modulation of macrophage phenotype through Akt2 or miR-146a could provide a potential therapeutic approach for aseptic ARDS; however, it may be deleterious in septic ARDS because of impaired bacterial clearance. ***The Journal of Immunology*****, 2014, 192: 000–000.**

Acute respiratory distress syndrome (ARDS) is a major cause of respiratory failure in critically ill patients, with no effective treatment reported (1). Acute lung injury, the pathologic presentation of ARDS, is characterized by alveolar barrier disruption and lung inflammation (2–7). Two phases of inflammatory response have been recognized in experimental acute lung injury: the acute phase, characterized by inflammatory cell infiltration and increased production of a variety of oxidants, cytokines, and proteolytic enzymes that promote tissue destruction (1, 2) and the resolving phase, during which phagocytosis of debris and alveolar structural repair are taking place (1, 8, 9).

Macrophages play an important role in the pathogenesis of lung injury, initiating the inflammatory response and promoting neutrophil infiltration and tissue damage in the lung (4, 5, 8–13). However, based on environmental stimuli, macrophages can possess the classical (M1) or alternative activation (M2) phenotype (14). Classically activated or M1 macrophages express high levels of inducible NO synthase (iNOS), generate NO, secrete IL-12β, and are prominent in the acute phase of inflammation (14). Genetic depletion or pharmacologic inhibition of iNOS was shown to confer protection against lung injury in several animal models (4, 13, 15–18), suggesting a crucial role for M1 macrophages in the pathogenesis of acute lung injury (ALI). Alternative macrophage activation, or M2, is characterized by high levels of arginase-1 (Arg-1), found-in-inflammatory zone-1 (Fizz1), chitinase-3–like-3 (Ym1), and macrophage galactose C-type lectin 1 and 2 (MGL1, MGL2) (8, 9, 19). M2 macrophages participate in the resolution of inflammation and are known to be beneficial in the outcome of several inflammatory diseases (14, 20–22).

The mechanisms that regulate macrophage activation phenotype are currently being investigated (14, 21, 22). Several signaling pathways, such as STAT-1 phosphorylation, IRF5 upregulation, and SOCS2 and SOCS1 were shown to promote M1 activation (21, 23–25). Also, SOCS3 suppression, STAT6 phosphorylation, and C/EBPβ and IRF4 upregulation were shown to regulate M2

*Department of Clinical Chemistry, University of Crete, Medical School, 71003 Heraklion, Greece; †Department of Intensive Care Medicine, University of Crete, Medical School, 71003 Heraklion, Greece; ‡Department of Pathology, University of Crete, Medical School, 71003 Heraklion, Greece; and §Cenix Bioscience, Dresden, Dresden BioInnovation Center, 01307 Dresden, Germany

Received for publication April 9, 2013. Accepted for publication October 25, 2013.

This work was supported by the European Commission FP7 programme "Translational Potential" (European Commission contract number 285948) and FP7 Industry-Academia Partnerships and Pathways (GA-2008-230725-TACIT), the Association for International Cancer Research (AICR11-0505), and by National and European Union funds under the APIΣTEIA Grant (2071). E.V. was supported by the Greek State Scholarships Foundation and a Manassaki Scholarship from the University of Crete.

Address correspondence and reprint requests to Dr. Christos Tsatsanis, Department of Clinical Chemistry-Biochemistry, School of Medicine, University of Crete, P.O. Box 2208, Heraklion 71003, Crete, Greece. E-mail address: tsatsani@med.uoc.gr

The online version of this article contains supplemental material.

Abbreviations used in this article: ALI, acute lung injury; ARDS, acute respiratory distress syndrome; Arg-1, arginase-1; BALF, bronchoalveolar lavage fluid; Fizz1, found-in-inflammatory zone-l; IC, inspiratory capacity; iNOS, inducible NO synthase; MGL, macrophage galactose C-type lectin; miRNA, microRNA; NS, normal saline; siAkt2, small interfering RNA against Akt2; siRNA, small interfering RNA; TRAF, TNFR-associated factor; WT, wild-type; Ym1, chitinase-3–like-3.

polarization (21, 23, 24). Akt is a family of three serine/threonine protein kinases (Akt1, Akt2, and Akt3) that are important to control cell survival, proliferation, and differentiation (26, 27). We showed that Akt kinases play a key role in the regulation of the macrophage activation phenotype (25, 28, 29). Depletion of the Akt2 isoform in peritoneal macrophages abrogates M1 activation and promotes M2 phenotype by inducing C/EBPβ (22, 25), a transcriptional regulator of Arg-1 expression (30). Akt2 depletion induces C/EBPβ via negative regulation of the microRNA (miRNA) miR-155, known to target C/EBPβ and promote M1 (22, 25, 31). Additionally, TLR4 signaling was shown to play an important role in alveolar macrophage activation in animal models of ALI (12, 32, 33). TLR4 signaling is regulated by the anti-inflammatory miRNA, miR-146a, which targets and suppresses downstream TLR4 mediators, such as TNFR-associated factor (TRAF)-6, IRAK1, and IRF5 (34, 35). Yet, the roles of the miR-146a macrophage activation phenotype and aseptic inflammation have not been investigated.

In the current study, we tested the hypothesis that a prominent M2 macrophage phenotype, such as the one possessed by Akt2$^{-/-}$ mice (22), would be protective in aseptic lung injury. Therefore, we compared the development of HCl acid aspiration–induced lung injury in wild-type (WT) and Akt2$^{-/-}$ mice. Additionally, we examined the molecular mechanisms involved in the regulation of the macrophage activation phenotype, focusing on the roles of Akt2, miR-155, and miR-146a. We also evaluated whether the macrophage activation phenotype can be modulated in vivo by targeting Akt2 or miR-146a. Last, we assessed the biological effect of Akt2 deletion in a septic model of lung injury induced by *Pseudomonas aeruginosa* to clarify the potential limitations of Akt2 suppression and M2 macrophage polarization under septic conditions in clinical practice.

Materials and Methods

HCl-induced ALI

For induction of ALI, 8–10-wk-old C57BL/6 WT and Akt2$^{-/-}$ mice were anesthetized and intubated oro-tracheally. HCl solution (0.05 N, pH ≈ 1.5), 2 ml/kg diluted in normal saline (NS, 0.9% NaCl), was instilled in the trachea, whereas age- and gender-matched mice received 2 ml/kg NS and served as controls. A bolus of 0.5 ml air was given to ensure that HCl solution reached the distal lung. Mice were then extubated and left to recover from anesthesia with oxygen supplementation. At specific time points following HCl administration, mice were sacrificed; a pressure-volume curve of the respiratory system was obtained, bronchoalveolar lavage fluid (BALF) was collected, and lung tissue was harvested.

In total, 262 mice (WT, $n = 145$; Akt2$^{-/-}$, $n = 117$) were used. Because of sample insufficiency, not all mice were used for all assays. The specific number of samples used is mentioned in the figure legends. All mice were kept in the pathogen-free animal facility of the Institute of Molecular Biology and Biotechnology in Heraklion, Crete. All procedures were approved by the Veterinary Department of Crete Prefecture and the University of Crete Medical School.

Evaluation of lung injury

The indices of lung injury examined included lung compliance, obtained from the pressure-volume curve of the respiratory system; protein concentration; inflammatory cells; cytokines in BALF; and lung histology.

A pressure-volume curve of the respiratory system was obtained by slow lung inflation to peak airway pressure of 25 cm H_2O, as previously described (36, 37). As an indicator of lung compliance we used the inspiratory capacity (IC), defined as the volume inflated at airway pressure of 25 cm H_2O normalized to body weight and expressed as a percentage of control.

Bronchoalveolar lavage, inflammatory cell counts, and protein/cytokine levels

BALF was obtained through intratracheal instillation of ice-cold PBS (Ca^{2+}- and Mg^{2+}-free, supplemented with 0.1 mM EDTA). First, 30 μl/g PBS was instilled, and the supernatant was used to evaluate cytokine concentrations. To collect alveolar macrophages, bronchoalveolar lavage was performed five times with 1 ml PBS.

Total WBC counts of cells isolated from BALF were estimated by hemocytometer counting using Kimura stain (38), whereas differential counts were determined by flow cytometry (see below). For cytospin preparations, the cell suspension was cytocentrifuged at 300 × *g* for 5 min using the Shandon Cytospin 4 (Thermo Scientific, Rockford, IL). Slides were air-dried overnight, stained with May-Grünwald Giemsa (Merck, Frankfurt, Germany), and evaluated under a light microscope.

Protein concentration of BALF was assessed by the BCA method (BCA Protein Assay, Thermo Scientific). IL-6, TNF-α, CXCL-1, and IL-1β protein levels in the lavage fluid were determined using a commercially available sandwich ELISA kit (Quantikine; R&D Systems, Abingdon, U.K.), according to the manufacturer's instructions.

Immunocytochemistry

Cells isolated from BALF were cytocentrifuged, as mentioned above, and placed on microscope slides. Immunocytochemistry for iNOS, IRF5, and Arg-1 was performed by immersing the slides in 4% paraformaldehyde in PBS and incubating with blocking serum, followed by incubation at 4°C overnight with rabbit polyclonal anti-mouse iNOS Ab (Santa Cruz Biotechnology, Santa Cruz, CA), rabbit polyclonal anti-mouse IRF5 Ab (Cell Signaling Technology, Beverly, MA), or mouse monoclonal anti-mouse Arg-1 (BD Biosciences, Franklin Lakes, NJ). Goat biotinylated anti-rabbit IgG or horse biotinylated anti-mouse IgG (both from Cell Signaling Technology) was used as secondary Ab. FITC-Avidin or Texas Red–Avidin (Vector Laboratories, Burlingame, CA) were used to detect binding of biotinylated primary Abs. Nuclei were counterstained with DAPI (Thermo Fisher Scientific, Waltham, MA).

Lung histology and lung injury score determination

For histology purposes, lungs were perfused with PBS through the right ventricle. An incision at the left atrium allowed outflow of the blood. Lungs were inflated intratracheally with 10% formalin at 25 cm H_2O pressure, fixed overnight at 4°C, and stored in 70% ethanol before embedding in paraffin. Lung tissue sections of 5 μm were prepared and further deparaffinized and rehydrated. Sections were stained with H&E and evaluated by a pathologist blinded to the interventions. Because of the patchy nature of the lesions, random high-power fields (400×) were scored. The selection was effectuated by successive haphazard displacements, each of which was at least one high-power field in length. To perform the histological assessment of lung injury, five independent variables were evaluated—neutrophils in alveolar spaces, neutrophils in the interstitial spaces, hyaline membranes, proteinaceous debris filling the airspaces, and alveolar septal thickening–and weighted according to the relevance ascribed to by the Official American Thoracic Society Workshop Report on Features and Measurements of Experimental Acute Lung Injury in Animals (39). The resulting injury score is a continuous value between 0 and 1.

Cell sorting and alveolar macrophage isolation

To discriminate alveolar macrophages, cells were stained with FITC–anti-mouse CD45 Ab (BD Biosciences), allophycocyanin–anti-mouse CD11c Ab (BD Biosciences), or PE-anti-mouse Ly-6G Ab (BioLegend, San Diego, CA) specific for WBCs, alveolar macrophages, or neutrophils, respectively. Cells were evaluated in a MoFlo Cell Sorter (Beckman Coulter, Fullerton, CA), and the percentages of macrophages and neutrophils were analyzed with Summit Software (Summit Software, Fort Wayne, IN). The $CD45^+CD11c^+Ly\text{-}6G^-$ cells (alveolar macrophages) were sorted further and isolated to purity > 90%.

RNA isolation and quantitative PCR

RNA from alveolar or thioglycolate-elicited peritoneal macrophages or total lung was isolated using TRIzol reagent (Life Technologies, Carlsbad, CA). In the case of in vivo–isolated and sorted alveolar macrophages, RNA precipitation was facilitated by the addition of 250 μg/μl RNase-free glucogen (Fermentas, St. Leon-Rot, Germany). One microgram of total DNA-digested RNA was used for cDNA synthesis (Thermoscript RT; Invitrogen, Carlsbad, CA). The SYBR Green method was followed in the PCR reaction. Primer sequences are shown in Supplemental Table I. Ribosomal protein S9 (RPS9) served as the housekeeping gene. Annealing was carried out at 60°C for 30 s, extension was at 72°C for 30 s, and denaturation was 40 cycles at 95°C for 15 s.

To isolate miRNAs from alveolar macrophages, total RNA was isolated as described above. TaqMan MicroRNA Assays (Life Technologies) were used for cDNA synthesis and quantitative PCR of specific miRNAs. The

miRNA sequence is described in Supplemental Table I. SnoRNA135 served as housekeeping miRNA. Annealing and extension were carried out at 60˚C for 30 s, and denaturation was 40 cycles at 95˚C for 15 s in a 7500 Fast Real-Time PCR System (Life Technologies). Analysis of the fold change was performed based on the Pfaffl method (40).

Flow cytometry

Expression of protein levels of iNOS, IL-12β, Arg-1, Fizz1, MGL-1/2, and IL-10 was determined by flow cytometry cell surface and intracellular staining, as previously described (41, 42). Cells isolated from BALF were incubated with Golgi inhibitor (monensin; BD Biosciences), and cell surface staining was carried out by incubation with PerCP-Cy5.5 anti-mouse CD11c (BioLegend), fixation and permeabilization (BD Fixation and Permeabilization Solution Kit; BD Biosciences), and staining with allophycocyanin-conjugated mAb against murine IL-10, FITC-conjugated mAb against murine iNOS, or PE-conjugated mAb against murine IL-12β (all from BD Biosciences). Mouse monoclonal anti-mouse Arg-1 (BD Biosciences) and rabbit polyclonal anti-mouse Fizz1 (Abcam, Cambridge, U.K.) were used in separate analyses. FITC goat anti-rabbit IgG (BD Biosciences) or allophycocyanin rat anti-mouse IgG1 (BioLegend) was used as secondary Ab for Fizz1 or Arg-1 staining, respectively. PE anti-mouse MGL1/2 (R&D Systems, Minneapolis, MN) was used for cell surface staining in separate analyses. The proper isotype controls were used in each case. The flow cytometry events were acquired in a MoFlo Legacy Cell Sorter (Beckman Coulter) and analyzed with Summit Software. Flow cytometry events were gated first based on forward and side scatter and then $CD11c^+$ cells (alveolar macrophages) were selected to evaluate the expression of activation markers.

Nitrite concentration and arginase activity assay

Determination of NO metabolite and nitrite concentration in BALF (based on Griess reaction). BALF supernatants from control mice and mice with acid-induced lung injury for 12 h were used. A total of 50 μl sulfanilamide solution (1% w/v sulfanilamide, 5% w/v phosphoric acid) was added to an equal volume of sample. Samples were incubated for 10 min in the dark, and 50 μl 0.1% w/v *N*-(naphthyl) ethyl-enediamidedihydrochloride was added, followed by a second incubation for 10 min at room temperature in the dark. Absorbance at 550 nm was measured, and the amount of nitrite was determined using a $NaNO_2$ standard curve.

Arginase activity. Arginase activity was assessed indirectly by measuring the concentration of urea generated by the arginase-dependent hydrolysis of L-arginine as previously described (43). Alveolar macrophages from animals with acid-induced lung injury (12-h time point) and control mice were harvested, washed, and lysed with 10 mM Tris-HCl (pH 7.4) containing 0.4% (w/v) Triton X-100 and protease inhibitor mixture (Complete; Roche, Basel, Switzerland). After 30 min on a shaker, 100 μl 25 mM Tris-HCl was added. Ten microliters of 10 mM $MnCl_2$ was added to 100 μl this lysate, and the enzyme was activated by heating for 10 min at 55˚C. Arginine hydrolysis was conducted by incubating the lysates with 100 μl 0.5 M L-arginine (pH 9.7) at 37˚C for 60 min. The reaction was stopped with 800 μl H_2SO_4 (96%)/H_3PO_4 (85%)/H_2O (1/3/7, v/v/v). The urea concentration was measured at 550 nm after the addition of 40 μl α-isonitrosopropiophenone (Sigma-Aldrich, St. Louis, MO) (dissolved in 100% ethanol), followed by heating at 100˚C for 30 min. One unit of enzyme activity is defined as the amount of enzyme that catalyzes the formation of 1 μmol urea/min.

Western blot analysis

Macrophage protein lysates were resuspended in SDS-containing loading dye. Twenty micrograms of protein was electrophoresed on 13.3% denaturing polyacrylamide gel prior to wet transfer to 0.45 μm polyvinylidene difluoride membrane (Bio-Rad, Hercules, CA). Briefly, after blocking with 5% skim milk in PBS (pH 7.4) containing 0.1% Tween 20 for an hour at room temperature, the membranes were incubated with rabbit polyclonal anti-mouse IRF5 Ab (Cell Signaling Technology), mouse polyclonal anti-mouse TRAF6 Ab (Santa Cruz Biotechnology), or mouse monoclonal anti-mouse B-actin (Cell Signaling Technology) at 4˚C overnight. The membranes were then incubated with 40 ng/ml peroxidase-conjugated anti-rabbit or anti-mouse secondary Ab (Santa Cruz Biotechnology), respectively, for 30 min at room temperature, followed by reaction with Lumi-Light ECL substrate (Thermo Fisher Scientific).

Cell cultures and cell transfections

For cell-transfection experiments, peritoneal fluid or BALF from control animals was obtained through instillation of 5 × 1 ml HBSS (without calcium or magnesium) supplemented with 10 mM EDTA and 1 mM HEPES and filtered twice via a 35-μm cell strainer to exclude contamination of epithelial cells. A total of 1×10^5 macrophages/well (four wells/group) was seeded in 48-well tissue culture plates in a volume of 0.2 ml macrophage complete medium (DMEM; Life Technologies) supplemented with 10% (v/v) FBS, 10 mM L-glutamine, 100 IU/ml penicillin, and 100 μg/ml streptomycin. Cells were incubated at 37˚C for 4 h, and the medium was replaced with serum-free, antibiotic-free DMEM prior to transfection. Lipofectamine served as transfection reagent (RNAiMAX; Life Technologies), and cells were transfected with either 30 nM small interfering RNA (siRNA) for *Akt2* (sense seq: ACC/OmeU/UAUGUUGGACAAA/OmeG/A/OmeU/OmeU/, antisense seq: 5Phos/UCUUUGUCCAACA/OmeU/AAG/OmeG/Utt; designed at Cenix Bioscience) or with negative-control dsRNA. For miR-146a experiments, transfection was carried out with 30 nM miR-146a mimic, anti–miR-146a inhibitor, and nontargeting controls that were purchased from Ambion (Life Technologies). Transfection efficiency and biological effect were assessed 72 h posttransfection.

To induce the M1 phenotype in alveolar macrophages and to recapitulate the in vivo stimuli, BALF (0.3 ml/kg) samples from WT mice were obtained 6 h after acid aspiration. After 24 h of serum starvation, BALF supernatant (free of cells) was applied in cultured WT and $Akt2^{-/-}$ alveolar macrophages isolated from BALF in a 1:1 dilution with fresh serum-free DMEM. Control cells received the same ratio of NS. Cells were harvested 12 h poststimulation.

LPS stimulation in peritoneal macrophages, which were transfected with miR-146a mimic, miR-146a inhibitor, or scramble miRNA (all from Life Technologies), was carried out by introduction of a final concentration of 100 ng/ml LPS *Escherichia coli* to the cell medium. Stimulation was applied 4 or 24 h prior to cell harvesting.

Application of siRNA and miRNAs in vivo

The siRNA used for in vivo targeting of *Akt2* contain 2′-*O*-methyl modifications, increasing their in vivo stability and reducing immune response activation (44, 45). Its effectiveness in suppressing *Akt2* was verified in vitro before in vivo application. Based on dose-response experiments and on previous reports that applied naked siRNA and miRNA in the lung (46–49), 5 nmol siRNA targeting *Akt2*, 1 nmol miR-146a mimic, or 0.6 nmol miR-146a inhibitor (anti–miR-146a) (Life Technologies) was instilled intratracheally in each mouse in 50 μl NS prepared from nuclease-free water. For siRNA experiments, two doses of siRNA were administered: the first 48 h before the instillation of HCl acid and the second 1 h after acid aspiration. miR-146a mimic and inhibitor were instilled 1 h after the instillation of HCl acid. In both cases, mice were sacrificed 24 h postacid aspiration. siRNA-targeting *Luciferase* and nontargeting miRNA control (scramble) were used as experimental controls, respectively.

To evaluate the distribution of siRNA in the lung, Cy3-conjugated siRNA targeting *Luciferase* was used. A total of 5 nmol/mouse was administered oro-tracheally, and lungs were harvested 24 h later. Lungs were inflated in 4% PFA, snap-frozen, immersed in 20% sucrose, and prepared for microtome sections. DAPI staining (Thermo Fisher Scientific) was carried out, and tissues were observed under fluorescent microscopy. Lungs from mice that received NS exhibited a mild fluorescence signal that was attributed to high autofluorescence of lung tissue.

Pseudomonas aeruginosa *lung infection*

A clinical strain of *P. aeruginosa* (kindly provided by Dr. E. Skoulika, Department of Microbiology, Medical School, University of Crete) was maintained frozen in glycerol stocks. One day before lung infection, bacteria were thawed, inoculated into Luria–Bertani broth, and incubated overnight at 37˚C. From this culture, an aliquot was taken to start a fresh culture that lasted 6–7 h. Bacterial concentrations were estimated from a standard curve based on OD (OD_{600}). *P. aeruginosa* was harvested by centrifugation (3500 rpm 10 min), followed by washes and an appropriate final dilution with sterile NS. The inoculum number was confirmed retrospectively through plating of serial dilutions and counting of CFU on Luria–Bertani plates.

C57BL/6 WT and $Akt2^{-/-}$ mice were anesthetized as described above, and 40 μl bacterial solution (2×10^7 bacteria) or the corresponding vehicle solution (NS) was applied intratracheally. Animals were sacrificed 12 h after inoculation, and a pressure-volume curve of the respiratory system as well as BALF and lung tissue for histology were obtained. Protein levels, cytokine concentration, and WBC numbers were determined in BALF. To determine bacterial load (CFU), serial 10-fold dilutions of BALF were plated on agar plates; the results are expressed as mean CFU/ml BALF.

Statistical analysis

All data were evaluated for normality using the Kolmogorov–Smirnov test (with Dallal–Wilkinson–Lillie test used for *p* values). The data that passed

the normality test were analyzed using one-way ANOVA with the Bonferroni multiple-comparison post test. Comparison of nonparametric results between groups was performed using the Mann–Whitney *U* test or the Kruskal–Wallis test with the Dunn multiple-comparison post test, using GraphPad InStat software (GraphPad, San Diego, CA). The p values < 0.05 were considered significant. Results are expressed as mean ± SD or as median (5–95 percentiles), as indicated, and are representative of at least three independent experiments.

Results

Akt2 deficiency protects from the development of acid-induced lung injury

To determine the role of Akt2 and M2 macrophages in aseptic lung injury, we exposed Akt2$^{-/-}$ mice, which possess M2-type macrophages, to acid-induced lung injury. This model induces tissue injury that initiates an aseptic inflammatory cascade. WT mice developed severe lung injury within hours of acid aspiration, which was characterized by decreased lung compliance (Fig. 1A, 1B) and increased protein concentration in BALF compared with control mice treated with NS (Fig. 1C). The severity of lung injury peaked at 12 h postacid aspiration and declined thereafter (Fig. 1B, 1C). Macrophage and neutrophil infiltration increased within 6 h after acid aspiration in WT mice and reached its highest level at 12 h (Fig. 2A–C). Furthermore, chemokines and cytokines, such as TNF-α, IL-6, CXCL-1, and IL-1β, also accumulated in BALF and reached their highest levels at 6 h postacid aspiration (Fig. 2D). Lung compliance, protein concentration, BALF cell counts, and cytokines returned to baseline at 72 h after acid aspiration (Figs. 1B, 1C, 2A, 2B).

Acid-induced lung injury was less severe in Akt2$^{-/-}$ mice compared with WT mice (Fig. 1A–C). A decrease in lung compliance and an increase in BALF protein concentration were observed in acid-treated WT mice when compared to saline-treated mice, which was profound in acid-treated Akt2$^{-/-}$ mice (Fig. 1A–C). In addition, the severity of inflammatory cell infiltration (Fig. 2A–C) and the cytokine levels in BALF (Fig. 2D) were lower in Akt2$^{-/-}$ mice compared with WT mice.

Histology on lung sections from WT mice at 12 h postacid aspiration demonstrated destruction of normal tissue architecture characterized by thickening of the alveolar walls due to increased cellularity and edema (Fig. 1Db). Proteinaceous debris in the

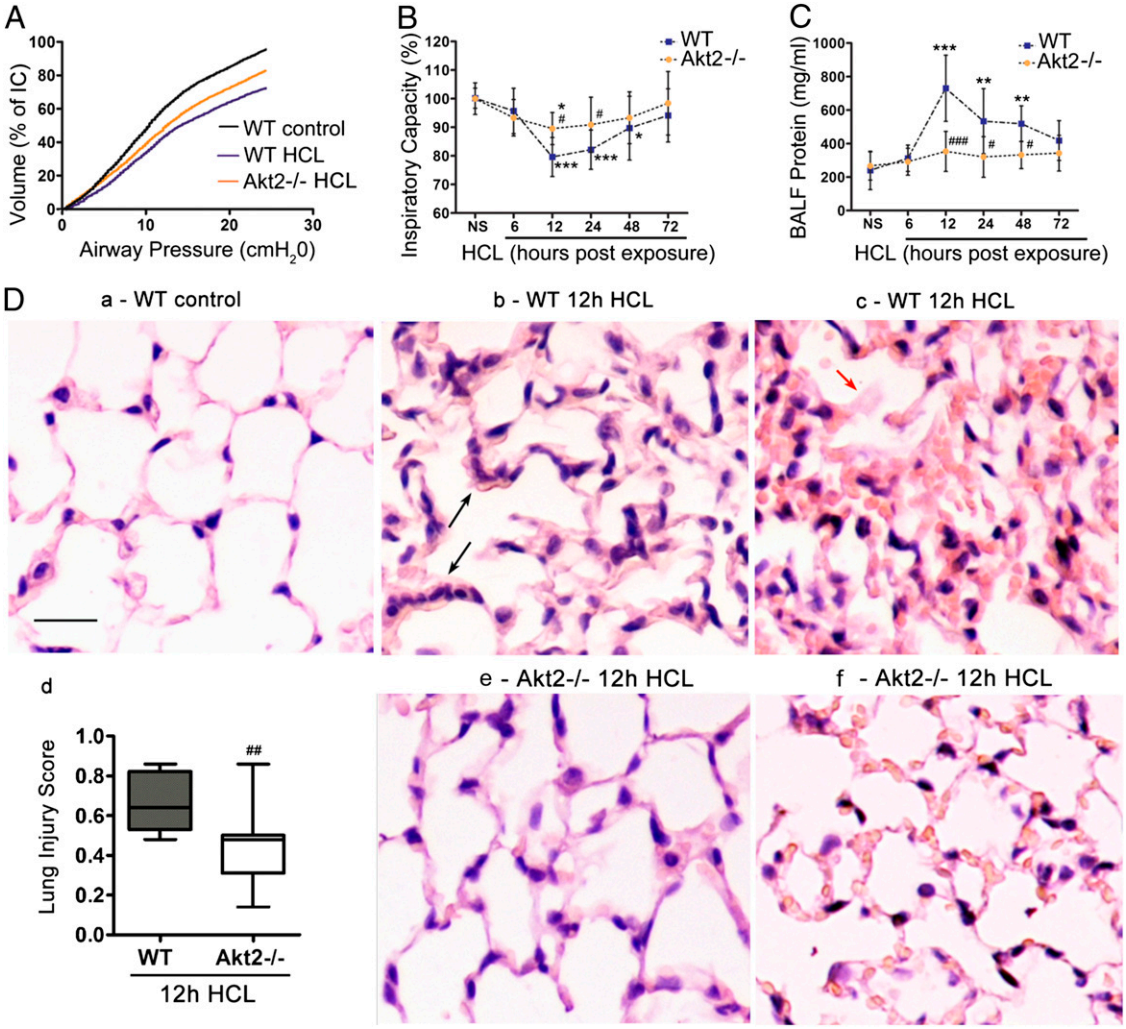

FIGURE 1. Acid aspiration–induced lung injury is reduced in Akt2$^{-/-}$ mice. Pressure-volume curve of the respiratory system (**A**), IC (**B**), and protein concentration in BALF (**C**) in WT and Akt2$^{-/-}$ mice at several time points after acid (HCl) aspiration compared with NS group. (**D**) Histological analysis of lung tissue of untreated control WT mice (**a**), WT mice (**b**, **c**), and Akt2$^{-/-}$ mice (**e**, **f**) at 12 h after HCl administration (H&E stain, original magnification ×400), as well as analysis of acute lung injury score (**d**). Black arrows in (b) demonstrate thickening of the alveolar walls as the result of increased cellularity. Red arrow in (c) indicates proteinaceous debris in the alveoli. Extravasated RBCs are also depicted. Scale bar, 25 μm. n = 5–8 mice/group. Graphs represent median ± SD. In (d), box shows 5–95 percentiles, horizontal line represents median, and whiskers represent minimum and maximum. $^{*}p < 0.05$, $^{**}p < 0.01$, $^{***}p < 0.001$, acid treatment versus NS treatment. $^{\#}p < 0.05$, $^{\#\#}p < 0.01$, $^{\#\#\#}p < 0.001$, Akt2$^{-/-}$ versus WT.

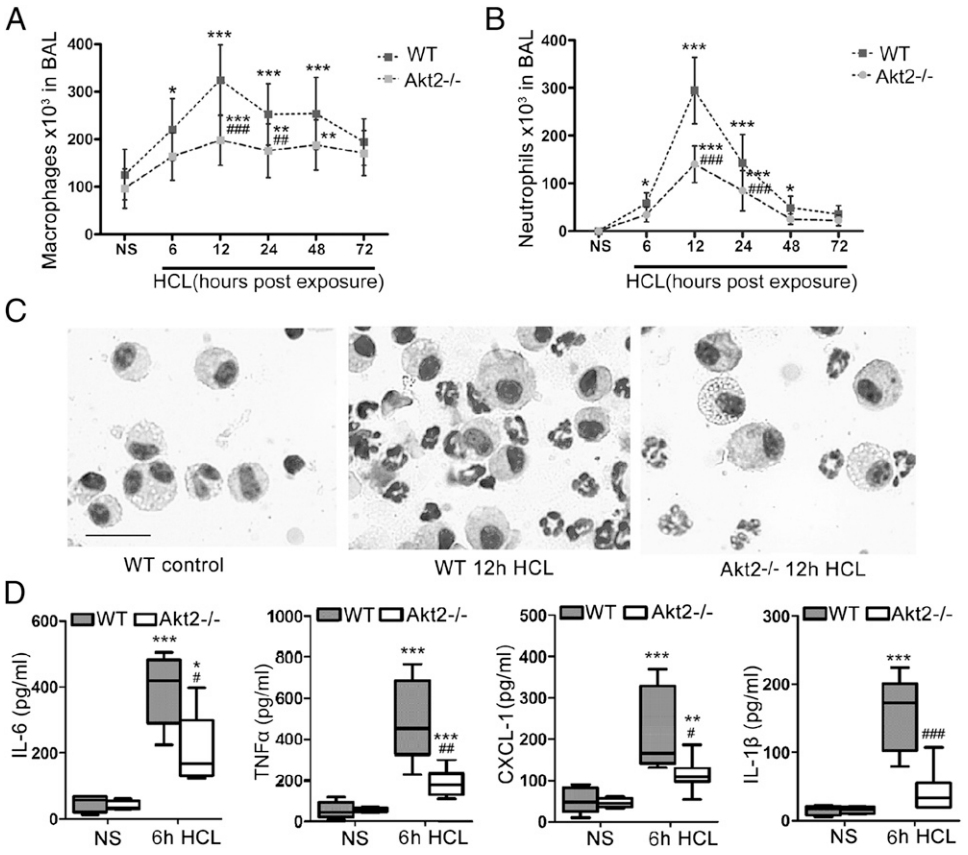

FIGURE 2. Lung inflammation upon acid aspiration was reduced in Akt2$^{-/-}$ mice. Macrophages (**A**) and neutrophils (**B**) accumulate in BALF soon after acid instillation. (**C**) Representative cytospin images of cells isolated from BALF from WT and Akt2$^{-/-}$ mice at 12 h after acid exposure. Scale bar, 25 μm. (**D**) Levels of TNF-α, IL-6, CXCL-1, and IL-1β in BALF of WT and Akt2$^{-/-}$ mice at 6 h after acid aspiration compared with NS aspiration group. n = 5–8 mice/group. Graphs in (A) and (B) represent median ± SD. In (D), box shows 5–95 percentiles, horizontal line represents median, and whiskers represent minimum and maximum. $^{*}p < 0.05$, $^{**}p < 0.01$, $^{***}p < 0.001$, acid treatment versus NS treatment. $^{\#}p < 0.05$, $^{\#\#}p < 0.01$, $^{\#\#\#}p < 0.001$, Akt2$^{-/-}$ versus WT.

alveoli and extravasated RBCs were also observed (Fig. 1Dc). Lung sections from acid-treated Akt2$^{-/-}$ mice at 12 h postinjury demonstrated less severe lung injury compared with WT mice (Fig. 1Dd). Only mild thickening of the alveolar walls with an inconspicuous presence of inflammatory cells, and focal congestion of capillaries, with mild red cell extravasation, were observed in Akt2$^{-/-}$ mice (Fig. 1De, 1Df).

These results suggested that ablation of Akt2 resulted in reduced manifestations of inflammation in the lung upon acid-induced lung injury.

Akt2 ablation suppresses M1 polarization and promotes M2 phenotype in acid-induced lung injury

To determine the inflammatory phenotype of infiltrated macrophages in the model of acid-induced lung injury, we measured the concentration of inflammatory mediators in the BALF and the presence of M1- and M2-type macrophages in the lungs of WT and Akt2$^{-/-}$ mice during the acute phase (12 h following acid aspiration), as well as at the resolution stage (24 h following acid aspiration). In the acute phase of injury, 12 h after acid aspiration, M1 activation of macrophages was observed in WT mice; alveolar macrophages overexpressed iNOS (Fig. 3A, 3C, 3D, 3F) and IL-12β (Fig. 3B, 3E). The expression of M1 markers returned to basal levels at 48 h of injury (Fig. 3A, 3B). The concentration of NO metabolites in BALF was increased in WT mice at 12 h postinjury (Fig. 3G). Expression of M1 markers after acid aspiration–induced lung injury was lower in Akt2$^{-/-}$ mice compared with WT mice (Fig. 3).

The expression of M2 activation markers Arg-1, Fizz1, and Ym1, at 12 h postacid aspiration, was evident in both WT and Akt2$^{-/-}$ macrophages. The levels of Arg-1, Fizz1, and Ym1, as well as arginase activity and MGL1 and MGL2 protein expression, were higher in Akt2$^{-/-}$ macrophages compared with WT ones (Fig. 4A–G, Supplemental Fig. 1A). Arg-1 mRNA was upregulated in WT and Akt2$^{-/-}$ macrophages 12 h following acid aspiration; however, upregulation of its protein and activity were not statistically significant at 12 h, but they were induced further at later time points (24 h following HCl instillation; data not shown). The expression of the anti-inflammatory cytokine IL-10, a characteristic of M2 macrophages, was similarly increased in WT and Akt2$^{-/-}$ macrophages after acid aspiration (Supplemental Fig. 1B), suggesting that its regulation is not under the control of Akt2.

In vitro application of siRNA targeting Akt2 in isolated alveolar macrophages from WT mice resulted in downregulation of Akt2 and concomitant upregulation of C/EBPβ, an M2 polarization-associated transcription factor (22), as well as Arg-1 and Fizz1 (Fig. 4H, 4I), further supporting the effect of Akt2 suppression in promoting M2 polarization in alveolar macrophages.

Involvement of miR-155 in macrophage-activation phenotype in acid-induced lung injury and the role of Akt2

Next, we sought to elucidate the mechanisms by which Akt2 deficiency regulates macrophage polarization and protects from acid-induced lung injury. Earlier studies (22, 25) from our group showed that miR-155 plays a central role in promoting M1 activation in macrophages following LPS stimulation and is under the control of Akt kinases. To investigate the involvement of miR-155 in the regulation of M1 phenotype in our model of aseptic lung injury, we measured miR-155 levels in alveolar macrophages from WT and Akt2$^{-/-}$ mice exposed to acid. We found that the expression of miR-155 did not increase in WT alveolar macrophages at 12 h after acid aspiration, but it was suppressed at 24 h postinjury (Fig. 5A). To exclude miR-155's involvement in M1 activation in our model, we stimulated alveolar macrophages in vitro

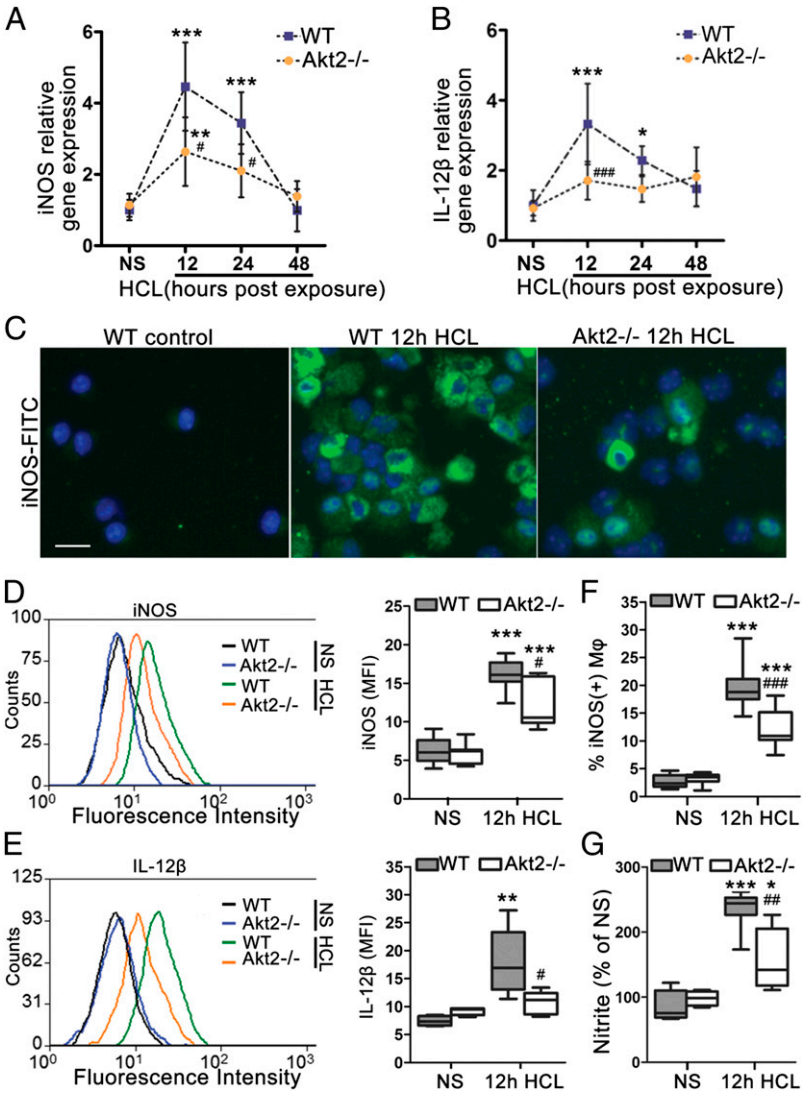

FIGURE 3. Classical (M1) macrophage activation in acid-induced lung injury was reduced in Akt2$^{-/-}$ mice. iNOS and IL-12β, markers of M1 activation, were evaluated in alveolar macrophages from WT and Akt2$^{-/-}$ mice at baseline and upon acid aspiration. iNOS (**A**) and IL-12β (**B**) mRNA induction was assessed at different time points after acid aspiration compared with the NS aspiration group. iNOS protein levels in WT and Akt2$^{-/-}$ alveolar macrophages were assessed by immunofluorescence (**C**) and fluorescence intensity (**D**) (measured by flow cytometry, MFI) 12 h after acid exposure. (**E**) Similarly, IL-12β protein levels were evaluated by fluorescence intensity (MFI) 12 h after acid exposure and compared with mice receiving NS. (**F**) iNOS^{+} WT and Akt2$^{-/-}$ macrophages based on flow cytometry cell counts. (**G**) Nitrite levels in BALF from WT and Akt2$^{-/-}$ mice after acid exposure. Scale bar, 25 μm. n = 5–8 mice/group. Graphs show mean ± SD. In box-and-whisker plots, box shows 5–95 percentiles, horizontal line represents median, and whiskers represent minimum and maximum. $^{*}p < 0.05$, $^{**}p < 0.01$, $^{***}p < 0.001$, acid treatment versus NS treatment. $^{\#}p < 0.05$, $^{\#\#}p < 0.01$, $^{\#\#\#}p < 0.001$, Akt2$^{-/-}$ versus WT. MFI, Mean fluorescence intensity of cells gated for CD11c.

with BALF collected from WT mice 6 h after acid aspiration. We found that exposure to BALF did not cause an increase in miR-155 levels, although it promoted iNOS expression (Fig. 4C, 4D), suggesting that miR-155 does not contribute to M1 activation of macrophages in this model of aseptic lung injury.

The development of M2 phenotype in WT alveolar macrophages 24 h after acid aspiration was associated with a decrease in miR-155 expression (Fig. 5A). The expression of miR-155 in Akt2$^{-/-}$ alveolar macrophages was lower compared with WT macrophages both at baseline and at 12 h postacid aspiration (Fig. 5A), in agreement with their inherent M2 phenotype. C/EBPβ levels, a target of miR-155, were inversely correlated with miR-155 levels (Fig. 5B). C/EBPβ expression increased in WT macrophages at 12 h after acid aspiration, and it was higher in Akt2$^{-/-}$ macrophages compared with WT ones (Fig. 5B). These results suggest that, even though miR-155 does not participate in the initial M1 activation of alveolar macrophages in aseptic lung injury, its suppression coincides with the emergence of M2 status.

Akt2-deficient macrophages overexpress miR-146a, which suppresses TLR signaling in acid-induced lung injury

Because macrophage activation and lung inflammation depend on TLR4 signals, we examined the impact of Akt2 ablation on TLR4-signaling components. We found that mRNA levels of TRAF6 and IRF5, but not of IRAK1, three downstream mediators of TLR4 signaling, were increased in WT alveolar macrophages at 12 h after acid aspiration (Fig. 6A, 6B). On the contrary, Akt2$^{-/-}$ macrophages expressed less TRAF6, IRF5, and IRAK1 compared with WT macrophages both at baseline and at 12 h after acid aspiration (Fig. 6A, 6B). Furthermore, application of siRNA targeting Akt2 to isolated alveolar macrophages resulted in downregulation of TRAF6 and IRF5 compared with cells that received nontargeting siRNA (Fig. 6C).

IRAK1, TRAF6, and IRF5 mRNA are regulated by the anti-inflammatory miRNA miR-146a (34, 35). Therefore, we evaluated the expression of miR-146a in alveolar macrophages after acid aspiration. miR-146a expression did not change significantly at 12 h after acid aspiration, but it increased at 24 h (Fig. 6E). Interestingly, in Akt2$^{-/-}$ macrophages, the expression of miR-146a was higher compared with WT macrophages prior to acid aspiration, as well as after 12 and 24 h (Fig. 6E). To further support that suppression of Akt2 results in miR-146a induction, we transfected macrophages with siRNA for Akt2 and found that miR-146a was upregulated (Fig. 6D). Additionally, miR-146a expression was higher, whereas TRAF6 and IRF5 mRNA and protein expression were lower in Akt2$^{-/-}$ peritoneal macrophages compared with WT macrophages (Fig. 6F, 6G). These findings suggested that miR-146a and its targets TRAF6 and IRF5 were affected by Akt2 deletion or suppression.

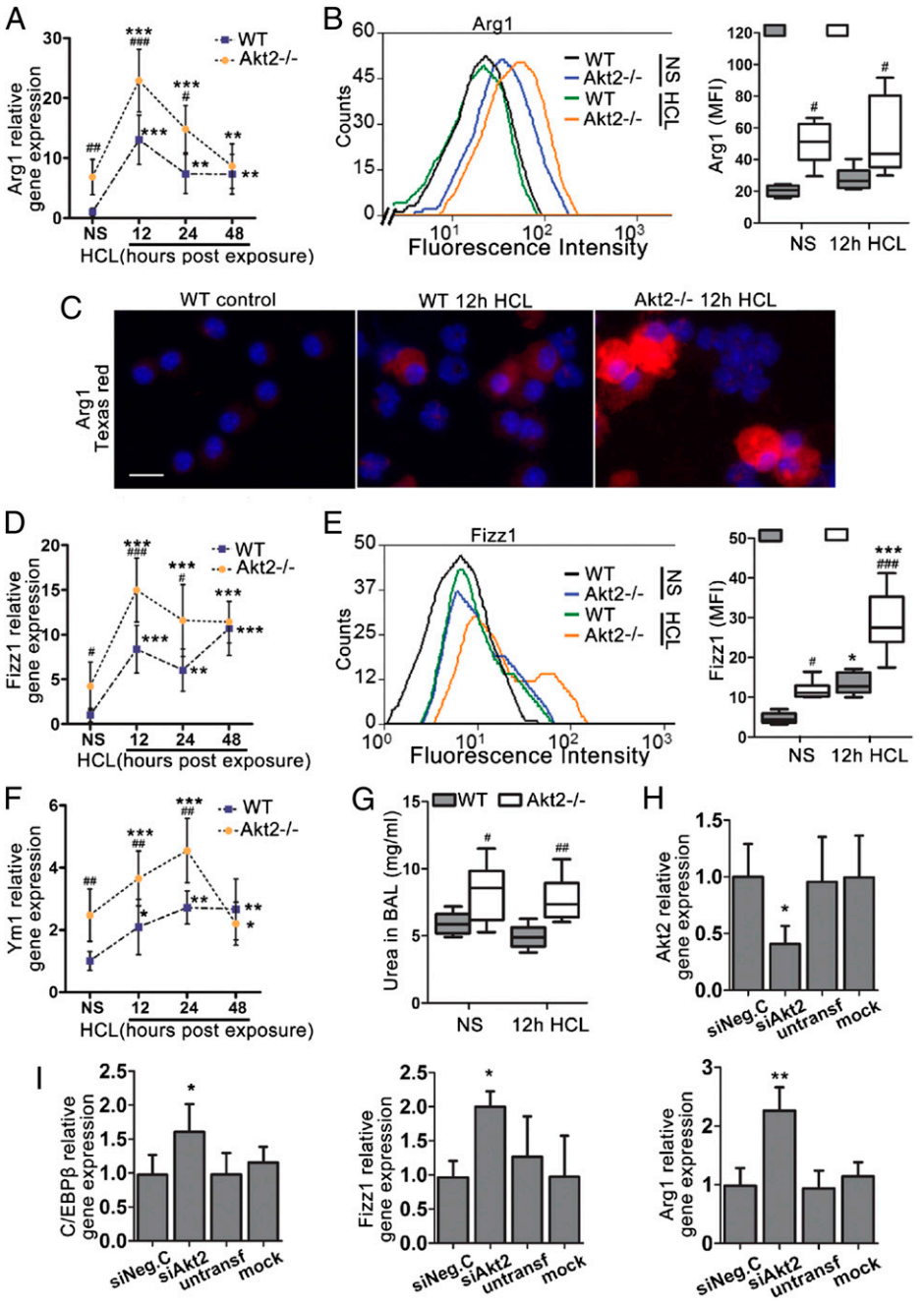

FIGURE 4. Akt2$^{-/-}$ alveolar macrophages exhibit M2 phenotype following acid-induced lung injury. Arg-1, Fizz1, and Ym1, markers of M2 macrophage activation, were evaluated in WT and Akt2$^{-/-}$ mice at baseline and upon acid aspiration. Arg-1 expression was assessed at mRNA levels (**A**) and protein levels (**B**) by flow cytometry (MFI) and immunofluorescence (**C**), 12 h after acid aspiration. Similarly, Fizz1 mRNA levels (**D**) and protein levels (**E**) (MFI) were evaluated in the same conditions. (**F**) Ym1 mRNA levels in WT and Akt2$^{-/-}$ macrophages in acid-treated mice compared with NS-treated mice. (**G**) Urea production, an index of arginase activity, was evaluated in WT and Akt2$^{-/-}$ alveolar macrophages after acid exposure. mRNA levels of Akt2 (**H**) and C/EBPβ, Arg-1, and Fizz1 (**I**) in isolated alveolar macrophages transfected with siAkt2 or nontargeting siRNA (siNeg.C). Cells that received only transfection reagent (mock) or were left untreated (untransfected) were used as controls. Scale bar, 25 μm. n = 5–8 mice/group. Graphs show mean ± SD. In box-and-whisker plots, box shows 5–95 percentiles, horizontal line represents median, and whiskers represent minimum and maximum. $^{*}p < 0.05$, $^{**}p < 0.01$, $^{***}p < 0.001$, acid treatment versus NS treatment. $^{\#}p < 0.05$, $^{\#\#}p < 0.01$, $^{\#\#\#}p < 0.001$, Akt2$^{-/-}$ versus WT. MFI, Mean fluorescence intensity of cells gated for CD11c.

miR-146a prevents M1 activation in vitro and in vivo and is critical for the protection observed in the absence of Akt2

To investigate whether miR-146a upregulation is essential for amelioration of the M1 response in Akt2$^{-/-}$ mice, we isolated peritoneal macrophages from WT and Akt2$^{-/-}$ mice; induced M1 polarization by treating them with LPS, a stimulus that promotes macrophage activation; and transfected them with either an miR-146a mimic or an miR-146a inhibitor. As controls, we used cells treated with negative-control miRNA (scramble), cells treated solely with transfection reagent (mock), and cells that remained untreated (i.e., nontransfected). Akt2$^{-/-}$ macrophages are hyporesponsive to LPS and maintain an M2 phenotype both in vitro and in vivo when mice are subjected to LPS-induced endotoxin shock (22).

Transfection of WT macrophages with miR-146a resulted in suppression of TRAF6 and IRF5. The effect of miR-146a on the suppression of TRAF6 and IRF5 in Akt2$^{-/-}$ macrophages was less prominent compared with WT macrophages (Fig. 7). Inhibition of miR-146a by an miR-146a inhibitor did not affect the expression of TRAF6 or IRF5 in WT macrophages, but it upregulated their expression in the absence of Akt2 (Fig. 7).

Furthermore, miR-146a transfection inhibited LPS-induced iNOS expression in WT macrophages (Fig. 8A) and led to the upregulation of C/EBPβ, Arg-1, and Fizz1 in control and LPS-treated WT macrophages (Fig. 8B–D, Supplemental Fig. 2A). Moreover, IL-6 and TNF-α expression was reduced in LPS-stimulated WT macrophages transfected with miR-146a (Fig. 8E, 8F). In contrast, transfection of miR-146a in Akt2$^{-/-}$ macrophages did not affect LPS-induced iNOS, IL-6, or TNF-α compared with LPS-treated Akt2$^{-/-}$ macrophages that received negative-control miRNA (Fig. 8A, 8E, 8F). However, inhibition of miR-146a in Akt2$^{-/-}$ macrophages increased LPS-induced iNOS, IL-6, and TNF-α, but it did not appear to cause a reduction in C/EBPβ, Arg-1, or Fizz1, sug-

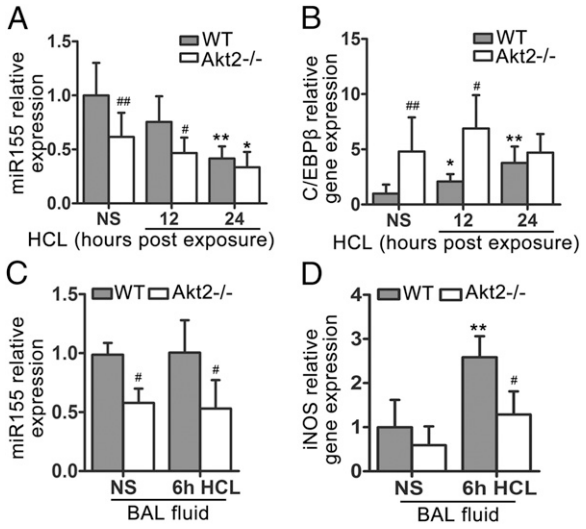

FIGURE 5. miR-155 expression in acid-induced lung injury. Expression of miR-155 (**A**) and its target mRNA C/EBPβ (**B**) in WT and Akt2$^{-/-}$ alveolar macrophages from mice exposed to acid for 12 or 24 h. miR-155 (**C**) and iNOS (**D**) mRNA levels in WT and Akt2$^{-/-}$ alveolar macrophages treated in vitro with BALF from WT mice that received either NS or HCl for 6 h in vivo. Data are mean ± SD for 4–8 mice or samples/group. $^{*}p < 0.05$, $^{**}p < 0.01$, acid treatment versus NS treatment. $^{\#}p < 0.05$, $^{\#\#}p < 0.01$, Akt2$^{-/-}$ versus WT.

gesting that these molecules are regulated by a different Akt2-dependent mechanism (Fig. 8B–F).

To further confirm that inhibition of Akt2 and induction of miR-146a inhibit M1 activation of alveolar macrophages in vivo, acid-treated WT mice received small interfering RNA against Akt2 (siAkt2) or miR-146a mimic or miR-146a inhibitor intratracheally to modulate Akt2 or miR-146a expression, respectively. Transfection efficiency was confirmed by assessing total lung mRNA levels of Akt2, TRAF6, and IRAK1 (Supplemental Fig. 2B–D), as well as miR-146a miRNA levels (Supplemental Fig. 2F). Distribution of siRNA into the lung parenchyma following its intratracheal administration was assessed by Cy3-conjugated control siRNA (Supplemental Fig. 2D). Because iNOS is the major marker of M1-activated macrophages, we evaluated the effect of siAkt2, miR-146a mimic, or miR-146a inhibitor on iNOS expression. Accordingly, iNOS was significantly suppressed in alveolar macrophages from mice treated with siAkt2 or miR-146a compared with those treated with scrambled RNA (Fig. 8G, 8H), suggesting that in vivo modulation of Akt2 or miR-146a could effectively suppress aseptic lung inflammation induced by acid aspiration. Moreover, administration of miR-146a inhibitor to Akt2$^{-/-}$ mice resulted in partial reversal of iNOS suppression in macrophages from those mice (Fig. 8I, Supplemental Fig. 2E), and it had no significant effect on Arg-1 levels (data not shown), suggesting that miR-146a induction is responsible, at least in part, for the suppressed M1 phenotype of Akt2$^{-/-}$ mice. Arg-1 expression in Akt2$^{-/-}$ alveolar macrophages was not affected by treatment with miR-146a inhibitor. Overall, these findings suggest that induction of M2 macrophages, either by inhibition of Akt2 or induction of miR-146a, may be protective against aseptic lung injury.

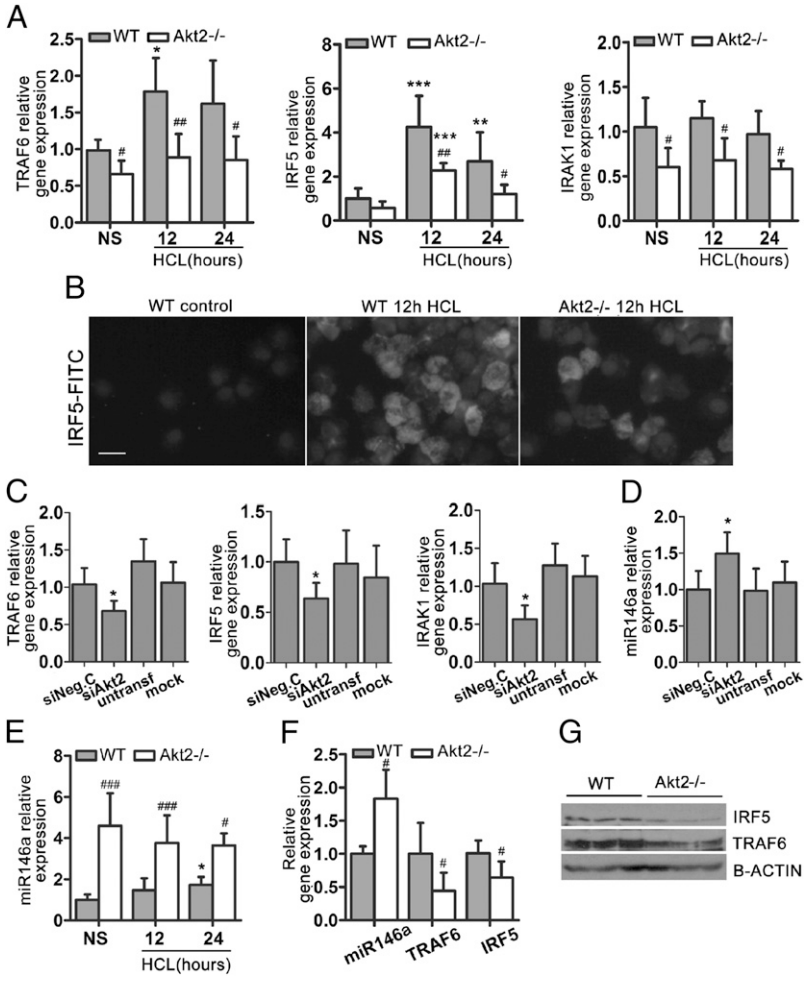

FIGURE 6. TLR4 signaling and miR-146a expression in acid-induced lung injury. mRNA levels of TRAF6, IRF5, and IRAK1 (**A**) and protein expression of IRF5 (**B**) in WT and Akt2$^{-/-}$ alveolar macrophages from mice exposed to acid aspiration for 12 h. Scale bar, 25 μm. mRNA levels of TRAF6, IRF5, and IRAK1 (**C**) and miR-146a in alveolar macrophages treated with siAkt2 or nontargeting siRNA (siNeg.C) (**D**). Cells that received only transfection reagent (mock) or were left untreated (untransfected) were used as controls. (**E**) Levels of miR-146a in WT and Akt2$^{-/-}$ alveolar macrophages from mice that received acid for 12 or 24 h. (**F**) Comparison of miR-146a, TRAF6, and IRF5 mRNA levels in unstimulated WT and Akt2$^{-/-}$ peritoneal macrophages. (**G**) Protein levels of IRF5 and TRAF6 in WT and Akt2$^{-/-}$ unstimulated peritoneal macrophages. B-actin was used as control. Data are mean ± SD for n = 4–8 mice or wells/group. $^{*}p < 0.05$, $^{**}p < 0.01$, $^{***}p < 0.001$, acid treatment versus NS. $^{\#}p < 0.05$, $^{\#\#}p < 0.01$, $^{\#\#\#}p < 0.001$, Akt2$^{-/-}$ versus WT.

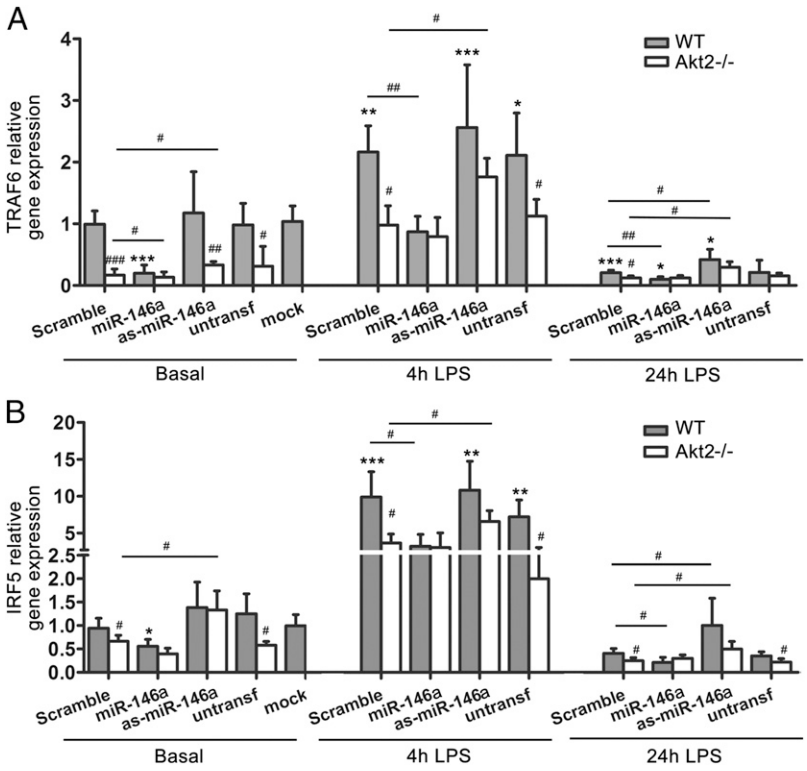

FIGURE 7. Modulation of miR-146a expression in WT and Akt2$^{-/-}$ macrophages in culture. mRNA levels of TRAF6 (**A**) and IRF5 (**B**) in WT and Akt2$^{-/-}$ peritoneal macrophages that were transfected with an miR-146a mimic, an inhibitor of miR-146, or a nontargeting control RNA (scramble). Untransfected cells, as well as cells that received only transfection reagent (mock), were used as experimental controls. Data are mean ± SD for n = 4–5 wells/group. On the x-axis, miR-146a represents the miR-146a mimic, and as-miR-146a represents the miR-146a inhibitor (antisense). $^{*}p < 0.05$, $^{**}p < 0.01$, $^{***}p < 0.001$, LPS treatment versus NS treatment. $^{\#}p < 0.05$, $^{\#\#}p < 0.01$, $^{\#\#\#}p < 0.001$, Akt2$^{-/-}$ versus WT.

Effect of Akt2 depletion in a septic lung injury model

Because aspiration-induced lung injury is frequently accompanied by the presence of pathogens, such as bacteria, we investigated whether Akt2 depletion and, therefore, M2 macrophage polarization, affects the response to live bacteria. For this purpose, we inoculated WT or Akt2$^{-/-}$ mice with *P. aeruginosa* (2×10^7 bacteria/mouse). Lung IC and protein concentration in BALF were similar between WT and Akt2$^{-/-}$ mice (Fig. 9A, 9B), whereas bacterial load (CFU/ml in BALF) was significantly higher in Akt2$^{-/-}$ mice compared with WT mice at 12 h after inoculation (Fig. 9C). Infiltration of macrophages and neutrophils, as well as iNOS expression, was less profound in Akt2$^{-/-}$ mice compared with WT mice (Fig. 9D–F). Macrophages from Akt2$^{-/-}$ mice retained their M2-prone phenotype in septic ALI and expressed more Arg-1 compared with those from WT mice (Fig. 9G). However, IL-6 and TNF-α concentrations in BALF did not differ between Akt2$^{-/-}$ and WT mice (Fig. 9H, 9I), but IL-6 and TNF-α levels appeared significantly reduced in Akt2$^{-/-}$ mice compared with WT mice when normalized to *P. aeruginosa* CFU (Fig. 9H, I), suggesting that the increase in these cytokines may be due to the increased bacterial load. Histological analysis of lung tissue upon *P. aeruginosa* infection revealed that both WT and Akt2$^{-/-}$ lung sections have severe distortion of normal lung architecture due to the presence of a dense interstitial and alveolar inflammatory infiltrate composed mainly of neutrophils, macrophages, and lymphocytes (Fig. 9J). However, the parenchymal damage was less severe in Akt2$^{-/-}$ mice compared with WT mice, because they demonstrated less parenchymal consolidation and better preservation of alveoli, probably as a result of reduced lung inflammation (Fig. 9J). Overall, these findings suggest that, although ablation of Akt2 and M2 polarization of macrophages protects from aseptic lung injury, it compromises the response of macrophages to live bacteria.

Discussion

In the present study we show that, in the mouse model of aseptic lung injury, macrophages first exhibit a proinflammatory M1 phenotype, followed by an M2 anti-inflammatory phenotype. Genetic ablation of Akt2 suppresses M1 activation via miR-146a induction, promotes an M2 phenotype, and protects mice from acid-induced lung injury.

ARDS, the devastating clinical syndrome of acute respiratory failure characterized by lung inflammation and alveolar barrier dysfunction, is a major cause of morbidity and mortality in patients in the intensive care unit. Although pneumonia and sepsis are the most common causes of ARDS, several aseptic conditions are associated with ARDS, such as acute pancreatitis, burns, near drowning, multiple trauma, and inhalation injury (1). With no effective treatment available, there is an urgent need to understand and, subsequently, modulate the pathogenesis of lung inflammation.

It is well established that macrophages play a central role in the pathogenesis of ARDS (4, 5, 12, 13). Most of the studies using animal models examined the role of macrophages in LPS-induced lung injury, a model that resembles septic ARDS (11, 18, 20). In this study, we used the model of acid-induced lung injury, a model of aseptic ARDS (2). Similarly to septic lung injury, we found that alveolar macrophages in acid-induced lung injury acquire a classical (M1) activation phenotype in the early phase that is characterized by increased iNOS expression and accumulation of NO metabolites, which are known to contribute to the pathogenesis of ARDS (4, 13, 15–18). Furthermore, we identified the onset of the resolving phase of inflammation, during which suppression of iNOS and predominance of Arg-1, Fizz1, and Ym1 expression, features of M2 polarization, take place. It was reported recently that stem cell–conditioned medium induced M2 polarization and suppressed lung inflammation in a model of LPS-induced lung injury (20), yet no molecular mechanism of M2 induction was suggested. In our study, Akt2-deficient mice exhibited an ameliorated M1 response and an accelerated M2 activation, resulting in significant protection from lung injury and suggesting that early induction of M2 macrophages, via Akt2 depletion, confers protection in the aseptic lung injury model.

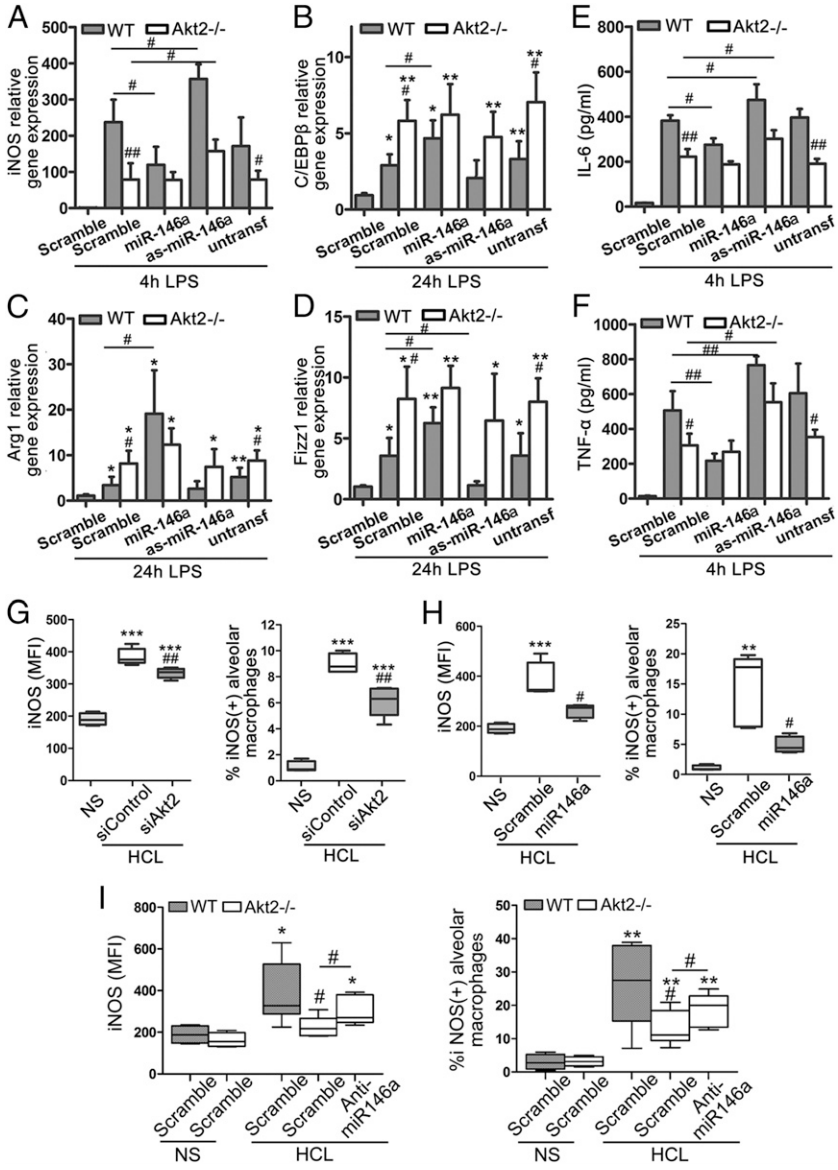

FIGURE 8. miR-146a modulates macrophage activation in WT and Akt2$^{-/-}$ macrophages. mRNA levels of iNOS (**A**), C/EBPβ (**B**), Arg-1 (**C**), and Fizz1 (**D**) in WT and Akt2$^{-/-}$ peritoneal macrophages that were treated with an miR-146a mimic, an inhibitor of miR-146, or a nontargeting control RNA (scramble). iNOS levels were assessed at 4 h post-LPS stimulation, whereas C/EBPβ, Arg-1, and Fizz1 were assessed at 24 h post LPS. Protein levels of IL-6 (**E**) and TNF-α (**F**) in supernatants of LPS-stimulated WT and Akt2$^{-/-}$ macrophages that were transfected with miR-146a mimic, an inhibitor of miR-146a, or a nontargeting control RNA. Nontransfected cells, as well as cells that received only transfection reagent (mock), were used as experimental controls. iNOS protein expression (MFI) and percentage of iNOS^{+} macrophages were measured in WT mice with acid-induced lung injury that were treated in vivo with siAkt2 (**G**), miR-146a mimic (**H**), or miR-146a inhibitor (anti–miR-146a) (**I**). n = 5–8 mice/group. Bar graphs show mean ± SD. In box-and-whisker plots, box shows 5–95 percentiles, horizontal line represents median, and whiskers represent minimum and maximum. $^{*}p < 0.05$, $^{**}p < 0.01$, $^{***}p < 0.001$, acid treatment versus NS treatment. $^{\#}p < 0.05$, $^{\#\#}p < 0.01$, Akt2$^{-/-}$ versus WT. MFI, Mean fluorescence intensity of cells gated for CD11c.

Therefore, we sought to investigate the mechanisms involved in the regulation of the macrophage-activation phenotype by Akt2 in this lung injury model. Activation of the PI3K/Akt pathway was demonstrated to mediate anti-inflammatory effects in macrophages (22, 25, 28, 29). The anti-inflammatory actions of the PI3K/Akt pathway are differentially controlled by the two Akt isoforms, Akt1 and Akt2, which also regulate the activation phenotype of macrophages (22). Hence, ablation of Akt2 suppresses LPS responses, promoting an M2 anti-inflammatory phenotype, whereas ablation of Akt1 renders macrophages hyperresponsive to LPS and M1 prone (22). We showed previously that miR-155, a proinflammatory miRNA, is differentially regulated by Akt kinases and plays a central role in M1 polarization of macrophages in several inflammatory models (22). Also, miR-155 was found to be important in the pathogenesis of LPS-induced lung injury (50). Yet, in the aseptic model of acid-induced lung injury, an increase in miR-155 expression was not necessary for the initial M1 polarization of macrophages, whereas a decrease in miR-155 levels was associated with the development of M2 phenotype. These findings suggest that, in this aseptic model, a distinct mechanism regulates macrophage activation.

Various signaling pathways, including STAT1/STAT6, SOCS2/SOCS3, TLR4, and IRF5/IRF4, were reported to regulate macrophage activation (21, 23, 24). Specifically, TLR4 signaling plays a central role in macrophage activation in both septic and aseptic inflammation, including ARDS (32, 33, 51–55), and is critical in the pathogenesis of disease (12, 32, 55). TLR4 signaling is controlled by MyD88- or TRIF-dependent downstream effectors, the signals of which converge for TRAF6 activation and NF-κB nuclear translocation (56). IRAK1 and IRF5 are primarily known to be involved downstream of MyD88 (52), but IRF5 is also involved in TRIF-mediated responses (57). In acid aspiration lung injury, TLR4/TRIF/TRAF6 signaling in lung macrophages was shown to determine the susceptibility to ARDS in vivo (12, 33). Both TRAF6 and IRF5 lead to NF-κB activation, but IRF5 is also an important regulator of iNOS and IL-12β expression and, thus, M1 polarization (23, 52, 57–60). We found that WT macrophages upregulate TRAF6 and IRF5 gene expression in line with their M1 phenotype, whereas Akt2-deficient macrophages, having an M2 phenotype, exhibit reduced levels of these factors both at baseline and upon acid injury.

miR-146a is an LPS-induced miRNA that plays a critical role in macrophage responses (61). miR-146a is considered an anti-inflammatory miRNA that mutes immune activation initiated by TLR4 by targeting the 3′−υντρανσλατεδ ρεγιον of TRAF6,

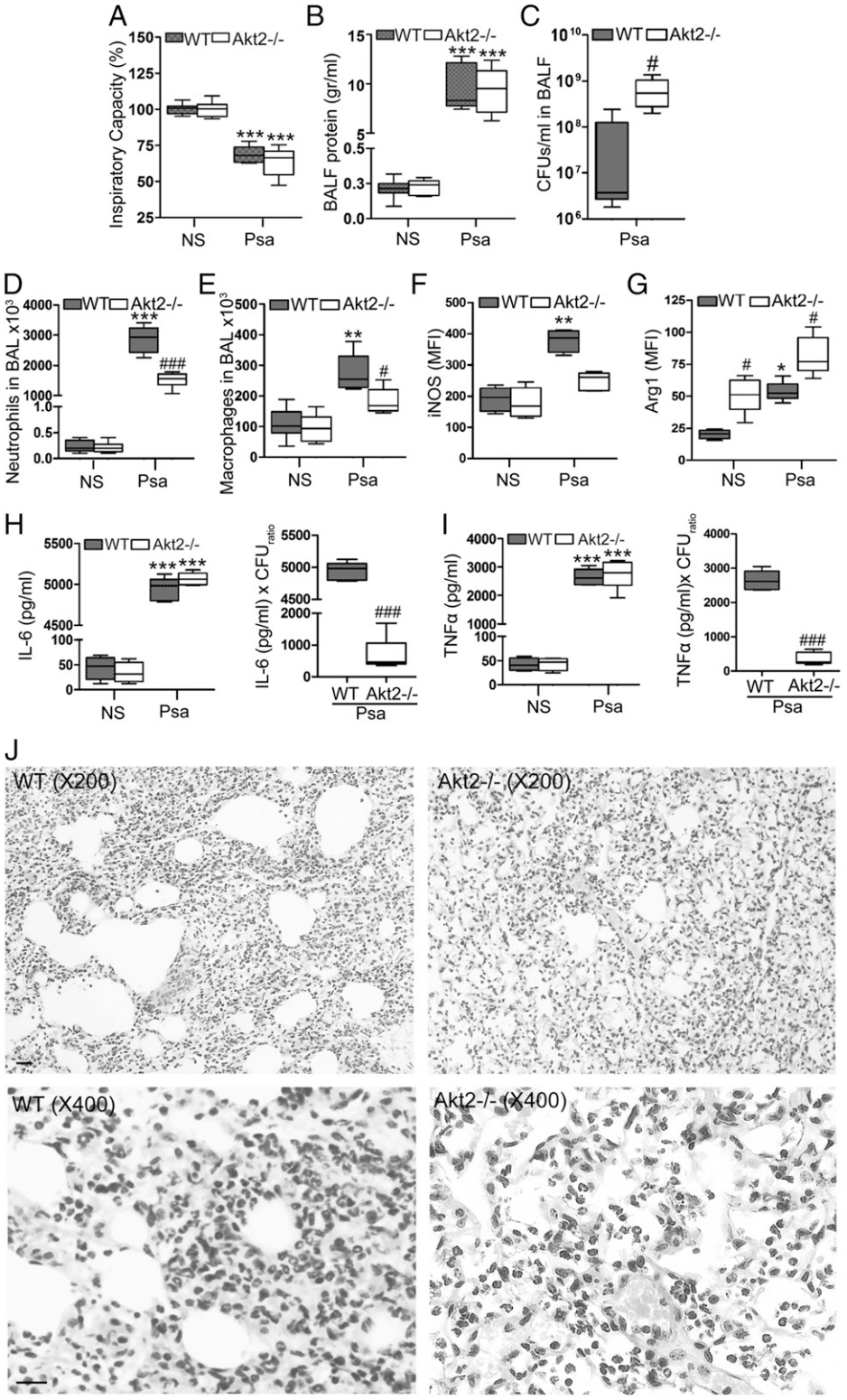

FIGURE 9. *P. aeruginosa* induced lung injury and inflammation in Akt2$^{-/-}$ mice. IC (**A**), protein concentration (**B**), and bacterial load (CFU/ml) (**C**) in BALF from WT and Akt2$^{-/-}$ mice at 12 h after *P. aeruginosa* inoculation (Psa). Neutrophil (**D**) and macrophage (**E**) cell numbers in BALF from WT and Akt2$^{-/-}$ mice after *P. aeruginosa* infection (Psa). Protein levels of iNOS (**F**) and Arg-1 (**G**) in alveolar macrophages (CD11c^{+} cells) of WT and Akt2$^{-/-}$ mice with *P. aeruginosa* lung infection assessed by flow cytometry and expressed as mean fluorescent intensity (MFI). Levels of IL-6 (**H**) and TNF-α (**I**) in BALF of WT and Akt2$^{-/-}$ mice at 12 h after *P. aeruginosa* inoculation. IL-6 and TNF-α levels are also shown normalized to bacterial load in BALF (CFU ratio = mean CFU/ml of WT mice/CFU/ml of Akt2$^{-/-}$ mice). (**J**) Histological analysis of lung tissue sections of WT and Akt2$^{-/-}$ mice after *P. aeruginosa* pneumonia (H&E stain) shows severe distortion of lung architecture in both sections as the result of the presence of dense interstitial and alveolar inflammatory infiltrates. Akt2$^{-/-}$ mice demonstrate slightly better preservation of alveoli and less parenchymal consolidation. Scale bars, 50 μm. $n = 6$ mice/group. In box-and-whisker plots, box shows 5–95 percentiles, horizontal line represents median, and whiskers represent minimum and maximum. $^{*}p < 0.05$, $^{**}p < 0.01$, $^{***}p < 0.001$, acid treatment versus NS treatment. $^{\#}p < 0.05$, $^{\#\#\#}p < 0.001$, Akt2$^{-/-}$ versus WT.

IRAK1, and IRF5 mRNAs (34, 35) and suppressing TLR4-induced NF-κB–regulated gene expression (61–64). In this study, we show that Akt2 deficiency resulted in a significant upregulation of miR-146a, which was of critical importance in suppressing the M1 phenotype. miR-146a transfection in WT macrophages was also able to inhibit iNOS induction, and miR-146a suppression in Akt2$^{-/-}$ mice resulted in upregulation of iNOS expression. It is of interest that introduction of miR-146a in WT macrophages induced expression of the transcription factor C/EBPβ, a master regulator of M2 polarization, indicating that miR-146a induction can promote alternative macrophage activation. However, inhibition of miR-146 in Akt2$^{-/-}$ macrophages did not suppress their M2 phenotype, suggesting that miR-146a is sufficient, but not necessary, for the induction of the M2 phenotype and that additional molecules regulated by Akt2, such as miR-155, maintain M2 activation.

Finally, we show that the pulmonary macrophage-polarization phenotype can be modulated in vivo by targeting local Akt2 or miR-146a expression. Intratracheal administration of siRNA

against Akt2 or of an miR-146a mimic in WT mice exposed to acid-induced lung injury resulted in a significant suppression of iNOS in alveolar macrophages. Because it is well established that suppression of iNOS and subsequent inhibition of M1 activation (4, 13, 15–18), as well as induction of M2 (20), can confer protection in ARDS, the identification of molecules that promote this mechanism in vivo is of the utmost importance. However, Akt2 suppression and M2 macrophages impair the innate immune response against live bacteria, such as *P. aeruginosa*, which limits the use of M2 induction for the protection from gastric acid aspiration–induced lung injury. Simultaneous treatment with antibiotics may overcome such a limitation in a clinical setting.

In summary, this study demonstrates the protective effect of alternative macrophage polarization in acid-induced lung injury and identifies Akt2 and miR-146a as key molecular determinants of alveolar macrophage polarization. Based on these findings, Akt2 and miR-146a appear to be promising therapeutic targets for aseptic ARDS. However, the impaired bacterial clearance as a result of M2 induction is a major limitation to the use of this therapeutic application in septic ARDS, which represents the great majority of cases in clinical practice either from a pulmonary or nonpulmonary source.

Disclosures

The authors have no financial conflicts of interest.

References

1. Ware, L. B., and M. A. Matthay. 2000. The acute respiratory distress syndrome. *N. Engl. J. Med.* 342: 1334–1349.
2. Matute-Bello, G., C. W. Frevert, and T. R. Martin. 2008. Animal models of acute lung injury. *Am. J. Physiol. Lung Cell. Mol. Physiol.* 295: L379–L399.
3. Frank, J. A., J. F. Pittet, H. Lee, M. Godzich, and M. A. Matthay. 2003. High tidal volume ventilation induces NOS2 and impairs cAMP-dependent air space fluid clearance. *Am. J. Physiol. Lung Cell. Mol. Physiol.* 284: L791–L798.
4. Frank, J. A., C. M. Wray, D. F. McAuley, R. Schwendener, and M. A. Matthay. 2006. Alveolar macrophages contribute to alveolar barrier dysfunction in ventilator-induced lung injury. *Am. J. Physiol. Lung Cell. Mol. Physiol.* 291: L1191–L1198.
5. Eyal, F. G., C. R. Hamm, and J. C. Parker. 2007. Reduction in alveolar macrophages attenuates acute ventilator induced lung injury in rats. *Intensive Care Med.* 33: 1212–1218.
6. Dolinay, T., M. Szilasi, M. Liu, and A. M. Choi. 2004. Inhaled carbon monoxide confers antiinflammatory effects against ventilator-induced lung injury. *Am. J. Respir. Crit. Care Med.* 170: 613–620.
7. Dreymueller, D., C. Martin, T. Kogel, J. Pruessmeyer, F. M. Hess, K. Horiuchi, S. Uhlig, and A. Ludwig. 2012. Lung endothelial ADAM17 regulates the acute inflammatory response to lipopolysaccharide. *EMBO Mol. Med.* 4: 412–423.
8. Johnston, L. K., C. R. Rims, S. E. Gill, J. K. McGuire, and A. M. Manicone. 2012. Pulmonary macrophage subpopulations in the induction and resolution of acute lung injury. *Am. J. Respir. Cell Mol. Biol.* 47: 417–426.
9. Gea-Sorlí, S., R. Guillamat, A. Serrano-Mollar, and D. Closa. 2011. Activation of lung macrophage subpopulations in experimental acute pancreatitis. *J. Pathol.* 223: 417–424.
10. Janssen, W. J., L. Barthel, A. Muldrow, R. E. Oberley-Deegan, M. T. Kearns, C. Jakubzick, and P. M. Henson. 2011. Fas determines differential fates of resident and recruited macrophages during resolution of acute lung injury. *Am. J. Respir. Crit. Care Med.* 184: 547–560.
11. Dhaliwal, K., E. Scholefield, D. Ferenbach, M. Gibbons, R. Duffin, D. A. Dorward, A. C. Morris, D. Humphries, A. MacKinnon, T. S. Wilkinson, et al. 2012. Monocytes control second-phase neutrophil emigration in established lipopolysaccharide-induced murine lung injury. *Am. J. Respir. Crit. Care Med.* 186: 514–524.
12. Imai, Y., K. Kuba, G. G. Neely, R. Yaghubian-Malhami, T. Perkmann, G. van Loo, M. Ermolaeva, R. Veldhuizen, Y. H. Leung, H. Wang, et al. 2008. Identification of oxidative stress and Toll-like receptor 4 signaling as a key pathway of acute lung injury. *Cell* 133: 235–249.
13. Kudoh, I., H. Miyazaki, M. Ohara, J. Fukushima, T. Tazawa, and H. Yamada. 2001. Activation of alveolar macrophages in acid-injured lung in rats: different effects of pentoxifylline on tumor necrosis factor-alpha and nitric oxide production. *Crit. Care Med.* 29: 1621–1625.
14. Mosser, D. M., and J. P. Edwards. 2008. Exploring the full spectrum of macrophage activation. *Nat. Rev. Immunol.* 8: 958–969.
15. Jian, M. Y., T. Koizumi, and K. Kubo. 2005. Effects of nitric oxide synthase inhibitor on acid aspiration-induced lung injury in rats. *Pulm. Pharmacol. Ther.* 18: 33–39.
16. Peng, X., R. E. Abdulnour, S. Sammani, S. F. Ma, E. J. Han, E. J. Hasan, R. Tuder, J. G. Garcia, and P. M. Hassoun. 2005. Inducible nitric oxide synthase contributes to ventilator-induced lung injury. *Am. J. Respir. Crit. Care Med.* 172: 470–479.
17. Liu, R., Y. Hotta, A. R. Graveline, O. V. Evgenov, E. S. Buys, K. D. Bloch, F. Ichinose, and W. M. Zapol. 2007. Congenital NOS2 deficiency prevents impairment of hypoxic pulmonary vasoconstriction in murine ventilator-induced lung injury. *Am. J. Physiol. Lung Cell. Mol. Physiol.* 293: L1300–L1305.
18. Farley, K. S., L. F. Wang, H. M. Razavi, C. Law, M. Rohan, D. G. McCormack, and S. Mehta. 2006. Effects of macrophage inducible nitric oxide synthase in murine septic lung injury. *Am. J. Physiol. Lung Cell. Mol. Physiol.* 290: L1164–L1172.
19. Herold, S., K. Mayer, and J. Lohmeyer. 2011. Acute lung injury: how macrophages orchestrate resolution of inflammation and tissue repair. *Front. Immunol.* 2: 65.
20. Ionescu, L., R. N. Byrne, T. van Haaften, A. Vadivel, R. S. Alphonse, G. J. Rey-Parra, G. Weissmann, A. Hall, F. Eaton, and B. Thébaud. 2012. Stem cell conditioned medium improves acute lung injury in mice: in vivo evidence for stem cell paracrine action. *Am. J. Physiol. Lung Cell. Mol. Physiol.* 303: L967–L977.
21. Gordon, S., and F. O. Martinez. 2010. Alternative activation of macrophages: mechanism and functions. *Immunity* 32: 593–604.
22. Arranz, A., C. Doxaki, E. Vergadi, Y. Martinez de la Torre, K. Vaporidi, E. D. Lagoudaki, E. Ieronymaki, A. Androulidaki, M. Venihaki, A. N. Margioris, et al. 2012. Akt1 and Akt2 protein kinases differentially contribute to macrophage polarization. *Proc. Natl. Acad. Sci. USA* 109: 9517–9522.
23. Honda, K., and T. Taniguchi. 2006. IRFs: master regulators of signalling by Toll-like receptors and cytosolic pattern-recognition receptors. *Nat. Rev. Immunol.* 6: 644–658.
24. Spence, S., A. Fitzsimons, C. R. Boyd, J. Kessler, D. Fitzgerald, J. Elliott, J. N. Gabhann, S. Smith, A. Sica, E. Hams, et al. 2013. Suppressors of cytokine signaling 2 and 3 diametrically control macrophage polarization. *Immunity* 38: 66–78.
25. Androulidaki, A., D. Iliopoulos, A. Arranz, C. Doxaki, S. Schworer, V. Zacharioudaki, A. N. Margioris, P. N. Tsichlis, and C. Tsatsanis. 2009. The kinase Akt1 controls macrophage response to lipopolysaccharide by regulating microRNAs. *Immunity* 31: 220–231.
26. Franke, T. F., S. I. Yang, T. O. Chan, K. Datta, A. Kazlauskas, D. K. Morrison, D. R. Kaplan, and P. N. Tsichlis. 1995. The protein kinase encoded by the Akt proto-oncogene is a target of the PDGF-activated phosphatidylinositol 3-kinase. *Cell* 81: 727–736.
27. Iliopoulos, D., C. Polytarchou, M. Hatziapostolou, F. Kottakis, I. G. Maroulakou, K. Struhl, and P. N. Tsichlis. 2009. MicroRNAs differentially regulated by Akt isoforms control EMT and stem cell renewal in cancer cells. *Sci. Signal.* 2: ra62.
28. Lee, Y. G., J. Lee, S. E. Byeon, D. S. Yoo, M. H. Kim, S. Y. Lee, and J. Y. Cho. 2011. Functional role of Akt in macrophage-mediated innate immunity. Front. Biosci. (Landmark Ed.) 16: 517–530.
29. Fukao, T., and S. Koyasu. 2003. PI3K and negative regulation of TLR signaling. *Trends Immunol.* 24: 358–363.
30. Gray, M. J., M. Poljakovic, D. Kepka-Lenhart, and S. M. Morris, Jr. 2005. Induction of arginase I transcription by IL-4 requires a composite DNA response element for STAT6 and C/EBPbeta. *Gene* 353: 98–106.
31. He, M., Z. Xu, T. Ding, D. M. Kuang, and L. Zheng. 2009. MicroRNA-155 regulates inflammatory cytokine production in tumor-associated macrophages via targeting C/EBPbeta. *Cell. Mol. Immunol.* 6: 343–352.
32. Prakash, A., K. R. Mesa, K. Wilhelmsen, F. Xu, J. M. Dodd-o, and J. Hellman. 2012. Alveolar macrophages and Toll-like receptor 4 mediate ventilated lung ischemia reperfusion injury in mice. *Anesthesiology* 117: 822–835.
33. Reino, D. C., V. Pisarenko, D. Palange, D. Doucet, R. P. Bonitz, Q. Lu, I. Colorado, S. U. Sheth, B. Chandler, K. B. Kannan, et al. 2011. Trauma hemorrhagic shock-induced lung injury involves a gut-lymph-induced TLR4 pathway in mice. *PLoS ONE* 6: e14829.
34. Williams, A. E., M. M. Perry, S. A. Moschos, H. M. Larner-Svensson, and M. A. Lindsay. 2008. Role of miRNA-146a in the regulation of the innate immune response and cancer. *Biochem. Soc. Trans.* 36: 1211–1215.
35. Taganov, K. D., M. P. Boldin, K. J. Chang, and D. Baltimore. 2006. NF-kappaB-dependent induction of microRNA miR-146, an inhibitor targeted to signaling proteins of innate immune responses. *Proc. Natl. Acad. Sci. USA* 103: 12481–12486.
36. Vaporidi, K., R. C. Francis, K. D. Bloch, and W. M. Zapol. 2010. Nitric oxide synthase 3 contributes to ventilator-induced lung injury. *Am. J. Physiol. Lung Cell. Mol. Physiol.* 299: L150–L159.
37. Reinhard, C., G. Eder, H. Fuchs, A. Ziesenis, J. Heyder, and H. Schulz. 2002. Inbred strain variation in lung function. Mamm. Genome: 13: 429–437.
38. Kimura, I., Y. Moritani, and Y. Tanizaki. 1973. Basophils in bronchial asthma with reference to reagin-type allergy. *Clin. Allergy* 3: 195–202.
39. Matute-Bello, G., G. Downey, B. B. Moore, S. D. Groshong, M. A. Matthay, A. S. Slutsky, and W. M. Kuebler; Acute Lung Injury in Animals Study Group. 2011. An official American Thoracic Society workshop report: features and measurements of experimental acute lung injury in animals. *Am. J. Respir. Cell Mol. Biol.* 44: 725–738.
40. Pfaffl, M. W. 2001. A new mathematical model for relative quantification in real-time RT-PCR. *Nucleic Acids Res.* 29: e45.
41. van Rijt, L. S., H. Kuipers, N. Vos, D. Hijdra, H. C. Hoogsteden, and B. N. Lambrecht. 2004. A rapid flow cytometric method for determining the cellular composition of bronchoalveolar lavage fluid cells in mouse models of asthma. *J. Immunol. Methods* 288: 111–121.

42. Shirey, K. A., L. E. Cole, A. D. Keegan, and S. N. Vogel. 2008. *Francisella tularensis* live vaccine strain induces macrophage alternative activation as a survival mechanism. *J. Immunol.* 181: 4159–4167.
43. Corraliza, I. M., M. L. Campo, G. Soler, and M. Modolell. 1994. Determination of arginase activity in macrophages: a micromethod. *J. Immunol. Methods* 174: 231–235.
44. Judge, A. D., M. Robbins, I. Tavakoli, J. Levi, L. Hu, A. Fronda, E. Ambegia, K. McClintock, and I. MacLachlan. 2009. Confirming the RNAi-mediated mechanism of action of siRNA-based cancer therapeutics in mice. *J. Clin. Invest.* 119: 661–673.
45. Robbins, M., A. Judge, and I. MacLachlan. 2009. siRNA and innate immunity. *Oligonucleotides* 19: 89–102.
46. Vaporidi, K., E. Vergadi, E. Kaniaris, M. Hatziapostolou, E. Lagoudaki, D. Georgopoulos, W. M. Zapol, K. D. Bloch, and D. Iliopoulos. 2012. Pulmonary microRNA profiling in a mouse model of ventilator-induced lung injury. *Am. J. Physiol. Lung Cell. Mol. Physiol.* 303: L199–L207.
47. Zhang, X., P. Shan, D. Jiang, P. W. Noble, N. G. Abraham, A. Kappas, and P. J. Lee. 2004. Small interfering RNA targeting heme oxygenase-1 enhances ischemia-reperfusion-induced lung apoptosis. *J. Biol. Chem.* 279: 10677–10684.
48. Alvarez, R., S. Elbashir, T. Borland, I. Toudjarska, P. Hadwiger, M. John, I. Roehl, S. S. Morskaya, R. Martinello, J. Kahn, et al. 2009. RNA interference-mediated silencing of the respiratory syncytial virus nucleocapsid defines a potent antiviral strategy. *Antimicrob. Agents Chemother.* 53: 3952–3962.
49. Gutbier, B., S. M. Kube, K. Reppe, A. Santel, C. Lange, J. Kaufmann, N. Suttorp, and M. Witzenrath. 2010. RNAi-mediated suppression of constitutive pulmonary gene expression by small interfering RNA in mice. *Pulm. Pharmacol. Ther.* 23: 334–344.
50. Guo, Z., Z. Wen, A. Qin, Y. Zhou, Z. Liao, Z. Liu, Y. Liang, T. Ren, and L. Xu. 2013. Antisense oligonucleotide treatment enhances the recovery of acute lung injury through IL-10-secreting M2-like macrophage-induced expansion of CD4+ regulatory T cells. *J. Immunol.* 190: 4337–4348.
51. He, Z., Y. Gao, Y. Deng, W. Li, Y. Chen, S. Xing, X. Zhao, J. Ding, and X. Wang. 2012. Lipopolysaccharide induces lung fibroblast proliferation through Toll-like receptor 4 signaling and the phosphoinositide3-kinase-Akt pathway. *PLoS ONE* 7: e35926.
52. Takaoka, A., H. Yanai, S. Kondo, G. Duncan, H. Negishi, T. Mizutani, S. Kano, K. Honda, Y. Ohba, T. W. Mak, and T. Taniguchi. 2005. Integral role of IRF-5 in the gene induction programme activated by Toll-like receptors. *Nature* 434: 243–249.
53. Connor, A. J., J. D. Laskin, and D. L. Laskin. 2012. Ozone-induced lung injury and sterile inflammation. Role of toll-like receptor 4. *Exp. Mol. Pathol.* 92: 229–235.
54. Krzyzaniak, M., G. Cheadle, C. Peterson, W. Loomis, J. Putnam, P. Wolf, A. Baird, B. Eliceiri, V. Bansal, and R. Coimbra. 2011. Burn-induced acute lung injury requires a functional Toll-like receptor 4. *Shock* 36: 24–29.
55. Hilberath, J. N., T. Carlo, M. A. Pfeffer, R. H. Croze, F. Hastrup, and B. D. Levy. 2011. Resolution of Toll-like receptor 4-mediated acute lung injury is linked to eicosanoids and suppressor of cytokine signaling 3. FASEB J. 25: 1827–1835.
56. Akira, S., S. Uematsu, and O. Takeuchi. 2006. Pathogen recognition and innate immunity. *Cell* 124: 783–801.
57. Ouyang, X., H. Negishi, R. Takeda, Y. Fujita, T. Taniguchi, and K. Honda. 2007. Cooperation between MyD88 and TRIF pathways in TLR synergy via IRF5 activation. *Biochem. Biophys. Res. Commun.* 354: 1045–1051.
58. Paun, A., R. Bankoti, T. Joshi, P. M. Pitha, and S. Stäger. 2011. Critical role of IRF-5 in the development of T helper 1 responses to *Leishmania donovani* infection. *PLoS Pathog.* 7: e1001246.
59. Krausgruber, T., K. Blazek, T. Smallie, S. Alzabin, H. Lockstone, N. Sahgal, T. Hussell, M. Feldmann, and I. A. Udalova. 2011. IRF5 promotes inflammatory macrophage polarization and TH1-TH17 responses. *Nat. Immunol.* 12: 231–238.
60. Lawrence, T., and G. Natoli. 2011. Transcriptional regulation of macrophage polarization: enabling diversity with identity. *Nat. Rev. Immunol.* 11: 750–761.
61. Nahid, M. A., K. M. Pauley, M. Satoh, and E. K. Chan. 2009. miR-146a is critical for endotoxin-induced tolerance: IMPLICATION IN INNATE IMMUNITY. *J. Biol. Chem.* 284: 34590–34599.
62. Hou, J., P. Wang, L. Lin, X. Liu, F. Ma, H. An, Z. Wang, and X. Cao. 2009. MicroRNA-146a feedback inhibits RIG-I-dependent Type I IFN production in macrophages by targeting TRAF6, IRAK1, and IRAK2. *J. Immunol.* 183: 2150–2158.
63. Tang, Y., X. Luo, H. Cui, X. Ni, M. Yuan, Y. Guo, X. Huang, H. Zhou, N. de Vries, P. P. Tak, et al. 2009. MicroRNA-146A contributes to abnormal activation of the type I interferon pathway in human lupus by targeting the key signaling proteins. *Arthritis Rheum.* 60: 1065–1075.
64. O'Connell, R. M., D. S. Rao, and D. Baltimore. 2012. microRNA regulation of inflammatory responses. *Annu. Rev. Immunol.* 30: 295–312.